Glacial and Interglacial Changes in Southwest Pacific Water Mass Ventilation and Circulation

Kumulative Dissertation zur Erlangung des akademischen Grades eines

Doktors der Naturwissenschaften: *Doctor rerum naturalium*

Dr. rer. nat.

am Fachbereich der Geowissenschaften

der Universität Bremen

vorgelegt von

Thomas Alexander Ronge

Bremen, Oktober 2014

Gutachter: **Prof. Dr. Ralf Tiedemann**

Alfred Wegener Institut – Helmholtz-Zentrum für Polar- und Meeresforschung, Bremerhaven

Universität Bremen FB 5 Geowissenschaften, Bremen

Prof. Dr. Michael Schulz

MARUM – Zentrum für Marine Umweltwissenschaften, Bremen

Universität Bremen FB 5 Geowissenschaften, Bremen

Erklärung

Hiermit erkläre ich an Eides statt, dass ich die vorliegende Arbeit ohne unzulässige Hilfe Dritter und unter Verwendung keiner als der von mir angegebenen Quellen und Hilfsmittel angefertigt habe. Die aus fremden Quellen wörtlich oder inhaltlich übernommenen Informationen sind als solche kenntlich gemacht.

Bremen, 7. Oktober 2014

Thomas Ronge

Some went out on the sea in ships […]. They saw the works of the Lord, his wonderful deeds in the deep.

Psalm 107, 23f

Acknowledgements

First off, I want to thank my supervisor Ralf Tiedemann, without whom this project would not have been possible. Thank you for the opportunity of working at the AWI, your encyclopedic expertise, advice, and for your ongoing support. Special thank goes also to Frank Lamy, my second supervisor for helping me throughout our numerous discussions.

Also, I want to thank Michael Schulz for reviewing this thesis and thanks to all the members of my committee.

I'd like to thank the entire senior scientists from our department, for your help and expertise.

Particularly, I want to thank Rita Fröhlking, Birgit Glückselig, Norbert Lensch, Lukas Ritzenhofen, Lisa Schönborn, Aysel Sorensen, Michael Seebeck, Marianne Warnkroß and Susanne Wiebe for technical support. Although the scientists get all the sunshine for the projects, without your terrific help in the background, none of us would be successful!

I want to thank all the awesome people (including captains and crews) who sailed the South Pacific with me aboard the infamous, storm-beaten cruise SO213. Together we survived Portuguese Man O' War, onboard fires, the myth-enshrouded *Point Nemo*, 12 m high waves, tropical cyclones and everything else the Roaring Forties tried to throw at us.

Furthermore, I want to thank all the legendary MarGeo PhD-students (current and former) for the great time we had.

I want to express my particular gratitude to my parents Edeltraud and Peter, my fiancée and best friend Melanie and my aunt Helga, who supported me in every detail of my life. Last but not least, I want to thank my little brother Jan whose slight indifference, regarding my travels and work, brought me back to Earth many times.

This PhD project was funded by the Federal Ministry of Education and Research (BMBF; Germany) project 03G0213A – SOPATRA and the Alfred Wegener Institute, Helmholtz Centre for Polar and Marine Research.

Abstract

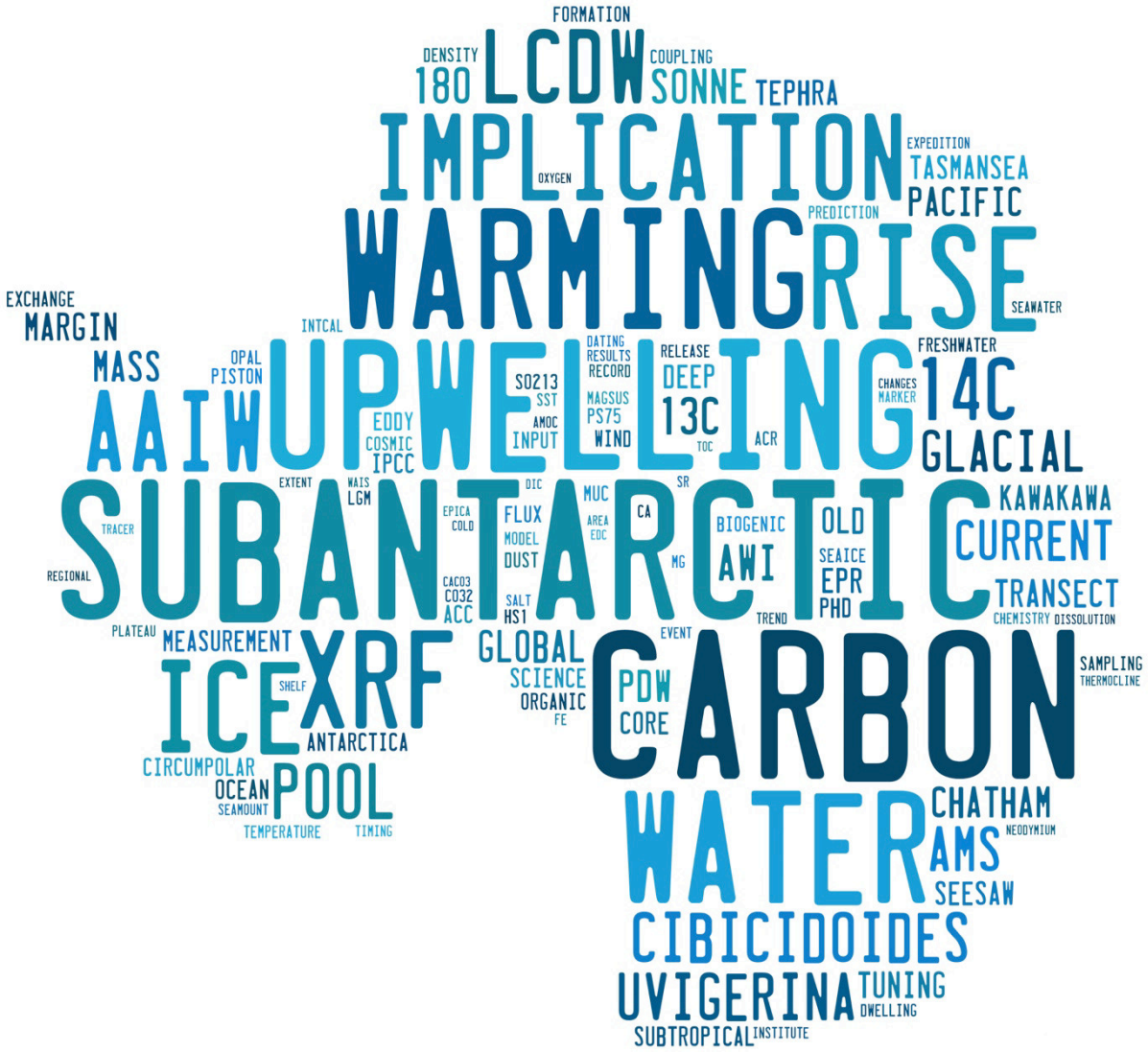

Reconstructions on Antarctic ice cores revealed pronounced, millennial-scale variabilities in atmospheric CO_2 over the past 800,000 years (e.g. Lüthi et al., 2008; Monnin et al., 2001; Petit et al., 1999; Raynaud et al., 2005; Siegenthaler et al., 2005). Despite these variabilities are known for several decades, the mechanisms, driving these patterns are still not fully resolved. As the ocean contains up to 60 times more carbon than the entire atmosphere, it is considered to be a major driver of the atmospheric CO_2 levels (Broecker, 1982): Storing CO_2 during glacials, releasing it during deglaciations. Because changes in the global thermohaline circulation are thought to operate on glacial/interglacial timescales, it has been suggested that

during glacials, the deep ocean was separated from surface-waters and therefore from the atmosphere by enhanced stratification, resulting in the pronounced accumulation of CO_2 and nutrients in the lower levels of the water column. These waters, isolated for millennia, then surfaced during interglacial periods and released their load of ancient CO_2. This hypothesis is strongly supported by the record of atmospheric radiocarbon activities ($\Delta^{14}C$; Reimer et al., 2013) in which a telltale drop in $\Delta^{14}C$ is shown during the interval of enhanced increase in atmospheric CO_2. This drop cannot be explained by the atmospheric formation of ^{14}C and is therefore indicative for the release of an old and hence ^{14}C-depleted and CO_2-enriched reservoir (e.g. the deep ocean) to the atmosphere. This release can therefore explain both records (atmospheric CO_2 and $\Delta^{14}C$). Indeed, several records from the Atlantic and Pacific Oceans point to the existence of this carbon pool in glacial deep-waters below 2000 m. However, the spatial extent (vertical and lateral) and particularly the pathways of upwelled waters during the interglacial remain elusive and even contradictory.

The aim of this thesis is to improve the knowledge of changes in South Pacific circulation and ventilation over different glacial to interglacial time-scales. The three manuscripts that form the backbone of this thesis are used to: 1) constrain the spatial extent and upwelling pathways of the glacial carbon pool in the South Pacific (0 – 30,000 years); 2) reconstruct boundary shifts between intermediate-waters and the underlying carbon pool in Circumpolar Deep Water over the last 350,000 years; 3) analyze changes in the South Pacific Gyre's thermocline during the past 200,000 years.

The focus of the first manuscript (*Chapter 3*) lies on the transition from the last glacial to the current interglacial. The $\Delta^{14}C$-reconstructions on a water mass transect of seven sediment cores from the New Zealand Margin and the East Pacific Rise identify a pool of radiocarbon depleted waters between ~2000 and ~4500 m in the glacial counterpart of Pacific Deep Water. The ^{14}C-depletion of this body of water is up to five times higher than in the modern South Pacific and reaches extreme apparent ventilation ages of ~8000 years. Despite the first deep-

water rejuvenation begins as early as ~21,000 years B.P., the main signal of rejuvenation and outgassing parallels the rise in atmospheric CO_2.

The vertical extent of southwest Pacific Antarctic Intermediate Water (AAIW) over the last four glacial/interglacial cycles is analyzed in the second manuscript (*Chapter 4*). Stable isotope records ($\delta^{13}C$ and $\delta^{18}O$) from epibenthic foraminifera of sediment cores bathed in AAIW and Upper Circumpolar Deep Water (UCDW) indicate a shoaling of AAIW during glacial periods. Further support for these findings arises from model reconstructions using the CCSM3-climate model. Throughout glacial maxima, pronounced input of freshwater by melting sea ice into the AAIW significantly increased its buoyancy and hampered its downward expansion. Hence, the upward displacement of the AAIW-UCDW boundary led to an expansion of the glacial carbon pool identified in *Chapter 3*.

In the third manuscript (*Chapter 5*) the evolution of Southern Ocean Intermediate Waters (SOIWs) is analyzed, using the Mg/Ca paleothermometry on surface- and deep-dwelling species of planktic (Emiliani, 1991) foraminifera. The results suggest opposing glacial subsurface conditions during the LGM and MIS 6 with colder-than-Holocene conditions during the former and warmer-than-LGM conditions during the latter interval. Because of the importance of SOIWs for the ventilation of the South Pacific Gyre (SPG), the results of *Chapter 5* reveal the relevance of Southern Ocean subsurface processes on the transfer of climatic signals from higher to lower latitudes via the SPG.

Ultimately, this thesis contributes to the broader understanding of ventilation and circulation changes in the Pacific Sector of the Southern Ocean. The combination of various proxies reveals the highly dynamic processes that affect the Southern Ocean on glacial/interglacial timescales. The results do not only constrain the vertical extent of the glacial carbon pool for the first time, but they also facilitate its integration in the global context of glacial circulation. Furthermore, the reconstructions shown in this study might help to improve model simulations that are used to both, reconstruct and predict changes in the global climate.

Kurzfassung

Untersuchungen an antarktischen Eiskernen enthüllten gravierende Schwankungen im atmosphärischen CO_2-Gehalt während der letzten 800.000 Jahre (Lüthi et al., 2008; Monnin et al., 2001; Petit et al., 1999; Raynaud et al., 2005; Siegenthaler et al., 2005). Obwohl schon seit Jahrzehnten bekannt, sind die Mechanismen, die diese atmosphärischen Muster bedingen, bis heute nicht vollständig verstanden. Die Tatsache, dass der Ozean etwa 60 mal mehr Kohlenstoff enthält als die gesamte Atmosphäre, macht ihn zu einem wahrscheinlichen Taktgeber für Veränderungen im atmosphärischen CO_2-Haushalt (Broecker, 1982) mit ozeanischer Aufnahme von CO_2 während Glazialen und Abgabe während Deglazialen. Da Veränderungen in der globalen thermohalinen Zirkulation auf glazialen/interglazialen Zeitskalen ablaufen, wird angenommen, dass der tiefe Ozean während Glazialen durch verstärkte Stratifizierung von Oberflächenwassern abgeschnitten war. Diese Trennung resultierte in der gesteigerten Anreicherung von CO_2 und Nährstoffen in der unteren Wassersäule. Diese Wassermassen, welche für Jahrtausende von der Oberfläche abgeschnitten waren, trieben während der Interglazialen auf und setzten das in ihnen gespeicherte alte CO_2 frei. Gestützt wird diese Hypothese durch den Verlauf der atmosphärischen Radiokohlenstoffaktivitäten ($\Delta^{14}C$; Reimer et al., 2013). Dieser Verlauf zeigt einen eindeutigen Abfall des atmosphärischen $\Delta^{14}C$ im selben Zeitintervall, in dem das atmosphärische CO_2 am stärksten ansteigt. Da dieser Abfall nicht mit der atmosphärischen Produktion von ^{14}C erklärt werden kann, deutet der Verlauf auf die Freisetzung eines alten und deshalb ^{14}C-abgereicherten aber CO_2-angereicherten Reservoirs (z.B. der tiefe Ozean) hin. Diese Freisetzung führte der Atmosphäre große Mengen an ^{14}C-armen CO_2 zu und kann somit beide Verläufe (CO_2 und $\Delta^{14}C$) erklären. Die Existenz dieses ozeanischen Kohlenstoffreservoirs wird in der Tat durch mehrere Untersuchungen im tiefen Atlantischen und Pazifischen Ozean unterhalb von ~2000 m bestätigt. Dessen ungeachtet sind die

räumliche Ausdehnung dieses Reservoirs (lateral und vertikal), aber auch die Routen des aufgetriebenen Wassers während der Interglaziale weiterhin unklar, seine Rekonstruktionen teils sogar widersprüchlich.

Das Ziel dieser Dissertation ist es, das Wissen über Veränderungen der Ventilation und Zirkulation des Südpazifiks auf unterschiedlichen glazialen/interglazialen Zeitskalen zu verbessern. Die drei Manuskripte, die den Kern dieser Arbeit bilden, befassen sich mit: 1) der Eingrenzung der räumlichen Ausdehnung des glazialen Kohlenstoffreservoirs sowie seiner Routen während des Interglazials im Südpazifik während der letzten 30.000 Jahre; 2) der Rekonstruktion der Grenzschichten von Zwischenwasser und dem unterliegenden Kohlenstoffreservoir im Zirkumpolaren Tiefenwasser über die letzten 350.000 Jahre; 3) der Analyse von Veränderungen der Thermoklinen der Südpazifischen Gyre während der letzten 200.000 Jahre.

Der Fokus des ersten Manuskriptes (*Kapitel 3*) liegt auf dem Übergang des letzten Glazials zum jetzigen Interglazial. Untersuchungen von $\Delta^{14}C$ an einem Wassermassentransekt aus sieben Sedimentkernen vor Neuseeland und am Ostpazifischen Rücken belegen ein Reservoir von radiokohlenstoffarmen Wasser zwischen ~2000 und ~4500 m Wassertiefe im glazialen Gegenstück des Pazifischen Tiefenwassers. Mit Ventilationsaltern von ca. 8000 Jahren war die glaziale Abreicherung des ^{14}C-Gehaltes in etwa fünfmal stärker als im heutigen Südpazifik. Obwohl die Erneuerung des Tiefenwassers bereits vor ~21.000 Jahren einsetzte, verläuft das Hauptsignal der Erneuerung parallel zum atmosphärischen CO_2-Anstieg.

Die vertikale Ausdehnung des Antarktischen Zwischenwassers (AAIW) wird im zweiten Manuskript (*Kapitel 4*) über den Zeitraum der letzten vier glazialen/interglazialen Zyklen rekonstruiert. Untersuchungen von stabilen Isotopen ($\delta^{13}C$ und $\delta^{18}O$) an epibenthischen Foraminiferen aus Sedimentkernen des heutigen AAIWs und Oberen Zirkumpolaren-tiefenwassers (UCDW) zeigen eine Verflachung des AAIWs während glazialer Perioden. Bestätigt wird dieses Ergebnis zusätzlich durch Modellrekonstruktionen mit Hilfe des

CCSM3-Klimamodells. Während glazialer Maxima erhöhte die verstärkte Zuführung von Süßwasser durch schmelzendes Meereis den Auftrieb von AAIW, was eine Abnahme der Tiefenausdehnung dieser Wassermasse zur Folge hatte. Als Resultat führte die Verflachung der AAIW-UCDW Grenzschicht zu einer Ausdehnung des glazialen Kohlenstoffreservoirs, wie es in *Kapitel 3* identifiziert wurde.

Die Evolution Südozeanischer Zwischenwasser (SOIW) wird im dritten Manuskript (*Kapitel 5*) mit Hilfe der Mg/Ca-Paläothermometrie untersucht. Diese Untersuchung, durchgeführt an oberflächen- und tieflebenden planktischen Foraminiferen, liefert gegenläufige Trends für das Letzte Glaziale Maximum (LGM) und das Marine Isotopen Stadium (MIS) 6. Die Bedingungen im tieferen Wasser während des LGMs waren kälter als das Holozän, während sie in MIS 6 deutlich wärmer als während des LGMs waren. Aufgrund der Bedeutung von SOIW für die Ventilation der Südpazifischen Gyre (SPG), zeigen die Resultate aus *Kapitel 5* die Relevanz von Prozessen des tieferen Südozeanes auf den Transport von Klimasignalen aus den höheren Breiten in die niederen Breiten via der SPG.

Letztendlich wird diese Dissertation zum besseren Verständnis der Ventilation und Zirkulation im pazifischen Sektor des Südozeans beitragen. Die Kombination von unterschiedlichen Methoden enthüllt die hochdynamischen Prozesse, die den Südozean auf glazialen/interglazialen Zeitskalen prägen. Diese Resultate grenzen nicht nur zum ersten Mal die vertikale Ausdehnung des glazialen Kohlenstoffreservoirs ein, sondern sie bringen dieses auch in den globalen Zusammenhang der glazialen Zirkulation. Weiterhin besitzen die hier gezeigten Rekonstruktionen das Potential, Computermodelle, welche für Rekonstruktionen und Vorhersagen des globalen Klimas genutzt werden, zu optimieren.

Table of contents

Acknowledgements I

Abstract II

Kurzfassung V

Chapter 1 Introduction 4

1.1 Preamble 4

1.2 The Southwest Pacific and the New Zealand Margin 7

1.2.1 Modern Oceanography 7

1.2.1.1 Surface Oceanography 7

1.2.1.2 Subsurface Oceanography 9

1.2.1.3 The SW-Pacific Deep Western Boundary Current 13

1.3 Previous work on water mass reconstructions 13

1.3.1 General framework 13

1.3.2 Previous work 17

1.4 Objective of this thesis 22

1.5 Author's contribution 24

Chapter 2 Material and methods 25

2.1 Research project SOPATRA 25

2.2 Sediment material 28

2.3 Methods 29

2.3.1 Sediment handling 29

2.3.2 Visual core description 29

2.3.3 Physical properties 30

2.3.4 XRF core scanning 31

2.3.5 Stable isotopes 32

2.3.6 Radiocarbon 32

2.3.7 Age model 34

Chapter 3 Constraining the extent and evolution of the Southwest Pacific glacial carbon pool 36

T.A. Ronge, R. Tiedemann, F. Lamy, F. Kersten, J. Fietzke, R. De Pol-Holz, K. Pahnke, B. V. Alloway, L. Wacker, J. Southon

Science (under review)

Chapter 4 Pushing the boundaries: Glacial / Interglacial variability of SW-Pacific intermediate-water over the last 350,000 years 60

T. A. Ronge, S. Steph, R. Tiedemann, M. Prange, U. Merkel, D. Nürnberg, G. Kuhn

Paleoceanography (under review)

Chapter 5 Glacial disparities in Intermediate Mode Water advection in the South Pacific gyre 89

R. Tapia, D. Nürnberg, **T. A. Ronge**, R. Tiedemann

Earth and Planetary Science Letters (under review)

Chapter 6 Conclusions and perspectives 116

6.1 Conclusions 116

6.2 The Last Ocean: Constraining the carbon pool in the glacial Indian Ocean 118

6.3 Improvement of data-model-comparisons 120

6.4 Beyond MIS 2-3 121

6.5 Assessing AAIW variability in other regions 122

Chapter 7 Epilogue 125

References 127

Appendix 146

A1 List of Abbreviations 146

A2 Core descriptions of SO213 sediment cores 148

Data handling 156

Chapter 1

Introduction

1.1 Preamble

Surrounding the Antarctic Continent, uninterrupted by landmasses, the Southern Ocean is of crucial importance for the oceanic overturning circulation and the global climate system (Kennicutt II and Chown, 2014). Water masses from the Pacific, Atlantic and Indian Oceans are mixed and spread into the major basins by the perpetual movement of eastbound winds and currents in this oceanic node (Fig. 1.1).

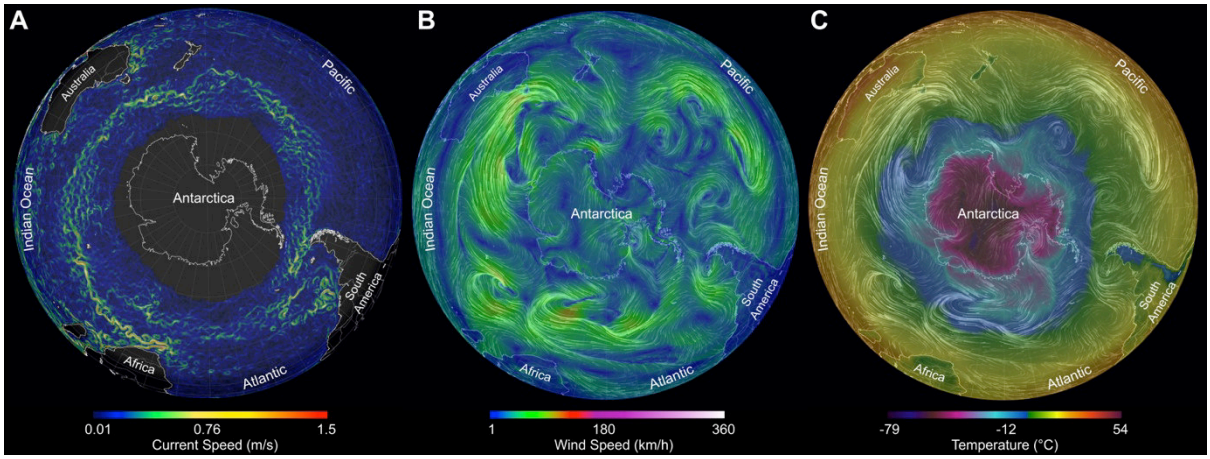

Figure 1.1: Surface properties of the Southern Ocean. **A)** Surface current speed. The grey area surrounding Antarctica indicates the winter sea ice extent. **B)** Surface wind speed. **C)** Surface temperatures. White lines in B and C indicate current wind tracks. Pictures taken in austral winter (July) 2014. Modified after http://earth.nullschool.net

Furthermore, the Southern Ocean constitutes an important window for the ventilation, formation and export of water masses (Charles and Fairbanks, 1992; Pahnke and Zahn, 2005). In this area old, CO_2- and nutrient-rich deep-waters are upwelled, mixed and transformed into newly formed intermediate- and bottom-waters (Fig. 1.2; Charles and Fairbanks, 1992).

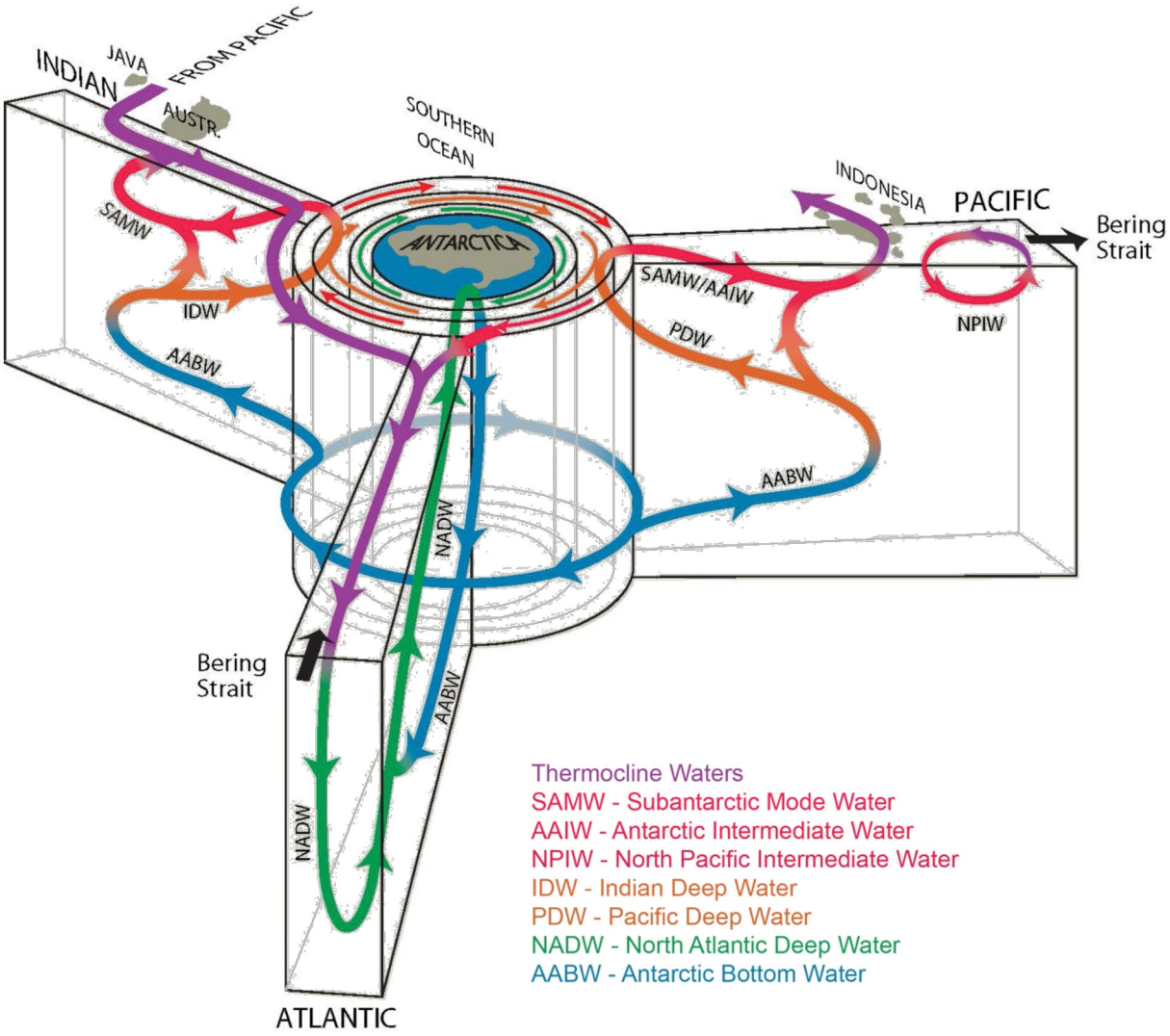

Figure 1.2: Schematic view of the global overturning circulation from an Antarctic point of view. Modified after (Talley, 2013).

This fact in particular has a potential global impact. Depending on upwelling rates (Skinner et al., 2010), biological productivity (Ziegler et al., 2013) and the partial pressure of atmospheric CO_2 (Takahashi et al., 2012), the Southern Ocean acts either as a sink or source for greenhouse gases. Thereby the extent, stratification and volume of the particular water masses play a prominent role, as these factors control a major part of ocean to atmosphere exchange rates. Despite the Southern Oceans key role in the global climate system (e.g. Anderson and Carr, 2010; Bianchi and Gersonde, 2004; Brix and Gerdes, 2003), its largest region, the South Pacific, is fundamentally underrepresented in paleoceanographic reconstructions. So far, most

studies, highlighting the importance of the Southern Ocean, concentrated on its Atlantic Sector or used Antarctic ice-core data.

With this study, I want to focus on glacial and interglacial mutabilities in the ventilation and formation of the major southwest Pacific water masses from the Antarctic Intermediate Water (AAIW) down to the Lower Circumpolar Deep Water (LCDW). The whereabouts of ^{14}C-depleted CO_2 in the glacial carbon cycle and its deglacial pathways in particular are still a matter of an ongoing debate (e.g. Broecker and Clark, 2010; De Pol-Holz et al., 2010; Marchitto et al., 2007; Skinner et al., 2010). In 1982, Wallace Broecker proposed that because the ocean contains up to 60 times more carbon than the atmosphere, atmospheric CO_2 is a "*slave to the oceans chemistry*". He concluded that the oscillation of atmospheric CO_2 as recorded in Antarctic ice cores (e.g. Lüthi et al., 2008) was driven by fluctuations in the ocean's carbon storage. Further support for this assumption arises from the record of atmospheric $\Delta^{14}C$ (Reimer et al., 2013). Especially during the so-called *mystery interval* of Heinrich Stadial 1 (17.5 – 14.5 kyr B.P.; Denton et al., 2006) atmospheric CO_2 rose, while its $\Delta^{14}C$ declined considerably. This pattern is a strong argument for the ventilation of an old and therefore ^{14}C-depleted carbon reservoir (e.g. the deep-ocean) to the atmosphere (Broecker, 2009). For though a large number of studies addressed the quest for this oceanic carbon reservoir, the results are still contradictory (Broecker and Barker, 2007; Broecker and Clark, 2010; Broecker et al., 2008; Burke and Robinson, 2012; Skinner et al., 2010; Stephens and Keeling, 2000). The reconstruction of pathways for old ^{14}C-depleted CO_2 from the deep-ocean to the atmosphere as well remains controversial (Bryan et al., 2010; De Pol-Holz et al., 2010; Marchitto et al., 2007; Rose et al., 2010; Stott et al., 2009). Analyzing radiocarbon data over the last 30,000 years from a depth transect of sediment cores (835 – 4339 mbsl), I want to shed new light on this issue, ultimately constraining the hypothesized carbon pool.

Since not only the ventilation of deep water masses but also the formation of intermediate-water is important for the global level of atmospheric CO_2 (Downes et al., 2010; Murata et al., 2010; Murata et al., 2007; Sabine et al., 2004), I furthermore studied the variability in the extent of AAIW off New Zealand over the last 350,000 years, using stable oxygen ($\delta^{18}O$) and carbon ($\delta^{13}C$) isotopes.

1.2 The Southwest Pacific and the New Zealand Margin

1.2.1 Modern Oceanography

1.2.1.1 Surface Oceanography

The dominant force in the Southern Ocean, the Antarctic Circumpolar Current (ACC; Fig. 1.3) is propelled by strong Southern Westerly Winds (SWW; Rintoul et al., 2001). In the region of this study, by the powerful winds of the infamous *Roaring Forties*. However, the wind stress is partly balanced by bottom stress, slowing down the eastward flow of the ACC (Rintoul et al., 2001). Measuring ~24.000 km in length (Whithworth, 1988) and moving a mean volume of 136.7±7.8 Sv (Cunningham et al., 2003) the ACC is the largest current system on the Planet. Because the ACC is connecting the Pacific, Atlantic and Indian Oceans, the current is of exceptional importance for the oceans and the global climate as it transports heat, salt and gases from one basin into another (Carter et al., 2009). Along its pathway, the ACC is steered by bottom topography like submerged plateaus or mid ocean ridges (Carter et al., 2009). The ACC is considerably constricted by the Campbell and Falkland plateaus, while the Kerguelen Plateau expands the current's surface (Carter et al., 2009; Orsi et al., 1995; Fig 1.3).

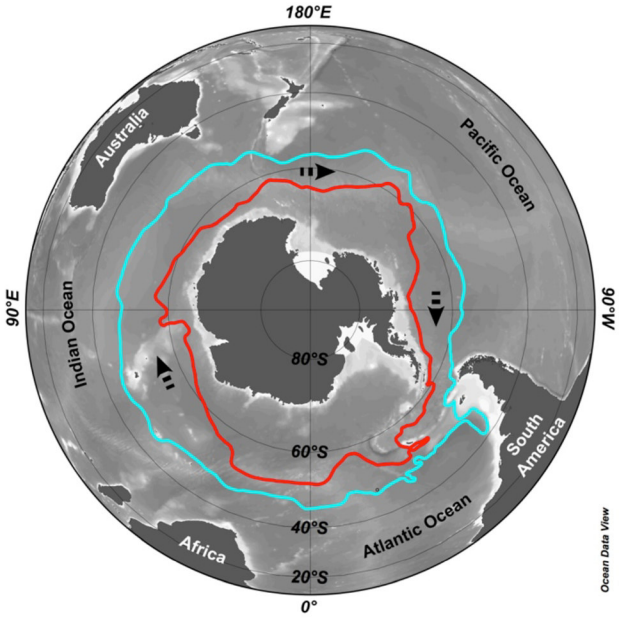

Figure 1.3: Bathymetric map of the Southern Ocean. Black arrows indicate the current direction of the ACC between the Sub Antarctic Front (blue) and the southern ACC boundary (red). Oceanic fronts and boundaries, according to Orsi et al. (1995).

The inflow of the ACCs northern edge, namely the Subantarctic Front (SAF), into the Pacific sector of the Southern Ocean is significantly affected by the New Zealand microcontinent (Carter and Wilkin, 1999). South of New Zealand, the Maquarie Ridge and the submerged Campbell Plateau force the SAF towards the north (Heath, 1981), before the parting SAF resumes its eastbound circumnavigation of Antarctica at ~55°S and ~50°S (Fig. 1.4; (Crundwell et al., 2008). Likewise the Subtropical Front (STF), locally known as the Southland Front (Sutton, 2003), is forced to follow the continental shelf of the submerged microcontinent (Crundwell et al., 2008; Sutton, 2003). The STF enters the Pacific at ~45°S in the Tasman Sea, is deflected to the south and along the landmass of New Zealand, until it turns to the east along the Chatham Rise at ~43°S (Fig. 1.4; Sutton, 2003). Above the crest of Chatham Rise, the STF spans a ~150 km wide area that widens to almost 400 km east off Chatham Rise, where no bathymetrical constrain is present (Carter et al., 1998). Southwest Pacific surface-waters are shaped by the influence of Subtropical Surface Water (STW) north and Subantarctic Surface Water (SAW) south of the STF (Crundwell et al., 2008; Morris et al., 2001). STW with its distinctive high salinity and temperature originates from the central Pacific and is transported towards the south along the East Australian Current (Heath, 1985)

and the Tasman Front (Fig. 1.4; Crundwell et al., 2008). Opposed to this, the southerly SAW is marked by low salinity and temperature (Heath, 1985).

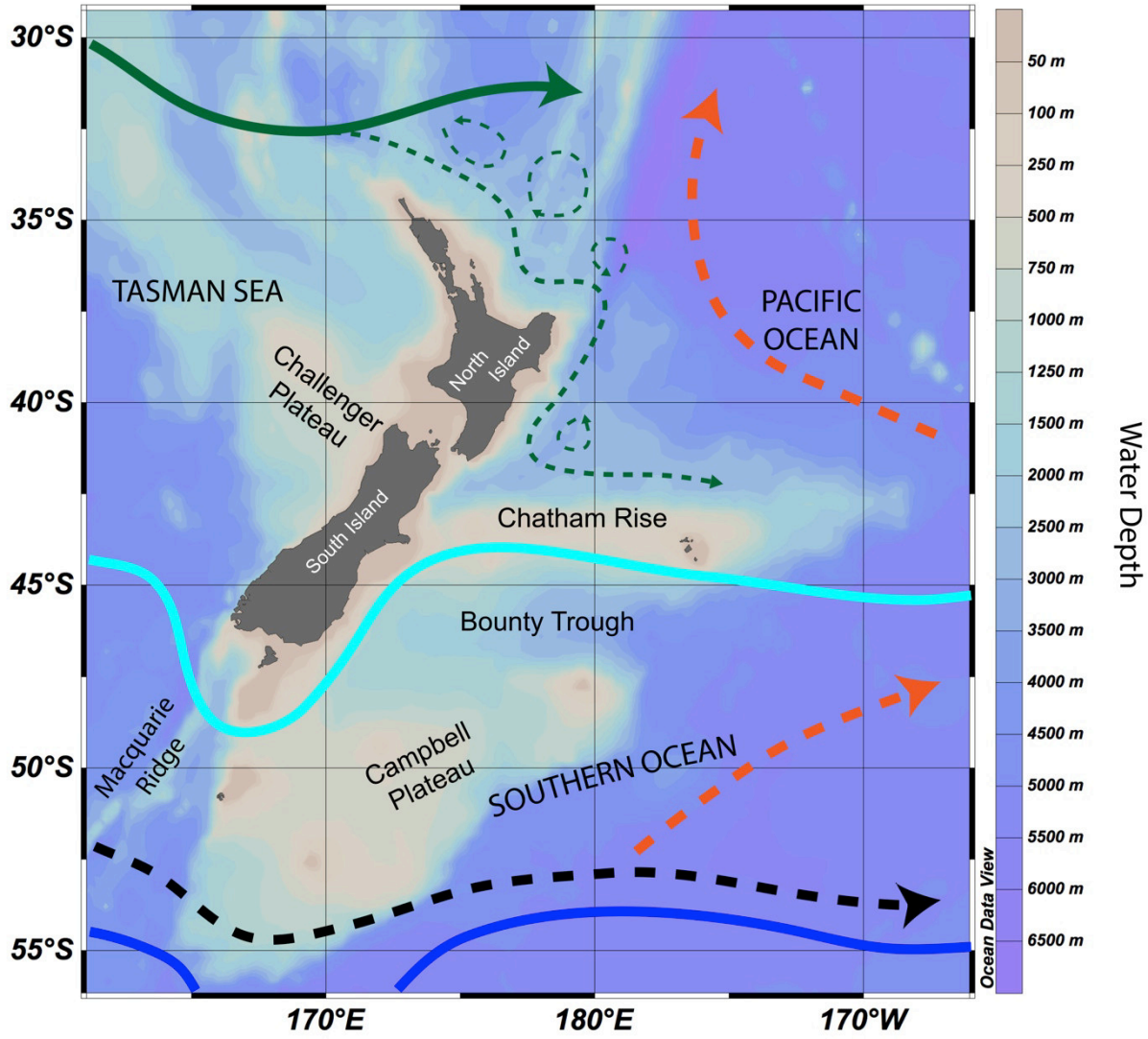

Figure 1.4: Bathymetric map of the New Zealand margin. ACC – Black arrow; STF – light blue line; SAF – dark blue line; Tasman Front and associated currents – green arrows; Deep Western Boundary Current – orange arrows. Currents, fronts and topographical features according to (Carter et al., 1998) and (Crundwell et al., 2008).

1.2.1.2 Subsurface Oceanography

The subsurface SW-Pacific is discriminated into four major water masses. Subantarctic Mode Water (SAMW), occupying the depth between ~300 – 800 m is formed during the southern winter by vigorous deep-convection of the equatorward ACC-side at the SAF (McCartney, 1977; Rintoul and England, 2002). Zillman (1972) suggests that cold southerly winds cool the

ocean surface mixed layer north of the SAF, ultimately leading to the formation of SAMW. Rintoul and Bullister (1999) however, state that the advection of cold and fresh waters across the SAF is the more likely reason for SAMW formation, due to the required air-sea fluxes. The prominent features of SAMW, namely its uniform density (pycnostad) and temperature (8 – 9°C), low vorticity and high oxygen content are developed via this process of deep mixing (Bostock et al., 2013a; McCartney, 1977). The SAMW is storing heat, freshwater and carbon and ventilates the thermocline of subtropical gyres between ~450 and 700 m (Rintoul and England, 2002; Toggweiler and Dixon, 1991; Toggweiler et al., 1991). Southeast of New Zealand, SAMW is distinctively colder than the SAMW-variety on the western side of the island in the Tasman Sea (Bostock et al., 2013a).

Below the SAMW, Antarctic Intermediate Water (AAIW) occupies the depth of ~800 – 1400 m (Crundwell et al., 2008). According to McCartney (1977), the formation of AAIW is intimately linked to the SAMW. He suggests that along its circumpolar pathway, SAMW is progressively cooled and freshened, with the coldest and freshest SAMW forming AAIW. However, Molinelli (1981) attributes the formation of AAIW to isopycnal exchange across the SAF. (Molinelli (1981) identifies the most pronounced subduction of AAIW in the southeast Pacific off Chile and off Kerguelen Island in the South Indian Ocean, although in theory, isopycnal mixing can be a circumpolar source of AAIW. Most likely both processes operate in different areas of AAIW formation, resulting in the observed range of AAIW features (Bostock et al., 2013a; Piola and Gordon, 1989). The bulk of AAIW is formed in the southeast Pacific off Chile, although several areas of AAIW subduction have been identified in the Pacific, Indian and Atlantic Ocean (Bostock et al., 2013a; Sallée et al., 2010; Fig. 1.5). In the Southern Ocean, recently formed AAIW is entrained in the eastward path of the ACC but is also diverted to the north into the subtropical gyres. A prominent salinity minimum (WOA; Antonov et al., 2010) traces AAIW throughout the gyres and into the major ocean basins (Bostock et al., 2013b).

In the southwest Pacific, south of New Zealand, AAIW (called Southern Ocean or SO AAIW) is formed that is less fresh and young than its AAIW-counterpart in the southeast Pacific (Bostock et al., 2013b). West of New Zealand in the Tasman Sea, SO AAIW is mixed with higher saline and more oxygenated thermocline waters of the Tasman Gyre forming the so-called Tasman AAIW (Bostock et al., 2013b). Tasman AAIW circles the north island of New Zealand and is separated from SO AAIW by the prominent Chatham Rise east of the islands (Bostock et al., 2013b).

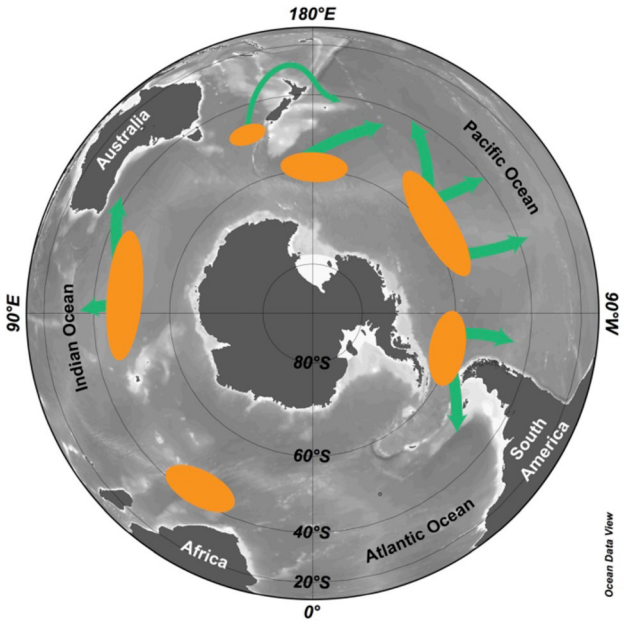

Figure 1.5: Bathymetric map of the Southern Ocean. Orange ellipses indicate the main areas of AAIW subduction. Green arrows indicate the main export to the interior. After Sallée et al. (2010).

Circumpolar Deep Water (CDW), the most voluminous Southern Ocean water mass, follows below the AAIW but outcrops along Antarctica's continental margin (Carter et al., 2009). The CDW is subdivided into two separate water masses. Upper Circumpolar Deep Water (UCDW; ~1400 – 2900 m) and Lower Circumpolar Deep Water (LCDW; ~2900 – 4500 m; (Crundwell et al., 2008). A distinctive oxygen minimum and high nutrient concentrations characterize the UCDW (Callahan, 1972; Carter et al., 2009; Fig. 1.6). This high CO_2 water mass (Bostock et al., 2013b) originates from the return flows of Indian Deep Water (IDW) and Pacific Deep Water (PDW; (Callahan, 1972; Rintoul and Bullister, 1999). South of the

Polar Front (PF), upwelling of UCDW (Bostock et al., 2013b) is contributing to the formation of AAIW. Increased salinity by the entrainment of North Atlantic Deep Water (NADW) into circumpolar waters marks the LCDW (Callahan, 1972; Orsi et al., 1995). Along deep western boundary currents (for more details, please refer to *Chapter 1.2.1.3*), LCDW is northward transported into the major ocean basins (Rintoul et al., 2001). In these basins, the chemistry of LCDW is altered by mixture with surrounding fresh water while biological activity is progressively depleting the oxygen levels of the aging water mass (Rintoul et al., 2001). The return flow of this altered water mass, from both the deep Pacific and Indian Oceans, is ultimately causing the oxygen minimum recorded in UCDW (Callahan, 1972; Rintoul et al., 2001).

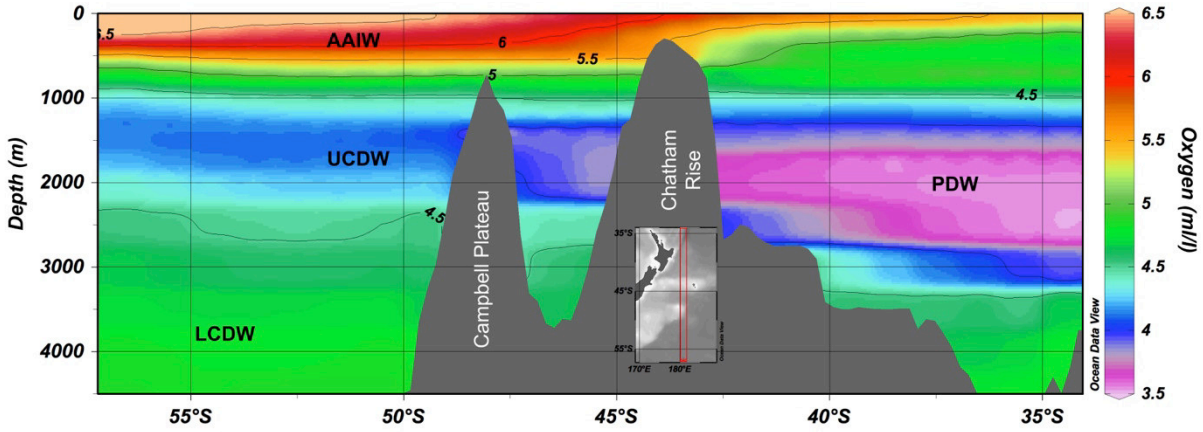

Figure 1.6: Oxygen concentration of the southwest Pacific along 179° W (WOA; (Garcia et al., 2010).

The lowermost Southern Ocean water mass, Antarctic Bottom Water (AABW), is characterized by increased salinity (e.g. Rintoul and Bullister, 1999). Nowadays, AABW is formed in the shelf-areas of the Weddell Sea (~50%), the Wilkes Land margin (~30%) and in the Ross Sea (~20%; Carter et al., 2009) by mixing of relatively warm deep-water (e.g. CDW) with winter surface water and shelf water (Rintoul et al., 2001). The high salinity of AABW is owed to the admixture of high saline waters to the shelf water via brine rejection during sea ice formation (Rintoul et al., 2001). Orsi et al. (1999) use the neutral density (γ^n) to define AABW, with γ^n >28.27 kg m^{-3}. Due to this high density, true AABW is limited to deep

circum-Antarctic Basins (Carter et al., 2009). Bottom-waters with a lower density (often also referred to as AABW) are not confined to these basins and are therefore able to propagate into all major ocean basins (Carter et al., 2009; Orsi et al., 1999).

In the southwest Pacific off New Zealand, the dispersal of AABW is hampered by the Pacific-Antarctic-Ridge (Orsi et al., 1999). However, the influence of AABW on SW-Pacific water masses can be traced in the isotopic composition of the lower LCDW (deeper ~4000 m; (McCave et al., 2008).

1.2.1.3 The SW-Pacific Deep Western Boundary Current

The majority of deep-water (>2000 m) entering the Pacific Ocean is transported via the distinct deep western boundary current (DWBC) south of New Zealand (Fig. 1.4; McCave and Carter, 1997). Transporting a volume of ~20 Sv, the Pacific DWBC is the strongest boundary current worldwide (Schmitz, 1995). Along with the ACC, the DWBC meanders around the Campbell Plateau and the Bounty Trough until it leaves the Southern Ocean east of the Chatham Rise (Carter et al., 2009; Crundwell et al., 2008).

1.3 Previous work on water mass reconstructions

1.3.1 General framework

The analysis of air, trapped in Antarctic ice core records, revealed significant changes of atmospheric CO_2 over the last 800,000 years (Lüthi et al., 2008). The close coupling of climate and CO_2 is revealed by the obvious correlation of Antarctic temperatures and atmospheric CO_2 (Fig. 1.7). As the ocean contains about 60 times more carbon than the atmosphere (Broecker, 1982), it is a very likely driver for the ~90 ppm fluctuations in atmospheric CO_2 (Fig. 1.7). Amongst all ocean basins, the Pacific is by far the largest carbon reservoir and thus should play an important role in the redistribution of CO_2.

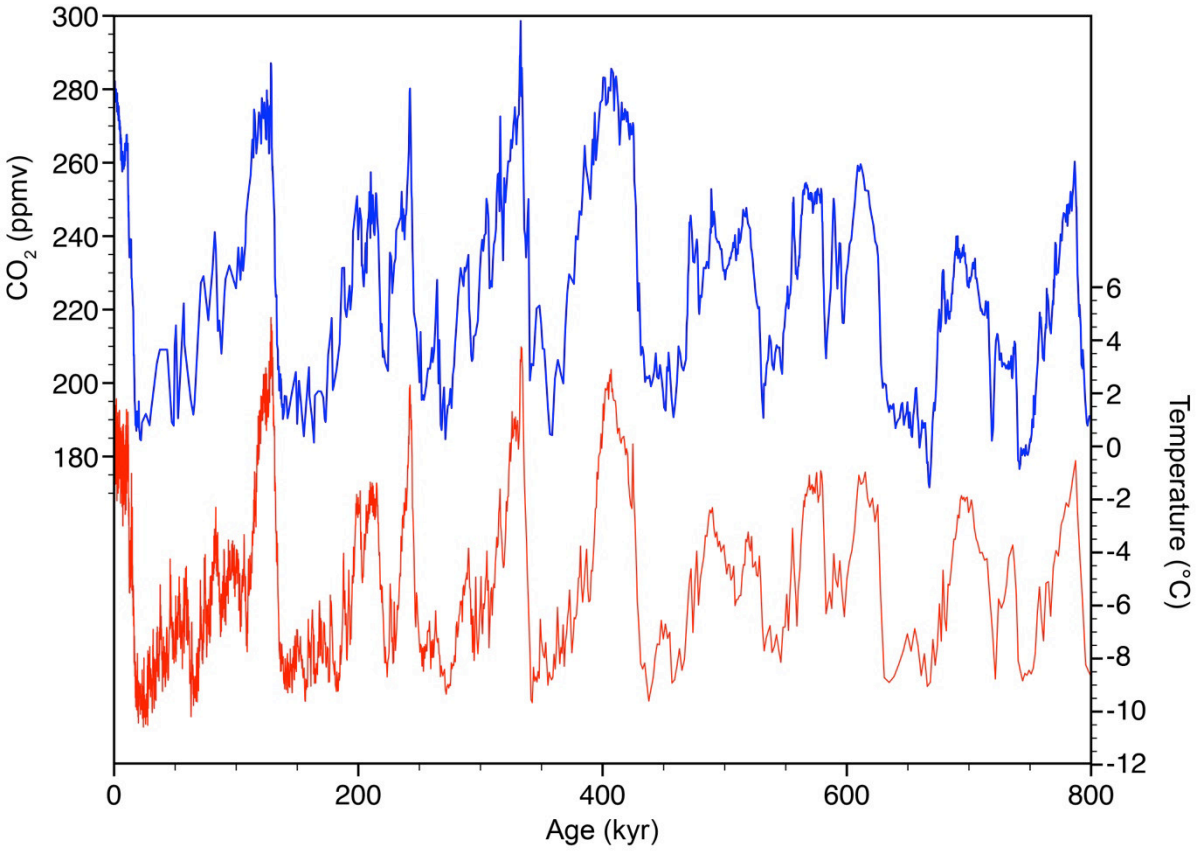

Figure 1.7: 800,000 years record of atmospheric CO_2 (blue line; Lüthi et al., 2008) and Antarctic temperature (red line; Jouzel et al., 2007), measured on the EDC ice core.

This scenario requires the storage of CO_2 in the oceans interior due to reduced communication of the deep-ocean and the surface water masses. In the course of a glacial, an aging water mass, trapped in the deep-ocean can accumulate large amounts of respiratory CO_2 (Anderson and Carr, 2010) and nutrients (e.g. Matsumoto et al., 2002) and release them once back in contact with the surface.

The whereabouts of these old and CO_2 rich water masses can be traced for example with reconstructions of stable isotopes ($\delta^{13}C$) or radiocarbon contents (^{14}C). The constant rain of organic matter (enriched in ^{12}C) from the surface into the deep-water leads to a progressive depletion in $\delta^{13}C$ (Zeebe and Wolf-Gladrow, 2001). Therefore, low $\delta^{13}C$ values are indicative of old water masses, even though other factors, like the *Phytodetritus Effect* (Mackensen et al., 1993) can also have a strong influence on benthic $\delta^{13}C$. Radiocarbon on the other hand is produced in the atmosphere by the interaction of cosmic rays and ^{14}N atoms. With a half-life

of 5730 ± 40 years (Godwin, 1962), ^{14}C decays back to ^{14}N. As a part of the carbon cycle, the oxidized variety of radiocarbon, namely $^{14}CO_2$, enters the surface ocean via air-sea gas exchange. Once a water mass is subducted, the ^{14}C in the dissolved inorganic carbon (DIC) begins to decay. For this reason, the longer the residence time of a water mass in the oceans interior, the more depleted its radiocarbon activity ($\Delta^{14}C$). This dependency leads to the highest $\Delta^{14}C$ values in surface waters and the lowest values in the return flows of the deep Pacific Ocean (Fig. 1.8). However, due to limitations in the rate of air-sea gas exchange and mixing with older deep-waters, surface-waters yield a higher radiocarbon age than the corresponding atmosphere. This age difference, called the surface reservoir age, amounts in average 400 years for the modern ocean but it can be as high as 1100 years in the upwelling areas of the Southern Ocean (Franke et al., 2008; Fig. 1.9). Thus, knowledge of the locations past reservoir age but also about the variability in the atmospheric ^{14}C content is necessary for accurate reconstructions of past water mass ventilation using the radiocarbon method.

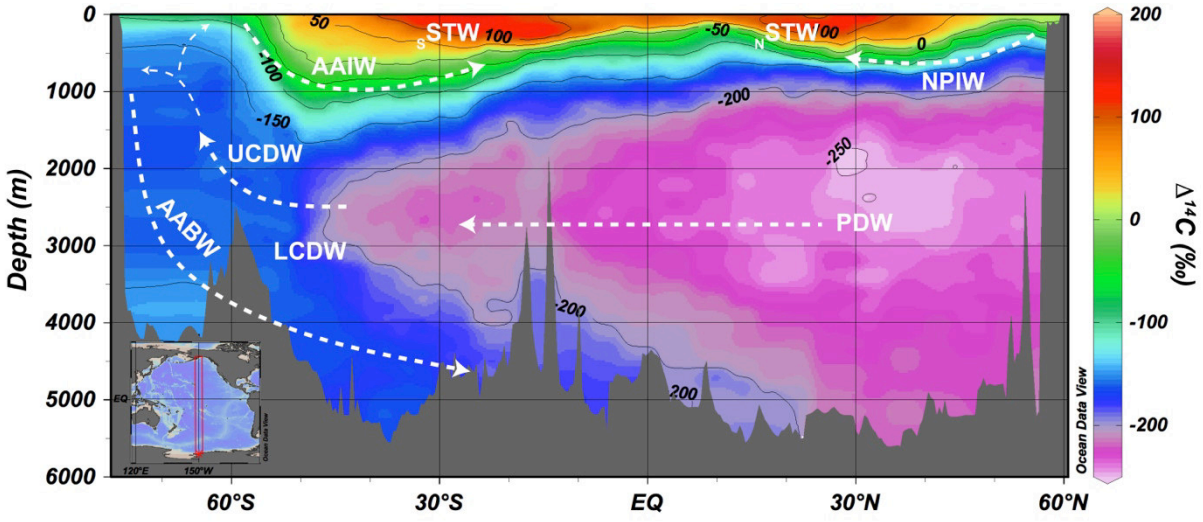

Figure 1.8: Pacific $\Delta^{14}C$ distribution (Key et al., 2004). $_{S/N}$STW – South/North Pacific Subtropical Surface Water; Antarctic Intermediate Water – AAIW; North Pacific Intermediate Water – NPIW; Upper and Lower Circumpolar Deep Water – UCDW/LCDW; Pacific Deep Water – PDW; Antarctic Bottom Water – AABW.

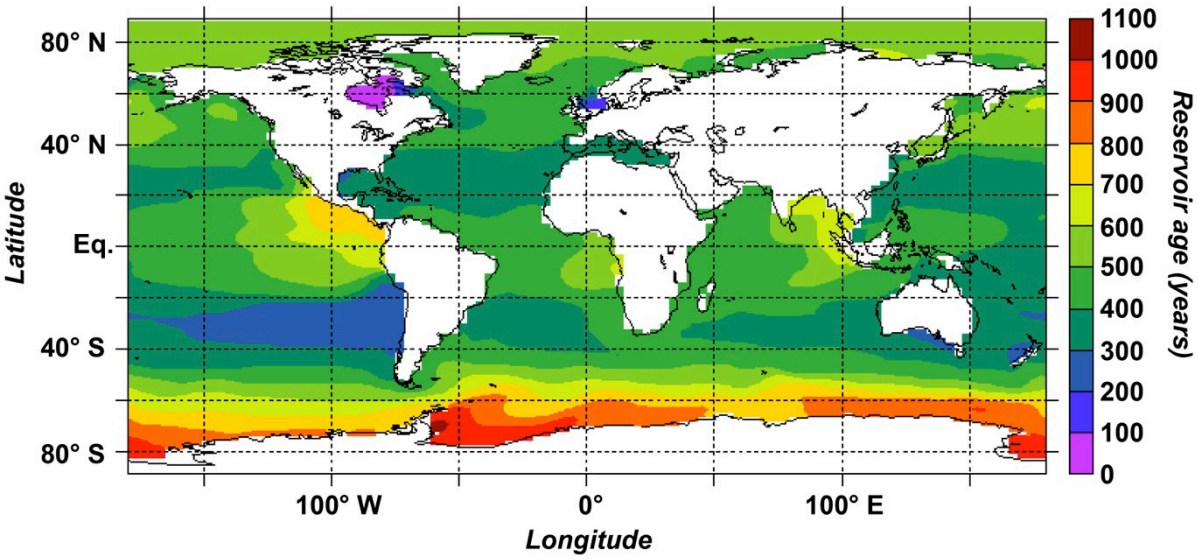

Figure 1.9: Modern surface reservoir ages. Modified after (Franke et al., 2008).

The atmospheric ^{14}C variability up to ~12,550 years B.P. can be reconstructed from tree ring chronology (Friedrich et al., 2004; Schaub et al., 2008). Before ~12,550 years B.P., the atmospheric record is anchored using plant macrofossils from varved lake sediments (Bronk Ramsey et al., 2012; Kitagawa and van der Plicht, 1998; Kitagawa and van der Plicht, 2000) or speleothems (Beck et al., 2001; Hoffmann et al., 2010; Southon et al., 2012). In turn these numerous records are included in the regularly updated IntCal calibration datasets (Reimer et al., 2004; Reimer et al., 2009; Reimer et al., 2013; Stuiver et al., 1998).

Considering all aforementioned factors, a common method to asses the ventilation of a water mass is to compare the ^{14}C-ages of benthic foraminifera (bathed by the respective water mass) to the contemporaneous atmospheric ^{14}C-value. In general, foraminifera incorporate the ^{14}C signal of the dissolved inorganic carbon ($DI^{14}C$) of their respective water mass during calcification. Therefore, the offset between benthic foraminifera (recording deep-water $DI^{14}C$) and planktic foraminifera (recording the atmospheric signal plus surface reservoir $DI^{14}C$) is indicative for the ventilation of the respective deep water mass (Fig. 1.10).

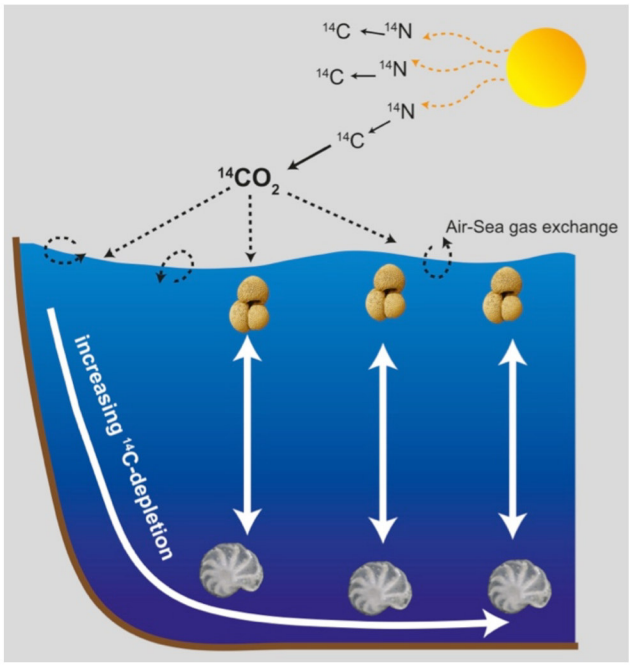

Figure 1.10: Schematic view of ^{14}C-related processes. In the atmosphere, ^{14}C is produced by the interaction of cosmic rays (orange arrows) with ^{14}N. Afterwards $^{14}CO_2$ enters the surface ocean via air sea gas exchange. Without contact to the atmosphere, the ^{14}C content of a subducted water mass is progressively depleted during it's residence-time in the ocean's interior. Thus the ventilation of a water mass can be reconstructed by the offset (white vertical arrows) of co-existing planktic and benthic foraminifera, which record the DI^{14}C-signal of their respective water mass.

1.3.2 Previous work

To date, the reconstruction of deep-water ventilation and water mass circulations has been addressed by numerous paleoceanographic studies, of which only a few concentrated on the Southern Ocean and even fewer on its Pacific Sector (cf. *Chapter 3*, Fig. 3.S1).

In the deep North Atlantic, stable and radiogenic isotope records off Iceland (Thornalley et al., 2010), Portugal (Skinner and Shackleton, 2004) and the USA (Keigwin, 2004) indicate decreased ventilation during the Last Glacial Maximum (LGM). Although, the low $\delta^{13}C$ values could be attributed to increased brine rejection (Thornalley et al., 2010), the increase in radiocarbon-derived ventilation ages (Keigwin, 2004; Skinner and Shackleton, 2004) points to a strengthened influence of old deep-water on the glacial North Atlantic. As Skinner et al. (2010) showed, the South Atlantic (MD07-3076, 3770 mbsl) as well experienced decreased ventilation during the LGM, reaching ventilation ages of up to 4000 years. In particular, the comparison of this Southern Ocean record to the North Atlantic sediment core MD99-2334K (Skinner and Shackleton, 2004) reveals an interesting pattern, the so-called ventilation seesaw (Skinner et al., 2014). In times of reduced NADW-formation like Heinrich Stadial 1 and the

Younger Dryas (McManus et al., 2004), the usual high offset in Southern Ocean to North Atlantic ventilation ages disappears (Fig. 1.11; Skinner et al., 2014).

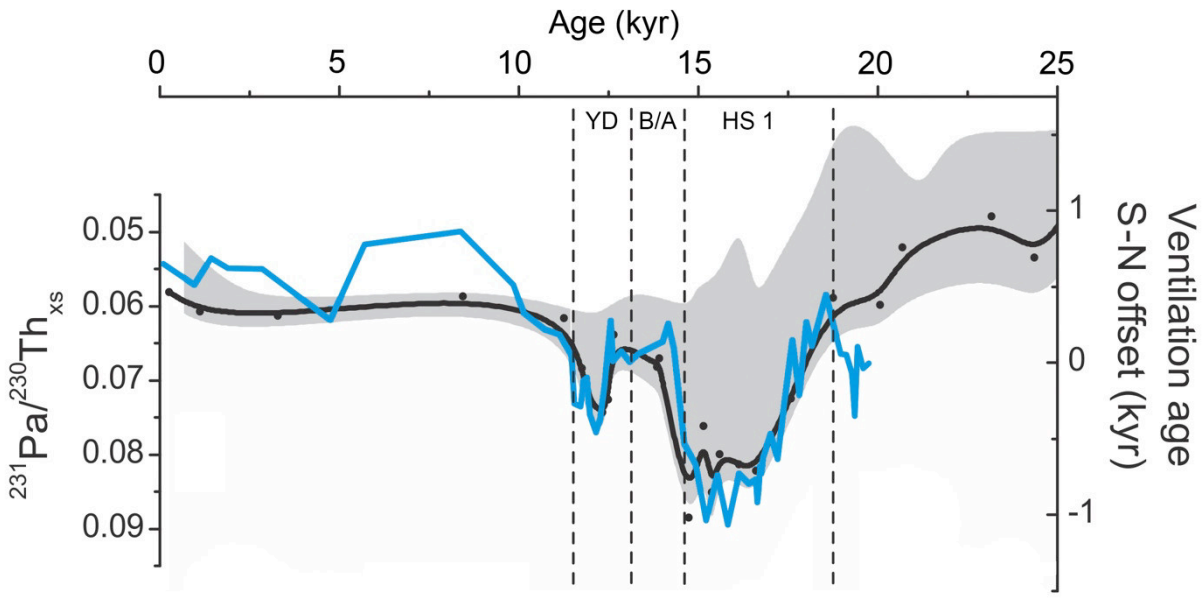

Figure 1.11: Atlantic ventilation seesaw. The black line and dots indicate the north-south offset in deep-water reservoir ages (Skinner et al., 2014). The Atlantic overturning circulation (blue line) is expressed by $^{231}Pa/^{230}Th$ ratios (McManus et al., 2004). YD – Younger Dryas; B/A – Bølling-Allerød; HS 1 – Heinrich Stadial 1. Modified after (Skinner et al., 2014).

However, Nd-records from the South Atlantic suggest a constant export of northern sourced deep-waters to the Southern Ocean (Piotrowski et al., 2004; Skinner et al., 2013), a fact that might imply the presence of old waters originating in the deep North Atlantic. For this reason one has to consider the operation of the ventilation seesaw only in terms of radiocarbon decay and not necessarily as a measure for water mass transport (Skinner et al., 2014).

Not unlike the North Atlantic, the North Pacific off Alaska (~3600 mbsl) and off Kamchatka (~2300 mbsl) as well shows increased ventilation ages of 1900 to 5100 years during the LGM (Galbraith et al., 2007; Sarnthein et al., 2007/2013). The intermediate water level however experienced a similar rate of ventilation as it does today (Galbraith et al., 2007). Therefore, the increased gradient between deep- and intermediate-waters argues for a pronounced North Pacific stratification, isolating the abyss from younger waters above (Galbraith et al., 2007).

Surprisingly, these results are contrasted by findings on a sediment core from 2710 mbsl off Oregon, showing similar glacial ventilation rates as today (Lund et al., 2011). Although, the North Pacific circulation remained similar to today (Lund, 2013), the $\Delta^{14}C$ at ~3600 mbsl was about 50‰ lower than at 2710 mbsl (Galbraith et al., 2007; Lund, 2013; Lund et al., 2011). Consequently, unlike the northernmost deep Pacific, the deep-waters off Oregon were not a significant part of the glacial carbon reservoir. Likewise, the waters from the western flank of the equatorial Pacific off West Papua (~2800 mbsl; MD01-2386) show a constant radiocarbon offset from the deep- to intermediate-water over the last 20,000 years (Broecker et al., 2008), excluding this area as well from the proposed carbon pool. At a first glance, Wallace Broecker and Elizabeth Clark (2010) present another discouraging record from the Pacific Ocean. Their analysis on sediment core TTN 013-18 (4400 mbsl; 2°S 140°W) apparently eliminated the existence of a glacial carbon pool. Then again, if the core location is plotted into the Pacific $\Delta^{14}C$ section shown in figure 1.8, the distinctive position of TTN 013-18 is revealed. Right at the edge of the modern PDW, it is not unlikely that the sediment core was located below the proposed glacial carbon pool. Furthermore, Broecker and Clark (2010) mention that despite large ^{14}C-differences between co-occurring planktic and benthic foraminifera (indicative for an old carbon reservoir) they used the coccolith to benthic-foraminifera ^{14}C-difference for their interpretation that showed only minor offsets for the analyzed interval. Their explanation for the use of coccoliths instead of *Globigerinoides sacculifer* is preferential bioturbation that apparently affected only the planktic foraminifera but not the coccoliths. What's more, the authors state that several age reversals occurred within their record. Together with the peculiar position of TTN 013-18 (at the modern carbon pools edge) these faunal and sedimentological uncertainties raise doubt over the meaningfulness of this record on the existence of the glacial carbon pool.

In the Southern Ocean, where circumpolar water masses are upwelled and new water masses are formed and spread into all major ocean basins (Talley, 2013), several studies indicate the existence of old and CO_2-enriched deep-water despite the negative findings of Broecker and Clark (2010). The ventilation ages of the South Atlantic were almost twice as high during the glacial than today (Barker et al., 2010; Skinner et al., 2010). Further to the west, radiocarbon analyses on deep-water corals from the Drake Passage highlighted the presence of an isolated carbon reservoir in the Circumpolar Deep Water (CDW; Burke and Robinson, 2012). Because the glacial $\Delta^{14}C$-concentration was reconstructed on corals retrieved close to the interface to overlying Antarctic Intermediate Water (AAIW; Burke and Robinson, 2012), boundary exchange with younger AAIW might have enriched the $\Delta^{14}C$-level in these samples. Therefore, the glacial depletion in $\Delta^{14}C$ might have been even more pronounced than recorded for the CDW by Burke and Robinson (2012).

The only study from the Pacific sector of the glacial Southern Ocean comes from Sikes et al. (2000). At the time of the Kawakawa/Oruaniu eruption ~25,000 years ago (Vandergoes et al., 2012) the Upper Circumpolar Deep Water reached ventilation ages of more than 5000 years (Sikes et al., 2000). However, Broecker and Clark (2010) are right when saying that this single measurement was never reproduced in the Pacific Southern Ocean again (a fact that will be changed by the results of this thesis).

During the deglaciation (~18 – 11.5 kyr B.P.), southern sourced AAIW had the potential to transport the signal of upwelled radiocarbon-depleted deep-water into the Atlantic, Pacific and Indian Oceans. Indeed, coupled measurements of U/Th and ^{14}C on deep-sea corals in the Atlantic off Brazil (781 mbsl; Mangini et al., 2010), $\Delta^{14}C$ reconstructions off Oman (820 mbsl; Bryan et al., 2010) and stable isotope measurements ($\delta^{13}C$) off Tanzania (446 mbsl; Romahn et al., 2014) trace a signature of old, Southern Ocean sourced deep-water in the Atlantic and Indian Ocean intermediate-waters.

Likewise in the Pacific Ocean, two intervals, showing a pronounced drop in $\Delta^{14}C$ have been recorded in intermediate waters off Baja California (Marchitto et al., 2007) and Galapagos (Stott et al., 2009). As these intervals (Heinrich Stadial 1 and the Younger Dryas) coincide with distinctive incursions in atmospheric $\Delta^{14}C$ (e.g. Denton et al., 2006; Reimer et al., 2013) it was argued that Southern Ocean upwelling during HS 1 and the YD led to a decrease in atmospheric $\Delta^{14}C$, further incorporating this signal in AAIW (Marchitto et al., 2007; Stott et al., 2009). Anyway, these findings are challenged by radiocarbon reconstructions close to the main formation area of AAIW. De Pol-Holz et al. (2010) measured the radiocarbon difference of planktic and benthic foraminifera on a sediment core off Chile (~1000 mbsl; SO161-SL22) but found no significant offset in intermediate water $\Delta^{14}C$ to the contemporaneous atmosphere over the last 20,000 years. Albeit, if the new east Pacific surface reservoir ages of Siani et al. (2013) are applied to the SO161-SL22 record, a slight imprint of old waters on this record is revealed throughout the deglacial period (Siani et al., 2013). Nevertheless, the radiocarbon depletion still remains by far less pronounced than in the Baja California (Marchitto et al., 2007) and Galapagos (Stott et al., 2009) records, leaving the sources of these low ^{14}C waters still under debate. Right in the center of the research area of this thesis, deglacial radiocarbon reconstructions on a sediment core from the Bounty Trough off New Zealand (1210 mbsl; MD97-2120) also suggest the ventilation of a CO_2-rich water mass via the Southern Ocean as well as the incorporation of this signal within AAIW (Rose et al., 2010). In this study as well, the AAIW radiocarbon-depletion is nowhere near the values measured by Marchitto et al. (2007) and Stott et al. (2009).

In summary, despite several negative examples, the majority of studies searching for a glacial deep-water carbon pool indicate widespread but insufficient clues for the existence of such aged waters. The pathways again, that these CO_2-enriched waters might have taken during the deglacial are still object of an ongoing debate.

1.4 Objective of this thesis

The superordinate objective of this thesis is to reconstruct and analyze changes in the ventilation and circulation of the southwest Pacific Ocean. In particular, the identification of the whereabouts of CO_2 during glacial times is one of the most controversial topics in paleoceanography. As it was mentioned in *Chapter 1.1*, contradicting studies emerged over the last decades that verified (e.g. Skinner et al., 2010) or falsified (e.g. Broecker and Clark, 2010) the existence of old and therefore CO_2-enriched waters in the deep, glacial-ocean. In particular, the Pacific sector of the Southern Ocean as well as the return flow of Pacific Deep Water (PDW) have been generally neglected in these reconstructions of the glacial carbon cycle. Another shortcoming of many studies is the use of single sediment cores from only one water depth. Despite their high resolution, these studies fail to grasp the vertical variability of proxies throughout the water column. However, knowledge about the vertical extent of old water masses is needed to reconstruct the amount of carbon stored in the deep glacial-ocean.

Furthermore, understanding the pathways of stored, ^{14}C-depleted carbon from the abyss towards the surface and ultimately to the atmosphere is of essential relevance for the reconstructions and modeling of past and future changes in the global carbon cycle. Yet, the ongoing search for these oceanic windows to the atmosphere is still a topic of an ongoing debate in the paleoceanographic community.

These two problems, the extent and the pathways of old carbon will be addressed in *Chapter 3*, using radiocarbon analyses on benthic and planktic foraminifera from seven sediment cores. The use of this sediment depth transect was especially well suited to constrain the long-yearned-for deep-water carbon pool.

The formation of AAIW and SAMW and their circulation within the subtropical gyres of the southern hemisphere are strongly influencing the redistribution of CO_2, heat and freshwater within the global upper ocean as well as the nutrient supply of the tropical thermocline

(Sarmiento et al., 2004; Spero and Lea, 2002; Toggweiler et al., 1991). Particularly in times where global CO_2-levels linger at ~400 ppm (Tans and Keeling, 2014), SAMW and AAIW display a significant sink for anthropogenic CO_2. Indeed, most of the anthropogenic CO_2 that is entrained into the oceans interior is transported via AAIW, a process without atmospheric CO_2-levels would be approximately 55 ppm higher than today (McNeil et al., 2003; Sabine et al., 2004). Despite the importance of AAIW, information on its vertical and lateral extent is scarce due to the lack of sufficient Pleistocene time series. By far exceeding the radiocarbon time-scale, the aim of *Chapter 4* is to reconstruct Pleistocene changes in the extent of AAIW. Five sediment cores from the Tasman Sea and the Bounty Trough are used to analyze depth-variations of the AAIW to UCDW boundary. These reconstructions can help to evaluate the influence of wind-stress, freshwater and upwelling rates on the extent of AAIW and therefore on the transport of atmospheric signals into the ocean.

In a similar way, the objective of *Chapter 5* is to reconstruct changes in the formation of Southern Ocean Intermediate Waters (SOIW) that include AAIW and SAMW. In this chapter, Mg/Ca temperature and stable isotope ($\delta^{18}O$) reconstructions are applied to a sediment core from the East Pacific Rise. This study area is of particular interest as it extends our knowledge on past circulation changes to the open-ocean realms of the Pacific Southern Ocean.

The combined reconstruction of (geologically) short-term ventilation changes of the entire southwest Pacific water column and long-term changes in the formation of SOIWs enables us to get a comprehensive overview of changes and forcing's in the global carbon cycle and oceanic circulation. This knowledge is urgently needed to draw the right conclusions from predictions of climatic evolution driven by anthropogenic forcing.

1.5 Author's contribution

Manuscript 1 (*Chapter* 3)

I performed the sediment treatment of all cores, but PS75/100-4, used in this chapter. Except for the part regarding the carbonate ion concentrations (please refer to (Kersten, 2013) and tephra analyses (done by Brent Alloway), I performed all methods and steps described in the manuscript. Subsequent to sample selection (picking of foraminifera), most samples were measured by third party contractors like the NOSAMS facility and the Keck laboratory in the USA. However, I measured all samples with ETH lab codes at the ETH in Zürich. I wrote the entire manuscript. Ralf Tiedemann and Frank Lamy contributed to the interpretation of the data. All co-authors reviewed the draft version and contributed to the discussion.

Manuscript 2 (*Chapter 4*)

I performed the stable isotope measurements on SO213-82-1 and SO213-84-1. Measurements on SO136-003, MD06-2986 and MD06-2990 were performed by Silke Steph. Dirk Nürnberg performed the Mg/Ca measurements at the Kiel University. Climate modeling was performed by Matthias Prange and Ute Merkel. I wrote the entire manuscript. Ralf Tiedemann contributed to the data-interpretation. All co-authors reviewed the draft version and contributed to the discussion.

Manuscript 3 (*Chapter 5*)

For this manuscript, I 1) measured the stable isotope record ($\delta^{18}O$) of sediment core SO213-59-2; 2) selected and provided the radiocarbon dating's used in SO213-59-2; 3) established the high-resolution age model as the basis of this study and 4) contributed in the interpretation and discussion of this manuscript during the writing process and journal review stages.

Chapter 2

Material and methods

2.1 Research project SOPATRA

This study was part of the international research project SOPATRA – **So**uth **Pa**cific Paleoceanographic **Tra**nsects (Tiedemann, 2012).

The aim of project SOPATRA was to generate comprehensive datasets to reconstruct Pleistocene changes in oceanic and atmospheric circulation patterns of the South Pacific. In detail, the project's objective was to reconstruct:

- The position and extent of oceanic frontal systems like the Subtropical and Subantarctic Fronts, the South Pacific Gyre and the Southern Westerly Winds and their impact on the formation of AAIW
- Oceanic stratification and its effect on biological productivity, nutrient concentrations, air-sea gas exchange and the formation of AAIW
- The intensity, heat- and salt-transfer of the Humboldt Current
- Changes in circulation and ventilation of AAIW, UCDW, LCDW and PDW along with changes in carbonate dissolution

In combination with the project BIPOMAC (**Bipo**lar Climate **Mac**hinery; Gersonde, 2011) these reconstructions shall increase the knowledge and understanding of the Polar and Equatorial Pacific as well as ocean-atmosphere interactions and shed new light on the Pacific's role in the global climate system.

Furthermore, SOPATRA should provide high-resolution bathymetric and seismic data for the IODP-proposal "Cenozoic Southern Ocean Pacific" (current status: *rejected*).

The SOPATRA expedition took place between December 2010 and March 2011 on the German research vessel *Sonne* (Fig. 2.1) and was subdivided into two legs of cruise SO213. Leg SO213/1 (Valparaíso, Chile – Valparaíso, Chile; Fig. 2.2) concentrated on the southeast Pacific Chile Rise (ChiRi) and the Chile Fracture Zone (CFZ). Throughout Leg 1, several low- to mid-resolution sediment cores were recovered, that span the last 5 million years.

Figure 2.1: R/V *Sonne* in the calm Pacific Ocean (M. Behrens, 2012).

The research areas of SO213/2 (Valparaíso, Chile – Wellington, New Zealand) were the CFZ, the East Pacific Rise (EPR), the Southwest Pacific Basin (SWB) and the New Zealand Margin (NZM; Fig. 2.2).

Most of the samples used in this study were recovered during SO213/2 in the Bounty Trough on the NZM. Two NZM sediment cores and one EPR-record recovered during the R/V *Polarstern* expedition ANT-XXVI (PS75) of project BIPOMAC were furthermore used to improve the vertical and lateral resolution of this study. As well, I used two sediment cores recovered during the R/V *Marion Dufresne* cruise MD152 (MD06-cores) of project MATACORE (Proust et al., 2006).

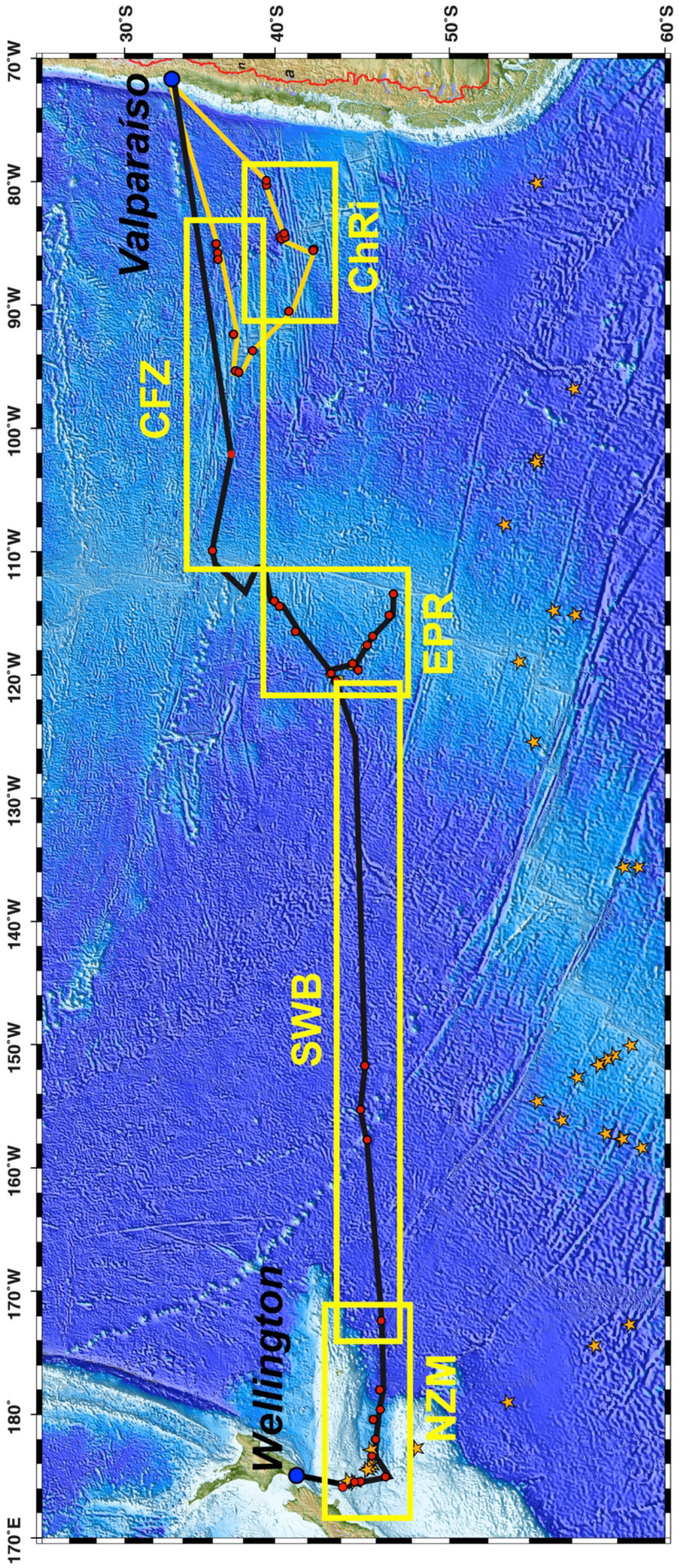

Figure 2.2: Cruise tracks of SO213/1 (orange line) and SO213/2 (black line). Red dots indicate stations of SO213, PS75 stations are indicated by orange stars. ChiRi – Chile Rise; CFZ – Challenger Fracture Zone; EPR – East Pacific Rise; SWB – Southwest Pacific Basin; NZM – New Zealand Margin.

2.2 Sediment material

All sediments used in this study that derive from the SO213 or PS75 cruises were recovered using a *Marinetechnik Kawohl Piston Corer* with a liner-diameter of 9 cm (Fig. 2.3; AWI system). The French *Calypso Giant Piston Corer* was applied to retrieve the MD06 samples used in *Chapter 4*. All sampling details described in the following of this chapter concentrate only on the SO213 and PS75 samples.

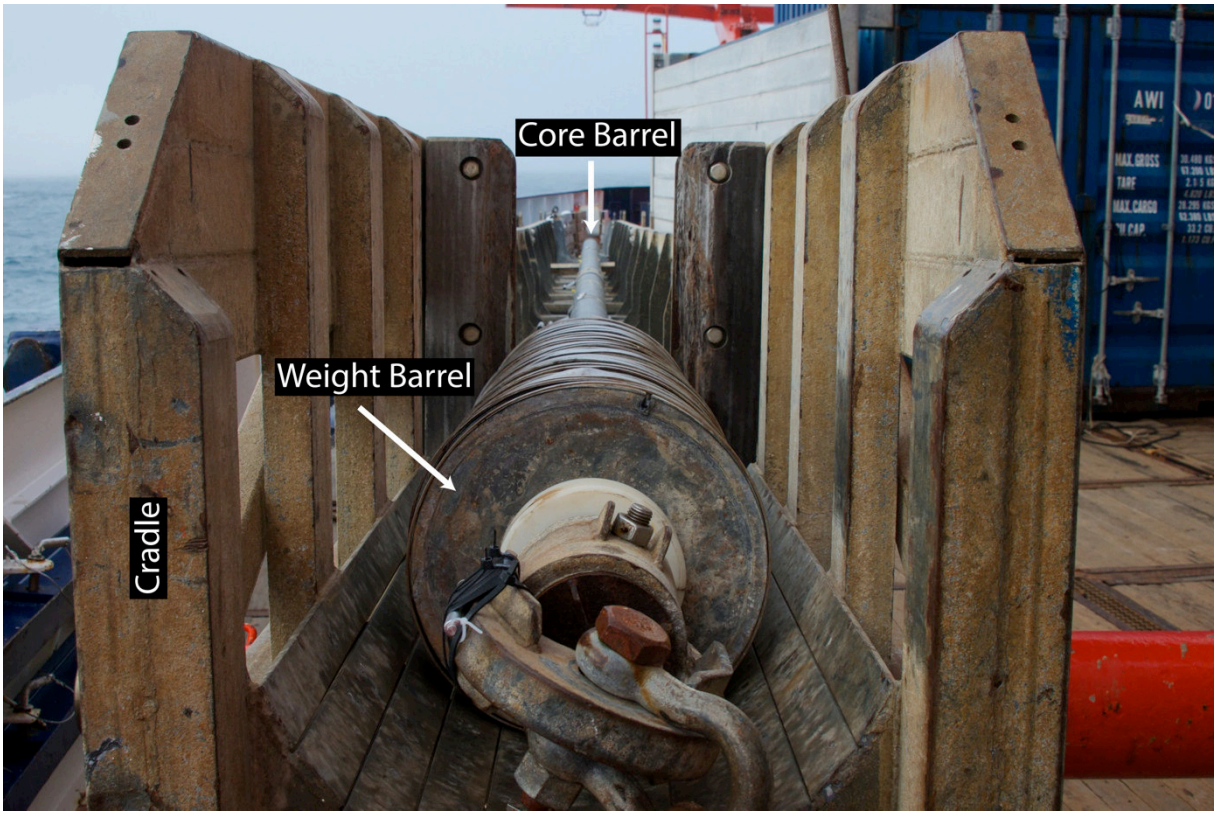

Figure 2.3: A *Kawohl Piston Corer* system in its cradle aboard R/V *Polarstern*.

Onboard, the five-meter long liners were cut into one-meter long sections. Before these sections were split into a working- and into an archive-halve, the magnetic susceptibility, density and P-wave velocity were measured using a *GEOTEK* Multi-Sensor Core Logger (Tiedemann, 2012; *Chapter 2.3.3*). The archive halve was exclusively used for non-destructive analyses like color-reflectance, visual core description (*Chapter 2.3.2*; Appendix A4) or XRF-scanning (*Chapter 2.3.4*). The working halve was sampled every centimeter in whole slices, while every second sample was assigned to the AWI. Until further analysis, all

samples were continuously stored in *Nasco Whirl-Paks*, the archive halves in D-tubes, both at ~4°C.

2.3 Methods

In this chapter, only methods are described that I applied to attain the results shown in the manuscripts of *Chapters 3, 4* and *5*. Methods that are not explained in this chapter but are part of the chapters below were contributed by the co-authors of the respective manuscripts and are therefore only described in the manuscripts method sections.

2.3.1 Sediment handling

Depending on their water content, all sediment samples were freeze-dried for two to three days. Subsequently, the sediments were sieved using a 63 µm mesh sieve and dried for two days at ~50°C. The >63 µm fraction was splitted into the size fractions of > 400µm, 315 – 400 µm; 250 – 315 µm; 125 – 250 µm and <125 µm. Using a reflective light microscope with a 50-fold magnification, foraminifera were picked (where possible) from the 250 – 315 µm fraction.

2.3.2 Visual core description

The visual core description (Appendix A4) was performed on the archive halve of each core directly after splitting of the respective core sections in order to avoid oxidative color-alteration. After removing the disturbed (by the splitting procedure) surface of each section, all prominent features like color changes, ice rafted debris, visible micro- and macrofossils, texture, degree of bioturbation, etc. were described. The revised version of the *1990 Munsell Soil Color Charts* was used for color determination. In order to assess the grain size as well as incorporated microfossils, several smear slides were taken over the entire length of each core.

Grain size and lithology were classified according to Mazzullo et al. (1988). Following these authors, lithological pattern according to IODP procedures were used to visualize the core descriptions (Appendix A4). According to the onboard procedures of SO213 (Tiedemann, 2012), the principal name used to describe the sediment consisted of the major biogenic component (e.g. calcareous or siliceous) and the degree of compaction (ooze, mud (mixture of silt and clay), sand and gravel (Wentworth, 1922). In case of further sediment components (~10 – 25%), the suffix "-bearing" was used to further distinguish the sediment type.

The attached core descriptions (Appendix A4) of SO213 sediment cores were made by me. PS75 core descriptions were conducted by the onboard scientific party of ANTXXVI-2 (please refer to Gersonde, 2011).

2.3.3 Physical properties

Aboard of R/V *Sonne* and R/V *Polarstern*, the physical properties of all sediment cores were measured, using a *GEOTEK* Multi Sensor Core Logger (MSCL; Fig. 2.4). The non-destructive method of logging entire unsplit core sections yields prompt output (a matter of only a few hours per sediment core) on the sediment cores magnetic susceptibility (magsus), P-wave velocity and Gamma Ray Attenuation (GRA)-density. Before the measurement started, each core was stored for 24 hours in the air-conditioned Magnetics- and Gravimetry Laboratory to ensure a constant core temperature. Gamma photons, emitted by a cesium (^{137}Cs) source, passing the sediment core were measured using a *Gammasearch2* gamma ray detector. Thereby, the number of gamma photons that pass the sediment without attenuation determines the sediment-specific GRA-density. The magsus was measured, using a *Bartington M.S.2* susceptibility meter with loop sensor. Passing through the loop sensor, the sediment-specific magsus alters the sensors oscillator frequency. This alteration is converted in the magnetic susceptibility values (SI) that are used as the output units for magsus measurements. Each core section was measured in 1 cm increments, with a count time of 10

seconds per step. Measurements were performed and processed using the *GEOTEK* MSCL 6.2 software and the *GEOTEK* Utilities 6.1 software.

Because P-wave velocities were not used in this study the measurement-process is not explained in detail.

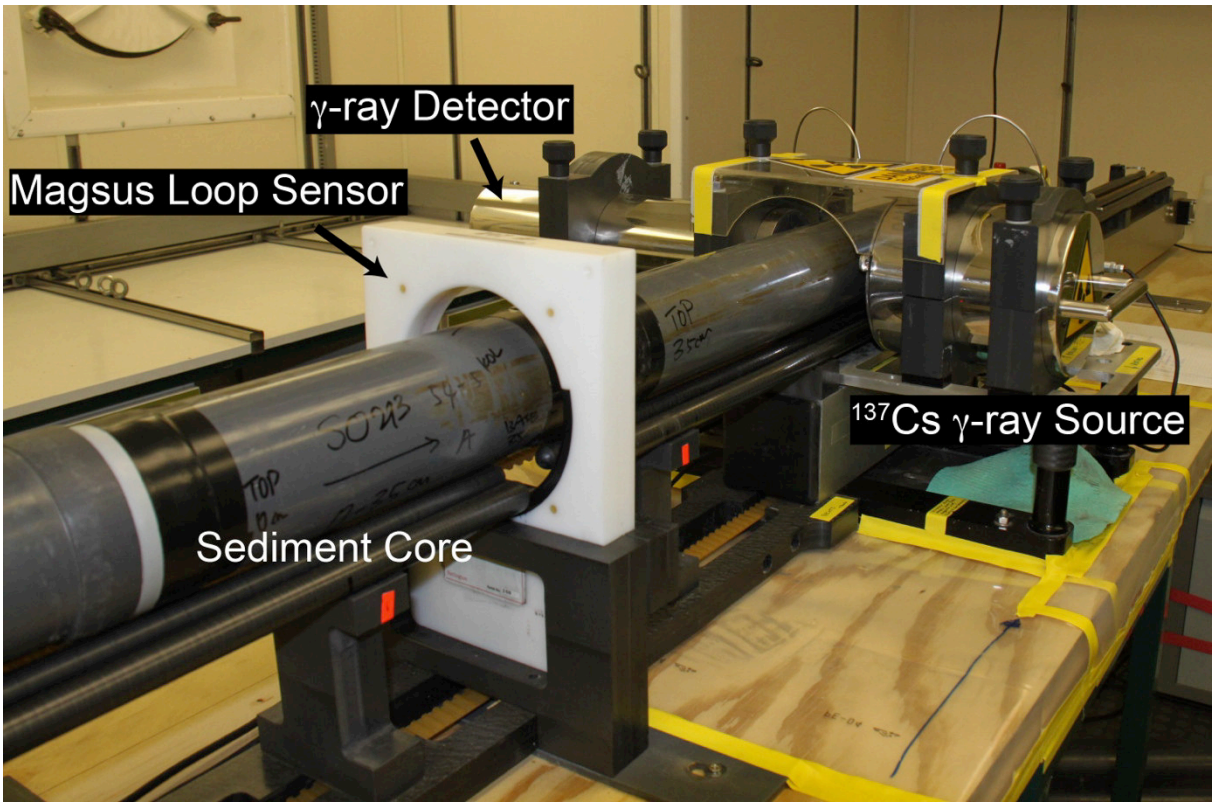

Figure 2.4: A *GEOTEK* MSCL in the Magnetics- and Gravimetry Laboratory aboard R/V *Sonne*.

2.3.4 XRF core scanning

The specific element abundances of all sediment cores were analyzed using an *Avaatech* X-ray fluorescence (XRF) core-scanner. All cores were measured with a step width of one cm. For each core-section, three runs with increasing X-ray intensities were performed. Elements up to Fe were measured at 10kV with a measurement time of ~12 seconds per centimeter. The elements Br to Sr were measured at 30kV for ~10 seconds and elements up to Ba were measured at 50kV for ~15 seconds per step.

The resulting element count data were corrected for section boundaries and core gaps in order to compile one uninterrupted depth-scaled record for each core.

Please note that the measurements used here do not represent absolute element concentrations but only measured counts of different element intensities. However, these results are absolute sufficient to enable a precise core-to-core correlation as it was performed in this study.

2.3.5 Stable isotopes

Stable isotopes were exclusively measured on benthic epi- or infaunal foraminifera. If available four specimens of the epifaunal species *Cibicidoides wuellerstorfi* (Hayward and Gross, 2014) were used to conduct the measurements. In case of intervals barren of *C. wuellerstorfi*, three specimens of the infaunal species *Uvigerina peregrina* (Gross, 2014) were measured. A *Finnigan MAT 253* mass spectrometer with a *Kiel IV Carbonate Device* was used to perform the measurements. Based on an internal standard of Solnhofen limestone, the one-year precision during the time of measurements was better than ±0.06‰ for $\delta^{13}C$ and ±0.08‰ for $\delta^{18}O$. A more detailed description for the methods used for $\delta^{18}O$ and $\delta^{13}C$ reconstruction is given in *Chapters 4.2.1.1* and *4.2.1.2*, respectively.

2.3.6 Radiocarbon

The radiocarbon measurements on foraminifera were used for different purposes in the different chapters of this study. In *Chapter 3*, ^{14}C measurements on corresponding pairs of planktic (*Globigerina bulloides*) and benthic (*C. wuellerstorfi and U. peregrina*) foraminifera were used to reconstruct ventilation changes of different water masses in the southwest Pacific. In *Chapter 4* however, the exclusive application of the radiocarbon method (measured on *G. bulloides*) was to constrain the age model for a sediment core from the East Pacific Rise.

The samples were measured at the W. M. Keck Carbon Cycle Accelerator Mass Spectrometer (AMS) Laboratory at the University of California in Irvine, USA (0.5 MV AMS), at the

National Ocean Science AMS facility in Woods Hole, USA (0.5 and 2.5 MV AMS), at the Leibniz-Laboratory for Radiometric Dating and Isotope Research of the University of Kiel, Germany (3 MV AMS) and at the Laboratory for Ion Beam Physics at the Eidgenössische Technische Hochschule (ETH) in Zürich, Switzerland (0.2 MV AMS; Fig. 2.5). In particular the ETH MICADAS (**Mi**cro **Ca**rbon **Da**ting **S**ystem) AMS-system is of special importance for ^{14}C-analyses in Polar Regions (often lacking a sufficient amounts of foraminifera or $CaCO_3$ in general), as it permits measurements of samples as small as ~0.1mg $CaCO_3$.

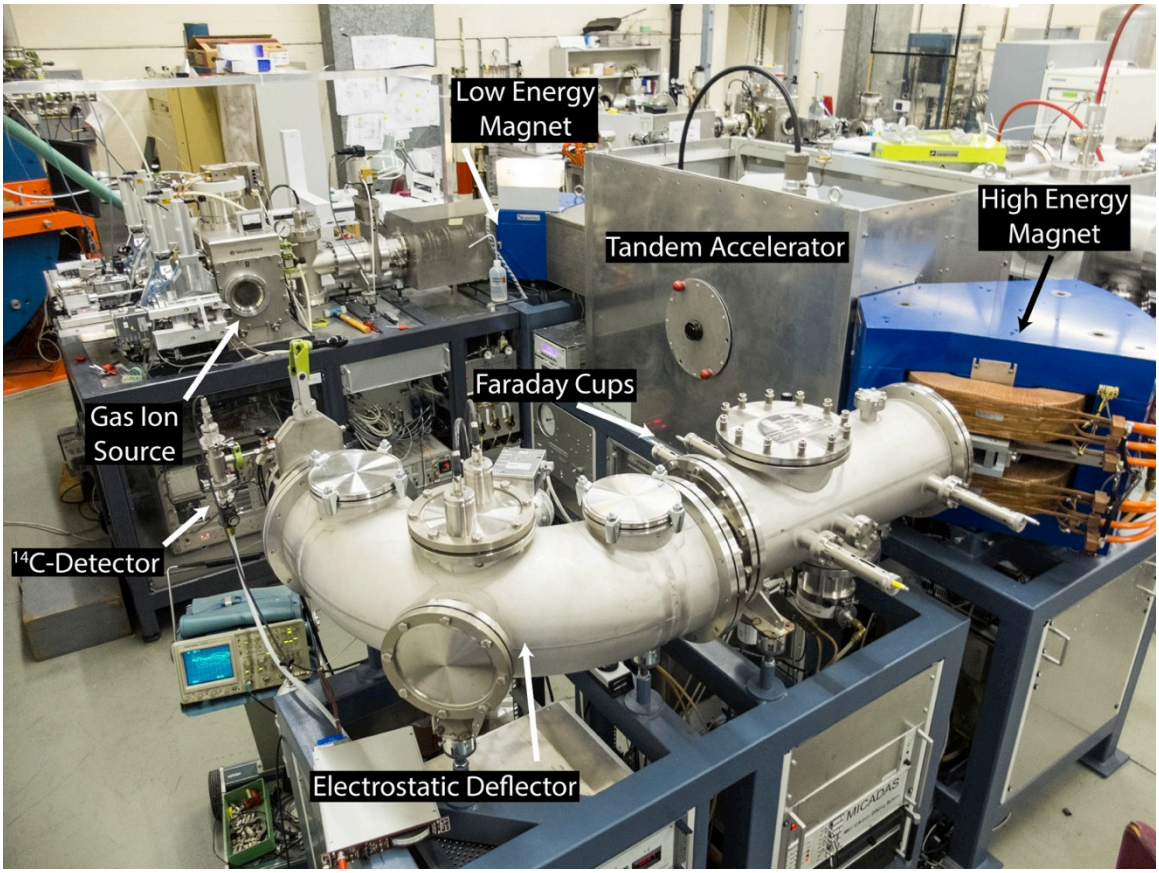

Figure 2.5: The 0.2 MV MICADAS AMS (Synal et al., 2007) at the ETH in Zürich. In the gas ion source, a He-CO_2 gas mixture (CO_2 is derived from the sample; in this study: foraminifera dissolved with phosphoric acid – H_3PO_4) enters a Ti-target and is sputtered with Cs^+, resulting in an ion beam. This beam is steered into the accelerator by a low energy electromagnet that additionally performs a first mass selection. The tandem accelerator (operating at 0.2 MV) is flushed with N_2-gas. The resulting collisions of the accelerated ion beam with the N_2-molecules destroy all larger molecules contained in the ion-beam, which would interfere with the ^{14}C-measurement. Leaving the accelerator, the beam is cleaned of remaining molecule-fragments using a high-energy (HE) electromagnet. Following the HE magnet, two faraday cups measure ^{12}C and ^{13}C ratios. Subsequently the beam is further purified and steered into the ^{14}C-detector for final measurement by an electrostatic deflector.

Surface (*G. bulloides*) ^{14}C-ages were converted to calendar ages, using the SHCal13 calibration curve (Reimer et al., 2013) embedded in the Calib 7.0 software (Stuiver and Reimer, 1993; Stuiver et al., 2005). As surface reservoir ages are different at every location, please refer to the respective chapter for more details on the reservoir correction necessary at the New Zealand Margin (*Chapter 3*) or the East Pacific Rise (*Chapter 3* and *5*).

2.3.7 Age model

The most important part of any paleoceanographic reconstruction is a sound age model, thus the age determination for every sample and the resulting proxy records. Without the knowledge of timing and length of reconstructed signals, the data themselves are meaningless. Still onboard, only hours after the core-retrieval, a first (approximate) age model was established using the MSCL-records as described in *Chapter 2.3.3*. Therefore, the magsus (representative for Fe) and GRA-density (indicating carbonate) were correlated to different marine isotope stages (MIS; e.g. Emiliani, 1955; Lisiecki and Raymo, 2005). Assuming that increased input of iron-rich dust in the ocean basins occurred during glacial periods (e.g. Lamy et al., 2014) and that carbonate deposition was pronounced during warmer interglacials, a comparison of these (preferentially) anti-correlated records enables a first, rough age determination. Supported by bio-stratigraphic age determination based on index fossils (foraminifera and nannofossils; Tiedemann, 2012), these rough age models were used to identify promising sediment cores or core intervals for further analysis (Fig. 2.6).

Depending on the study-area, the analyzed time interval and applied proxies, different methods for the precise age determination were used and/or combined.

For a precise descriptions of methods used for the age model of the respective studies in this thesis, please refer to *Chapters 3* to *5*.

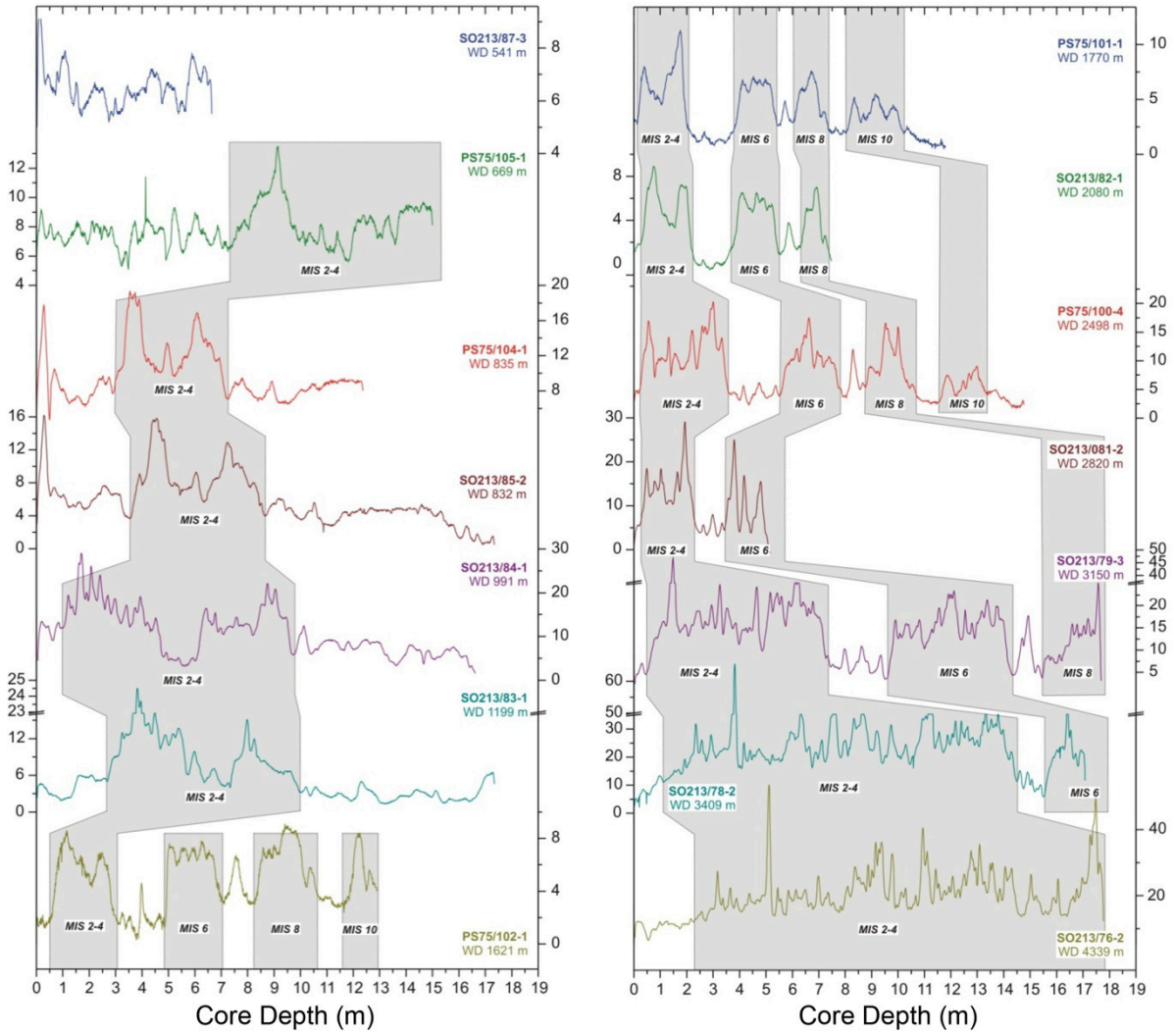

Figure 2.6: Approximate classification of sediment intervals in different Marine Isotopic Stages (MIS), based on the magnetic susceptibility of sediment records from the New Zealand margin. The y-axes display the magnetic susceptibility (SI). Modfied after Lamy, pers. comm.

Chapter 3

Constraining the extent and evolution of the Southwest Pacific glacial carbon pool

T. A. Ronge[1]*, R. Tiedemann[1], F. Lamy[1], F. Kersten[1], M. Frische[2], J. Fietzke[2], R. De Pol-Holz[3], K. Pahnke[4], B. V. Alloway[5], L. Wacker[6], J. Southon[7]

[1] Alfred Wegener Institute Helmholtz Centre for Polar and Marine Research, Bremerhaven, Germany

[2] GEOMAR Helmholtz Centre for Ocean Research, Kiel, Germany

[3] Departamento de Oceanografía and Center for Climate and Resilience Research (CR)[2], Universidad de Concepción, Chile

[4] Max Planck Research Group – Marine Isotope Geochemistry, Institute for Chemistry and Biology of the Marine Environment, Carl von Ossietzky University, Oldenburg, Germany

[5] School of Geography, Environment and Earth Sciences, Victoria University, Wellington, New Zealand

[6] Laboratory of Ion Beam Physics (HPK), Eidgenössische Technische Hochschule, Zürich, Switzerland

[7] School of Physical Science, University of California, Irvine, USA

*Correspondence to: Thomas.Ronge@awi.de

Under review at *Science*

Abstract:

The deglacial pattern of rising atmospheric CO_2 and the associated drop in its radiocarbon activities is thought to be partly driven by the release of old CO_2 from a marine carbon inventory. However, the extent and location of the oceanic carbon pool is still elusive. Here, we present radiocarbon records from a Southwest Pacific transect of sediment cores and identify a significant radiocarbon-depletion in glacial Pacific Deep Water between ~2000 and 4500 m. Glacial radiocarbon levels are up to five times lower than throughout the Holocene and equate to apparent ventilation ages as high as ~8000 years. Although the redistribution of

old carbon from the deep- into the intermediate-water begins at ~21,000 years B.P., the major outgassing pulse from the deep Pacific parallels the rise in atmospheric CO_2.

One Sentence Summary: Localization of the glacial carbon pool and its deglacial pathways in the Southwest Pacific.

3.1 Main text

Ice core records show an increase in atmospheric CO_2 of ~90 ppmv during the last glacial/interglacial transition, from 18.5-11 kyr B.P. (Monnin et al., 2001). This change was accompanied by a significant drop in atmospheric radiocarbon activities ($\Delta^{14}C$), most pronounced between 17.5 and 14.7 kyr B.P. (Parrenin et al., 2013; Reimer et al., 2013). The obvious dependency of both records argues for a deglacial process that links the release of radiocarbon depleted (i.e. old) reservoir to the increase of atmospheric CO_2 (Broecker and Clark, 2010). Hence, outgassing of an old deep-water carbon pool, enriched in CO_2 but depleted in ^{14}C, might have caused a substancial part of these atmospheric CO_2 variations (Broecker and Clark, 2010; Skinner et al., 2010). So far, only isolated findings of old glacial water masses, exceeding ventilation ages of ~4500 yrs in the North and South Pacific as well as in the South Atlantic argue for the storage of CO_2 in the deep glacial ocean (Burke and Robinson, 2012; Sarnthein et al., 2013; Sikes et al., 2000; Skinner et al., 2010; Fig. 3.S1). The circum-Antarctic upwelling region is regarded as the most likely pathway of stored old carbon from the abyss to the atmosphere. In this oceanic window, carbon rich deep-waters like Pacific Deep Water (PDW) are mixed and upwelled and provide a major source for Antarctic Intermediate Water (AAIW), formed close to the Subantarctic Front (Pahnke and Zahn, 2005). Hence, AAIW is able to propagate the circulation- and outgassing-signals (high CO_2 and low ^{14}C) into the major ocean basins. In this context, numerous intermediate-water records have been analyzed to track the timing and export of upwelling deep-water from the

Southern Ocean (SO) (De Pol-Holz et al., 2010; Marchitto et al., 2007; Rose et al., 2010). Despite these efforts, the spatial and temporal dimension of this reservoir as well as the pathway, magnitude, and process of the deglacial CO_2 release remain elusive (De Pol-Holz et al., 2010; Marchitto et al., 2007).

We use $\Delta^{14}C$ records from six sediment cores at the New Zealand Margin (NZM; Fig. 3.1A), covering the major water masses AAIW and Upper/Lower Circumpolar Deep Water (UCDW/LCDW) between ~830 and 4500 m water depth (WD; Fig. 3.1B). This transect is supplemented by $\Delta^{14}C$ data from an open ocean core from the East Pacific Rise (EPR; PS75/059-2, 3613 m; ~4200 km east of the NZM; Figs. 3.S1, 3.S2). Our NZM depth-transect is well suited for the analysis of SO water mass ventilation as we can record ^{14}C-depleted deep-waters on their way to the upwelling region further south, as well as recently subducted intermediate-waters moving towards the north, still carrying deep-water signals modified by upwelling and air-sea gas exchange (Fig. 3.1B). To trace the outgassing signal of CO_2 over the last 30 kyr, we combined B/Ca measurements that act as a proxy for carbonate ion concentrations [CO_3^{2-}] (Yu et al., 2014) with $\Delta^{14}C$ reconstructions. The age control for our sediment cores is based on a correlation to the nearby reference core MD97-2120 (Pahnke and Zahn, 2005; Fig. 3.S8) that we had previously fine-tuned to the EDML ice core, using SST and $\delta^{18}O$-records (EPICA Community Members, 2006).

The most striking feature of our reconstructed $\Delta^{14}C$ values over the last 30 kyr is the large glacial range of $\Delta^{14}C$ between ~830 and 4500 m WD (400‰ to -550‰; Fig. 3.2). This exceeds the modern and Holocene range by a factor of ~5 and indicates large age gradients, strongly suggesting enhanced stratification of the intermediate and deep glacial Southern Ocean. Today's oldest water mass is PDW that is fed into circumpolar-waters along its pathway in the global thermohaline circulation. This ^{14}C-depleted PDW presently extends

from 2000 to 2500 m WD north of the Chatham Rise close to New Zealand (Bostock et al., 2011; Fig. 3.1B).

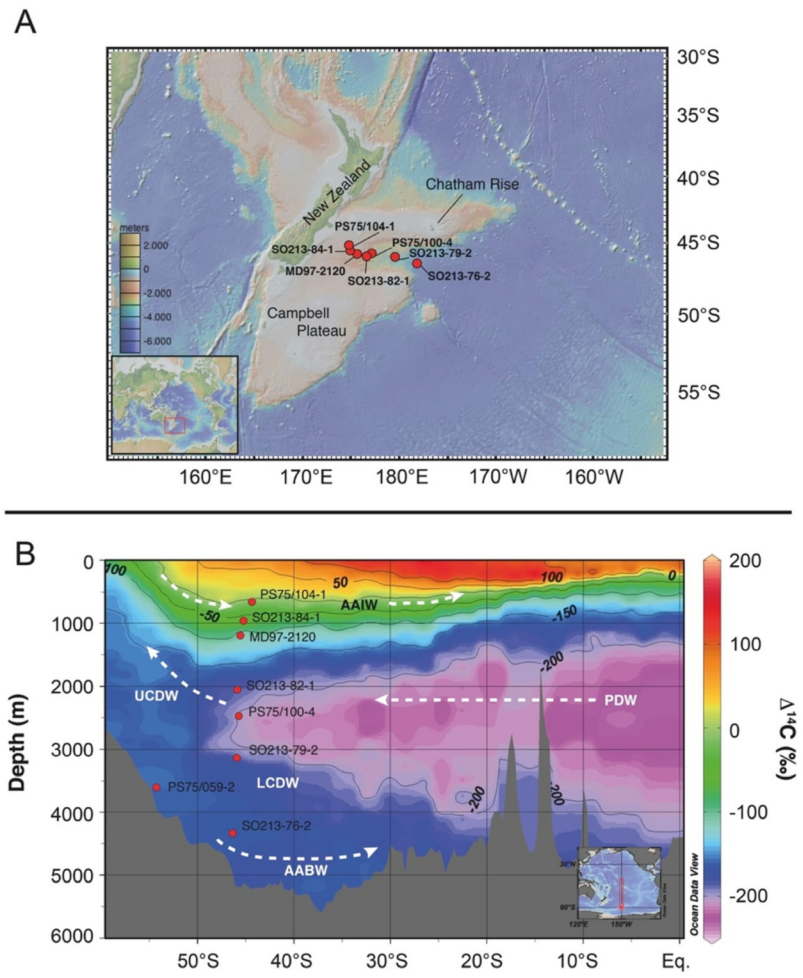

Figure 3.1: Overview of the New Zealand Margin showing core locations and major water masses (A) Bathymetric map of the New Zealand Margin (for the location of our open ocean core PS75/059-2 please refer to Fig. 3.S2. Sediment core locations are indicated by red dots. (B) Water mass section indicating the $\Delta^{14}C$ concentrations of the modern South Pacific. Sediment cores (red dots) were projected into WOCE line P16 (~152°W; Key et al., 2004). Antarctic Intermediate Water (AAIW); Upper and Lower Circumpolar Deep Water (UCDW and LCDW); Antarctic Bottom Water (AABW); Pacific Deep Water (PDW). Reference core MD97-2120 (1210 m; Pahnke and Zahn, 2005).

With our transect, we are able to show that during the Last Glacial Maximum (LGM), significantly aged and ^{14}C-depleted water masses occupied CDW depths between 2000 m and 4500 m in the SW Pacific (Fig. 3.3A; Fig. 3.4A). Our data locate the core of the old water mass at ~2500 m WD (PS75/100-4; modern depth of UCDW; Fig. 3.3A), yielding a maximum deep-water to atmosphere offset in radiocarbon activities ($\Delta\Delta^{14}C$) of ~-1000‰, corresponding roughly to an apparent ventilation age (benthic minus reservoir corrected

planktic ^{14}C age) of ~8000 yrs. The upper and lower boundary of this old water mass is marked by higher $\Delta\Delta^{14}C$ values of -550‰ to -600‰ indicating mixing with younger water masses above and below (Fig. 3.2).

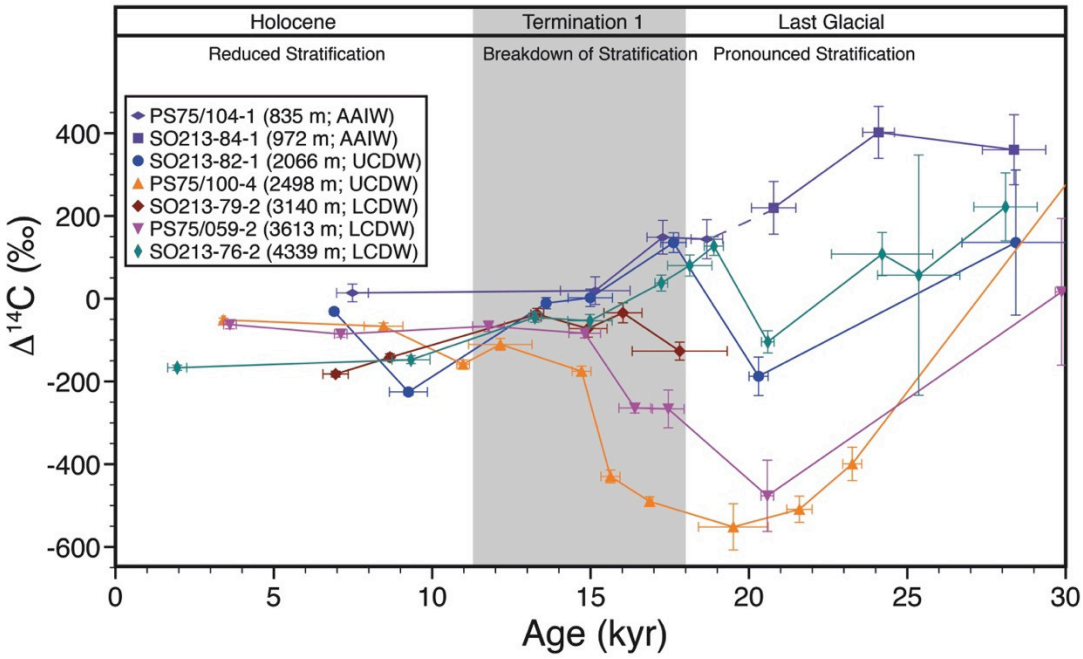

Figure 3.2: $\Delta^{14}C$ changes of the major South Pacific water masses. AAIW – Antarctic Intermediate Water; UCDW/LCDW – Upper and Lower Circumpolar Deep Water; LGM – Last Glacial Maximum. The large glacial range in $\Delta^{14}C$ indicates a pronounced water mass stratification.

In accordance, (McCave et al., 2008) reported the highest glacial nutrient concentrations between 2000 and 3500 m WD indicative of aged water masses north of the Chatham Rise close to our main research area. Our open ocean sediment record traces the old carbon reservoir eastward to the EPR, where $\Delta\Delta^{14}C$ values are as negative as -900‰ at 3600 m WD (Figs. 3.2, 3.3A). Hence this old water mass was not only restricted to the New Zealand region but seems to have occupied the entire South Pacific. This suggestion is corroborated by findings of old glacial waters in the Drake Passage (Burke and Robinson, 2012). In the South Atlantic oldest water masses have been identified at ~3700 m WD with $\Delta^{14}C$ values similar to our Pacific records characterizing the upper and lower boundary of the old carbon pool (Skinner et al., 2010).

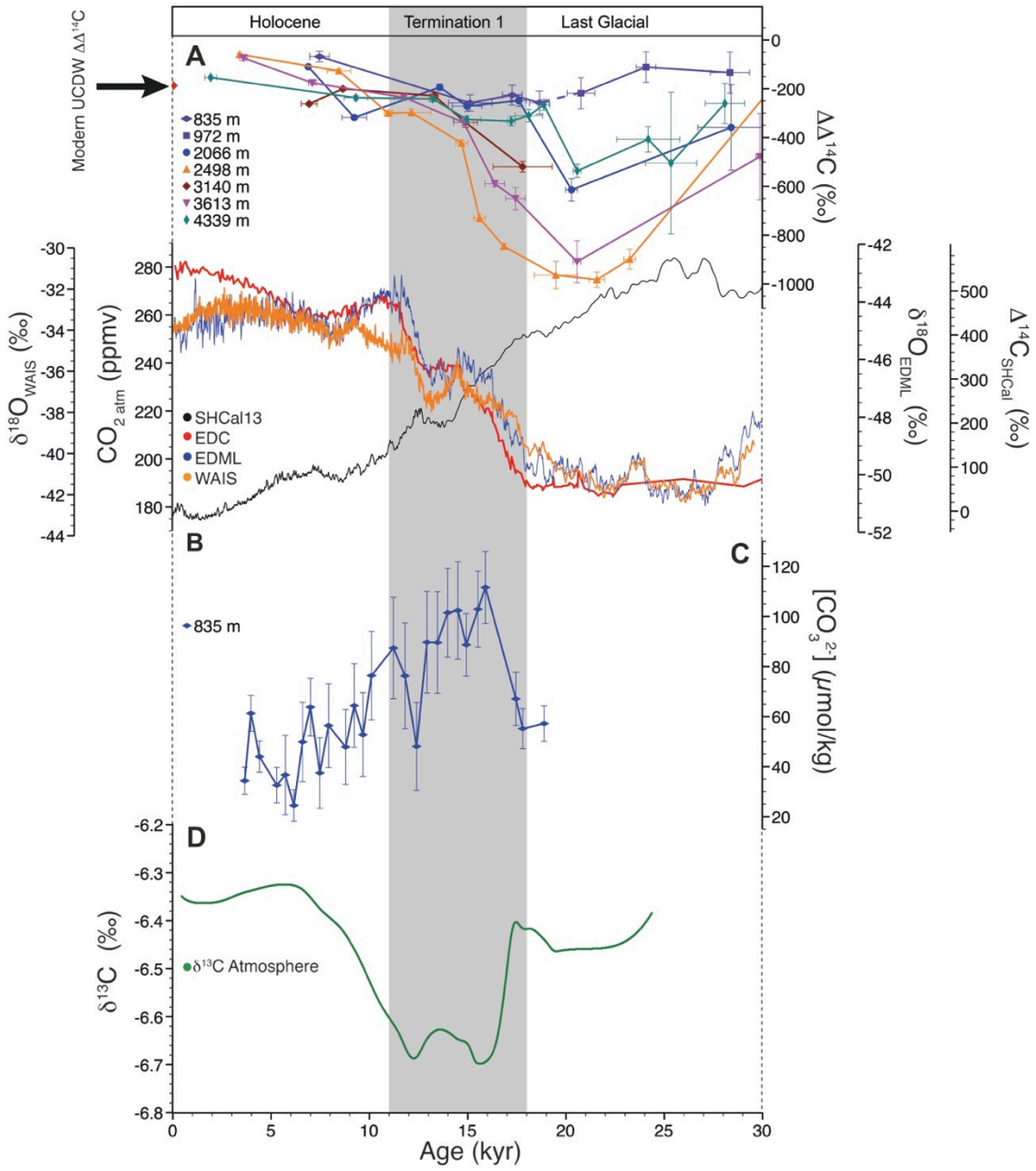

Figure 3.3: Comparison of oceanic and atmospheric proxy records (A) $\Delta\Delta^{14}C$ values (the difference of measured $\Delta^{14}C$ values to the corresponding atmosphere) of the intermediate and deep SW-Pacific; Modern SW-Pacific UCDW $\Delta\Delta^{14}C$ (red diamond; Key et al., 2004). (B) Atmospheric CO_2 concentrations in EDC (red line) (Monnin et al., 2001; Parrenin et al., 2013); EDML (blue line; EPICA Community Members, 2006; Veres et al., 2013) and WAIS $\delta^{18}O$ records (orange line WAIS Divide Project Members, 2013) and atmospheric $\Delta^{14}C$ values (black line; Reimer et al., 2013). (C) Carbonate ion concentrations of SW-Pacific AAIW. (D) Atmospheric $\delta^{13}C$ concentrations (Schmitt et al., 2012).

We hypothesize that the sill depth of the Drake Passage at ~2500 WD hampered the inflow of extreme old Pacific water masses to the South Atlantic, only permitting the access of ^{14}C-depleted waters from the upper boundary of the glacial carbon pool (Fig. 3.S4). Compared to the deep-water records, our intermediate-water record (SO213-84-1; modern depth of AAIW) shows the highest $\Delta\Delta^{14}C$ values during the LGM (~-90‰). This strong contrast supports previous findings of a glacial chemocline in the SO between ~1500 m and 2000 m (Ninnemann and Charles, 2002), separating nutrient depleted, younger AAIW above from older water masses below. Consistent with old deep waters in both the North (~5200 yrs) (Sarnthein et al., 2013) and South Pacific (~4700 yrs; Lowe et al., 2012; Sikes et al., 2000), we suggest that our ^{14}C-depleted waters represent the very old return flow of SO-sourced glacial water masses from the North Pacific (PDW), similar to the modern circulation pattern shown in figure 3.1B.

Any explanation for the pronounced glacial radiocarbon depletion of the deep Southern Ocean has to involve a limited ocean-atmosphere exchange due to strengthened ocean stratification under glacial boundary conditions (Sigman et al., 2010; Fig. 3.4A). Northward-expanded Antarctic sea ice and Southern Westerly Winds (SWW; Gersonde et al., 2005; Kohfeld et al., 2013) contribute to reduced air-sea gas-exchange and upwelling of deep-waters. Surface freshening by melting sea-ice in the source regions of intermediate-waters (Saenko and Weaver, 2001) and enhanced formation of highly saline Antarctic Bottom Water (Adkins, 2013) may have set a density structure that led to reduced mixing and the encasement of old PDW (Fig. 3.4A). In addition, the shoaling of North Atlantic Deep Water (NADW; Curry and Oppo, 2005) is expected to reduce the input of freshly ventilated waters into South Pacific CDW below ~2000 m. Our finding of very high deep-water ventilation ages can be plausibly explained by these interacting key processes and is consistent with the glacial storage of atmospheric CO_2 in the deep-ocean (Adkins, 2013).

At the end of the last glacial and during the transition to the modern interglacial from ~21-11.5 kyr B.P.), converging $\Delta\Delta^{14}C$ values across the entire water column argue for a progressive destratification (Fig. 3.3A; 3.4B).

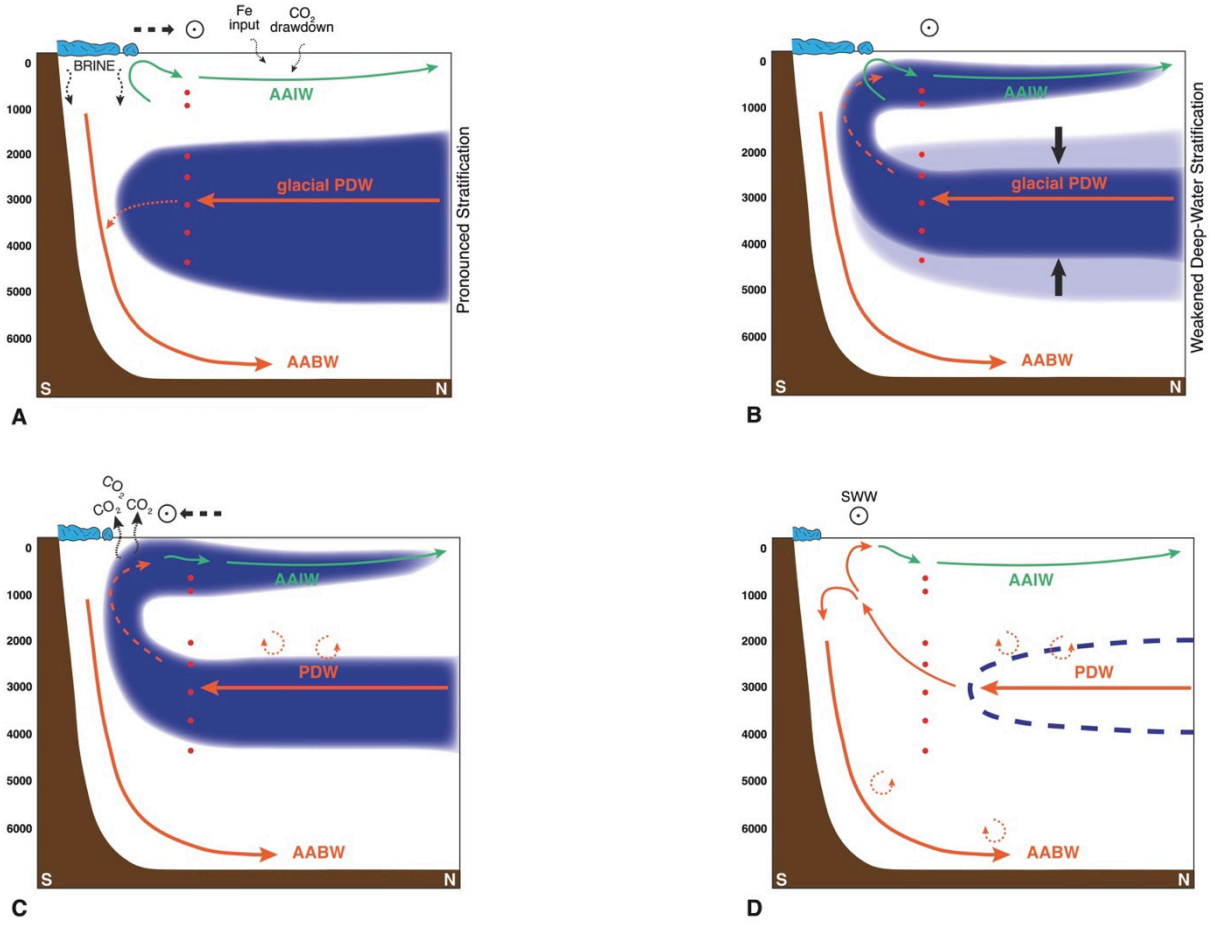

Figure 3.4: Schematic view of South Pacific overturning circulation. Green arrows: intermediate-water circulation; orange arrows: deep-water circulation; blue shading: poorly ventilated old and CO_2 rich waters; ice-blue areas: sea ice; SWW: Southern Westerly Winds; red dots: approximate depth of sediment cores; circular arrows: diffusional and diapycnal mixing. (A) LGM: Northernmost extent of Antarctic sea ice and SWW. Increased AABW salinity by brine rejection favors ocean stratification. The resulting chemocline at ~2000m water depth separates intermediate and deep water masses, resulting in extremely poor ventilated PDW. Increased glacial dust input promotes primary production and drawdown of atmospheric CO_2. (B) Early West Antarctic warming interval (~21 kyr B.P.): First signs of a weakened stratification. Old and ^{14}C depleted water is incorporated in AAIW; outgassing of CO_2 still hampered by sea ice. (C) Termination 1 (~18-11.5 kyr BP): Intensive SO upwelling induced by the southward shift of Antarctic sea ice and SWW from their glacial positions. Pronounced release of ^{14}C-depleted CO_2. Increased AAIW carbonate ion concentrations. (D) Holocene: SWW and sea ice extent in their modern position. Circumpolar Deep Water is upwelled in the Southern Ocean (SO).

First signs of a weakening in stratification characterize the interval from ~21-18 kyr B.P., thereby preceding the deglacial CO_2 rise by a few thousand years (Fig. 3.3). During this interval, the intermediate-water to atmosphere offset in radiocarbon starts to increase while the $\Delta\Delta^{14}C$ at ~2000 and 4300 m WD decreases. This pattern points to a process that combines an early onset of SO upwelling with a transfer of old carbon into the intermediate-water level due to a strongly restricted air sea gas exchange (Fig. 3.4B). The timing of this process might be closely linked to the early deglacial temperature increase in the West Antarctic region (WAIS Divide Project Members, 2013).

Later, during Termination 1, when the most radiocarbon-depleted waters at 2500 m WD rejuvenate, no further pronounced depletion in AAIW $\Delta\Delta^{14}C$ is recorded (Fig. 3.3A). However, the intermediate-water $\Delta\Delta^{14}C$ values remain low and form a minimum from ~19-15 kyr B.P (this study; Rose et al., 2010). Such upwelled old SO deep-waters have also been traced by enhanced deglacial reservoir-ages in Southeast Pacific surface waters (Siani et al., 2013) and are also considered to be a major source for the formation of AAIW. This relationship between the old carbon pool and the newly formed and radiocarbon depleted AAIW strongly suggests that the additional amount of upwelled old carbon was not buffered by an intensified incorporation in AAIW, but that it was instead transferred to the atmosphere (Fig. 3.4C). This inference is consistent with our $\Delta^{14}C$ and $[CO_3^{2-}]$ reconstructions, which document SO outgassing coinciding with the rise in atmospheric CO_2 (Fig. 3.3). At the core depth of the old glacial water mass (~2500 m WD; Fig. 3.3), the deglacial increase in $\Delta\Delta^{14}C$ by ~800‰ implies a substantial deep-water rejuvenation by ~7000 years. The strongest $\Delta\Delta^{14}C$-rise from ~17 to 14.5 kyr B.P. is paralleled by a pronounced transient maximum in intermediate water carbonate ion concentrations from ~55 to 115 μmol/kg (835 m WD; Fig. 3.3C). The magnitude of this southwestern Pacific intermediate-depth $[CO_3^{2-}]$ change (~60 μmol/kg) is significantly higher than the 24 μmol/kg increase recently reported for the deep

South Atlantic during the same time window (Yu et al., 2014), indicating that the bulk of CO_2 outgassing occurred in the Pacific sector of the SO. According to the calcite compensation theory, a transient high in oceanic carbonate ions is interpreted to result from CO_2-loss (Broecker and Peng, 1987) and supports the hypothesis of a SO window for stored glacial CO_2 to the atmosphere. At the end of the deglacial CO_2-release, the initial state of [CO_3^{2-}] is restored, probably by the extraction of alkalinity by calcite compensation in the deep ocean and coral reef growth during the Holocene (Fig. 3.3C). These deglacial changes parallel rising atmospheric CO_2 and decreasing $\delta^{13}C$-values recorded in Antarctic ice-cores (Parrenin et al., 2013; Schmitt et al., 2012; Fig. 3.3), suggesting close mechanistic links. Along with intensified upwelling (Anderson et al., 2009) the breakdown of stratification favored the erosion of the glacial carbon pool and supplied old deep-waters to the ocean surface. These processes ultimately culminated in the release of ^{13}C and ^{14}C depleted CO_2 to the atmosphere (Fig. 3.4C). This deglacial CO_2-release reduced the maximum atmosphere to deep-water offset of the carbon reservoir from ~-1000‰ during the LGM to ~-200‰ in the Holocene (Fig. 3.3A). At the end of the glacial termination (~11.5 kyr), the uniform and high Southwest Pacific $\Delta\Delta^{14}C$, the beginning decrease in carbonate ion concentrations and the paralleled increase in atmospheric $\delta^{13}C$ (Schmitt et al., 2012) mark the end of the deglacial oceanic outgassing period that contributed to the ~90 ppmv rise in atmospheric CO_2.

Our reconstructions provide new insights into the evolution and dynamic of the marine carbon inventory, its aging and the process of CO_2-release to the atmosphere. Surprisingly, our data do not record changes in deep-water chemistry, caused by the pronounced millennial-scale fluctuations of the Atlantic Meridional Overturning Circulation (AMOC). For example, a strong reduction in AMOC during Heinrich Stadial 1 (McManus et al., 2004) would have diminished the input of ^{14}C-enriched NADW into the deep Pacific, leading to a depletion of $\Delta^{14}C$. In contrast, we record an uninterrupted increase in deep-water $\Delta^{14}C$ throughout the

deglaciation (Fig. 3.2). Although the deglacial geometry of NADW and its injection to the Atlantic sector of the Southern Ocean have strongly varied, its changing capacity was too low to affect the $\Delta^{14}C$ signatures in the South Pacific. However, the timing of the most pronounced increase in deep-water $\Delta^{14}C$ parallels Heinrich Stadial 1. This may indicate a response of SO processes (Denton et al., 2010) to the bipolar seesaw, influencing the dynamic of ventilation and outgassing.

Our radiocarbon records show an extensive body of very old ^{14}C-depleted water between 2000 m and 4500 m WD extending across large parts of the South Pacific (Figs. 3.2; 3.S4). If this water mass reflects the return-flow of aged water from the North Pacific, we would expect that a similar pattern in the Indian Ocean would further expand the volume of the old carbon pool.

Acknowledgements

We thank: Captains, crews and scientific parties of R/V *Sonne* and R/V *Polarstern* for their support during SO213/2 and ANTXXVI-2; M. Sarnthein for helpful comments; R. Gersonde and P. Köhler for sample material and data; R. Fröhlking, B. Glückselig, N. Lensch, L. Ritzenhofen, L. Schönborn, M. Seebeck, R. Sieger, M. Warnkroß and S. Wiebe for technical support. TAR was funded by the Federal Ministry of Education and Research (BMBF; Germany) project 03G0213A – SOPATRA and the Alfred Wegener Institute, Helmholtz Centre for Polar and Marine Research. BVA received funded support from an internal Victoria University of Wellington Science Faculty Research Grant. RDPH received support from FONDAP-15110009 and Iniciativa Científica Milenio NC120066 and IC120019. Data will be made available at http://doi.pangaea.de/10.1594/PANGAEA.833663.

3.2 Supplementary Materials:

3.2.1 Sediment cores

The water mass transect that is forming the backbone of this study consists of seven sediment cores retrieved during the *R/V Polarstern* cruise ANTXXVI/2 (Gersonde, 2011) and *R/V Sonne* SO213/2 (Tiedemann, 2012) cruises from the Bounty Trough off New Zealand (New Zealand Margin, NZM) and from the East Pacific Rise (EPR; Fig. 3.S1 and 3.S2). In combination, these sediment cores record all water masses between 835 m and 4339 m, thus the modern water depths of the AAIW down to the LCDW with an imprint of AABW (McCave et al., 2008). Positions, water depth, modern water masses and average sedimentation rates are reported in table A2.1 (Appendix).

An advantage of the NZM core transect is that it was not affected by potential glacial/interglacial shifts of the Subtropical Front (STF) or the Subantarctic Front (SAF) (Hayward et al., 2008). The STF is bathymetrically fixed by the Chatham Rise, while the SAF is topographically steered by the submerged Campbell-Bounty Plateau (Hayward et al., 2008). As all sediment cores were permanently south of the STF and due to their close proximity to each other, we assume that changes in surface reservoir ages would affect all locations in a similar way. An exception is core PS75/059-2, which was retrieved ~4200 km east of the Bounty Trough, at the western flank of the East Pacific Rise (Fig. 3.S1 and 3.S2) about 2° north of the SAF.

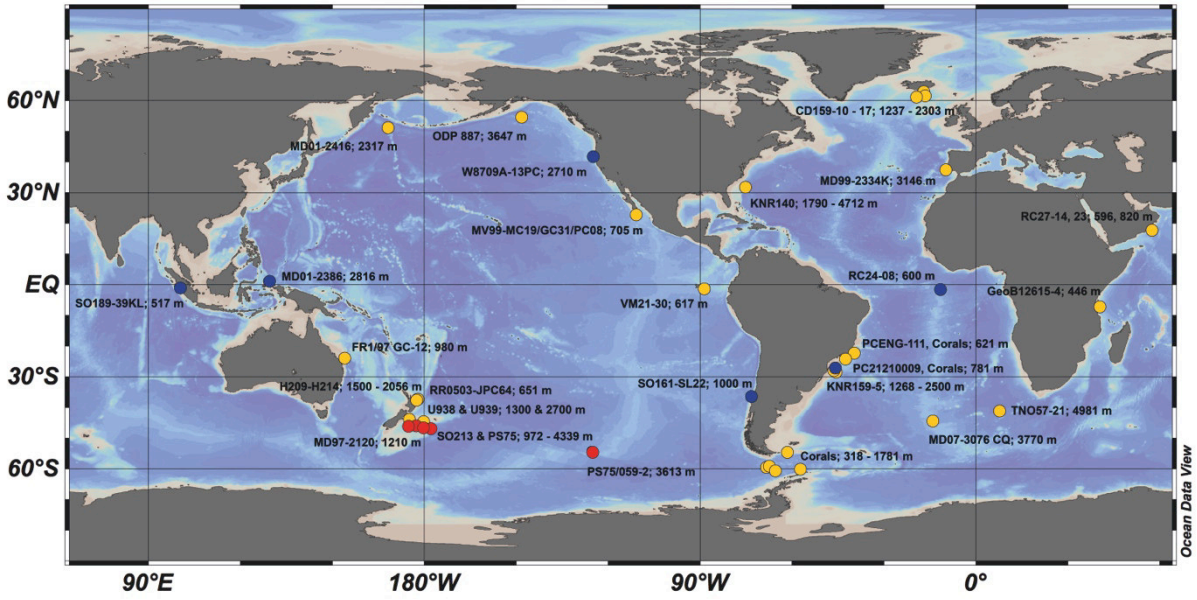

Figure 3.S1: Overview map of worldwide sediment cores used to constrain the glacial carbon pool or its pathways. Red dots – this study; orange dots – evidence for old glacial/deglacial water; blue dots – no significantly aged water. See table A2.4 (Appendix) for core references. Map generated using ODV 4.6.1 (Schlitzer, 2014).

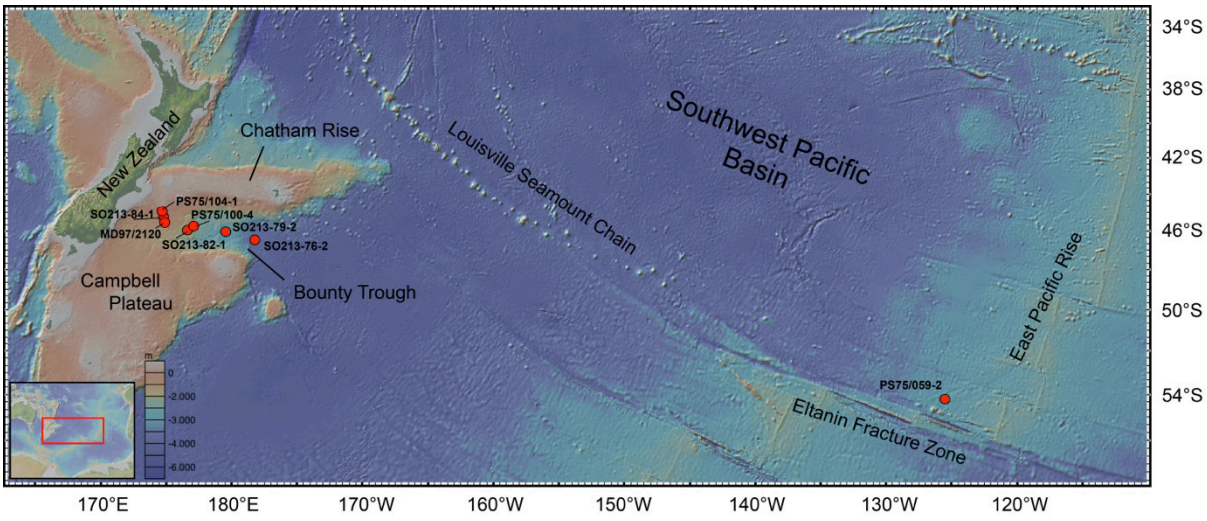

Figure 3.S2: Map of the SW Pacific showing the core locations used in this study (red dots) and major topographic features. Map generated using GeoMapApp (www.geomapapp.org)

3.2.2 Radiocarbon dating

For every sample, corresponding pairs of planktic (monospecific *Globigerina bulloides*) and benthic (mix of *Cibicides wuellerstorfi* and *Uvigerina peregrina*) foraminifera were picked from the 250-315 µm and 315-400 µm size fractions. To minimize the effect of contamination on our analyses, we paid special attention not to pick any broken, discolored or filled tests. Radiocarbon measurements were performed at the National Ocean Science AMS (NOSAMS) facility in Woods Hole, USA, the W. M. Keck Carbon Cycle AMS Laboratory at the University of California at Irvine, USA and at the Laboratory for Ion Beam Physics at the Eidgenössische Technische Hochschule (ETH) in Zurich, Switzerland.

To reconstruct the apparent ventilation ages, the offset in deep-water to surface ^{14}C ages, of different water masses, we calculated the difference in benthic and reservoir corrected planktic (B-P) ^{14}C-ages (Fig. 3.S3).

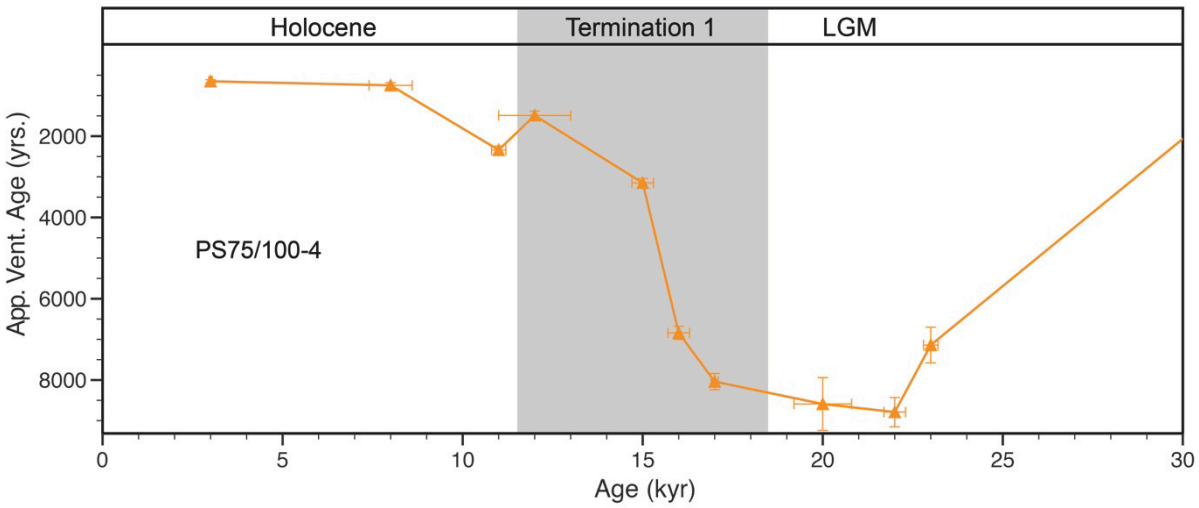

Figure 3.S3: Apparent ventilation ages of PS75/100-4 calculated from the ^{14}C age difference of benthic to reservoir corrected planktic foraminifera.

The radiocarbon activity ($\Delta^{14}C$) is the offset between the *absolute international standard* and the samples activity corrected for age (Stuiver and Polach, 1977) and is generally utilized in

mass and balance calculations (Sarnthein et al., 2013). We used the equation of (Adkins and Boyle, 1997) to determine the initial (paleo) $\Delta^{14}C$ of the benthic samples:

$$\Delta^{14}C = \left[\left(\frac{e^{-^{14}Cage/8033}}{e^{-cal.age/8266}}\right) - 1\right] \times 1000$$

To correct the $\Delta^{14}C$-values for variations in atmospheric $\Delta^{14}C$, we calculated the water mass $\Delta^{14}C$ offset to the corresponding atmospheric $\Delta^{14}C$ ($\Delta\Delta^{14}C$). The $\Delta\Delta^{14}C$ of our CDW records to records from the Drake Passage (Burke and Robinson, 2012) and the South Atlantic (Skinner et al., 2010) is shown in figure 3.S4. Taking the atmospheric values into account, the use of $\Delta\Delta^{14}C$ facilitates the direct comparison of water mass $\Delta^{14}C$ to the corresponding atmosphere.

The radiocarbon details for all cores are shown in table A2.2 (Appendix). Ventilation age errors were calculated from combined errors in ^{14}C ages and the error of the calibrated calendar ages (please refer to the chapter Age models). The error in $\Delta^{14}C$ was calculated from ^{14}C and calibrated age errors.

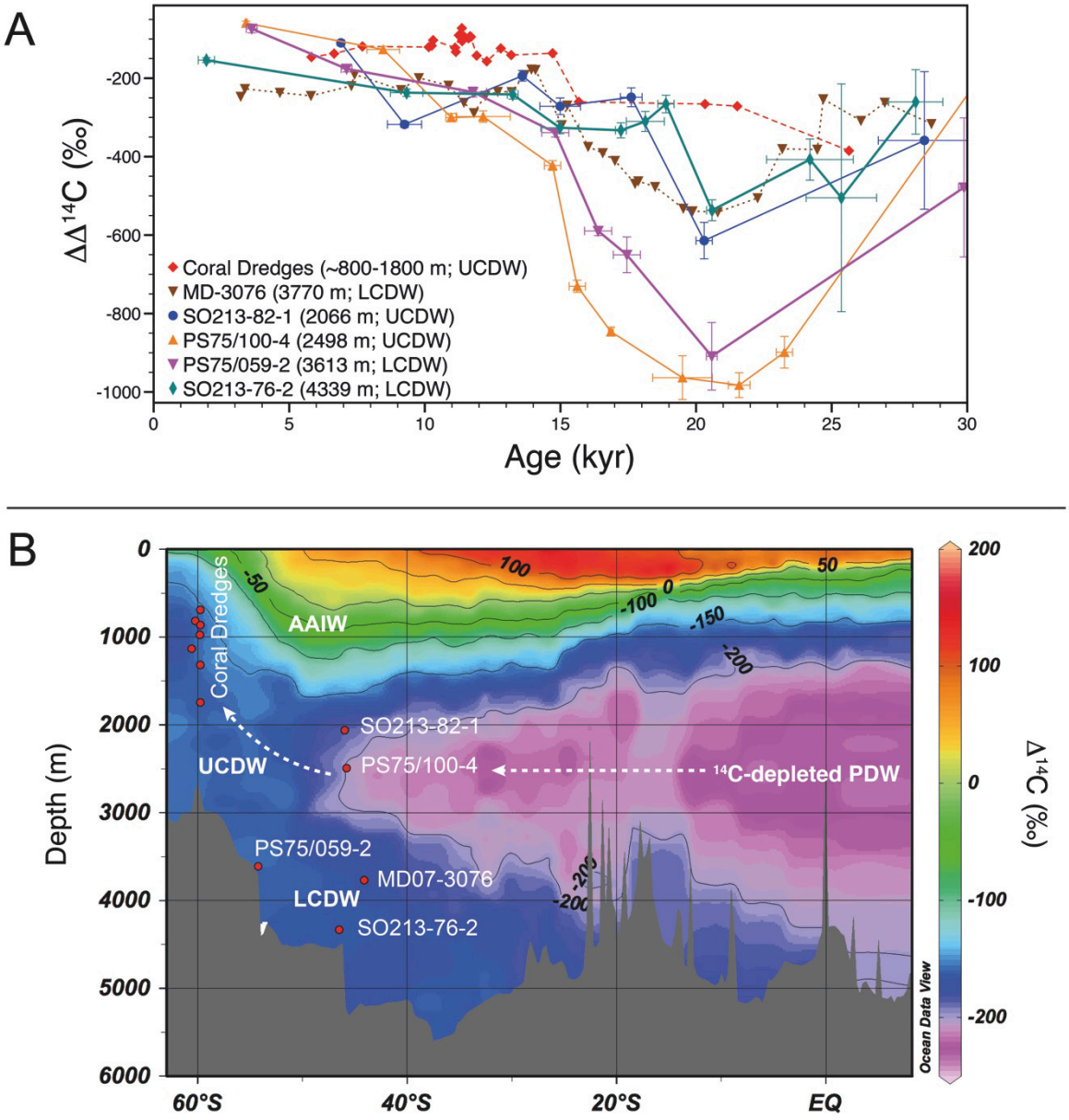

Figure 3.S4: $\Delta^{14}C$ offset between different CDW records and the contemporaneous atmosphere ($\Delta\Delta^{14}C$; Reimer et al., 2013). (A) $\Delta\Delta^{14}C$ measured on deep-water corals (red diamonds; Burke and Robinson, 2012) from the Drake Passage, and in South Atlantic sediment record MD07-3076 (brown inverted triangles; Skinner et al., 2010) in comparison to SW-Pacific $\Delta\Delta^{14}C$ data (this study). The clear offset in $\Delta\Delta^{14}C$ of the coral dredges (from UCDW depth) to the other CDW records at ~20 – 22 kyr BP, may be a result of AAIW influence at this site, since the samples are from a depth close to the AAIW/UCDW boundary at 819 m (Burke and Robinson, 2012). (B) Sediment cores plotted into the $\Delta^{14}C$ section of WOCE line P16 at 152°W (Key et al., 2004). The LGM depth distribution of $\Delta\Delta^{14}C$ shown in figure 3.S4 A, clearly resembles the modern radiocarbon distribution, with the highest depletion found at ~2500 m WD. Anyway, the LGM values prove a more pronounced depletion during this interval. The Holocene pattern differs slightly from picture shown in figure 3.S4 B, as a more uniformly distribution of $\Delta^{14}C$ in prevails in modern CDW off New Zealand. Section generated using ODV 4.6.1 (Schlitzer, 2014).

3.3.3 B/Ca ratios in epibenthic foraminifers

For our B/Ca measurements on sediment core PS75/104-1 (Appendix A2), we used the epibenthic foraminifer species *Cibicidoides wuellerstorfi*. We only used specimens of the 315-400 µm size-fraction that did not show any signs of alteration or secondary mineral fillings.

B/Ca ratios were analyzed at the GEOMAR Helmholtz Centre for Ocean Research Kiel, Germany, using a 193 nm Excimer laser ablation system (Coherent, GeoLasPro) coupled to a double-focusing magnetic sector mass spectrometer (Nu Instruments, AttoM) in low resolution mode (300 Res, 10% valley definition). For each sample 3-6 shells were used and trace elemental composition was analyzed on four spots with 90 µm diameter each in the three oldest chambers on the umbilical side. The NIST 615 standard (Jochum et al., 2011) was measured before and after sets of five foraminifer shells and used for signal calibration. Given standard deviations include analytical uncertainties and natural variations within a single sample and the standard. In order to exclude contamination effects, foraminifer shells as well as the NIST 615 standard were pre-ablated before analysis. Samples with Mn/Ca above 0.2 mmol/mol and Al/Ca above 0.4 mmol/mol were discarded from the dataset.

Downcore carbonate ion concentration reconstructions were calculated, using the B/Ca-$\Delta[CO_3^{2-}]$ calibration for *C. wuellerstorfi* of (Yu and Elderfield, 2007):

$B/Ca = 1.14 \pm 0.048\ (\Delta[CO_3^{2-}]) + 177.1 \pm 1.41\ (R^2 = 0.86)$

Past carbonate ion concentrations in deep- to intermediate-water can be derived from calcite saturation ($\Delta[CO_3^{2-}]$) and carbonate ion concentration at saturation ($[CO_3^{2-}]_{sat}$): $[CO_3^{2-}] = \Delta[CO_3^{2-}] + [CO_3^{2-}]_{sat}$.

3.3.4 Tephra analyses

In cores SO213-76-2 (507-508 cm) and SO213-79-2 (150-151 cm) a distinctive vitric-rich tephra layer was identified (Fig. 3.S5). Morphological expression, grain size and thickness of

this tephra were indistinguishable and hence, most likely to represent the same eruptive event. Glass shard major element chemistry of this tephra layer was then determined by electron microprobe analysis (EMA) and the results were compared with selected onshore and offshore Kawakawa/Oruanui Tephra (KOT) correlatives (Table A2.3; Fig. 3.S6). The glass shard geochemistrys were consequently indistinguishable which a) affirms correlation to KOT, and b) augments the overall chronology of this study. All major element determinations were made on a JEOL Superprobe (JXA-8230) housed at Victoria University of Wellington, using the ZAF correction method. Analyses were performed using an accelerating voltage of 15 kV under a static electron beam operating at 8 nA. The electron beam was defocused between 10 to 20 μm. All elements calculated on a water-free basis, with H_2O by difference from 100%. Total Fe expressed as FeO_t. Mean and ± 1 standard deviation (table A2.3; in parentheses), based on *n* analyses. All samples normalized against glass standards VG-568 and ATHO-G.

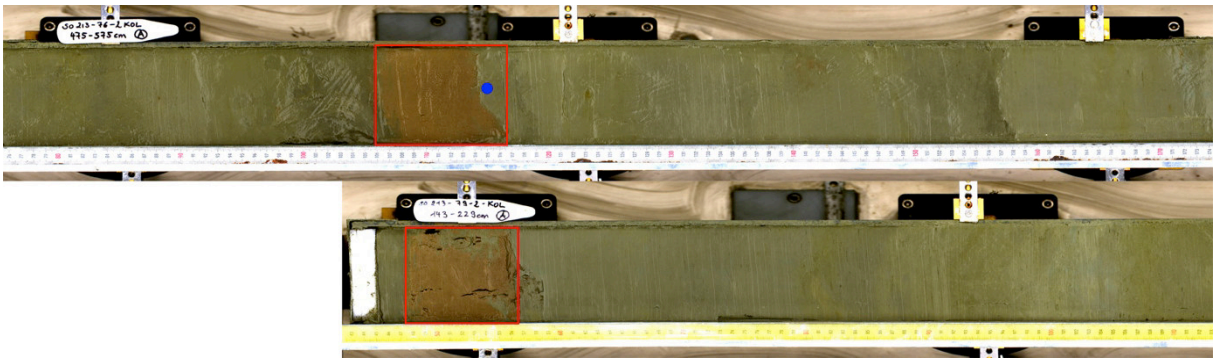

Figure 3.S5: Core pictures of SO213-76-2 (top) and SO213-79-2 (bottom) showing the 25.36 kyr B.P. Kawakawa/Oruanui Tephra (indicated by red boxes). The blue dot indicates the sample depth of SO213-76-2 515 cm, used to constrain the surface reservoir age. Scale is in centimeters.

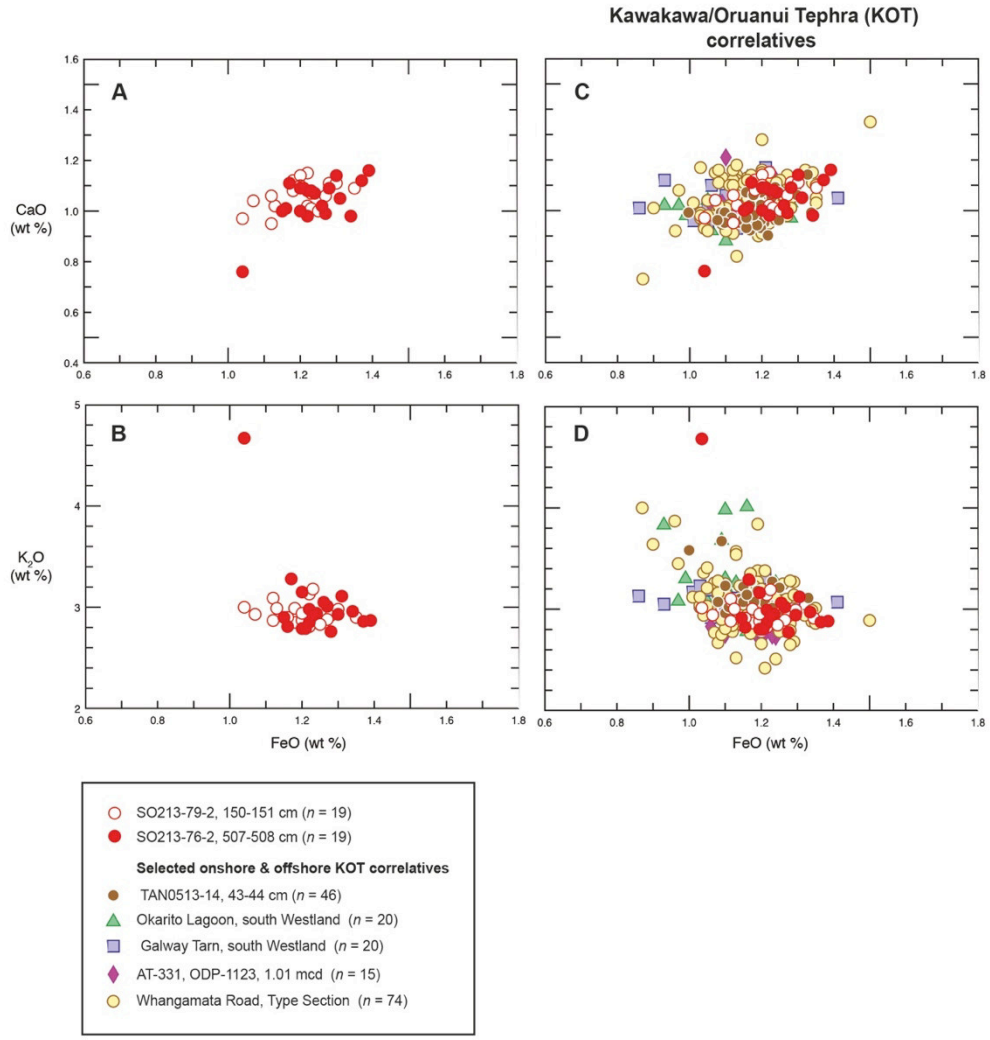

Figure 3.S6: CaO **(A)** and K_2O **(B)** to FeO ratios of SO213-79-2 (red circles) and SO213-76-2 (red filled circles) in comparison to element ratios of reference samples of the Kawakawa/Oruanui Tephra (KOT) (**C** and **D**). TAN0513-14 (Ryan et al., 2012); Okarito Lagoon, Galway Tarn (Newnham et al., 2007); AT-331; ODP-1123 (Alloway et al., 2005); Whangamata Road (Villamor et al., 2007).

3.3.5 XRF scanning

All sediment cores were analyzed at the Alfred Wegener Institute for their specific element abundances using an Avaatech X-ray fluorescence (XRF) core-scanner with a preset step width of 1 cm. These measurements only represent counts of element intensities and not absolute element concentrations but are sufficient for the use in core-to-core correlation.

3.3.6 Age models

We chose the high-resolution core MD97-2120 (1210 m water depth) as a reference core due to its position close to our sediment cores in the Bounty Trough. Following the approach applied by Rose et al. (2010), we correlated the planktic $\delta^{18}O$ and Mg/Ca derived SST records of MD97-2120 (Pahnke et al., 2003) with the EDML ice core $\delta^{18}O$ record (EPICA Community Members, 2006; Veres et al., 2013; Fig. 3.S7). This correlation considered the new age model of EDML ice core (Veres et al., 2013) and thus improves the previous correlation (Rose et al., 2010).

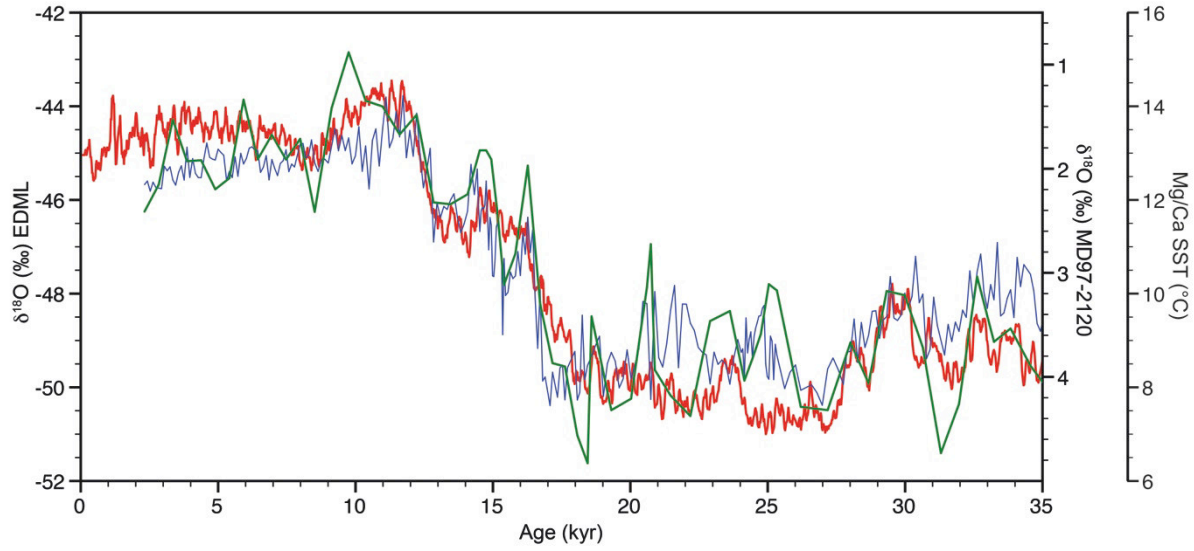

Figure 3.S7: Planktic $\delta^{18}O$ (blue curve) and SST (green curve) records of sediment core MD97-2120 (Pahnke et al., 2003) fine-tuned to the EDML $\delta^{18}O$ record on the AICC12 time scale (red curve; Members, 2006; Veres et al., 2013).

To establish a robust core-to-core correlation, the XRF element content records (Sr, Ca, Fe and Sr/Fe) were then correlated to respective age-scaled XRF records of the sediment core MD97-2120 from the southern Chatham Rise (Fig. 3.S8, 3.S9; Pahnke and Zahn, 2005; Pahnke et al., 2003) using the computer program AnalySeries 2.0.4.2 (Paillard et al., 1996). In particular, the Sr-counts were useful for the core-to-core correlation, as Sr represents $CaCO_3$-variability, but is barley affected by differences in grain size or the water-content. In some

sediment cores, the Sr-counts display an early deglacial increase at ~19.7 kyr (Fig. 3.S8). However, the timing of this increase is in phase when using Sr/Fe-counts instead, enabling a better core-to-core correlation (Fig. 3.S9). To achieve the best correlation we considered the reservoir corrected planktic ^{14}C ages in intervals lacking pronounced XRF-features (e.g. in the Holocene). Furthermore, we were able to use a distinctive tephra layer as a radiocarbon-independent stratigraphic marker in two sediment cores (SO213-76-2 and SO213-79-2; Fig. 3.S5). The layer in both cores represents the widespread Kawakawa/Oruanui tephra (KOT). The KOT is a silicic tephra erupted from Taupo Volcanic Centre (TVC) in the central North Island of New Zealand with an age of ~25.36 kyr B.P. (Vandergoes et al., 2012) and is the most important isochronous tephra marker erupted in the SW Pacific region during the last 30,000 years (Alloway et al., 2007). This tephra was likewise found in reference core MD97-2120 (Pahnke et al., 2003). In this sediment core, we updated the KOT age used by (Pahnke et al., 2003) to the revised age by Vandergoes et al. (2012). The age model of our open ocean core PS75/059-2 from the East Pacific rise (Lamy et al., 2014) has been adjusted to our NZM age model, by correlating it to the XRF Fe-counts of PS75/100-4.

To assess the quality of the age model described above, we established a second age model based solely on calibrated planktic ^{14}C-ages and the KOT age. Planktic radiocarbon ages were calibrated to calendar ages, using the calibration software Calib 7.0 (Stuiver and Reimer, 1993; Stuiver et al., 2005) with the embedded SHCal13 calibration curve (Reimer et al., 2013). To account for reservoir effects, we corrected all ^{14}C-ages younger than 18 kyr with a reservoir age of 640 ± 40 years (Sikes et al., 2000). For the glacial interval, we used a ^{14}C surface reservoir-age of 838±160 years. This age represents the reservoir age for the ^{14}C sample (SO213-76-2 515cm), taken directly below the tephra shown in figure 3.S5.

As both age models are in good agreement, but not identical (shown in figure 3.S10), their age differences have been considered as uncertainties in our age assignments of the age model

used in the main text. Because of these comparable results, we assume our XRF based age models to be robust.

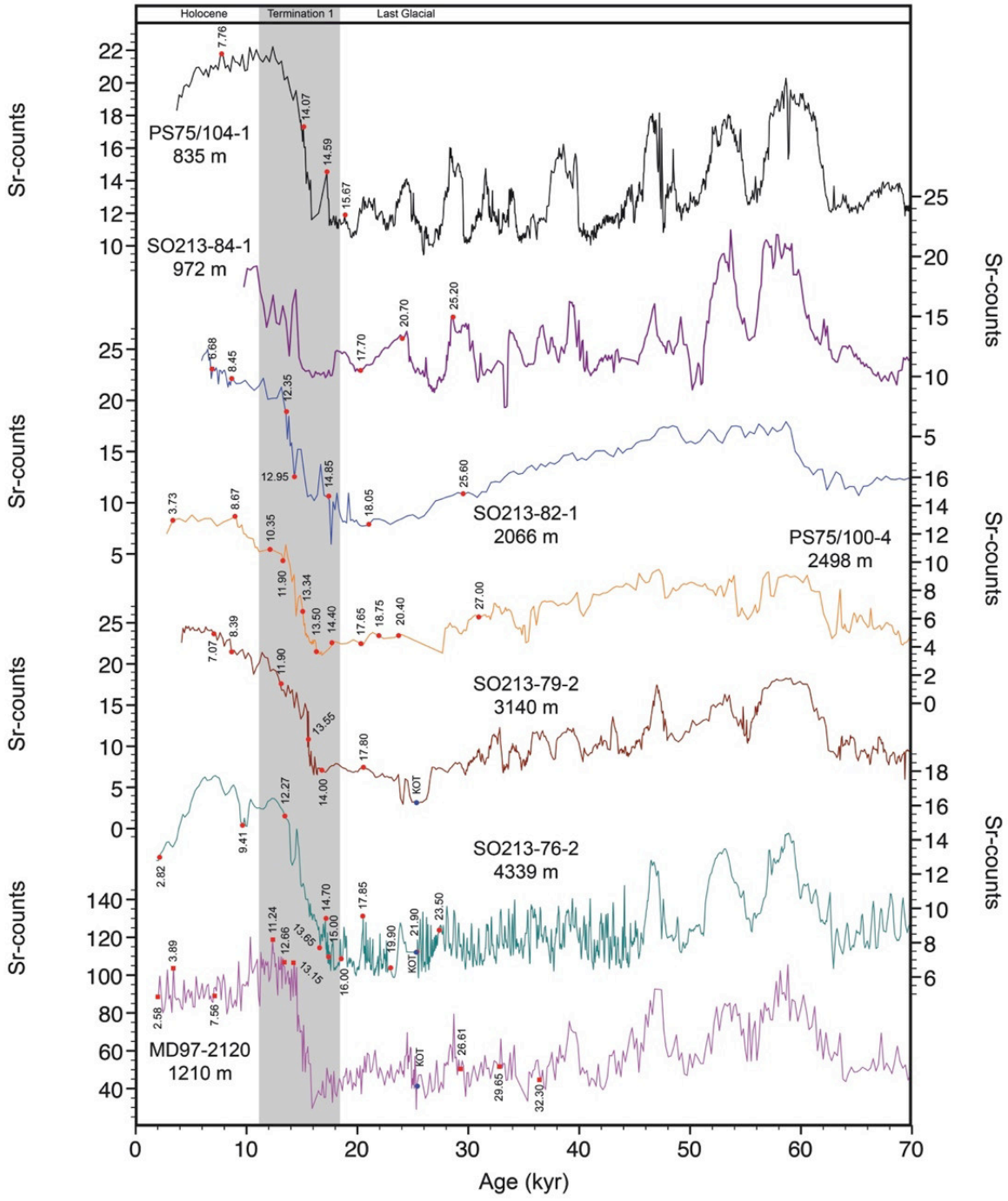

Figure 3.S8: XRF correlation of all sediment cores to the reference core MD97-2120 (Pahnke and Zahn, 2005) for the past 70 kyr. Displayed here are solely Sr-count curves (scale ∗1000). Likewise, Ca-, Sr/Fe- and Fe-counts, stable isotope records, and tephra analyses were used to establish an optimal correlation. Red dots indicate ^{14}C-sampling positions of this study; red squares are sampling positions by Pahnke and Zahn (2005). Black numbers indicate raw ^{14}C ages. YD – Younger Dryas; ACR – Antarctic Cold Reversal; HS1 – Heinrich Stadial 1; LGM – Last Glacial Maximum; KOT – Kawakawa/Oruanui Tephra.

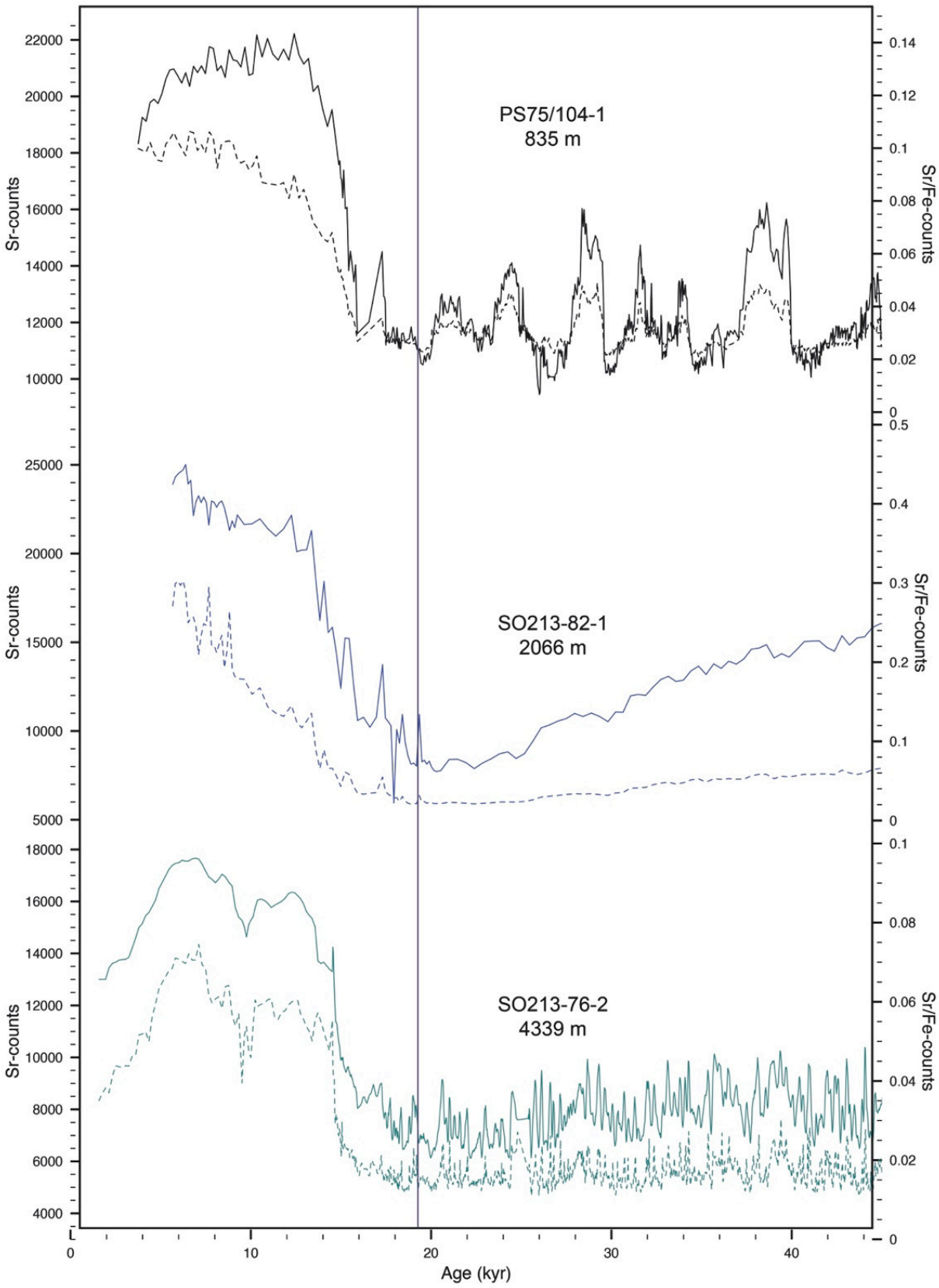

Figure 3.S9: Comparison of Sr- (solid lines) to Sr/Fe-counts (stippled lines). The early increase in Sr-counts at ~19.7 kyr (vertical line) that is obvious in some cores shown in Fig. 3.S8 is detrended, when using Sr/Fe instead, enabling a better core-to-core correlation.

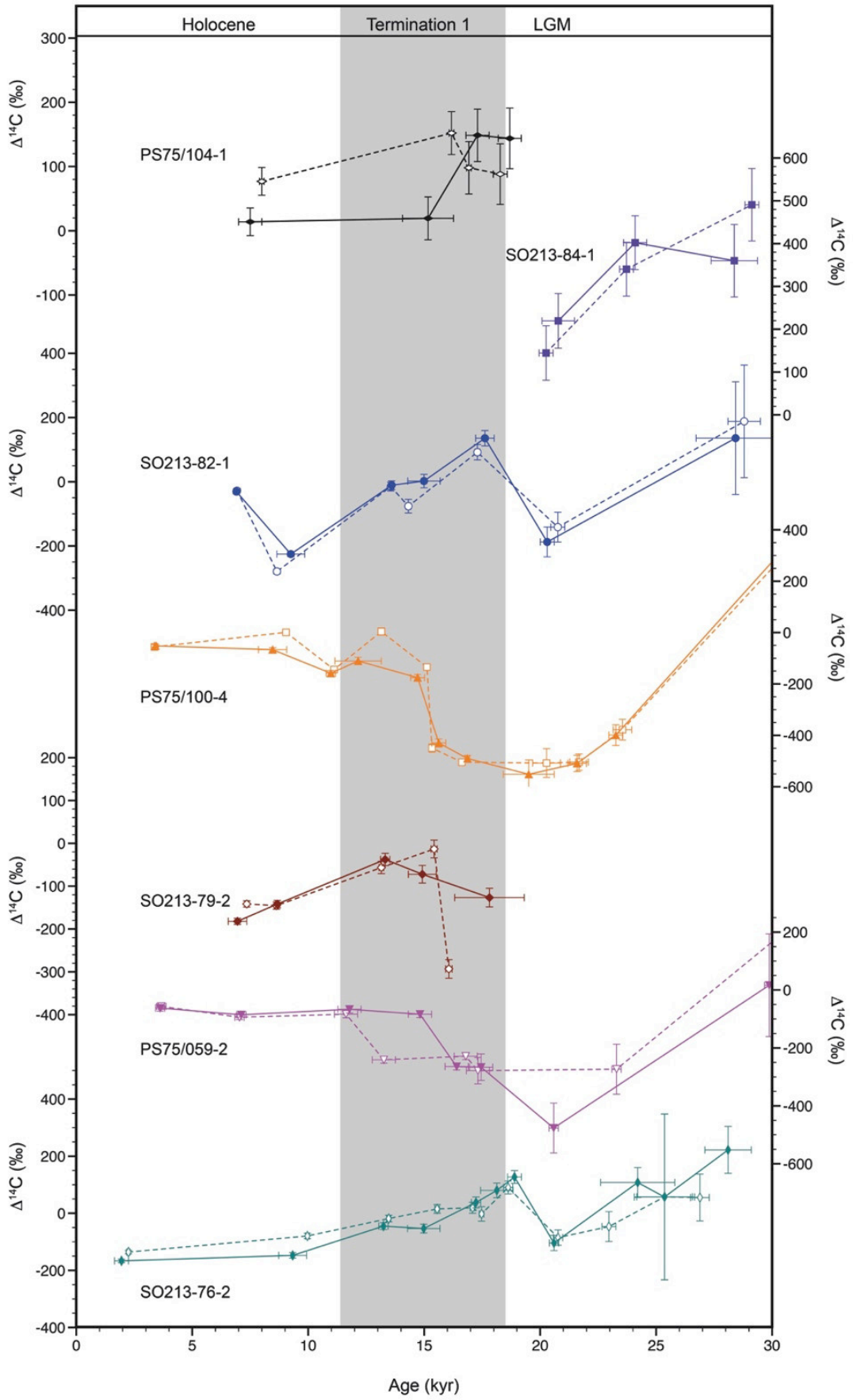

Figure 3.S10: Comparison of $\Delta^{14}C$ records generated using different age models. The solid lines are based on the XRF-correlation-method, while the stippled lines are based on calibrated planktic ^{14}C ages.

Chapter 4

Pushing the boundaries: Glacial / Interglacial variability of SW-Pacific intermediate-water over the last 350,000 years

Thomas A. Ronge[1], Silke Steph[1], Ralf Tiedemann[1], Matthias Prange[2], Ute Merkel[2], Dirk Nürnberg[3], Gerhard Kuhn[1]

[1] Alfred Wegener Institute Helmholtz Center for Polar and Marine Research, Bremerhaven, Germany

[2] University of Bremen – MARUM and Geoscience Department, Bremen, Germany

[3] GEOMAR Helmholtz Center for Ocean Research, Kiel, Germany

Correspondence to: T. Ronge, Thomas.Ronge@awi.de

Under review at *Paleoceanography*

Abstract

Glacial/interglacial changes in Southern Ocean's air-sea gas exchange have been considered as important mechanisms contributing to the glacial/interglacial variability in atmospheric CO_2. Hence, understanding past variability in Southern Ocean intermediate- to deep-water chemistry and circulation is fundamental to constrain the role of these processes on modulating glacial/interglacial changes in the global carbon cycle. Our study focused on the glacial/interglacial variability in the vertical extent of southwest Pacific Antarctic Intermediate Water (AAIW). We compared carbon and oxygen isotope records from epibenthic foraminifera of sediment cores bathed in modern AAIW and Upper Circumpolar Deep Water (UCDW; 943 – 2066 m water depth) to monitor changes in water mass circulation spanning the past 350,000 years. We propose that pronounced freshwater input by melting sea ice into the glacial AAIW significantly hampered the downward expansion of SW-Pacific AAIW. This process led to a pronounced upward displacement of the AAIW-

UCDW interface during colder climate conditions and therefore to an expansion of the glacial carbon pool.

4.1 Introduction

In the Southern Ocean, Antarctic Intermediate Water (AAIW) forms in regions close to the Subantarctic Front (SAF; Bostock et al., 2013a; Georgi, 1979; Piola and Georgi, 1982). Off New Zealand, in the SW-Pacific, the SAF meanders between 45° and 55° S (Fig. 4.1; Crundwell et al. (2008). South of the Chatham Rise, in our research area, the intermediate waters originate directly from the Antarctic Circumpolar Current (ACC; Hayward et al., 2002), while the waters to the North derive from the Coral and Tasman Seas (Bostock et al., 2013a; Tomczak and Godfrey, 1994). Bostock et al. (2013a) refer to the intermediate waters, formed in a small region close to the SAF off New Zealand as Southern Ocean (SO) AAIW. This SO AAIW forms from upwelled nutrient- and CO_2-rich Circumpolar Deep Water (CDW). Accordingly, AAIW's chemical signature carries information about the efficiency of the biological pump and air-sea gas exchange (Sigman et al., 2010). Simplified, the remaining nutrient concentration of sinking AAIW is a measure of the difference of upwelled nutrients and biological consumption in the uppermost water column, while the overturning intensity is modified by the strength of the wind-induced upwelling. The associated processes within this loop from upwelling to sinking are crucial for the oceanic release or uptake of atmospheric CO_2.

During the past, the transport of AAIW was crucial for the redistribution of nutrients, heat and freshwater (Schmitz, 1995; Toggweiler and Dixon, 1991) within the global ocean. On glacial/interglacial timescales, climate signals of upwelling deep-water were transported to the major ocean basins within the AAIW (Marchitto et al., 2007; Stott et al., 2009; Basak et al., 2010; Bryan et al., 2010) and, at least during the last Deglacial, AAIW displayed an important indicator for the transport of CO_2 from old deep water masses (CDW) to the

atmosphere. Today, most of the anthropogenic CO_2 entering the ocean depths is contained within AAIW (Downes et al., 2010; Murata et al., 2010; Murata et al., 2007; Sabine et al., 2004). The importance of the oceanic uptake of CO_2 (not only via AAIW) becomes evident by the fact that without this process, the atmospheric CO_2 concentration would be about 55 ppm higher than it is today (~400 ppm; Sabine et al., 2004). Despite the importance of AAIW for the global climate, especially in view of the current climate change, only scarce information about the temporal changes in its vertical and lateral expansion exists. In this study, we present new epibenthic $\delta^{13}C$ and $\delta^{18}O$ records from the Chatham Rise and the Tasman Sea off New Zealand that span the last 350 kyr. In comparison to a previously published record from sediment core MD97-2120 (1210 m; 45°32S 174°55E; Pahnke and Zahn, 2005) we are able to constrain the vertical extent of AAIW over different climatic cycles by using isotope records from multiple sediment cores from different water depths.

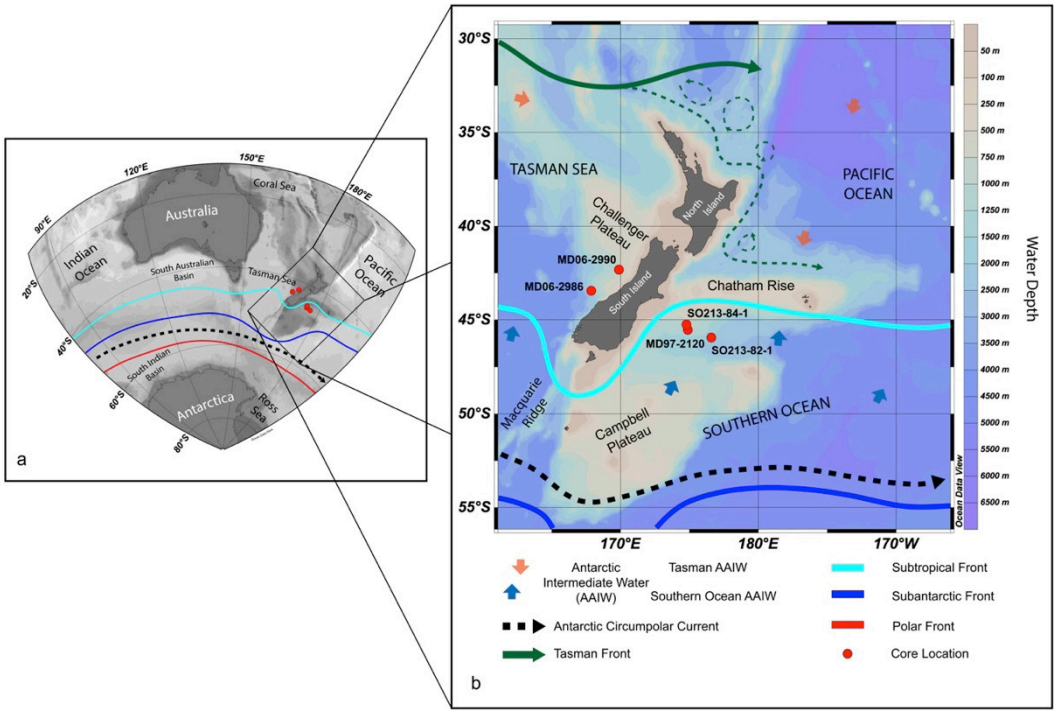

Figure 4.1: Bathymetric and oceanographic map of the study area showing the major oceanic fronts and current systems in the Southern Ocean. a) Supraregional overview map of the SW-Pacific and Indian Sector of the Southern Ocean. b) Regional setting of the New Zealand subcontinent (After Bostock et al., 2013b; Crundwell et al., 2008; Orsi et al., 1995).

4.2 Material and Methods

We analyzed four sediment cores from the Tasman Sea and the Bounty Trough off New Zealand, collected during R/V *Marion Dufresne* MD152 and R/V *Sonne* SO213/2 (Proust et al., 2006; Tiedemann, 2012) cruises in 2006 and 2011, respectively. Cores MD06-2990 (943 m; 42°19S 169°55E) and MD06-2986 (1477 m; 43°27S 167°54E) were collected in the Tasman Sea west of New Zealand. Cores SO213-84-1 (972 m; 45°07S 174°34E) and SO213-82-1 (2066 m; 45°46S 176°36E) are located on the eastern side of the island, in the Bounty Trough south of the Chatham Rise. Today, SO213-84-1 and MD06-2990 are bathed by AAIW, MD06-2986 and SO213-82-1 on the other hand by Upper Circumpolar Deep Water (UCDW). The uppermost part of MD06-2990 was significantly disturbed during core recovery. We therefore used the top section of R/V *Sonne* core SO136-003 (42°17.74'S / 169°52.66'E; 958 m water depth; (Thiede, 1999) to replace the affected sediment sequence (see description of the age model for additional information). The core SO213-82-1 yields an average sedimentation rate of 3 cm/kyr, SO213-84-1 shows a sedimentation rate of 6 cm/kyr while MD06-2986 and MD06-2990 yield sedimentation rates of 8 cm/kyr and 3 cm/kyr, respectively. The working-halves of both SO213 cores were sampled at 2 cm intervals. The top 13.50 m of core MD06-2990 (33.55 m length) and the top 2.50 m of core SO136-003 were sampled at 2 cm intervals, core MD06-2986 (32.68 m length) was sampled at 4 cm intervals. Subsequently the samples were frozen and freeze-dried for two to three days, depending on the samples' water content. After freeze-drying, the samples were wet sieved through a sieve with a mesh size of 63µm and dried for two days at ~50°C. When dry, the samples were fractionated through different mesh sieves (125 µm, 250 µm, 315 µm and 400 µm). The foraminifera were picked from the size fractions 250-315 µm and 315-400 µm using a reflective light microscope with a 50-fold magnification.

4.2.1 Stable Isotopes

Isotope ratios (reported in delta notation versus VPDB calibrated via international standard NBS19) of $\delta^{13}C$ and $\delta^{18}O$ were measured on 4 specimens of *Cibicidoides wuellerstorfi* or in samples lacking a sufficient amount of *C. wuellerstorfi*, on 3 specimens of *Uvigerina peregrina* (Fig. 4.2). All measurements were conducted at the Alfred Wegener Institute in Bremerhaven, using a *Finnigan MAT 253* mass spectrometer with a *Kiel IV Carbonate Device*. The long-term precision based on an internal laboratory standard (Solnhofen limestone) measured over a one-year period together with samples was better than ±0.06‰ for $\delta^{13}C$ and ±0.08‰ for $\delta^{18}O$.

In all cores but one we were able to find sufficient specimens of *C. wuellerstorfi* over the whole record to perform the isotope measurements. Sediment core SO213-82-1 presents us with the problem that in sporadic samples, no *C. wuellerstorfi* could be found, so that we used *U. peregrina* to fill these gaps.

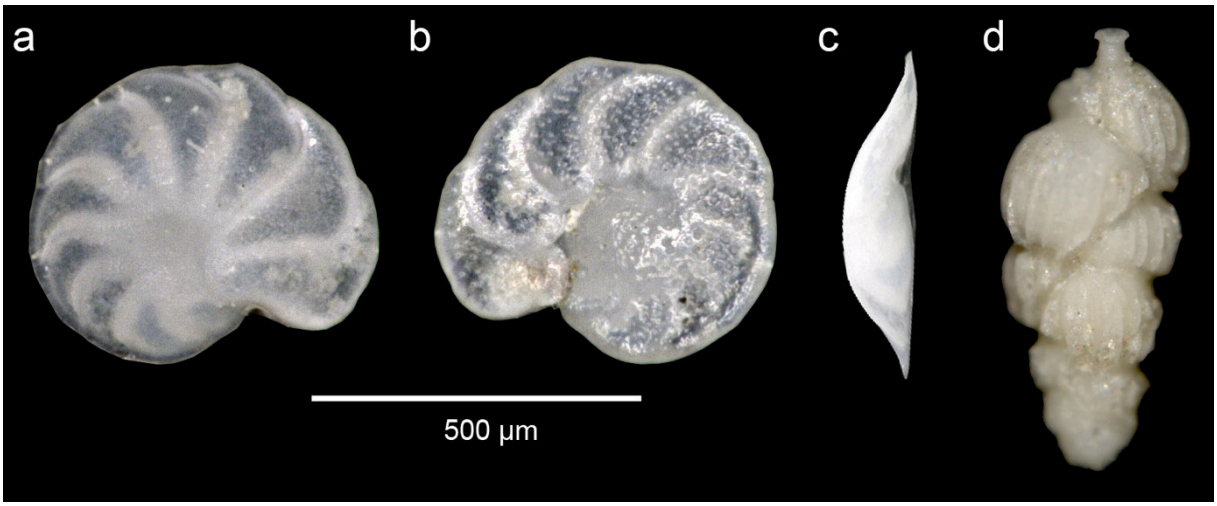

Figure 4.2: Pictures of foraminifera, used for isotopic measurements. Umbilical view a), spiral view b) and apertural view c) of *Cibicidoides wuellerstorfi*. Figure 4.2 c was digitally rendered from figure 4.2 a using a *Keyence VHX-5000* digital microscope. d) Lateral view of *Uvigerina peregrina*.

4.2.1.1 Oxygen Isotopes

Primarily, we used the benthic $\delta^{18}O$-signal for the development of our age-models. In addition to changes in global ice volume (Shackleton, 1977), which provide the stratigraphic basis in our study, the benthic $\delta^{18}O$-signal reflects variations in local temperature and/or salinity (Emiliani, 1955; Epstein and Mayeda, 1953). In general, the $\delta^{18}O$-values recorded by *C. wuellerstorfi* deviate by ~0.64‰ from *U. peregrina* values (Shackleton and Opdyke, 1973). The $\delta^{18}O_{Cib\ \&\ Uvi}$ values in the records of SO213-84-1 and SO213-82-1 show a very high correlation with a mean offset *C. wuellerstorfi* – *U. peregrina* of 0.48‰. Therefore, we used this offset of 0.48‰ to correct the Bounty Trough $\delta^{18}O$ values of *C. wuellerstorfi* for species-specific fractionation (McCave et al., 2008; Pahnke & Zahn, 2005) instead of using an offset of 0.64‰ (Duplessy et al., 1988; Shackleton and Opdyke, 1973). However, the Tasman Sea records MD09-2986 and MD06-2990/SO136-003 were rendered Uvi-equivalent by adding 0.64‰, as these records are in good agreement with the accepted method.

4.2.1.2 Carbon Isotopes

In paleoceanography, the epibenthic $\delta^{13}C$-records of the foraminifer *C. wuellerstorfi* are commonly used as a proxy for changes in water mass nutrient concentrations (Kroopnick, 1985; Zahn et al., 1991). The $\delta^{13}C$-values in the water column strongly depend on the remineralization of ^{12}C-enriched organic matter, which leads to the consumption of oxygen and the release of nutrients. Low $\delta^{13}C$-values are therefore indicative of high nutrient concentrations and weakly ventilated water masses. Furthermore, oceanic $\delta^{13}C$-values are influenced by the release of terrestrial carbon during glacial times (Peterson et al., 2014) as well as by thermodynamic (Broecker and Maier-Reimer, 1992) and biological effects (Farquhar et al., 1989).

As described above, we used *U. peregrina* to fill the intervals barren of *C. wuellerstorfi*. Following the methods of Pahnke and Zahn (2005) and McCave et al. (2008), we disregarded the usual +0.9‰ *U. peregrina* to *C. wuellerstorfi* offset. As these authors showed, the epi- to infaunal $\delta^{13}C$ difference off New Zealand is far from constant but varies on glacial to interglacial timescales as a function of $\delta^{18}O_{Uvi}$. Over the whole record, the average offset $\Delta\delta^{13}C_{Cib\text{-}Uvi}$ is 0.81‰ and therefore close to the offset of 0.9‰. However, the addition of 0.9‰ proves to be impractical for the conversion of $\delta^{13}C_{Uvi}$ in SO213-82-1, if just the epi- to infaunal offset of the Holocene and the LGM are compared. During the Holocene, the mean $\Delta\delta^{13}C_{Cib\text{-}Uvi}$ of SO213-82-1 is as high as 1.09‰ while the LGM offset is only 0.47‰. To account for this variable offset, we used the regression equation of McCave et al. (2008):

$$\Delta\delta^{13}C_{Cib\text{-}Uvi} = 0.464\delta^{18}O_{Uvi} - 2.753 \; (r=0.629;\; n=57)$$

A comparison of raw isotopic data to the corrected values of SO213-82-1 is shown in figure 4.3.

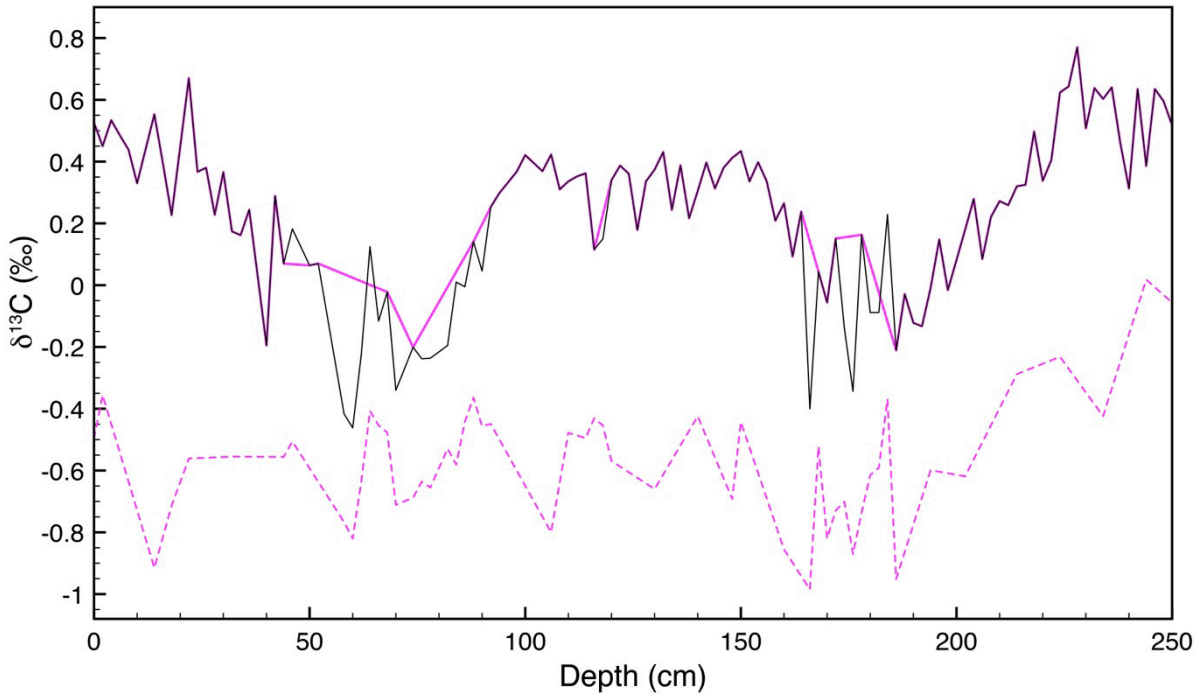

Figure 4.3: Comparison of benthic $\delta^{13}C$ values in sediment core SO213-82-1. Raw data of *C. wuellerstorfi* (pink line) and *U. peregrina* (stippled pink line). The black line shows a combination of *C. wuellerstorfi* and corrected *U. peregrina* values.

4.2.2 Sea surface temperature reconstructions

The Mg/Ca measurements were conducted on ~30 tests of the planktic foraminiferal species *Globigerina bulloides*, picked from the size fraction 355-400 µm. Sample treatment and analyses followed the procedure as described in Nürnberg and Groeneveld (2006). We followed the cleaning protocol of Barker et al. (2003), applying only the oxidative cleaning step. All samples were measured at Kiel University, using an ICP-AES (*ISA Jobin Yvon-Spex Instruments S.A. GmbH*). The relative analytical error for the Mg/Ca was ~0.1%. Replicate samples showed an average standard deviation of ~0.1 mmol/mol.

Mg/Ca data were converted into paleo-seasurface temperatures ($SST_{Mg/Ca}$), using the calibration of Mashiotta et al. (1999) for *G. bulloides*:

$$Mg/Ca = 0.474\ e^{(0.107 * T)} \text{ with } R^2 = 0.98$$

4.2.3 Total Organic Carbon

In order to assess the influence of phytodetritus (high in ^{12}C) on the benthic $\delta^{13}C$ signals, we measured the total organic carbon content (TOC) on sediment cores SO213-82-1 and SO213-84-1 (Bounty Trough), with a spacing of 10 cm, using a PC controlled Eltra CS-2000 Carbon Sulfur element analyzer. We reconstructed the organic carbon accumulation rates (TOC_{AR}) as follows:

$$TOC_{AR}\ (g/cm^2/kyr) = \text{sedimentation rate (cm/kyr)} * \text{dry density } (g/cm^3)/10$$

4.2.4 Age determination

Our age models reflect a combination of radiocarbon dating and $\delta^{18}O$-correlation to age scaled reference records. The age model for the upper section of cores MD06-2986 and MD06-2990/SO136-003, SO213-82-1 and SO213-84-1 is based on Accelerator Mass Spectrometry (AMS) ^{14}C dates. AMS ^{14}C dating was performed on mixed planktic

foraminifera (MD06-2986, 8 samples; Table A3.1), on *Globorotalia inflata* (SO136-003, 6 samples; Table A3.1) or on *Globigerina bulloides* (SO213-82-1, 7 samples; SO213-84-1, 3 samples; Ronge et al., submitted to Science, 2014). The samples were prepared and analyzed in the Leibniz-Laboratory for Radiometric Dating and Isotope Research at the Christian-Albrechts-University of Kiel (MD06-2986), at the AMS ^{14}C Laboratory at the Eidgenössische Technische Hochschule (ETH) Zürich (SO136-003) and at the NOSAMS facility in Woods Hole, USA (SO213-82-1 and SO213-84-1). AMS ^{14}C ages were converted to calendar ages using Calib 7.0 of (Stuiver et al., 2005), applying a local reservoir correction of 640 years for interglacial (cf. Sikes et al., 2000; Pahnke and Zahn, 2005) and 840 years for glacial age samples (Ronge et al., submitted to Science, 2014). Beyond the range of radiocarbon dating, the age scale for our cores was obtained by correlating the benthic oxygen isotope records (mainly indicative of changes in global ice volume) with the astronomically dated LR04 global benthic δ^{18}O reference stack (Lisiecki and Raymo, 2005; Fig. 4.4). In the course of this process, we combined the benthic δ^{18}O records for cores SO136-003 and MD06-2990. The uppermost part comprising the interval of Marine Isotope Stage (MIS) 1 to MIS 4 (0 – 65 kyr) is based on SO136-003, while the record below, down to 350 kyr (MIS 4 to MIS 10) is based on MD06-2990. Tuning our benthic δ^{18}O records to the LR04 stack resulted in a generally good agreement with the previously published benthic δ^{18}O record of core MD97-2120, collected from 1200 m water depth on Chatham Rise east of New Zealand (Fig. 4.4; Pahnke and Zahn, 2005). To further improve our age models, we fine-tuned the epibenthic δ^{18}O records of MD06-2986 and MD06-2990/SO136-003 to the benthic δ^{18}O record of MD97-2120.

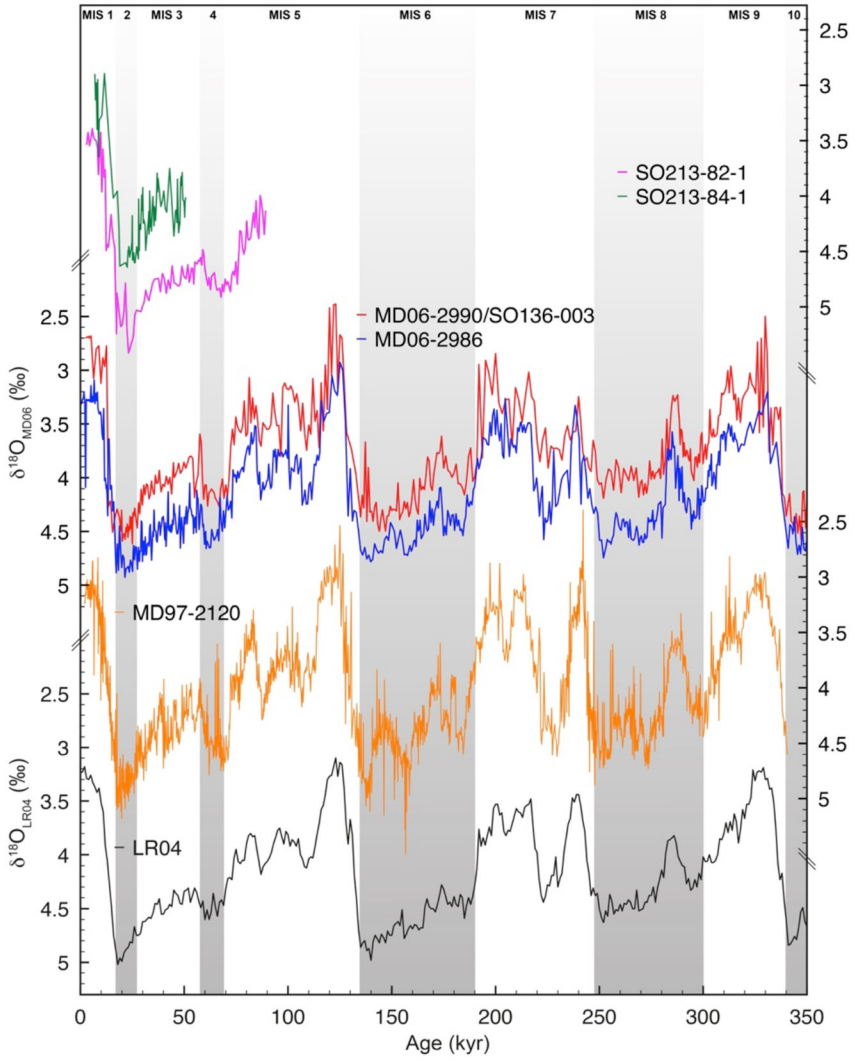

Figure 4.4: Benthic $\delta^{18}O_{Cw}$ isotope records. Bounty Trough sediment cores SO213-82-1 (pink) and SO213-84-1 (green); Tasman sea records MD06-2986 (blue) and MD06-2990 (red). Isotope record of MD97-2120 (orange; Pahnke and Zahn, 2005). Benthic stack LR04 (black; Lisiecki and Raymo, 2005). Marine Isotope Stages: MIS 1 to MIS 10. Grey shadings indicate glacial maxima.

4.2.5 Climate Modeling

In order to test hypothesized mechanisms that may have affected the characteristics and distribution of AAIW during glacial climates, we analyzed results from a glacial climate simulation using the Community Climate System Model version 3 (CCSM3). CCSM3 is a state-of-the-art fully coupled global general circulation model which is composed of four components representing the atmosphere, the ocean, the land surface and sea ice (Collins et al., 2006). For the simulation in this study, the atmosphere model has a resolution of ~3.75° (T31 spectral truncation) with a vertical discretization of 26 levels, while the ocean and sea-ice components are run on a nominal 3° grid with 25 levels in the ocean (Yeager et al., 2006).

Besides a pre-industrial control run, a simulation of the LGM has been carried out (Merkel et al., 2010). This simulation takes into account the orbital parameters, the greenhouse gas concentrations and the ice-sheet distribution of the LGM (21 kyr before present). Moreover, a sea level lowering of 120 m has been taken into account by a modification of the land-sea distribution, which for instance, leads to closure of the Bering Strait. For details of the experimental setup and spin-up procedure to obtain statistical equilibrium climates, the reader is referred to Merkel et al. (2010).

4.3 Results

Here we present proxy-records from the four sediment cores described in section 4.2, which are indicative of changes in SST-variability (planktic Mg/Ca), intermediate- and deep-water circulation (benthic $\delta^{13}C$ and $\delta^{18}O$) and biogenic productivity (TOC_{AR}) in our study area. These records allow us to register climate-driven variations in the vertical extent of AAIW and UCDW. The two Tasman Sea records MD06-2086 and MD06-2990 span at least the last four glacial/interglacial cycles from 0 to 350 kyr, while SO213-84-1 and SO213-82-1 form the Bounty Trough do not exceed the last 100 kyr.

The close correlation of the Bounty Trough and Tasman Sea isotopic-records in both AAIW (Fig. 4.5 top) and UCDW (Fig. 4.5 bottom) enables us to compare the water masses on both sides of the island.

4.3.1 Benthic $\delta^{13}C$

All sediment cores analyzed show similar $\delta^{13}C$ patterns over the whole time interval, oscillating between glacial lows and interglacial highs, with a mean offset of ~0.7‰ between the AAIW and UCDW. The sediment cores bathed by modern AAIW (SO213-84-1 and MD06-2990) and by modern UCDW (SO213-82-1 and MD06-2986) show similar isotopic

values, alternating between ~0.6 and 1.2‰ and ~ -0.2 and 0.8‰, respectively (Table A3.2). Nevertheless, minor differences between Tasman Sea and Bounty Trough δ^{13}C-values are evident especially during the last glacial (Fig. 4.5). Throughout the LGM, the isotopic minima in Bounty Trough cores SO213-84-1 (AAIW) and SO213-82-1 (UCDW) are more pronounced than in their Tasman Sea counterparts. Therefore we would like to mention that the δ^{13}C-values of the respective time-interval from core SO213-82-1 partly derive from adjusted *U. peregrina* values. Despite similar amplitudes in SO213-84-1 and SO213-82-1 a certain bias, introduced by the recalculation of *U. peregrina* values in SO213-82-1 cannot be completely excluded. In this context, it is noteworthy that the amplitudes for MIS 4 are nearly identical for SO213-82-1 and MD06-2986 as both records exclusively base on *C. wuellerstorfi* (Fig. 4.5).

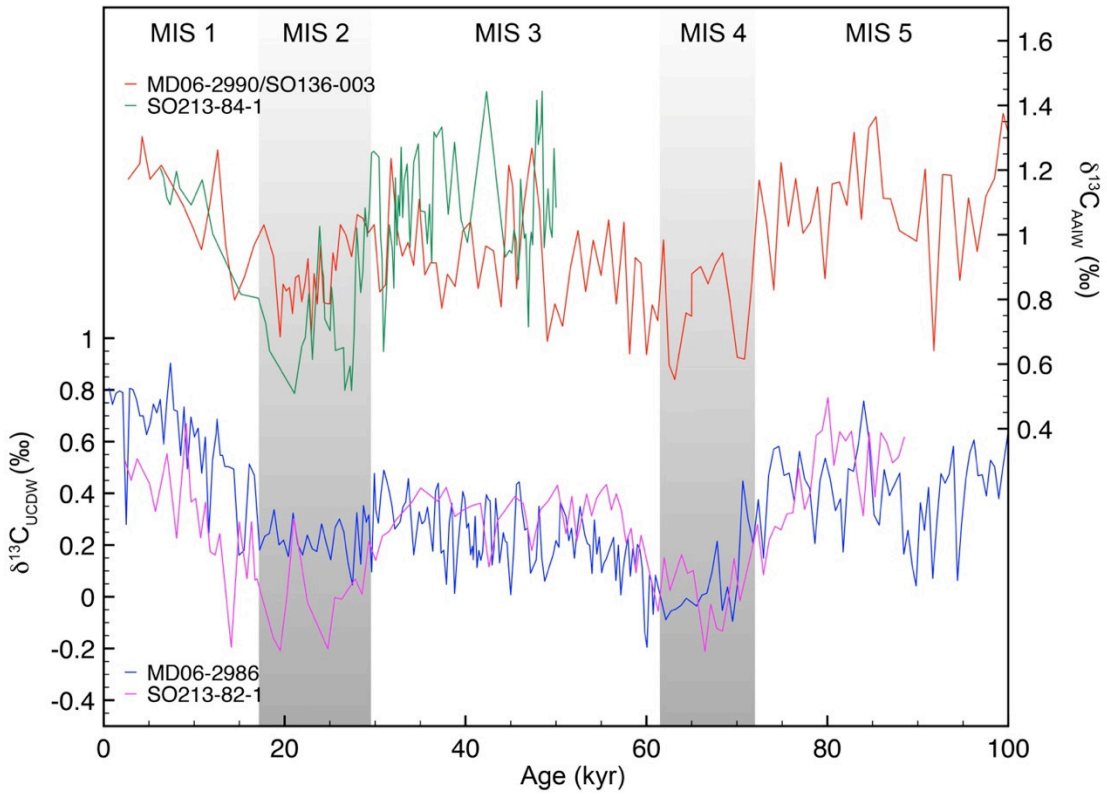

Figure 4.5: Comparison of Bounty Trough (SO213) and Tasman Sea (MD06) AAIW and UCDW benthic δ^{13}C records. Throughout the whole time interval MD06-2986 (blue) and SO213-82-1 (pink) are bathed by UCDW, while MD06-2990/SO136-003 (red) and SO213-84-1 (green) are bathed by AAIW. Grey shadings as shown in figure 4.4. The pronounced offset of SO213-82-1 and MD06-2986 during MIS 2 might derive from the use of *U. peregrina* in SO213-82-1 in this time interval.

4.3.2 Benthic $\delta^{18}O$

Except for SO213-82-1, where occasional samples of *U. peregrina* had to be analyzed to complement the record in depths barren of *C. wuellerstorfi* (see methods), benthic $\delta^{18}O$ records were measured on monospecific samples of *C. wuellerstorfi*.

All records display similar distinctive glacial-interglacial cycles. The variability of the epibenthic $\delta^{18}O$ ($\delta^{18}O_{Cw}$) signal in our sediment cores reflects to a large part changes in global ice volume (Shackleton, 1977). Yet the fact that the glacial/interglacial $\delta^{18}O_{Cw}$ amplitudes of up to ~2 ‰ in all cores generally exceed the sea level-related mean ocean $\delta^{18}O$ change of 0.8 to 1.1 ‰ (e.g. Waelbroeck et al., 2002) indicates that a relevant portion of the $\delta^{18}O_{Cw}$ signal can be attributed to changes in water temperature and/or salinity (Emiliani, 1955; Epstein and Mayeda, 1953). Although the glacial/interglacial $\delta^{18}O_{cw}$ amplitudes are very similar in our records, $\delta^{18}O_{Cw}$ at the shallow cores MD06-2990/SO136-003 (945 m) and SO213-84-1 (972 m) was generally lower than at the deeper core sites MD06-2986 (1477 m) and SO213-82-1 (2066 m) during the last four glacial/interglacial cycles (on average ~0.46‰). This pattern points to higher temperatures and/or lower salinity in the intermediate-water (Fig. 4.4).

4.3.3 Total Organic Carbon

The TOC_{AR} for cores SO213-82-1 and SO213-84-1 range from 0.26 to 0.58 g/cm^2/kyr and 0.38 to 1.39 g/cm^2/kyr, respectively (Table A3.3). Due to these low TOC_{AR} values (less than 1.5 g/cm^2/kyr), we assume that the $\delta^{13}C$ results measured on the epibenthic foraminifer species *C. wuellerstorfi* were not affected by the Phytodetritus Effect (Mackensen et al., 1993).

4.3.4 Modeling study

The overall distribution of South Pacific water masses with the characteristic low-salinity tongue of AAIW is clearly expressed in the pre-industrial control simulation with the CCSM3 model (Fig. 4.6 a,c). Compared to observations, however, AAIW forms too far north which is likely related to simulated Southern Westerly Winds (SWW) that are biased towards north (Varma et al., 2011), a common shortcoming in most coarse-resolution climate models (e.g. Rojas et al., 2009). Moreover, the modeled AAIW is too shallow and too salty, despite a surface low-salinity bias south of ~40°S (Fig. 4.6 a,c). These model-data mismatches hamper direct geographical comparisons with proxy records from a specific location and imply that changes in the South Pacific hydrography are likely simulated somewhat too far north. Nevertheless, since the model captures the large-scale water masses relevant for this study, the model results are helpful in explaining glacial-interglacial changes of water mass characteristics and water mass distribution. In particular, enhanced surface freshwater input near the AAIW formation regions from melting sea ice in the LGM simulation (Fig. 4.6 b) leads to further freshening of the glacial AAIW (<33.5 psu) which spreads towards the north at a much shallower depth compared to the modern (Fig. 4.6 d).

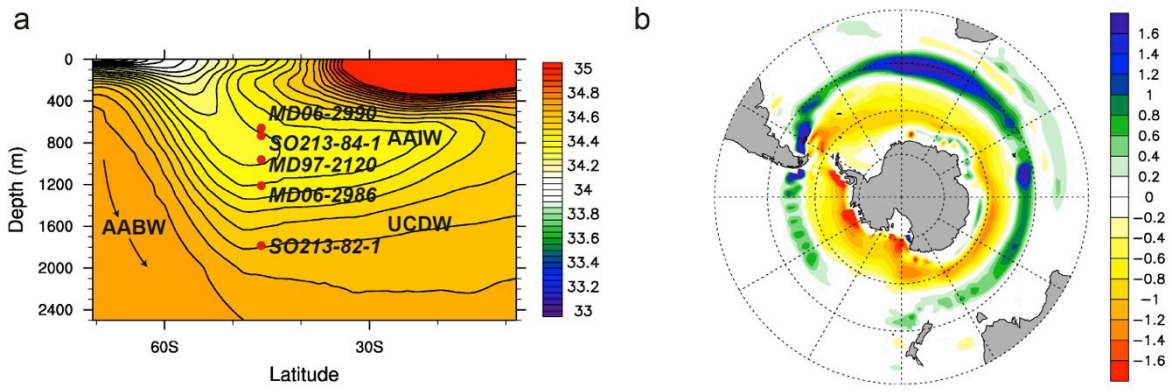

Figure 4.6: Pacific salinity distributions. a) Observed present-day salinity, zonally averaged across the South Pacific (WOA; Antonov et al., 2010). Red dots indicate the approximate water depth of sediment cores used in this study. b) Modeled LGM Southern Ocean surface freshwater flux anomaly (m/yr; positive means freshwater flux into the ocean) relative to pre-industrial (annual mean; 100-yr average).

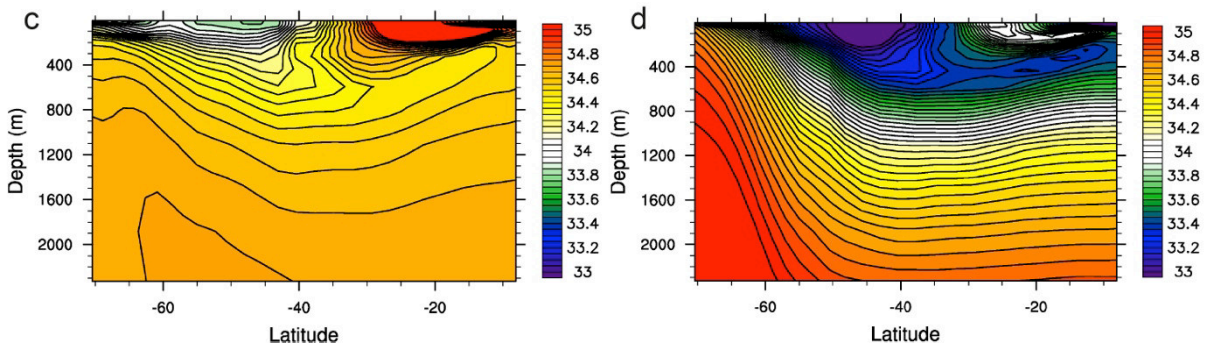

Figure 4.6 continued: Pacific salinity distributions. c) Modeled pre-industrial salinity, zonally averaged across the South Pacific (annual mean; 100-yr average). d) As c) but for the LGM (salinity adjusted such that global mean salinity is identical to pre-industrial). AAIW – Antarctic Intermediate Water; UCDW – Upper Circumpolar Deep Water; AABW – Antarctic Bottom Water.

4.4 Discussion

The most obvious result of our study is the constant offset of AAIW to UCDW $\delta^{13}C$ over the last 350 kyr, indicating no significant changes in water mass geometry. However, this interpretation is revealed as spurious by including another record bathed in modern AAIW-depth (MD97-2120; 1210 m; Pahnke and Zahn, 2005), located between the records obtained from in this study, right at the boundary from AAIW to UCDW (Fig. 4.7).

Today, SW-Pacific AAIW extends from ~500 m to about 1450 m (Hayward et al., 2002; Heath, 1985; Sloyan et al., 2010). Below, in depths between 1450 m and 2500 m follows UCDW (Carter and McCave, 1997) with its distinctive oxygen minimum and CO_2 maximum (Bostock et al., 2013b and references therein). This pattern locates the sediment cores MD06-2990/SO136-003 (943/958 m) and SO213-84-1 (972 m) close to the core of modern AAIW, today at about 700 m (Heath, 1985). The deep-water cores MD06-2986 (1477 m) and SO213-82-1 (2066 m) are therefore located in UCDW. Despite the proximity of MD06-2986to the interface of AAIW and UCDW (Fig. 4.7), the very close correlation with the deeper core SO213-82-1 illustrates that MD06-2986 remained in UCDW throughout the last 100 kyr (Fig. 4.5). Therefore we infer that this setup was maintained over the whole record of 350 kyr. This

leaves MD97-2120 (1210 m) that also lies close to the intersection of AAIW and UCDW, in a crucial position for the investigation of AAIW extent through time.

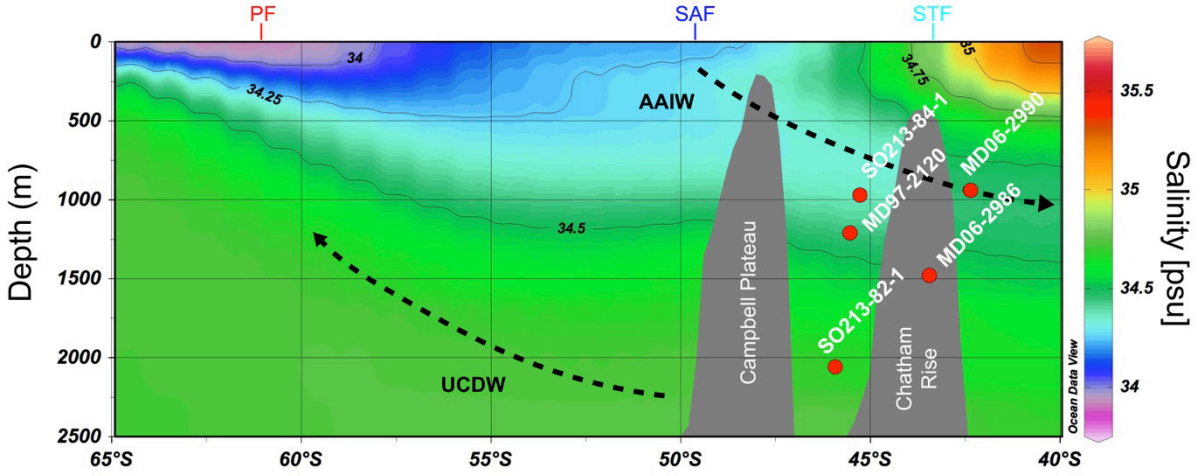

Figure 4.7: Salinity section along the 180° meridian (WOA; Antonov et al., 2010). To project the analysed sediment cores (red dots) in this section, their longitudes were adjusted to 180°. Arrows indicate the prevailing current regime of SW-Pacific water masses. AAIW – Antarctic Intermediate Water; UCDW – Upper Circumpolar Deep Water; PF – Polar Front; SAF – Subantarctic Front; STF – Subtropical Front.

As it was explained in section 4.3.1, the $\delta^{13}C$-gradient between SO213-84-1/MD06-2990/SO136-003 (AAIW) and SO213-82-1/MD06-2986 (UCDW) remained stable for the last 350 kyr (~0.7‰). Therefore we argue that the cores, interpreted as AAIW and UCDW were bathed by these respective water masses throughout the whole time interval. Accepting this general framework, we can use the record of MD97-2120 (Fig. 4.8; Pahnke and Zahn, 2005) to reconstruct changes in the vertical extent of AAIW.

During the LGM the $\delta^{13}C_{Cib}$ of AAIW (SO213-84-1 and MD06-2990/SO136-003) and UCDW (SO213-82-1 and MD06-2986) were lower by 0.43‰ and 0.45‰, respectively, than during the Holocene (Table A3.4). Thus this difference fits to the mean whole-ocean $\delta^{13}C$-shift of 0.38±0.08‰ (Peterson et al., 2014) and is clearly lower than the AAIW difference found by Bostock et al. (2010) of 0.8‰ Taking all cycles over the past 350 kyr into account, the isotopic offset between glacials and interglacials for MD06-2990/SO136-003 and MD06-

2986 is 0.19‰ and 0.27‰ respectively. However, the LGM/Holocene offset of MD97-2120 is 0.53‰ and the 350 kyr average offset (MIS1 – MIS9) is 0.41‰. Therefore, we argue that the pronounced depletion in glacial $\delta^{13}C$ of core MD97-2120 indicates an upward displacement of the AAIW-UCDW interface during glacial maxima. As it is shown in Table A3.4, the offset of MD97-2120 to MD06-2990/SO136-003 (943/958 m; AAIW) and MD06-2986 (1477 m; UCDW) is almost equal during interglacials, slightly leaning to the well-ventilated AAIW. However, during glacial maxima the $\Delta\delta^{13}C_{2120\text{-}UCDW}$ decreases to only 0.19‰ while $\Delta\delta^{13}C_{AAIW\text{-}2120}$ increases to 0.52‰.

Throughout the Holocene, the $\delta^{13}C$ values of MD97-2120 resemble those of SO213-84-1, yielding average values of 0.83‰ and 1.14‰, respectively (Fig. 4.8). On the other hand, SO213-82-1 shows significantly lower values of 0.4‰. This pattern reflects the modern water mass distribution (Fig. 4.9), locating MD97-2120 and SO213-84-1 in AAIW and SO213-82-1 in UCDW (Fig. 4.7).

During the Last Glacial Maximum $\delta^{13}C$ of MD97-2120 approaches the values of SO213-82-1 (0.33‰ and 0‰, respectively). Even though the values of SO213-84-1 also decline, they remain at an average of 0.74‰ and thus considerably higher than the deeper cores. The deep-water to intermediate-water difference, $\Delta\delta^{13}C_{84\text{-}82}$ (0.74‰) remains similar to the Holocene offset of 0.74‰. Therefore, on a glacial/interglacial timescale, MD97-2120 appears to alternate between the water masses assigned to the sediment cores above and below, approaching the water mass interpreted as UCDW in glacial times. This pattern is particularly revealed in figure 4.9 (black arrows), where the Glacial-to-Holocene offset in both, $\delta^{13}C$ and $\delta^{18}O$ of MD97-2120 is the largest from all sediment cores.

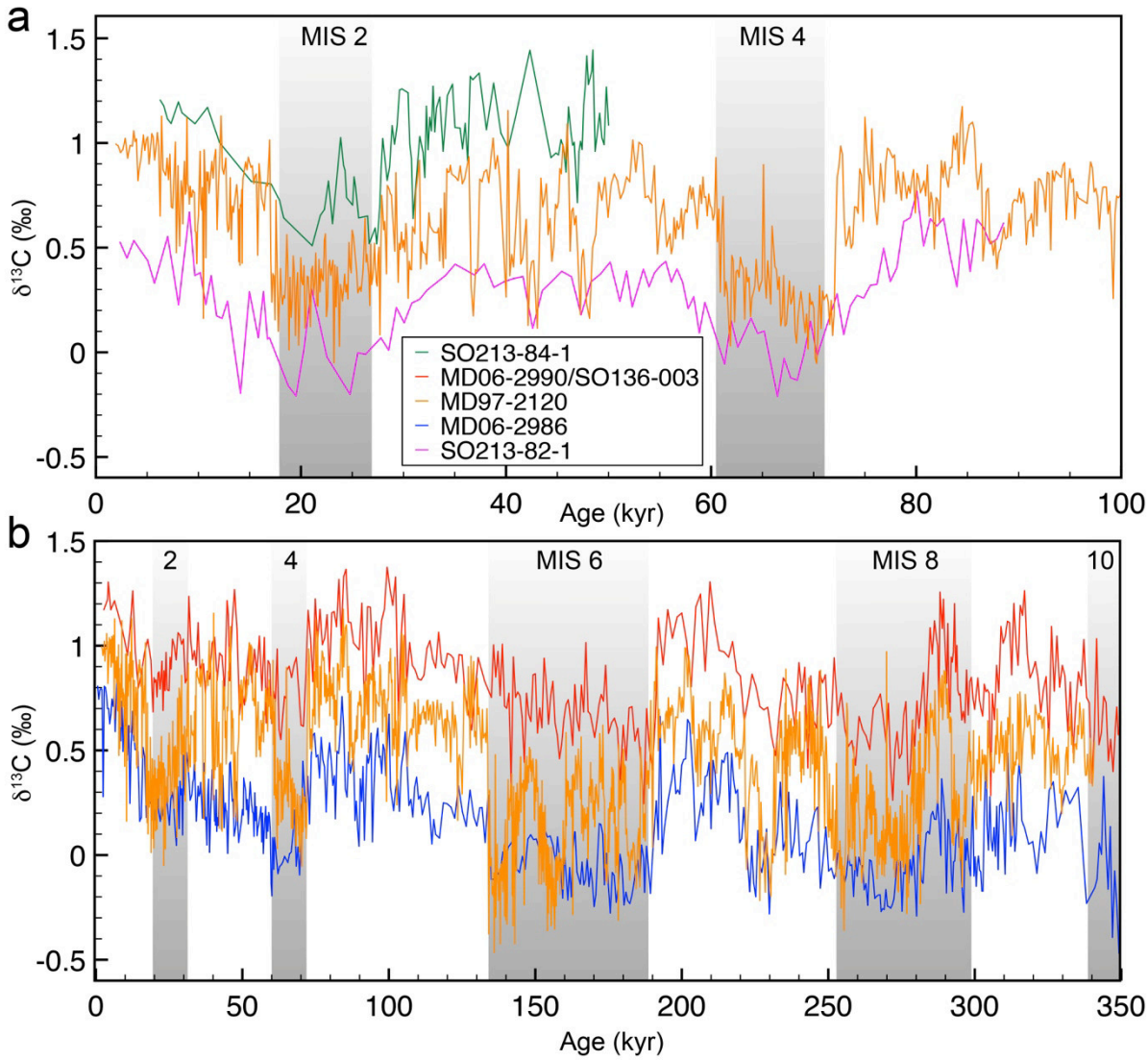

Figure 4.8: Comparison carbon isotope records for the last a) 100 kyr (Bounty Trough) and b) 350 kyr (Tasman Sea) b) to the Bounty Trough record MD97-2120 (Pahnke and Zahn, 2005).

The pattern, with MD97-2120 $\delta^{13}C$ moving towards UCDW values during glacial maxima and towards AAIW during warmer periods, is repeated throughout the whole time interval analyzed (Table 4). We compared MD97-2120 to MD06-2990/SO136-003 and MD06-2986 on longer timescales, as both SO213-cores span only the last glacial to interglacial cycle.

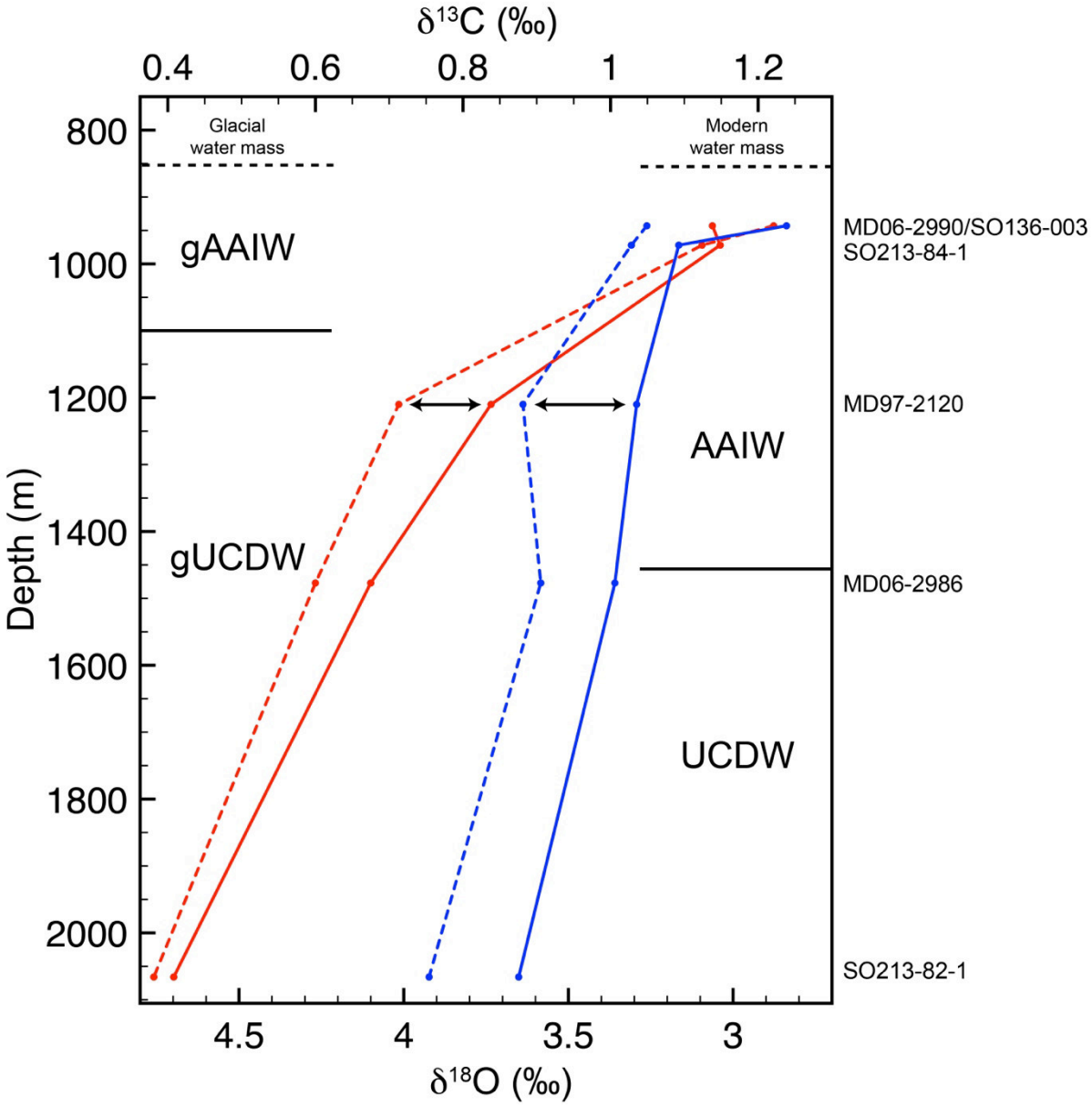

Figure 4.9: Comparison of averaged Holocene (solid lines) and LGM (dashed lines) benthic $\delta^{13}C$ (red) and $\delta^{18}O$ (blue) depth profiles. The glacial $\delta^{13}C$ values were corrected for the global isotopic shift by adding 0.38‰ (Peterson et al., 2014). Glacial $\delta^{18}O$ values were adjusted according to Waelbroeck et al. (2002) by subtracting 1.1‰. Black arrows indicate the pronounced isotopic shift in MD97-2120 caused by the shift from AAIW to UCDW. Glacial water mass distribution (gAAIW & gUCDW) as proposed in chapter 4.4; modern distribution after Heath (1985), Carter and McCave (1997), Hayward et al. (2002) and Sloyan et al. (2010). Sediment core (modern water depths) are indicated on the right axis.

During the warmer stages 3, 5, 7 and 9, the average $\delta^{13}C$ values of the shallowest core MD06-2990/SO136-003 (interpreted as AAIW) are as high as 0.91‰, while MD97-2120 and MD06-2986 display lower averages with 0.6‰ and 0.24‰, respectively The isotopic offset between

MD06-2990/SO136-003 and MD97-2120 ($\Delta\delta^{13}C_{2990\text{-}2120}$) rises in the course of glacial maxima (MIS 6 and MIS 8) from interglacial values of 0.31‰ to a $\Delta\delta^{13}C_{2990\text{-}2120}$ of 0.53‰ (Fig. 4.10 b).

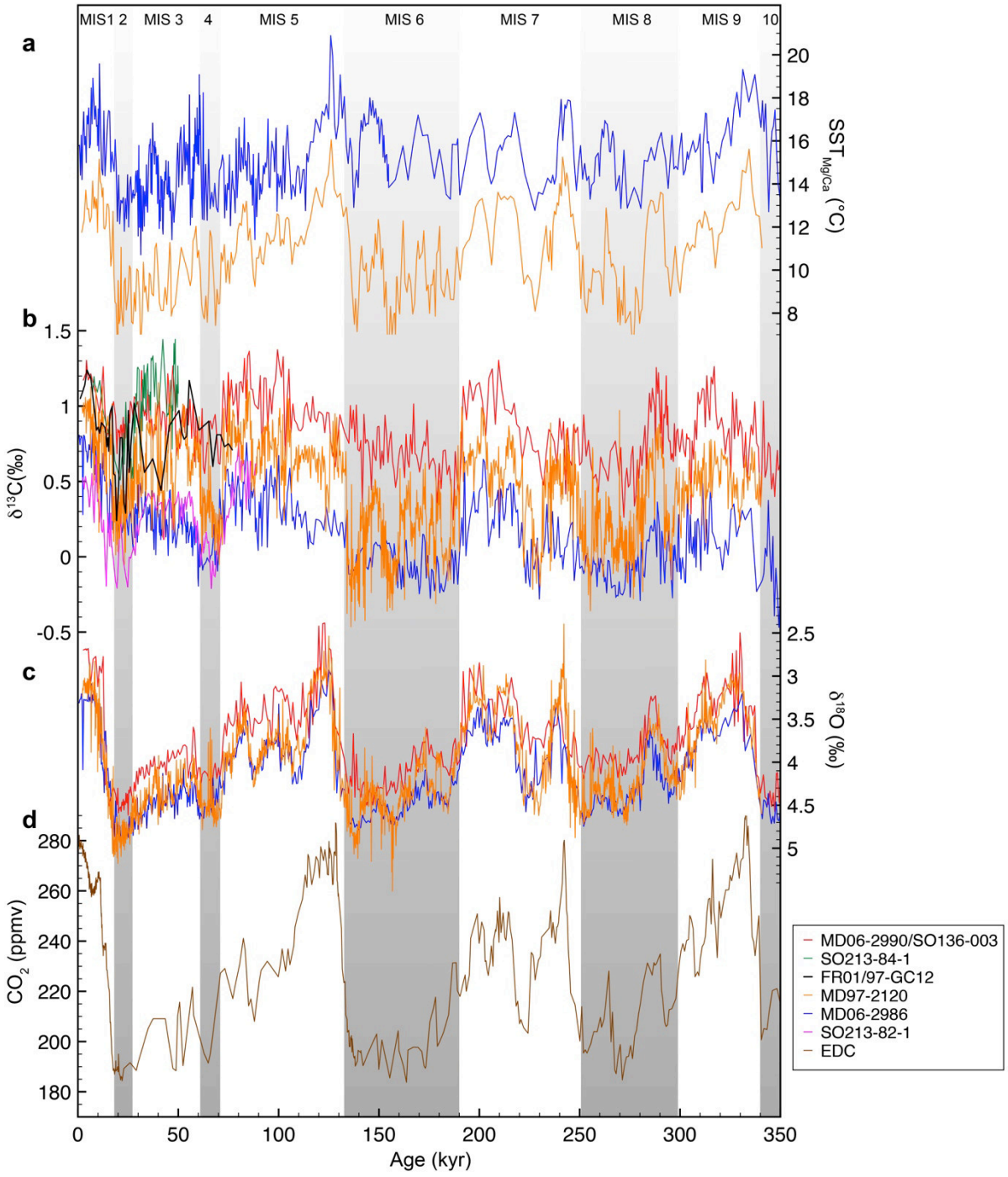

Figure 4.10: Multiple proxy records of SW-Pacific AAIW and UCDW compared to an Antarctic ice core record over the past 350,000 years. a) Planktic $SST_{Mg/Ca}$ of MD97-2120 (orange; Pahnke and Zahn, 2005) and MD06-2986 (blue) measured on *G. bulloides*. b) Benthic (*C. wuellerstorfi*) $\delta^{13}C$ records of Tasman Sea cores MD06-

2986 (blue) and MD06-2990/SO136-003 (red), Bounty Trough cores SO213-82-1 (pink) and SO213-84-1 (green) compared to MD97-2120 $\delta^{13}C$ (orange; Pahnke and Zahn, 2005) and FR1/97-GC12 (black; Bostock et al., 2004). c) Benthic (*C. wuellerstorfi*) $\delta^{18}O$ records of sediment cores MD06-2986 (blue), MD06-2990/SO136-003 (red) and MD97-2120 (orange). d) Composite CO_2 curve for the last 350 ky. (brown; 0-22 ky.: EPICA Dome C, Monnin et al., 2001; 22-350 ky.: Vostok, (Pépin et al., 2001; Petit et al., 1999; Raynaud et al., 2005). Grey shadings as shown in Fig. 4.4.

The comparison of sediment cores above and below MD97-2120, suggests an upward displacement of the AAIW-UCDW interface, locating MD97-2120 in poorer ventilated UCDW during the LGM, MIS 4, MIS 6 and MIS 8. These findings are supported by the analysis of the CDW oxygen minimum, which was found at substantially shallower water depths throughout the LGM (Hayward et al., 2004).

The similarity of benthic $\delta^{13}C$ patterns in our cores over the last three glacial-interglacial cycles suggests that source-water preformed nutrient changes of AAIW or changes in temperature-dependent fractionation during air-sea gas exchange in the convection region (Broecker and Reimer, 1992) are negligible.

Similar to, but less pronounced than the AAIW to UCDW shift displayed in the $\delta^{13}C$ record of MD97-2120, the $\delta^{18}O$ record shows a shift from low salinity, higher temperature AAIW during warmer climatic periods to higher saline and/or lower temperature UCDW during glacial maxima like the LGM or MIS 4 (Fig. 4.10 b,c).

4.4.1 Proposed Mechanisms

Throughout glacial maxima, the boundary, separating high-nutrient (low $\delta^{13}C$) and CO_2 rich waters from a better ventilated and low-nutriend water mass rises from ~2000 m (interglacials and interstadials) to a depth shallower than 1200 m. This shift could be attributed to several factors, which will be discussed in the following: A northward displacement of the AAIW source region, endmember $\delta^{13}C$ depletion, increased stratification, decreased biological

productivity, increased UCDW upwelling, a reduction in the formation of SO AAIW as proposed by Bostock et al. (2004) and Pahnke and Zahn (2005) or reduced AAIW subduction owed to increased buoyancy.

During the LGM, the winter sea ice (WSI) surrounding Antarctica advanced to about the position of the modern Polar Front (PF; Gersonde et al., 2005). This advance was accompanied by a northward displacement of Antarctic cold waters, where the strongest cooling occurred within the modern Sub Antarctic Zone (SAZ; Gersonde et al., 2005). According to some authors (e.g. Gersonde et al., 2003; Sikes et al., 2009), the major oceanic fronts as well advanced towards the North, expanding the surface area of the Southern Ocean. As AAIW is closely associated with Subantarctic Mode Water (SAMW; Bostock et al., 2004) and SAMW in turn is coupled to the SAF (Hanawa and Talley, 2001), the upward displacement of the AAIW-UCDW interface could be assigned to a northward displacement of the SAF during the LGM. This process would cause SAMW/AAIW to be subducted further to the North (in relation to warmer intervals) extending only to shallower depths at the core locations analyzed in this study. However, Hayward et al. (2008) showed that, in the region off East New Zealand, neither the SAF nor the Subtropical Front shifted during glacial/interglacial cycles, due to topographic constraints by the Campbell Plateau and the Chatham Rise (Fig. 4.1), respectively. Therefore, we assume a northward shift of the formation region of SO AAIW south of New Zealand (Bostock et al., 2013a) as an unlikely process to explain the upward displacement of UCDW.

A decline of air-sea exchange during glacials due to the northward expansion of sea ice (Gersonde et al., 2005) and/or an equatorward shift in SWW (e.g. Mohtadi and Hebbeln, 2004; Stuut and Lamy, 2004) could have depleted the $\delta^{13}C$ due to reduced thermodynamic fractionation in the source region of AAIW (Mackensen, 2012). However, as our intermediate-water records show a similar glacial drop in $\delta^{13}C$ as the UCDW records, we

propose that this process did not play the dominant role in driving the $\delta^{13}C$ pattern in MD97-2120. Increased upper-ocean stratification has the potential to lower the $\delta^{13}C$ level of a water mass by its separation from high $\delta^{13}C$ surface waters. Radiocarbon analyses on cores south of the Chatham Rise indeed constrain a pronounced stratification of the glacial SW-Pacific (Ronge et al., submitted to Science, 2014) but place the cline, which separates poorly ventilated waters from overlying waters, below the AAIW at a depth of ~2000 m. Therefore a stratified upper ocean cannot explain the low glacial $\delta^{13}C$. However, mixing with $\delta^{13}C$-depleted waters below the cline cannot be excluded.

The preferential uptake of isotopically lighter ^{12}C through biological productivity based on photosynthesis (Farquhar et al., 1989) enriches the $\delta^{13}C_{DIC}$ (Dissolved Inorganic Carbon) in a surface water mass. A decrease in biological export production (Francois et al., 1997) in the formation area of AAIW would therefore decrease the $\delta^{13}C_{DIC}$ in source waters. Although this process cannot be completely excluded, we argue it to be unlikely as Hayward et al. (2004) report increased biological productivity in SAZ off New Zealand. The Phytodetritus Effect (Mackensen et al., 2000) on the other hand has the potential to decrease the $\delta^{13}C$ in epibenthic foraminifera. However, as we mentioned in the results, we assume that our sediment cores were not affected by a pronounced increased input of organic carbon.

Pahnke and Zahn (2005) already discussed the process of increased UCDW upwelling as a possible explanation for the very low glacial $\delta^{13}C$ values. This process, being in agreement with the $\delta^{13}C$ data (Pahnke and Zahn, 2005; this study), could in general explain the upward displacement of the AAIW-UCDW boundary. However, several studies point to decreased glacial upwelling (Boyle and Keigwin, 1982; Sigman and Boyle, 2000) and ventilation (Sikes et al., 2000; Skinner et al., 2010; Ronge et al., submitted to Science, 2014). Even though increased upwelling cannot be completely ruled out, we consider this scenario as relatively unlikely.

Although the northern Tasman Sea record FR1/97-GC12 (990 m; 23°34S 153°46E; Bostock et al., 2004) is located close to the core depth of modern AAIW (Heath, 1985), its LGM $\delta^{13}C$ values are as low as the $\delta^{13}C$ of UCDW records MD06-2986 (1477 m) and SO213-82-1 (2066 m). This implies that in the Tasman Sea as well, glacial AAIW (gAAIW) did not reach as deep as during the Holocene. We argue that despite findings of increased glacial AAIW formation (Herguera et al., 2010; Martínez-Méndez et al., 2013; Meissner et al., 2005; Muratli et al., 2010), southern sourced AAIW in the southwest Pacific may not always have reached the core-depth of FR1/97-GC12 during the LGM. As Ribbe (2001) suggested, the production of AAIW is closely coupled to the wind stress applied on subantarctic surface waters. He showed that the volume of transported AAIW is in direct proportion to the forcing of Southern Hemispheric wind stresses. During glacial peak times, the northward displacement of SWW (Mohtadi and Hebbeln, 2004; Moreno et al., 1999; Stuut and Lamy, 2004; Toggweiler et al., 2006) in combination with static oceanic fronts (Hayward et al., 2008) led to a reduction of wind stress in the formation area of SW-Pacific AAIW. In addition, the advancing winter sea ice edge increased the glacial import of freshwater by melting sea ice into the AAIW (e.g. Saenko and Weaver, 2001) and thereby intensified the SAZ salinity anomaly (Gersonde et al., 2005; Jenkins, 1999; Pahnke and Zahn, 2005), ultimately hampering the subduction of AAIW (Fig. 4.11). Furthermore, highly saline bottom waters, stabilized by brine rejection (Adkins, 2013) increased the water column density gradient and thus supported the positive buoyancy of fresher AAIW. A salinity-controlled pattern, leading to shallower penetration of glacial AAIW, is also supported by our CCSM3 model runs (Fig. 4.6) that point to an increased density gradient between glacial water masses (Fig. 4.12). Separately and even more in combination, the processes described here might have significantly reduced the downward extension of AAIW within the SW-Pacific. This void,

created by the diminishing influence of gAAIW was then filled by an upward displacement of underlying UCDW.

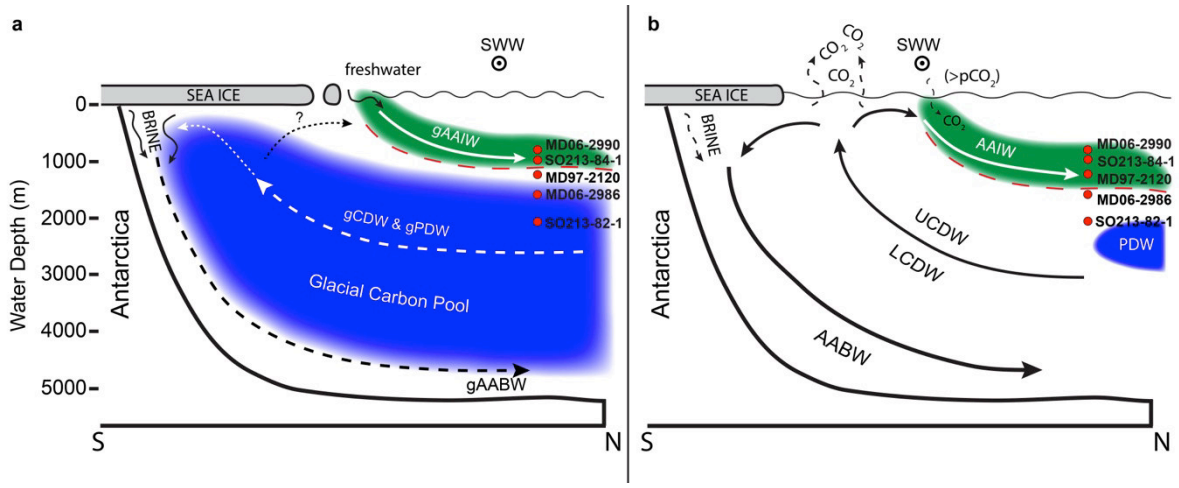

Figure 4.11: Conceptual schemes of SW-Pacific water mass structures. a) Glacial pattern: Associated with advancing winter sea ice, the Southern Westerly Winds (SWW; dotted circle) shift towards the North, away from the formation region of glacial (g)AAIW (green shaded area). Freshwater input from the close sea ice edge enhances gAAIW buoyancy, locating it above the depth of reference core MD97-2120. The blue-shaded area indicates the very old (low $\Delta^{14}C$) glacial deep-water carbon pool, rich in CO_2 and nutrients (low $\delta^{13}C$). During glacial maxima, the AAIW/UCDW interface (red dashed line) shifts above 1200 m, bathing the reference core location of MD97-2120 in low $\delta^{13}C$ gUCDW. Dashed arrows indicate a more sluggish deep-water circulation than during interglacial times. Red dots show the modern water depth of sediment cores analysed in this study. b) Interglacial pattern: During the warmer stages like the Holocene, the sea ice derived meltwater input in AAIW declines, while the SWW shift towards a poleward position. Increased AAIW salinity favours a deepening of the AAIW-UCDW interface. Retreating sea ice enables air-sea gas exchange of upwelled CDW, releasing stored CO_2 towards the atmosphere (e.g. Ronge et al., submitted to Science, 2014). During times of high atmospheric partial pressure of CO_2 ($>pCO_2$) like today (due to anthropogenic forcing), CO_2 is being subducted into the ocean interior via AAIW. Thus today the Southern Ocean acts as a CO_2 sink, while in preindustrial times (and other interglacials), the SO released upwelled CO_2 to the atmosphere (e.g. Gruber et al., 2009). Thick, continuous arrows indicate enhanced ventilation, water mass circulation and exchange compared to glacial maxima. The old Pacific Deep Water (PDW) carbon pool diminishes and retreats towards it modern dimension (see Key et al., 2004).

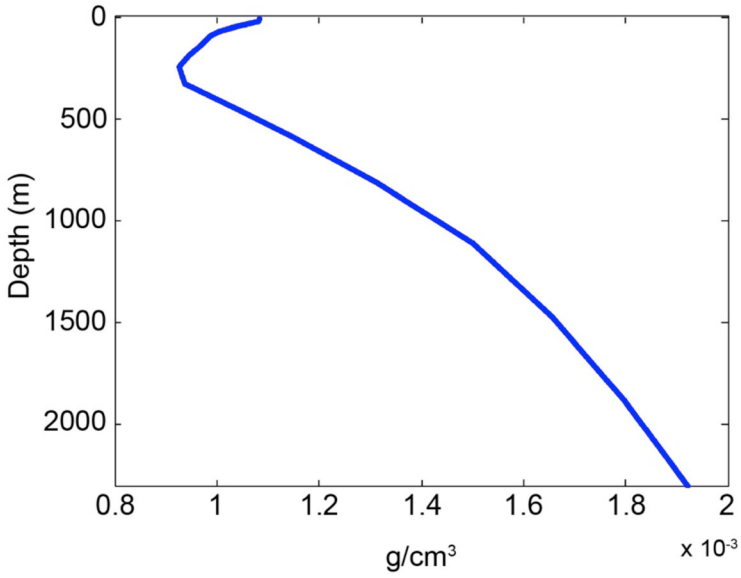

Figure 4.12: Vertical profile of modeled LGM in-situ density anomaly relative to pre industrial, zonally averaged across the South Pacific at 30°S (annual mean; 100-yr average).

The close correlation between deep- and intermediate-water $\delta^{13}C$ and SSTs (Pahnke and Zahn, 2005; this study; Fig. 4.10 a, b) points to Southern Hemisphere climatic events as the driving force of the proposed processes. At the end of each glacial cycle, parallel to $SST_{Mg/Ca}$, the low $\delta^{13}C$ of MD06-2990/SO136-003/SO213-84-1 and MD97-2120 increase and approach the same absolute values, while simultaneously, UCDW $\delta^{13}C$ of SO213-82-1 and MD06-2986 rises just as rapid (Fig. 4.10). Increasing temperatures in the Southern Hemisphere (e.g. Parrenin et al., 2013) reverse the sequence of glacial processes outlined above. Sea ice retreats and therefore reduces the SAZ freshwater anomaly, the SWW shift towards a poleward position, both increasing the formation and ventilation of deep- and intermediate-waters (Toggweiler et al., 2006; Ronge et al., submitted to Science, 2014).

At the end of each glacial cycle, atmospheric CO_2 displays a rapid departure from low glacial values (Monnin et al., 2001). The good correlation between atmospheric CO_2 and UCDW $\delta^{13}C$ (Fig. 4.10 b,d) suggests a close coupling of increased deep-water ventilation, AAIW formation and global climate. Assuming that SST-changes in the Tasman Sea and the Bounty Trough are broadly synchronous to Antarctic ice-core temperatures, the temporal difference between SST and benthic $\delta^{13}C$-records can provide evidence for differences in water mass

ventilation. In this context, Pahnke and Zahn (2005) proposed that a transient buoyancy inertia caused by meltwater-export, delayed the ventilation of AAIW, as the SSTs of sediment core MD97-2120 lead the increasing $\delta^{13}C$-trend by 1-3 kyr. However, as the $\delta^{13}C$-values in our record interpreted as AAIW (MD06-2990/SO136-003) increase at the same time as the SSTs (Fig. 4.10; Table A3.5), we argue that the lead/lag of MD97-2120 $\delta^{13}C/SST_{Mg/Ca}$ is not a consequence of delayed ventilation but of a delayed downward expansion of AAIW and decelerated UCDW ventilation. As already proposed, the enhanced import of meltwater likely led to a buoyancy gain of recently formed AAIW. Only upon a reduction of freshwater input, the AAIW would be able to advance to depths larger than about 1200 m. Although the AAIW ventilation occurred at the onset of rising temperatures, the UCDW lagged behind, due to the huge pool of old and CO_2 rich water that had to be ventilated as shown by Ronge et al. (submitted to Science, 2014).

We further speculate that changes in the AAIW freshwater budget might cause global reorganizations in the oceanic Themohaline Circulation (THC). Saenko et al. (2003) showed that the endmember freshwater budget of the THC controls the density gradients of AAIW and North Atlantic Deep Water (NADW) and therefore their formation rate. Freshwater input in one hemisphere can significantly alter the AAIW-NADW density gradient, enhancing or hampering the formation rate of the respective water mass on the opposed hemisphere (Weaver et al., 2003).

4.5 Conclusions

Recent benthic $\delta^{13}C$ and $\delta^{18}O$ records from the Bounty Trough and the Tasman Sea off New Zealand allow new insights into the formation and extent of SW-Pacific AAIW over the last 350 kyr. The new proxy data and modeling results presented in this study, question the hypothesis that stronger water column stratification resulted in reduced production of glacial

AAIW (Pahnke and Zahn, 2005). Our results suggest that a northward displacement of the WSI edge (Gersonde et al., 2005) led to a significantly shallower AAIW subduction in the SW-Pacific during glacial maxima. Warmer climatic conditions on the other hand favor the enhanced downward extent of AAIW (Fig. 4.11).

Following the synchronous timing of these observations and published SSTs (Pahnke and Zahn, 2005), we conclude that pronounced climate changes in the Southern Hemisphere are the dominating factor, driving changes in AAIW formation, its vertical expansion as well as the ventilation and the associated carbon cycling of CDW.

Radiocarbon analyses on planktic and benthic foraminifera proved the presence of exceptional old waters within glacial CDW in the SW-Pacific and South Atlantic (Skinner et al., 2010; Ronge et al., submitted to Science, 2014). At the onset of the most recent deglaciation, deep-water ventilation improved simultaneously with the increase in AAIW formation, outlined above. The restart of the Southern Ocean Meridional Overturning Circulation (SOMOC; e.g. Fischer et al., 2010) conveyed ancient CO_2 from the deep-ocean towards the atmosphere, thus increasing the ventilation of CDW while the expansion of SW-Pacific AAIW was favored.

Vast amounts of anthropogenic CO_2 are transported towards the deep-ocean via the AAIW (Sabine et al., 2004; Murata et al., 2007, 2010; Downes et al., 2010), while at the same time stored CO_2 is upwelled within CDW (Gruber et al., 2009; Fig. 4.11). As model predictions suggest, the current CO_2 sink of the Southern Ocean (Gruber et al., 2009) might evolve into a source due to the poleward shift of SWW and the accompanying increase in CDW upwelling (Le Quéré et al., 2007). Additional modeling studies (e.g. Downes et al., 2010; Manabe and Stouffer, 1993) showed that this process might be reversed on longer time scales, leading to increased ocean stratification and decreased AAIW formation and consequently to a reduction in the uptake of anthropogenic CO_2. Thus, in order to specify the Southern Ocean's role in the

carbon cycle of a changing climate system, improved insight in this highly dynamic system is essential.

Acknowledgements

This work was funded by the Federal Ministry of Education and Research (BMBF; Germany) project 03G0213A – SOPATRA and the Alfred Wegener Institute, Helmholtz Centre for Polar and Marine Research.

We thank captains, crews and scientific parties of R/V *Sonne* cruise SO213/2 and R/V *Marion Dufresne* cruise MD152 for their support during sample collection; K. Pahnke and A. Sturm for data; A. Mackensen and J. Wollenburg for discussion; R. Fröhlking, N. Lensch, G. Meyer, L. Ritzenhoven. L. Schönborn, M. Seebeck and S. Wiebe for technical support. Data will be made accessible at http://doi.pangaea.de/10.1594/PANGAEA.835498

Chapter 5

Glacial disparities in Intermediate Mode Water advection in the South Pacific Gyre

R. Tapia[1], D. Nürnberg[1], **T. A. Ronge**[2] and R. Tiedemann[2]

[1] GEOMAR Helmholtz Centre for Ocean Research, Wischhofstr. 1-3, 24148, Kiel, Germany.

[2] Alfred Wegener Institute Helmholtz Centre for Polar and Marine Research, Am Alten Hafen 26, 27568, Bremerhaven, Germany.

Corresponding author: R. Tapia, GEOMAR Helmholtz Centre for Ocean Research, Wischhofstr. 1-3, 24148, Kiel, Germany. (rtapia@geomar.de)

Under review at *Earth and Planetary Science Letters*

Abstract

The Intermediate Mode Waters formed in the Southern Ocean are crucial for the lower thermocline ventilation processes in Southern Hemisphere Gyres. They might also have served as the most relevant pathways transporting climatic signals from high to low latitudes via "oceanic tunneling" on glacial/interglacial time scales. Despite the importance of the Southern Ocean Intermediate Waters (SOIWs), our understanding on the long–term evolution, exact advection paths, and impact on the South Pacific Gyre's thermocline is still fragmentary.

Here, we present a 200 kyr record of paired Mg/Ca ratios and stable oxygen isotopes from surface- and deep-dwelling planktic foraminifera, from the South Pacific Gyre (SPG). On

average, the Mg/Ca–derived sea surface temperatures (*Globigerina bulloides*) show similar conditions during the LGM and Marine Isotope Stage (MIS) 6 (9.4 °C versus 9.9 °C). In contrast, our Mg/Ca–derived subsurface temperatures (*Globorotalia inflata* and *Globorotalia truncatulinoides*) suggest the LGM ~3 to ~2 °C colder than MIS 6. The reconstructed subsurface ice volume corrected stable oxygen isotope ratio of seawater ($\delta^{18}O_{sw\text{-}ivc}$, proxy for local salinity changes) suggests opposing glacial subsurface conditions, i.e., slightly saltier–than–Holocene during MIS 6 to fresher–than–Holocene during MIS 2. Considering that subsurface hydrography at the core site is plausibly driven by the formation and/or advection of SOIWs from the South East Pacific, our results provide further support on the relevance of subsurface processes in the Southern Ocean transferring climatic signals (temperature and salinity) to the SPG. Furthermore, the contrasting subsurface glacial scenarios at the SPG's thermocline imply that the advection of SOIWs could be highly variable during different glacial stages.

5.1 Introduction

The Southern Ocean Intermediate Waters (SOIWs), such as Antarctic Intermediate Water (AAIW) and Subantarctic Mode Water (SAMW), are critical pathways for atmospheric gases (e.g. anthropogenic CO_2 (Sabine, 2004) and oxygen (Russell and Dickson, 2003)) to enter the oceans interior and for nutrients from upwelled deep-waters in the Southern Ocean to return to the thermoclines of the subtropical gyres (Sarmiento et al., 2004). Different studies have suggested that these water masses located at intermediate depths played a relevant role in glacial/interglacial climate change (Bostock et al., 2004; Pahnke et al., 2008; Pahnke and Zahn, 2005; Pena et al., 2008/2013; Spero and Lea, 2002).

The South East Pacific (SEP; a list of acronyms is given in Table A1) is the principal formation area of SAMW and AAIW (Fig. 5.1; Bostock et al., 2010/2013a; Hartin et al., 2011; Hasson et al., 2011; Holte et al., 2013; Sallée et al., 2006). The SAMW is formed just

north of the Subantarctic Front (SAF) via the deepening of mixed layers during wintertime convection (Sloyan et al., 2010). The temperature and salinity properties of the SAMW are controlled by the incorporation of fresh water (i.e., via precipitation, melting sea ice and northward Ekman transport of the Subantarctic Surface Water (SASW)) during its formation in the SEP (Schneider and Bravo, 2006).

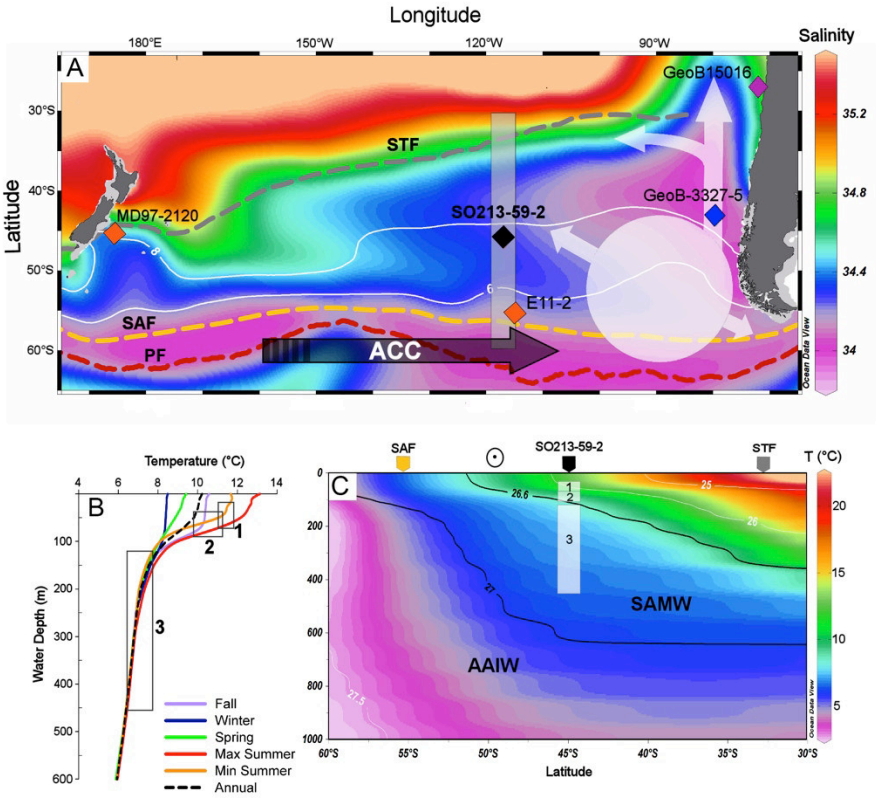

Figure 5.1: A) Location of sediment core SO213-59-2 and reference sites discussed in the text (diamonds). The main SOIW formation area and advection (large white area and arrows; after (Hartin et al., 2011; Herraiz-Borreguero and Rintoul, 2011), including salinity (color) and temperature (white contour lines and numbers; WOA09) at 150 m water depth (~26.8 kg/m^3) are indicated. Dashed lines denote the oceanographic frontal boundaries: the Subtropical Front (STF; gray), the Subantarctic Front (SAF; yellow), and the Polar Front (PF; red; Orsi et al., 1995). **B)** Vertical profile of the annual mean, the seasonal mean, the minimum and the maximum summer temperature of the uppermost 600 m of the water column at the core site (WOA09). The average Holocene Mg/Ca temperature for *G. bulloides* (1), *G. inflata* (2) and *G. truncatulinoides* (3) are plotted against the estimated habitat water depth of each species. The depth ranges of *G. bulloides* (< 50 m), *G. inflata* (50 – 100 m) and *G. truncatulinoides* (> 150 m) are used to define surface-water, thermocline-water and deep–thermocline-water. Boxes mark ranges of Mg/Ca temperatures in surface sediments and Holocene sediments. **C)** Detail of the S-N transect denoted in A), indicating the vertical distribution of SAMW (26.6 – 27 kg/m^3; ~ 100 –

600 m) and AAIW (> 27 kg/m^3; > 600 m) (Hanawa and Talley, 2001; Tsuchiya and Talley, 1998). Numbers in the white boxes correspond to the assumed habitat depth range of the planktic foraminifera species analyzed as in B). Notice that the inferred habitat depth range of *G. inflata* is located close to boundary between SAMW and Subtropical waters (<26.6 kg/m^3). Open circle with dot denotes eastward-directed flow of the maximum SWW. Color-coded arrows mark oceanic fronts depicted in A).

The SAMW becomes progressively colder, fresher, and denser as it approaches the Drake Passage (~4 °C; McCartney, 1977) forming the coldest, and densest variety of SAMW known as AAIW (McCartney, 1977). The AAIW is characterized by a vertical salinity minimum and high gas content (Hartin et al., 2011). SAMW and AAIW are exported to the Atlantic Ocean through the Drake Passage, and to the lower thermocline in the Subtropical Gyres of Southern Hemisphere oceans (Hanawa and Talley, 2001; McCartney, 1977). These water masses play a fundamental role in the ventilation of the modern thermocline in the subtropical South Pacific Gyre (SPG; Hartin et al., 2011; Herraiz-Borreguero and Rintoul, 2011; Holte et al., 2012) as well as transporting heat, salt and nutrients from the Southern Ocean to lower latitudes, via processes as "oceanic tunneling" at glacial/interglacial timescales (Liu et al., 2002; Pena et al., 2008/2013).

To date, the enhanced presence of SOIWs during cold periods in mid and low latitudes of the East Pacific has been explained by invoking either latitudinal displacement and/or stronger Southern Westerly Wind (SWW; Martínez-Méndez et al., 2013; Muratli et al., 2010; Pena et al., 2008; Pena et al., 2013). An opposite situation, i.e. increased formation of SOIWs during warm periods, has been proposed for the South West Pacific off New Zealand (Pahnke and Zahn, 2005). These regional differences emphasize further need of geographical constraint in the data-poor South Pacific, in order to better understand the spatial pattern of SOIWs formation and distribution in the South Pacific.

Here we present paired Mg/Ca and $\delta^{18}O$ records of three species of planktic foraminifera (*Globigerina bulloides, Globorotalia inflata* and *Globorotalia truncatulinoides*) from

sediment core SO213–59–2 in the central South Pacific covering the last 200 kyr. The aim of this study is to reconstruct the structure of the water column in the subtropical SPG during the late Quaternary, and to evaluate the subsurface variability (thermocline water depth) potentially influenced by the enhanced injection of SOIWs (SAMW/AAIW) formed in the SEP during glacial stages.

5.2 Material and Methods

The age model of the gravity core SO213–59–2 (45°49' S, 116°52' W; 3161 m water depth; Fig. 5.1 A), retrieved from the East Pacific Rise during R/V *Sonne* cruise SOPATRA, is based on correlation of benthic foraminiferal $\delta^{18}O$ record (*Cibicidoides wuellerstorfi*, 250–315 µm) to the global benthic $\delta^{18}O$ stack LR04 (Lisiecki and Raymo, 2005) using the software package AnalySeries 2.0 (Paillard et al., 1996; Fig. 5.2 A). The age model is further supported by two ^{14}C accelerator mass spectrometer (AMS) dates of *G. bulloides* measured at the Leibniz-Laboratory for Radiometric Dating and Isotope Research of the University of Kiel (Fig. 5.2 A). AMS ^{14}C ages were converted to calendar age using the software CALIB 7.0 (Stuiver et al., 2005) with the Marine13 (Reimer et al., 2013) dataset and ΔR correction of 560 years correction (Bard, 1988). The uppermost sediment (0–1 cm) from multicorer SO213–59–1 (same location) was also dated (details are given in the Supplementary Information).

Three planktic foraminiferal species of mixed layer dwellers i.e., *G. bulloides* and deep dwellers i.e., *G. inflata*, and *G. truncatulinoides* (dextral) were picked from surface sediments (top 1 cm of multicorer) and SO213–59–2 at 2 cm intervals. The Mg/Ca and stable isotope ($\delta^{18}O$) measurements were performed on the same sample composing 30 to 40 shells from the size fraction 355−400 µm. Occasionally, we extended the size fraction to 315–400 µm to recover enough calcite material from *G. inflata* and *G. truncatulinoides*.

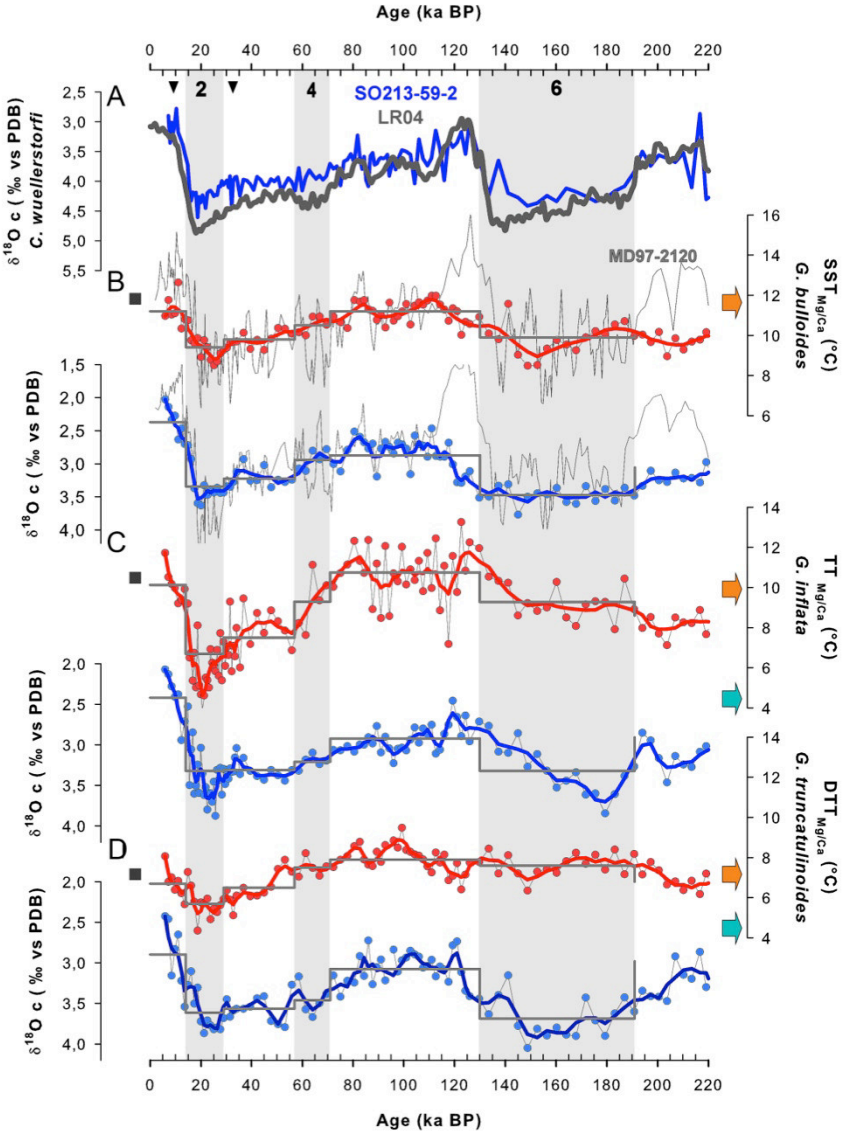

Figure 5.2: Foraminiferal (isotope) geochemical data of core SO213-59-2. **A)** Age model for core SO213–59–2 based on the graphical alignment of the benthic foraminiferal $\delta^{18}O$ record (blue curve) to the benthic $\delta^{18}O$ stack LR04 (gray curve; Lisiecki and Raymo, 2005). Auxiliary AMS ^{14}C age control points are indicated by black inverted triangles (see Supplementary material Table 5.S1). Shaded bars indicate glacial intervals; black numbers in the bars represent the Marine Isotope Stages. Calculated seawater Mg/Ca−temperatures (red circles, red curve illustrates 3-points running average) and $\delta^{18}O$ (blue circles, blue curve illustrates 3-points running average) derived from **B)** *G. bulloides*, **C)** *G. inflata* and **D)** *G. truncatulinoides*. $SST_{Mg/Ca}$ = sea surface temperature, $TT_{Mg/Ca}$ = thermocline temperature, $DTT_{Mg/Ca}$ = deep thermocline temperature. Surface sediment data from MUC SO213−59−1 are indicated by black squares. Continuous gray lines denote average temperatures values computed per each isotopic stage (MIS1 to MIS 6). Orange arrows indicate the summer ocean temperature at 50 m (b; assumed mean living depth of *G. bulloides*), 75 m (c; assumed mean living depth of *G. inflata*) and 300 m (d; assumed mean living depth of *G. truncatulinoides*) water depth (WOA09); green arrows denote the modern temperature of SOIWs in the SE Pacific (~4 − 5 °C; Hartin et al., 2011). The downcore $SST_{Mg/Ca}$ record of core SO213−59−2 shows smaller variability than the high resolution $SST_{Mg/Ca}$ (*G. bulloides*) reconstruction from MD97−2120 at 45° S (Pahnke et al., 2003).

Pretreatment and analytical procedures followed the method described by Nürnberg and Groeneveld (2006) and the cleaning protocol proposed by Barker et al. (2003) including an additional reductive cleaning step. Analyses were performed on an ICP-OES (VARIAN 720–ES) with and analytical long-term precision of ±0.1 mmol/mol for Mg/Ca of ECRM752–1 standard. The efficiency of the cleaning was evaluated by monitoring the elements Fe and Mn, which were measured alongside Mg (details in supplementary information 5.7).

The $\delta^{18}O$ measurements were performed at GEOMAR, Kiel, using a MAT 253 mass spectrometer (*Thermo Scientific*, Germany) coupled with a *Kiel IV Carbonate device* (*Thermo Scientific*, Germany). Results were referenced to the NBS19 standard and calibrated to the PDB scale. Analytical errors were ±0.06‰ for $\delta^{18}O$.

The conversion of Mg/Ca values to temperatures was conducted according to the calibrations of Mashiotta et al. (1999): $Mg/Ca = 0.474\ e^{(0.107 * T)}$); Groeneveld and Chiessi (2011): $Mg/Ca = 0.72\ e^{(0.076 * T)}$); and Regenberg et al. (2009): $Mg/Ca = 0.84\ e^{(0.083 * T)}$) for *G. bulloides, G. inflata*, and *G. truncatulinoides*, respectively.

Dissolution is known to affect the preservation of the Mg/Ca signal in planktic foraminifera, however we considered that dissolution did not drive the glacial−interglacial changes observed along the core SO213–59–2 (details discussed in supplementary information).

To estimate habitat depth range of each species, we averaged the Mg/Ca–temperatures from surface sediments (top 1 cm of multicorer) and Holocene sediments (0 – 10 kyr) from core SO213–59–2, and compared them with modern climatological data from World Ocean Atlas 2009 (WOA09; Antonov et al., 2010; Locarnini et al., 2010). To estimate the amplitude of temperature changes across each Marine Isotope Stage (MIS), we averaged the temperature estimates within each of the glacial (MIS 2 and MIS 6) and interglacial (MIS 1 and MIS 5) intervals. The intervals were defined according to the boundaries stated by Lisiecki and Raymo (2005).

Although numerous biological vital processes (symbiont activity, ontogeny) may affect the $\delta^{18}O$ fractionation processes in planktic foraminifera (Rohling and Cooke, 1999), we assume no vital effect in this study (details discussed in supplementary information 5.7), because local $\delta^{18}O_{sw}$ correlates linearly with ocean water salinity on regional scales (Le Grande and Schmidt, 2006).

We used the seawater $\delta^{18}O_{sw}$ as a proxy for local salinity changes. However, we did not convert the $\delta^{18}O_{sw}$ signal into salinity because the variation of $\delta^{18}O$ in the ocean is more complicated than salinity. Other processes, such as sea ice formation affect seawater $\delta^{18}O$ and salinity differently. These additional complications result in only regionally–coherent $\delta^{18}O$ to salinity relationships (Le Grande and Schmidt, 2011).

The $\delta^{18}O_{sw\text{-}ivc}$ calculation involves the subtraction of the temperature effect from the planktic $\delta^{18}O$ data ($\delta^{18}O_{sw}$ (VSMOW) = $\delta^{18}O$ + 0.27 - (4.38 - (4.382 - 4 * 0.1 (16.9 - T))1/2)/(0.1 x 2); (Shackleton, 1974), followed by the removal of the ice volume component (IVC) of the seawater $\delta^{18}O$ composition (Waelbroeck et al., 2002). We linearly interpolated the Waelbroeck et al. (2002) record at the time step of the core SO213–59–2 profile and subtracted the mean ocean $\delta^{18}O_{sw}$ from the reconstructed $\delta^{18}O_{sw}$ values. The absolute error in calculating $\delta^{18}O_{sw}$ is ~ ±0.3‰ (Rohling, 2007).

5.3 Results

5.3.1 Planktic foraminiferal Mg/Ca – temperatures

The Mg/Ca (temperature) values of *G. bulloides, G. inflata* and *G. truncatulinoides* in surface sediments (top 1 cm of multicorer) are 1.66 mmol/mol (~11.7 °C), 1.59 mmol/mol (~10.4 °C) and 1.52 mmol/mol (~7.1 °C), respectively (Fig. 5.2). The averaged reconstructed temperatures (surface sediments + Holocene) range between 11.3 (±0.4) °C for *G. bulloides*, 10.6 (±0.8) °C for *G. inflata* and 7.1 (±0.6) °C for *G. truncatulinoides* (Fig. 5.2), consistent with climatological austral summer temperatures (WOA09; Locarnini et al., 2010) typical for

water depths < 70 m; ~50 – ~100 m and 150 – ~400 m, respectively (Fig. 5.1 B). The inferred seasonality of the Mg/Ca signals is in agreement with sediment trap data east of New Zealand, which suggest that the maximum fluxes of *G. bulloides* and *G. inflata* are mainly bound to Southern Hemisphere's late spring to summer in subantarctic waters (King and Howard, 2003; Northcote and Neil, 2005). Based on the correlation with the WOA09 temperatures, we interpret these species as reflecting the austral summer water temperature at the surface (*G. bulloides* – $SST_{Mg/Ca}$), the thermocline (*G. inflata* – $TT_{Mg/Ca}$) and the deep thermocline (*G. truncatulinoides* – $DTT_{Mg/Ca}$).

Downcore SO213–59–2, Mg/Ca ranges between 1.17 – 1.83 mmol/mol in *G. bulloides*, 0.96 – 1.97 mmol/mol in *G. inflata* and 1.21 – 1.85 mmol/mol in *G. truncatulinoides* over the past 220 kyr, with higher ratios during interglacials. Large $TT_{Mg/Ca}$ amplitude variations of ~8 °C (from ~5 to ~13 °C) are observed at the thermocline level. Smaller temperature variabilities are observed at the surface (*G. bulloides*) and the deep thermocline (*G. truncatulinoides*), with $STT_{Mg/Ca}$ ranges of ~4 °C (~9 to ~13 °C) and $DTT_{Mg/Ca}$ of ~ 6°C (~4 to ~10 °C), respectively (Fig. 5.2). The inferred $SST_{Mg/Ca}$, $TT_{Mg/Ca}$, and $DTT_{Mg/Ca}$ show glacial–interglacial amplitudes of ~2, ~4 and ~2 °C, respectively (Fig. 5.2). Our results suggest, on average, similar interglacial surface conditions (MIS 1 vs. MIS 5) in the subtropical SPG, with no differences in $SST_{Mg/Ca}$ during both interglacials (~11.2 °C). This pattern is paralleled by the situation observed at thermocline level, $TT_{Mg/Ca}$ of ~10.1 °C (MIS 1) vs. ~10.8 °C (MIS 5; Fig. 5.2 B, C). On the other hand, slightly larger temperature differences between interglacials can be observed at $DTT_{Mg/Ca}$ of ~6.7 °C (MIS 1) vs. ~7.9 °C (MIS 5; Fig. 5.2 D).

The average glacial $SST_{Mg/Ca}$ is similar during MIS 2 and MIS 6 (9.4 °C versus 9.8 °C, respectively). In contrast, marked glacial differences are observed at the thermocline, where $TT_{Mg/Ca}$ suggests a glacial difference of ~3 °C between MIS 2 and MIS 6 (~6.7 °C versus ~9.3 °C, respectively). The minimum temperature of ~4.6 °C centered at ~20 kyr, is ~3 °C colder than the lowest temperature observed in MIS 6 (~8.1 °C). At the deep thermocline, a similar

trend can be observed, where the $DTT_{Mg/Ca}$ show on average ~2 °C colder conditions during MIS 2 than MIS 6 (~5.7 °C versus ~7.6 °C, respectively) and minimum temperatures of ~4.4 °C and ~6.4 °C at ~20 kyr and ~148 kyr, respectively.

5.3.2 Planktic foraminifera stable oxygen isotopes and relative salinity reconstruction

The $\delta^{18}O$ values of *G. bulloides*, *G. inflata* and *G. truncatulinoides* from the surface sediments (top 1 cm of multicorer) are 1.87, 2.27 and 2.37‰, respectively. Along the analyzed time interval, the $\delta^{18}O$ values show glacial/interglacial fluctuations ranging between 3.8 and 2.02‰ at the sea surface, between 3.8 and 2.07 ‰ at the thermocline, and between 4.05 and 2.12‰ at the deep−thermocline (Fig. 5.2). Although the isotopic values at all three water depths increase synchronously at ~30 kyr, the heaviest $\delta^{18}O$ values are reached at different time intervals. At the thermocline level, the maximum is reached at ~25 kyr, while at the surface the values continue to increase until the heaviest value is reached at ~20 kyr.

Along the water column the averaged planktic $\delta^{18}O$ values during MIS 1 range from 2.4 to 2.9‰ and from 2.9 to 3.1‰ during MIS 5, with *G. bulloides* and *G. inflata* showing lighter $\delta^{18}O$ values and *G. truncatulinoides* the heavier $\delta^{18}O$ values. During MIS 2 the $\delta^{18}O$ values oscillate between 3.3 and 3.6 ‰ similar to MIS 6 with $\delta^{18}O$ values ranging from 3.3 to 3.7 ‰ (Fig. 5.2).

The foraminiferal $\delta^{18}O$ values are determined by water temperature and the $\delta^{18}O$ of seawater at the moment of calcification. Therefore, the foraminiferal $\delta^{18}O$ can be used as a qualitative thermal monitor. The thermal gradient inferred from the $\delta^{18}O$ gradient between MIS 1 – 2 and MIS 2 – 6 varies for each species but in general suggest temperature gradients ≤ 1 °C at all water depth. The lack of accordance between the thermal gradients inferred from Mg/Ca–temperatures (see Section 5.3.1) and $\delta^{18}O$, suggests large changes in the seawater isotopic composition.

The calculated $\delta^{18}O_{sw\text{-}ivc}$ values range from 0.35‰ to 2.23‰ at the sea surface (*G. bulloides*), from -0.73 to 2.35‰ at the thermocline (*G. inflata*), and from -0.51 to 1.59‰ at the deep–thermocline (*G. truncatulinoides*), respectively. These results suggest fresher conditions during the glacial and saltier conditions during the interglacial. The species-specific $\delta^{18}O_{sw\text{-}ivc}$-deviations from the averaged Holocene (0 – 10 kyr) and surface sediment ($\Delta\delta^{18}O_{sw\text{-}ivc}$) range between -0.39 to 1.25‰ at the surface, -1.40 to 1.68‰ at the thermocline and -0.89 to 1.21‰ at the deep thermocline (Fig. 5.3). The $\Delta\delta^{18}O_{sw\text{-}ivc}$ values at all three water depths are highest during MIS 5 (Fig. 5.3 C, D, E). Moreover, our results suggest differences in glacial $\delta^{18}O_{sw\text{-}ivc}$ at all water depths, where slightly saltier–than–Holocene conditions prevailed during MIS 6, contrasted by the fresher–than–Holocene conditions during MIS 2 (Fig. 5.3 C, D, E).

5.4 Discussion

Since the environmental niche of some species can potentially vary trough time (Cléroux et al., 2007/2009), the ecology of the studied species must be taken into account when interpreting Mg/Ca record. In this study the effect of this caveat is minimized, since our interpretations are restricted to changes of the main ocean state (glacial and/or interglacial stages) and the co–variation of the different planktic foraminiferal species.

5.4.1 Evolution of water column structure in the South Pacific

The ~4 °C of total glacial sea surface cooling observed at our study site is weaker than the cooling suggested by previous studies from similar latitudes between the Subtropical Front (STF) and the SAF in the South Pacific, such as Geob3327−5 in the SEP (43°S; Ho et al., 2012) and MD97−2120 in the South West Pacific (45°S; Pahnke et al., 2003), which show a larger glacial sea surface cooling ~8 °C (Fig. 5.2 B). At our study site the $SST_{Mg/Ca}$ and surface $\Delta\delta^{18}O_{sw\text{-}ivc}$ fluctuations commonly suggest fresh and cool glacial and salty and warm

interglacial conditions, as previously described for the South West Pacific (Fig. 5.3 B; Pahnke et al., 2003).

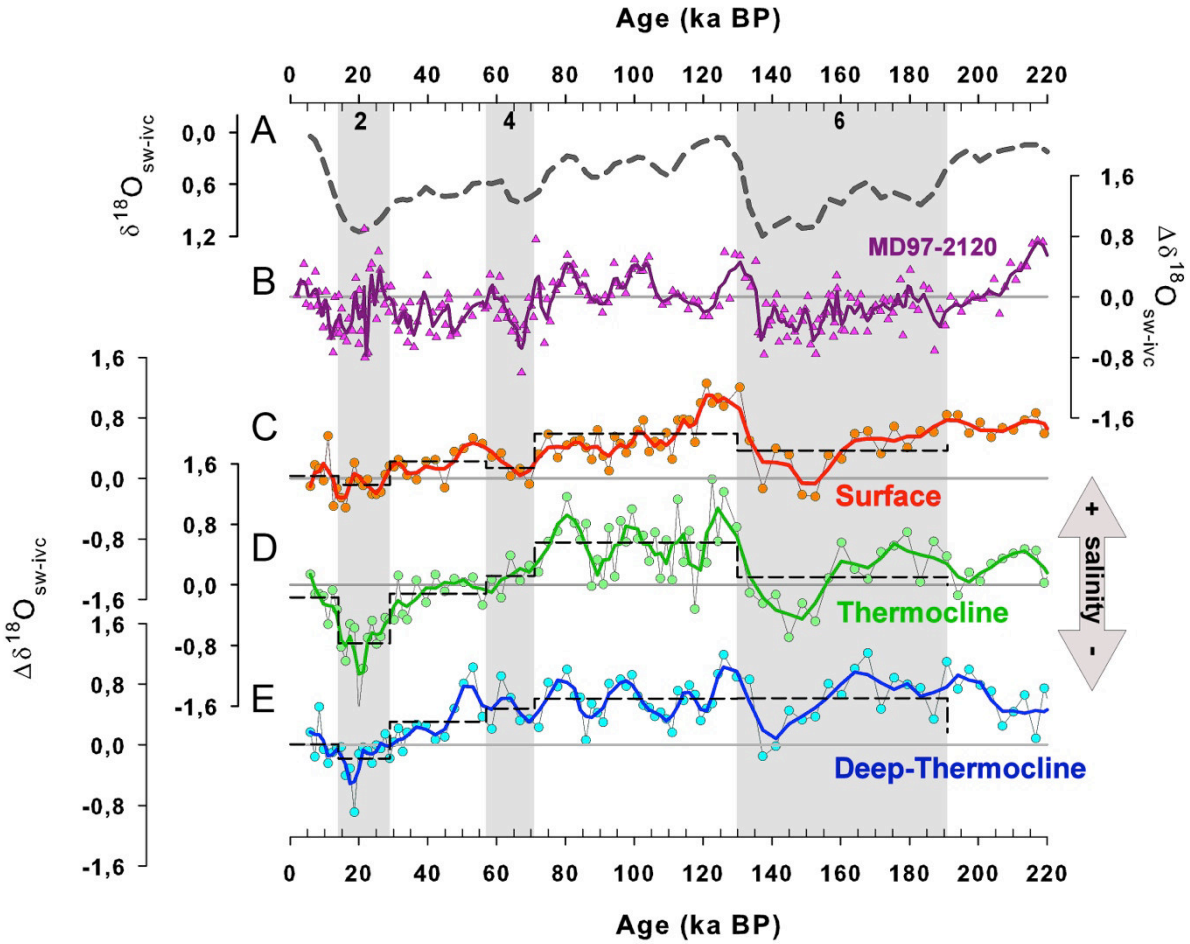

Figure 5.3: Comparison of **A)** mean ocean $\delta^{18}O_{sw}$ (Waelbroeck et al., 2002) and the reconstructed local salinity anomalies for **B)** Chatham Rise core MD97−2120 (Pahnke et al., 2003) and our study site SO213-59-2 in the South Pacific Gyre at **C)** surface, **D)** thermocline and **E)** deep thermocline level. Gray continuous lines denote species-specific averaged mean Holocene values (surface sediments + 0 − 10 kyr). Thick lines are the 3 points running average of the data (circles). Black dashed lines denote average values computed per each isotopic stage (MIS1 to MIS 6).

The co−variation of sea surface temperature and salinity at similar latitudes has been attributed to a northward migration of the SAF and/or larger influence of SASW during glacial stages that results in lower surface temperature and salinity (Nürnberg and Groeneveld, 2006; Pahnke et al., 2003). However, this mechanism is unlikely to operate at our core location since siliceous microfossil transfer functions suggest no large

glacial−northward displacement (>4°) of the frontal system in the central South Pacific (Gersonde et al., 2003/2005). Furthermore, unlike the relative similar glacial $SST_{Mg/Ca}$ (9.4°C (LGM) versus 9.9°C (MIS 6)) during the past 200 kyr, our glacial subsurface Mg/Ca–temperatures and $\Delta\delta^{18}O_{sw\text{-}ivc}$ records are characterized by larger differences between the LGM and MIS 6, from ~3 to ~2 °C and 0.9 to 0.8 ‰ ($\delta^{18}O_{sw}$) at thermocline and deep thermocline water depth as recorded by *G. inflata* and *G. truncatulinoides*, respectively (Fig. 5.2 and 5.3). These contrasting surface and subsurface conditions argue against glacial frontal migration as the controlling factor of the glacial/interglacial hydrographic changes at the core-site, as the shifting of the SAF would have affected the entire upper water column. Our data show that despite a lack of variability at the sea surface in the subtropical SPG, substantial changes occurred at subsurface water depths (at thermocline level). Considering the importance of the SOIWs in ventilating the thermocline in this region (Hartin et al., 2011; Sloyan et al., 2010), we interpret the subsurface Mg/Ca–temperatures and the according $\Delta\delta^{18}O_{sw\text{-}ivc}$ variations as driven by the changes in the supply of SOIWs formed in the SEP. Various other proxy reconstructions suggest an enhanced SOIW formation and/or advection to lower latitudes during cold/glacial periods (Martínez-Méndez et al., 2013; Muratli et al., 2010; Pena et al., 2013). In general, our subsurface reconstructions are in accordance with these observations, showing colder and fresher subsurface conditions during the glacial in comparison with the preceding interglacial stage (Fig. 5.2 and 5.3). Interestingly, our subsurface records (*G. inflata* and *G. truncatulinoides*) suggest temperature (ΔT) and relative salinity ($\Delta\delta^{18}O_{sw\text{-}ivc}$) differences during the LGM two times larger than MIS 6 (Fig. 5.4 A). These differences imply a high variability in the formation process and/or the advection of the SOIWs to the SPG thermocline during glacial stages.

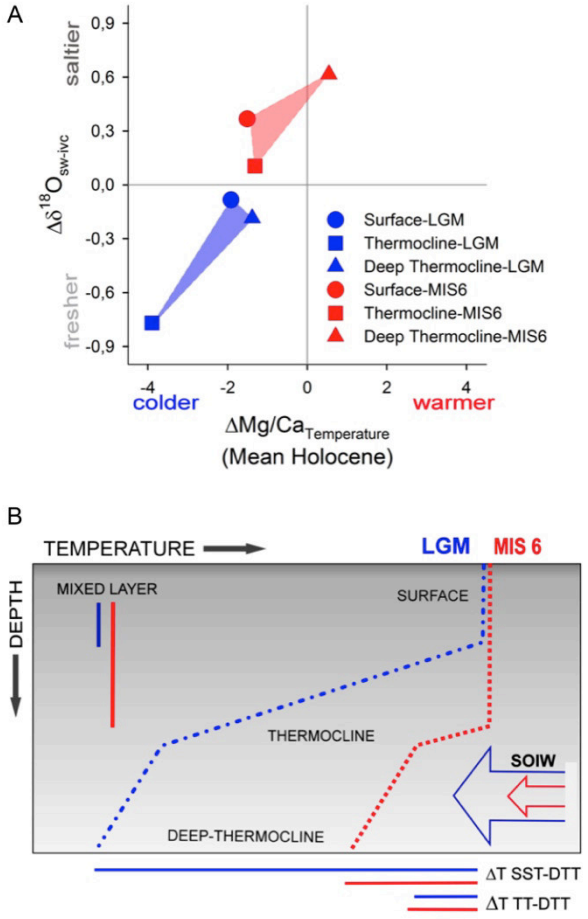

Figure 5.4: A) Salinity and temperature differences ($\Delta\delta^{18}O_{sw\text{-}ivc}$ and ΔT) during the LGM (blue) and MIS 6 (red) in comparison to mean Holocene values at the surface (circle), the thermocline (square) and the deep-thermocline (triangle). Colder and fresher than-the-Holocene subsurface-waters characterize the LGM. In contrast, MIS 6 shows subsurface waters saltier than-the-Holocene and warmer than-the-LGM. The pronounced subsurface differences of MIS 2-6 in temperature (ΔT ~2 to ~3 °C) and salinity ($\Delta\delta^{18}O_{sw\text{-}ivc}$ ~0.8 and ~0.9 ‰), suggest differences in the subsurface advection of SOIWs. **B)** Schematic overview of water column conditions in MIS 6 (red) and the LGM (blue). The saltier and warmer MIS 6 (a) shows small $\Delta T_{SST\text{-}DTT}$ (~2.2 °C) and $\Delta T_{TT\text{-}DTT}$ (~1.6 °C), suggesting a shallower mixed layer. Since MIS 6 and the LGM display similar surface temperatures, their ΔT is most likely controlled by the subsurface temperature. Therefore, subsurface co-variations in temperatures and salinities (cold/fresh LGM and warm/salty MIS 6), suggest relevant differences in the advection of cold and fresh SOIWs to the thermocline at the core site.

Assuming no temporal change in the habitat depth range of the planktic foraminifera as shown in figure 5.1 B and C, we calculate the thermal gradient between $SST_{Mg/Ca}$ and $DTT_{Mg/Ca}$ ($\Delta T_{SST\text{-}DTT}$), $SST_{Mg/Ca}$ and $TT_{Mg/Ca}$ ($\Delta T_{STT\text{-}TT}$) and $TT_{Mg/Ca}$ and $DTT_{Mg/Ca}$ ($\Delta T_{TT\text{-}DTT}$) to reconstruct the upper ocean structure.

The $\Delta T_{SST\text{-}DTT}$ values range on average from ~5 to ~2 °C, and increased continuously from MIS 6 to the Holocene, i.e. from on average ~2.2 °C (MIS 6), ~3.2 °C (MIS 5), ~3.7 °C (MIS 2), to ~4.5 °C (MIS 1; Fig. 5.5 A). The increasing $\Delta T_{SST\text{-}DTT}$ suggests a continuous shoaling of the thermocline since MIS 6, resulting in a thinned mixed layer towards the present. Similarly, the $\Delta T_{STT\text{-}TT}$ of ~0.5 °C (MIS 6) suggests a lower stratification and deeper mixed layer, in contrast a larger $\Delta T_{STT\text{-}TT}$ (~2.7 °C) occurs during LGM. A similar scenario is suggested by the $\delta^{18}O_{sw}$ gradient between surface and deep–thermocline ($\Delta\delta^{18}O_{sw}$ STT–DTT), showing small differences in salinity during MIS 6 in comparison to MIS 2 (Fig. 5.5 B).

Although, at thermocline water depths the $\Delta T_{TT\text{-}DTT}$ shows a similar pattern than the $\Delta T_{SST\text{-}DTT}$ during interglacial stages with large thermal gradients between upper and deeper thermocline depths i.e. ~3.4 °C (MIS 1) and ~2.9°C (MIS 5). Interestingly, in both glacial stages MIS 2 and MIS 6 low $\Delta T_{STT\text{-}TT}$ occurs (~1 °C and ~1.6 °C, respectively; Fig. 5.5 A).

The isotopic composition of the seawater at different water depths can act as a proxy for the mixing/advection of subsurface water masses (Rohling and Cooke, 1999). Adopting this approach, we take the $\Delta\delta^{18}O_{sw}$ *G. inflata – G. truncatulinoides* as a qualitative indicator of the subsurface mixing/advection (Fig. 5.5 B). The $\Delta\delta^{18}O_{sw}$ of *G. inflata – G. truncatulinoides* of the past 220 kyr is the smallest during the LGM and MIS 6 suggesting stronger subsurface mixing/advection ratios during full glacial stages.

5.4.2 Thermocline differences during the LGM and MIS 6

Taken together two general glacial scenarios emerge, with an emphasis on the thermocline. Firstly, during MIS 6 a highly homogenized water column (deep mixed layer, with low values of $\Delta T_{SST\text{-}TT}$, $\Delta T_{SST\text{-}DTT}$, $\Delta\delta^{18}O_{sw}$ *G. bulloides – G. truncatulinoides* and $\Delta\delta^{18}O_{sw}$ *G. inflata – G. truncatulinoides*) existed, with slightly saltier than−the−Holocene and warmer than LGM waters. Secondly, during the LGM, the water column was more stratified (thinner mixed layer, higher values of $\Delta T_{SST\text{-}TT}$, $\Delta T_{SST\text{-}DTT}$, $\Delta\delta^{18}O_{sw}$ *G. bulloides – G. truncatulinoides*) with

subsurface water fresher and colder than−the−Holocene. The resemblance of the subsurface temperatures ($TT_{Mg/Ca}$ and $DTT_{Mg/Ca}$) to the modern coldest variety of SOIWs (AAIW; 4 – 5°C; Hartin et al., 2011; McCartney, 1977) the substantial reduction of the temperatures differences between $TT_{Mg/Ca}$ and the $SST_{Mg/Ca}$ at the core site of sediment core E11-2 (Mashiotta et al., 1999; Fig. 5.1) and low $\Delta\delta^{18}O_{sw}$ *G. inflata – G. truncatulinoides* suggest an enhanced subsurface inflow of SOIWs to the site in comparison to the MIS 6 (Fig. 5.4 B).

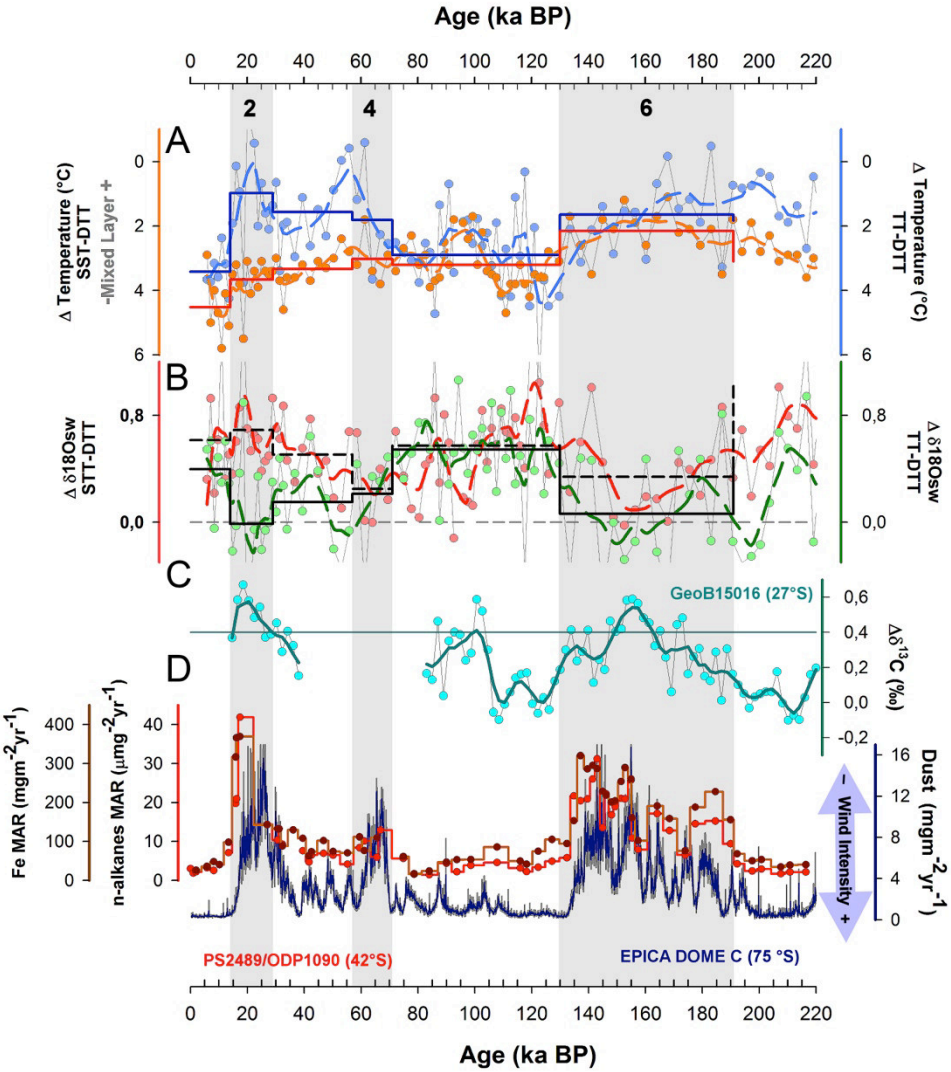

Figure 5.5: Vertical temperature differences (Δ Temperature) in the water column. **A)** Orange color indicates ΔTemperature between sea surface ($SST_{Mg/Ca}$) minus deep-thermocline ($DTT_{Mg/Ca}$). Light blue color denotes Δ Temperature between thermocline ($TT_{Mg/Ca}$) minus deep-thermocline ($DTT_{Mg/Ca}$). **B)** Calculated water isotopic difference ($\Delta\delta^{18}O_{sw}$). Red color indicates the $\Delta\delta^{18}O_{sw}$ between *G. bulloides* (surface) minus *G. truncatolinoides* (deep-thermocline; Gb-Gt). Green color denotes $\Delta\delta^{18}O_{sw}$ between *G. inflata* (thermocline) and *G. truncatolinoides* (Gi-Gt). Continuous lines correspond to 3-point running averages of the data (circles). Black dashed lines denote average values computed per isotopic stage (MIS 1 to MIS 6). The co-variation of $\Delta\delta^{18}O_{sw}$

$_{Gb\text{-}Gt}$, $\Delta\delta^{18}O_{sw\ Gi\text{-}Gt}$; $\Delta T_{SST\text{-}DTT}$ and $\Delta T_{TT\text{-}DTT}$ to lower values suggests a general scenario of a relative homogenous water column (lower stratification) during MIS 6. However, opposing LGM-gradient surface to deep-thermocline ($\Delta T_{SST\text{-}DTT}$ and $\Delta\delta^{18}O_{sw\ Gb\text{-}Gt}$) and thermocline to deep-thermocline ($\Delta T_{TT\text{-}DTT}$ and $\Delta\delta^{18}O_{sw\ Gi\text{-}Gt}$) suggest a stratified water column and stronger advection of cold and fresh water restricted to thermocline levels. **C)** The $\delta^{13}C$ gradient between GeoB15016 and the PDW stack ($\Delta\delta^{13}C_{DIC}$) reflects the site-specific variations on the $\delta^{13}C$ signal, which are driven by changing contributions of PDW and AAIW. Positive $\Delta\delta^{13}C_{DIC}$ values indicate measurable presence of AAIW. The dashed cyan line denotes the modern $\Delta\delta^{13}C_{DIC}$ (0.4 ‰) for site GeoB15016 (Martínez-Méndez et al., 2013). **D)** Insoluble dust flux in EPICA Dome C ice core (blue; Lambert et al., 2008) and the long-chain odd carbon-numbered n-alkanes (brown) and Fe-flux (red) at core location PS2489-2/ODP1090 (Martinez-Garcia et al., 2009).

5.4.3 Enhanced Pacific Intermediate Mode Water formation

Different glacial scenarios for the thermocline (discussed in Section 5.4.2) suggest glacial discrepancies in the lateral flux (advection) of the SOIWs to the SPG. Both, northward displacement and stronger SWW have been invoked to explain enhanced SOIW signals in the tropical and subtropical SEP during cold periods (Martínez-Méndez et al., 2013; Muratli et al., 2010; Pena et al., 2008/2013). However, a general consensus on the displacement or strengthening of the SWW during glacial stages is still lacking. Proxy reconstructions and models simulations suggest either an equatorward or poleward displacement of the SWW or an increase in wind-strength without latitudinal shift in comparison to today (e.g. Lamy et al., 2004; Markgraf et al., 1992; Otto-Bliesner et al., 2006; Shin et al., 2003; Sime et al., 2013).

Although the relationship between SST and wind displacements is not straightforward (Kohfeld et al., 2013), previous SST reconstructions from the SEP have been interpreted as reflecting a northward displacement of SWW and its associated oceanic frontal system during the LGM (Kaiser et al., 2005; Lamy et al., 2004). Glacial displacements of 7° and ~9° for the SAF and the Polar Front (PF) have been suggested to be recurrent features in this region during the last 700 kyr (Ho et al., 2012), similar in magnitude during the LGM and MIS 6. For this reason, it seems unlikely that a comparable extent in the glacial northward displacement of SWW could generate distinctly different SOIWs and contrasting subsurface

waters in the SPG (i.e., fresher−waters−than−Holocene during the LGM and saltier waters−than−Holocene during MIS 6; Fig. 5.4).

On the other hand, numerical experiments (Ribbe, 2001) and reconstructions for the LGM in the SEP (Muratli et al., 2010) have suggested a close link between the strength of the SWW and the SOIW formation. The intensification of the SWW have been often invoked among the factors controlling the increased glacial dust fluxes in East Antarctica (Lambert et al., 2008), South Pacific (Lamy et al., 2014) and as far north as 42° S in the South Atlantic (Martínez-Garcia et al., 2009). The comparison of Holocene and LGM proxy data suggest an intensification of the Antarctic Circumpolar Current (ACC; Noble et al., 2013), with no significant change of its mean location (Matsumoto et al., 2001). Since the ACC is partially driven by the SWW, the current intensification has been interpreted as an evidence for stronger winds during the LGM (Matsumoto et al., 2001). Another analogue to evaluate the response of the ocean to changes in wind intensity is the Southern Annular Mode (SAM). The SAM is the main climatic mode controlling the winds in the Southern Hemisphere (Thompson and Solomon, 2002), defined as the alternating pattern of strengthening and weakening of westerly winds between the mid and high latitudes in the Southern Hemisphere. The SAM alters 1) the strength of northward Ekman Flow, 2) the upwelling along the Antarctic Continent, 3) the vertical tilt of the isopycnals, and 4) inducing downwelling at ~45°S (Hall and Visbeck, 2002; Lenton and Matear, 2007; Lovenduski and Gruber, 2005; Oke and England, 2004). The tight coupling between SAM and the water properties of SAMW formed in the Pacific Basin (160°E to 80°W) has been suggested by field studies (Ayers and Strutton, 2013; Lovenduski and Gruber, 2005). During positive SAM events, the belt of strong SWW contracts, therefore intensifying SWW over the ACC and weakening the SWW north of 45°S. Conversely, a negative SAM event reflects the expansion of the strong SWW belt towards the equator. In the Pacific Basin, these wind anomalies are significantly correlated with nutrient and temperature properties of the SAMW (Ayers and Strutton, 2013).

During positive SAM-events, the intensified SWW produce negative wind stress curl anomalies south of the maximum wind stress, a higher northward Ekman transport throughout the region of the SWW, and positive wind stress curl anomalies north of the maximum wind stress. These conditions result in anomalous surface divergences and convergences (Hall and Visbeck, 2002; Saenko et al., 2005), which drive increased upwelling south of and in the ACC-area, ultimately causing the northward transport of colder water toward the regions of SAMW and AAIW formation (Oke and England, 2004). Therefore, increased downwelling in the Subantarctic Zone results in a rapid formation of SAMW (Ayers and Strutton, 2013; Lovenduski and Gruber, 2005).

Although a decadal oscillation like SAM cannot be resolved by the resolution of this record, we assume that SAM-like changes operated over longer time scales (e.g. Moreno et al., 2014). Hence, we speculate that the subsurface temperature and salinity conditions at our study site are mainly controlled by the strength of the SWW, modulating the vigor of the Ekman transport toward the formation-regions of SAMW and AAIW (Oke and England, 2004). Furthermore, stronger winds in the Southern Ocean generally imply deeper mixing, and hence deeper mixed layers. These factors are a crucial pre−requisite for the formation of AAIW and SAMW (Hanawa and Talley, 2001; McCartney, 1977).

5.4.4 Reconstructed glacial variability of SOIW

Proxy reconstructions from the western side of South America suggest a constant formation and northward advection of colder modes of SOIW, namely AAIW, during glacial stages (Martínez-Méndez et al., 2013). Notably, this process increased during the LGM in comparison with other glacial stages (Martínez-Méndez et al., 2013) and the Holocene (Muratli et al., 2010). This increase is in good agreement with our subsurface records, which show a pronounced cooling and freshening at the subsurface during LGM in comparison with the Holocene (Fig. 5.4). In spite of the differences in proxies used, an enhanced presence of

colder modes of SOIWs (AAIW) seems ubiquitous in different LGM settings along the Chilean slope (Martínez-Méndez et al., 2013; Muratli et al., 2010) and the subsurface SPG (cooling and freshening, this study). Lower thermal differences between the reconstructed subsurface temperatures in the SPG and the $SST_{Mg/Ca}$ further south (E11-2; Mashiotta et al., 1999) during LGM, support the idea of a stronger meridional transport, resulting in a tighter connection between the SPG and the main formation area of SOIWs in the SEP.

On the other hand the homogenous water column with warmer and saltier subsurface conditions (relative to the LGM) during MIS 6 (Fig. 5.4), is probably owed either to a reduction and/or to ceasing SOIW advection to the South Pacific Gyre's thermocline from the SEP. These conditions are contrasted by the SOIWs signal observed at 27° S, whereas the signal during MIS 6 is on average weaker than that during the LGM, but still stronger than that during the Holocene (Fig. 5.5; Martínez-Méndez et al., 2013). Divergent observations at the Chilean slope and in the open ocean suggest differential variations in the advection of SOIWs during glacial stages, with a relatively stable northward advection of the denser modes of SOIWs along the South American continent and a more fluctuating advection of SOIWs that feed the SPG's thermocline. It is noteworthy that the variations in the intensification of the advection process and possibly also the formation of SOIWs, are tightly linked to temporal trends in dust fluxes (a proxy for wind strength), in the South Atlantic and Antarctica (Fig. 5.5 D; Lambert et al., 2008; Martínez-Garcia et al., 2009). The decrease in the salinity during the youngest part of MIS 6 (Fig. 5.3 D, E) corresponds to an increase in dust flux since ~160 kyr B.P., further reinforcing the role of SWW intensity as the main driver of the SOIWs injection to the SPG (Fig. 5.5 D). Strong winds could break down the ocean stratification, thereby allowing a rapid development of deep mixed layers, which in turn lead to the formation of AAIW and SAMW, and promoting the subduction of these waters to the South Pacific Gyre.

5.5 Conclusions

Glacial–interglacial changes in the reconstructed temperatures and relative salinities from deep-dwelling foraminifera (*G. inflat*a and *G. truncatulinoides*) suggest variations in the presence of SOIWs in the South Pacific Gyre.

The results of this study indicate, that the inflow of SOIWs to the South Pacific Gyre can be highly variable during different glacial stages, resulting in subsurface waters during LGM, which are colder and fresher than−the−Holocene. Comparatively, MIS 6 is characterized by warmer (DT ~3 to ~2°C) and saltier ($\delta^{18}O_{sw}$ ~ 0.9 to ~ 0.8 ‰) subsurface waters (relative to LGM). These findings provide a competing hypothesis to previous findings that propose a stable and continuous influence of the SOIWs during glacial stages.

Various scenarios of SOIWs formation/advection, inferred from our data in the South Pacific Gyre and previously published data in the South East Pacific and South West Pacific, suggest spatial heterogeneity in the northward transport of the SOIWs signal in the Pacific basin. The modern relationship between advection/formation processes of the SOIWs and SWW intensity indicates the influence of wind–strength (SWW) on the SOIWs advection/formation, rather than solely its glacial latitudinal migration.

5.6 Acknowledgments

This study is part of the project SOPATRA (SOuth PAcific paleoceanographic TRAnsect) funded by the German Ministry of Education and Research (BMBF) trough grant No. 03G0213B. Technical support and laboratory assistance from N. Gehre, L. Haxhiaj (GEOMAR) and L. Schönborn (AWI) are highly appreciated. We are grateful to S.L. Ho, S. Contreras and J. Groeneveld for their comments and suggestions during the preparation of this manuscript, and two anonymous reviewers for their valuable comments that improved the final version of this article.

5.7 Supplementary Material

5.7.1 Age Control

Three radiocarbon measurements were performed at the Leibniz-Laboratory for Radiometric Dating and Isotope Research of the University of Kiel, Germany. The purpose of this analysis was to 1) confirm the Holocene age of the surface sediment (multicorer SO213−59−1) and, 2) improve the age model of the gravity core SO213−59−2.

Table 5.S1 ^{14}C AMS ages analyzed on planktic foraminifera and calibrated ages 1) confirming the Holocene age for SO213−59−1 (multicorer, MC) and; 2) ^{14}C AMS ages supporting the age model for the gravity core SO213−59−2 (GC).

Core	Depth (cm)	Species	Conventional age (yr BP)	Standard deviation (± yr)	Reservoir Age (yr)	Laboratory code
SO213-59-1 (MC)	0-1	Planktic mix	8001	210	560	KIA 45888
SO213-59-2 (GC)	9-10	*G. bulloides*	10669	122	560	KIA 47137
	45-46	*G. bulloides*	33487	366	560	KIA 47139

5.7.2 Assessing data quality and cleaning efficiency

The covariance of Mg/Ca with other secondary phase elemental ratios, such as Fe/Ca or Mn/Ca, can be used as an indicator of contamination on the measured Mg/Ca. The presence of clays and/or authigenic minerals may be indicated by high Mg/Ca ratios in association with elevated Fe/Ca. Similarly, the presence of authigenic ferromanganese carbonate overgrowths, or ferromanganese oxide precipitates, may be indicated by elevated values and positively correlated Fe/Ca and Mn/Ca ratios (Barker et al., 2003). In figure 5.S1, both Fe/Ca and Mn/Ca show no clear positive correlation with Mg/Ca, therefore suggesting no obvious control on the Mg/Ca variability.

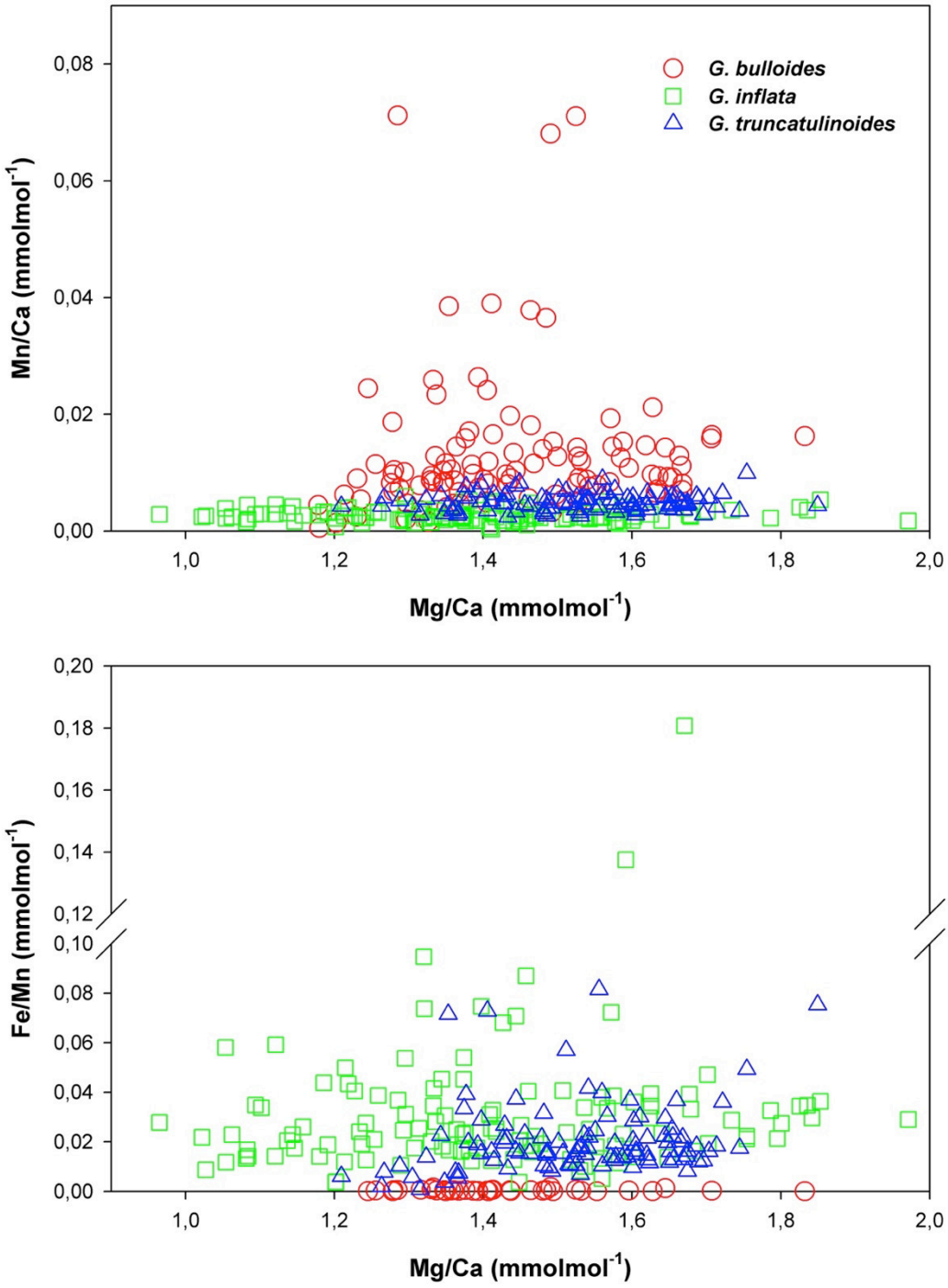

Figure 5.S1: Mg/Ca plotted against (a) Mn/Ca and (b) Fe/Ca, indicating that contamination has not controlled Mg/Ca variability.

5.7.3 Assessing the impact of dissolution on Mg/Ca–derived temperatures in the South Pacific

Dissolution is known to affect the preservation of the Mg/Ca signal in planktic foraminifera (Brown and Elderfield, 1996; Dekens et al., 2002; Regenberg et al., 2006; Regenberg et al., 2014), in particular in bottom waters undersaturated with respect to calcite when $\Delta[CO_3^{2-}] < 0$ mol/kg and $\Omega_{calcite}$ <1 (Brown and Elderfield, 1996; Regenberg et al., 2014) until its final absence from sediments at the snowline of the calcite–compensation depth (100% CaCO dissolution).

Dissolution not only reduces Mg/Ca and therefore lowers the paleotemperature estimates, but also foraminiferal test–weight (Dekens et al., 2002; Brown et al., 1996; Regenberg et al., 2006, 2014). Notwithstanding the aforementioned, high fidelity of temperature estimates have been suggested for *G. bulloides* based on the comparison of Mg/Ca–derived temperatures against dissolution proxies (Mekik et al., 2007) and results from laboratory experiments (Marr et al., 2013). In addition, we also do not observe any systematic trend in the shell weight and Mg/Ca ratios of the *G. bulloides* in our core (Fig. 5.S2).

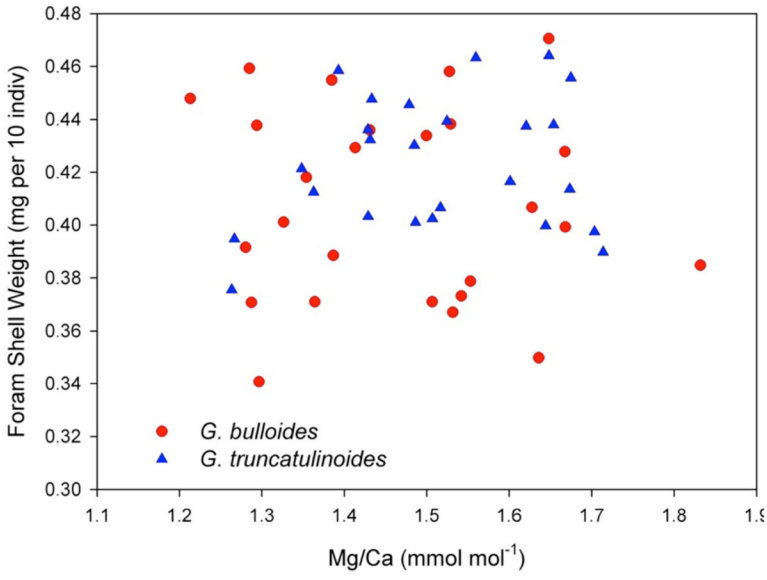

Figure 5.S2: Random selection of shell weights plotted against Mg/Ca in *G. bulloides* and *G. truncatulinoides*, in both cases the coefficient of correlation (R^2) is < 0.1, discarding dissolution as the main factor controlling Mg/Ca variability.

Moreover, *G. bulloides*–Mg/Ca values along core SO213–59–2 (1.1 – 1.8 mmol/mol) are within the range of 0.9 – 2.4 mmol/mol (< 220 kyr) at a shallower site in the Southwest Pacific (1200 m water depth) with good foraminifera preservation (Pahnke et al., 2003). In spite that the core SO213–59–2 is close to the modern calcite saturation horizon (CSH, defined as $\Omega_{calcite}$ = 1) at ~ 3100 m water depth observed in the SW Pacific (Bostock et al., 2011), roughly $\Delta[CO_3^{2-}] < 0$ µmol/kg (Regenberg et al., 2014; Fig. 5.S3).

Although it is true that Mg is most likely selectively removed from the foraminiferal tests and related Mg/Ca–temperatures are presumably underestimated. However, we refrained from applying the Mg/Ca correction of 0.1 – 0.2 °C per µmol/kg for surface and 0.4 – 0.6 °C per µmol/kg for subsurface-dwellers (Regenberg et al., 2014), as it leads into unrealistic corrected (modern) subsurface temperatures ~8 to 12 °C warmer.

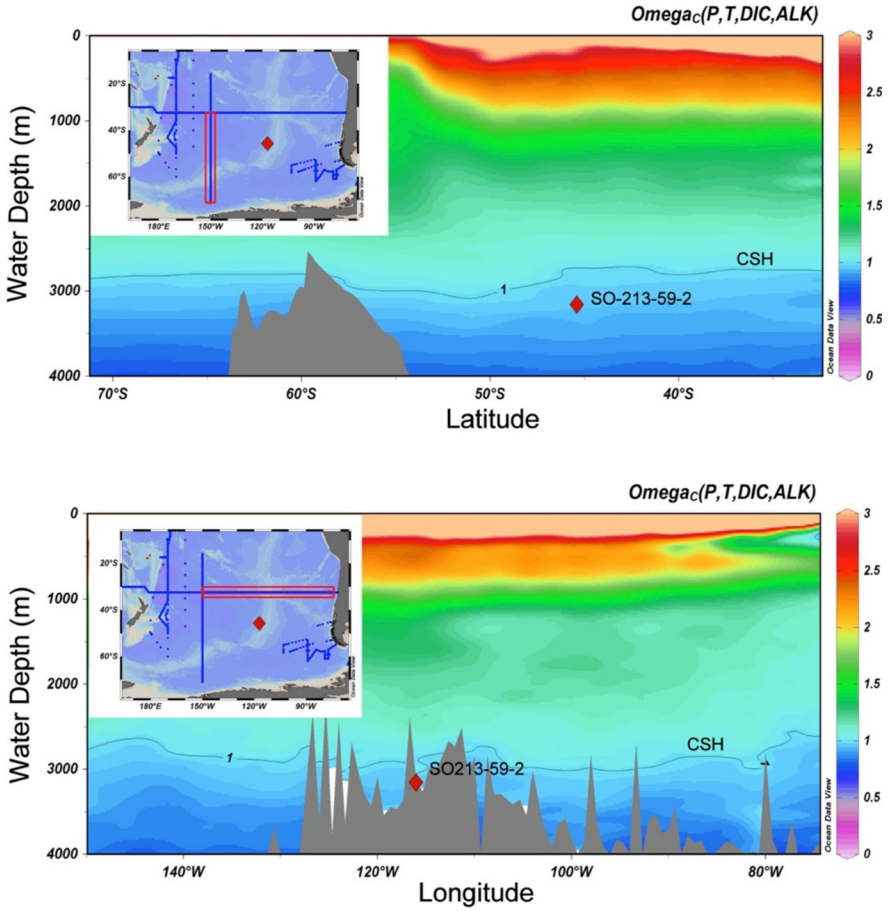

Figure 5.S3: Calcite saturation ($\Omega_{calcite}$) for transects P16S 2005 (upper panel) and P06 2003 (lower panel), calculated from the DIC and alkalinity in the CARINA database (Brown and Elderfield, 1996; Key et al., 2010) using the Ocean Data View software (Schlitzer, 2014). Location of transects and sediment core SO213-59-2 (red diamond) is shown on the maps. Calcite saturation horizon (CSH, $\Omega_{calcite}$ = 1) contour is highlighted to show the extrapolated depth of the CSH across the basin.

Additionally, glacial SST–cooling of ~4 °C observed in our record is in agreement with previous paleoceanographic studies in the Subantarctic South Pacific based on foraminiferal census counts and Mg/Ca ratios (111 – 123 °W; Barker et al., 2003; Luz, 1977; Mashiotta et al., 1999). Taken together, these observations suggest that the downcore Mg/Ca-derived temperature variations reconstructed at our site are unlikely to be affected by dissolution.

5.7.4 Additional Factors of variability in the foraminiferal $\delta^{18}O$

We are aware that not all the planktic foraminifera calcify in equilibrium with seawater due to a number of different biological processes (symbiont activity, ontogeny) that may affect the $\delta^{18}O$ fractionation processes (Rohling et al., 1999). This offset (vital effect) varies between species and is particularly difficult to estimate for species with large vertical habitat ranges, and for species lacking available culture data (Spero and Lea, 1996).

Previous works (Mortyn and Charles, 2003; Spero et al., 2003; Steph et al., 2009; Wilke et al., 2009) suggest that the species considered here (*G. inflata* and *G. truncatulinoides*) have large a spread of disequilibria frequently centered about a zero offset (Table 5.S2). Consequently there is no consensus on a possible oxygen isotopic disequilibrium. For this reason and because *G. inflata* and *G. truncatulinoides* are nonsymbiotic species that are believed to precipitate their shell calcite at/or close to equilibrium (Fairbanks et al., 1980), we assume that the vital effect did not affect the results of this study.

Table 5S2 :Values of vital effects reported in the literature.

	Disequilibrium (‰)	Size Fraction (µm)	Reference
G. inflata	-0.4 to +0.4	> 200	(Niebler et al., 1999)
	+0.01 to +0.25	350 – 450	(Loncarcic et al., 2006)
	0.94	150 – 250	(Mortyn and Charles, 2003)
	-0.2	NA	(Deuser and Ross, 1989)
G. truncatulinoides	-0.3 to +0.2	>250	(Niebler et al., 1999)
	+0.2	NA	(Steph et al., 2009)
	-0.10 to +0.16	350 – 450	(Loncaric et al., 2006)
	1.1	150 – 250	(Mortyn and Charles, 2003)
	-0.11	280 – 440	(Wilke et al., 2009)
	0	NA	(Deuser and Ross, 1989)

Chapter 6

Conclusions and perspectives

6.1 Conclusions

In this thesis, a combination of different paleoceanographic proxies was used to reconstruct the ventilation and circulation history of the South Pacific. The principle aim of these reconstructions was to decipher oceanic processes, influencing the global carbon cycle, which ultimately affect the global climate on millennial time-scales via variations in ocean-to-atmosphere interactions.

The $\Delta^{14}C$-reconstructions on sediment records from the New Zealand Margin (NZM) and the East Pacific Rise (EPR) indicate the existence of a glacial pool, enriched in ^{14}C-depleted CO_2 in Circumpolar Deep Waters between ~2000 and ~4500 m water depth (*Chapter 3*). This pattern shows a striking analogue to the modern radiocarbon-distribution in the Pacific Ocean (Key et al., 2004). Similar as today (but by far more depleted), the most pronounced radiocarbon-depletion was recorded in water depths between ~2500 and ~3600 m. During the glacial, these waters yielded a maximum deep-water to atmosphere radiocarbon offset ($\Delta\Delta^{14}C$) of up to ~-1000‰ that equates to an apparent ventilation age of ca. 8000 years. These findings (extreme depletion at ~2500 m water depth; lower depletion above and below) are corroborated by stable isotope analyses on sediment cores north of the Chatham rise, which also indicate poorly ventilated glacial waters between 2000 and 3500 m water depth (McCave et al., 2008). This carbon reservoir was not only restricted to the NZM but also extended through the entire South Pacific, as our analyses at the EPR and records from the Drake Passage (Burke and Robinson, 2012) suggest. The large glacial range in the $\Delta^{14}C$ distribution (~5 times higher than in the Holocene) between ~830 and ~4500 m water depth suggests that an increase in water mass stratification of the deep and intermediate Southern Ocean resulted in the separation of the deep-ocean from the surface and therefore from the atmosphere.

Different glacial boundary conditions (Sigman et al., 2010), like the northward expansion of Antarctic sea ice (Gersonde et al., 2005), the northward shift of the Southern Westerly Winds (Kohfeld et al., 2013) and increased buoyancy differences between deep- and intermediate-waters (Adkins, 2013; Saenko and Weaver, 2001) have the potential to trigger and maintain this pronounced glacial stratification. Paralleled by an early warming in the west Antarctic (WAIS Divide Project members, 2013), the retreat of the Amundsen Sea shelf ice (Klages et al., 2014), and the rise in Southern Hemisphere midsummer insolation at ~65°S (Schulz and Zeebe, 2006), a first rejuvenation of the upper and lower boundaries of the glacial carbon pool is observed at ~21,000 years B.P. These waters were incorporated into the intermediate-waters as a drop in the AAIW $\Delta\Delta^{14}C$ indicates. However, the persistent restriction in air-sea gas exchange prevented the release of CO_2 via this pathway. During Termination 1 (~18 – 11.5 kyr B.P.), the rejuvenation of the most depleted waters at ~2500 m water depth parallels the increase in atmospheric CO_2. The conclusion that these deep-waters contributed to the rise in $CO_{2\ atm}$ is corroborated by the intermediate-water record of carbonate ion concentrations (*Chapter 3*; Kersten, 2013), which indicates the release of CO_2 in the formation area of this water mass (AAIW) that clearly parallels the rise in deep-water $\Delta\Delta^{14}C$. Summarizing, the results of *Chapter 3* prove the existence of the glacial carbon pool in the deep South Pacific and indicate its importance for the variability in atmospheric CO_2.

On longer timescales as well, the results of this thesis provide new implications for water mass and circulation changes in the southwest Pacific as well as for the evolution of the glacial carbon pool trough time (*Chapter 4*). Stable isotope records from the AAIW and UCDW, covering the last 350,000 years indicate a significant upward displacement of the AAIW-UCDW boundary during glacial intervals. In contrast to Pahnke and Zahn (2005) who suggested that enhanced water mass stratification affected the AAIW, the results of *Chapter 4* point to a shift in water mass boundaries. Freshwater input in AAIW by the northward

expansion of Antarctic sea ice (Saenko and Weaver, 2001; Gersonde et al., 2005) and increased bottom-water salinity by enhanced brine rejection (Adkins, 2013), increased glacial differences in deep- and intermediate water buoyancy, ultimately triggering the upward displacement of AAIW. Modeling runs as well point to this setup as the driving process, influencing the AAIW-UCDW boundary. It is furthermore suggested that the observed expansion of glacial UCDW also increased the volume of the glacial carbon pool. This finding might prove important for future reconstructions of the oceanic carbon budget during glacial periods.

In the open South Pacific (EPR), Mg/Ca derived temperature reconstructions on planktic foraminifera suggest important variations in the thermocline of Southern Ocean Intermediate Waters (SOIWs; *Chapter 5*). The temperature gradient, reconstructed on *G. bulloides* (surface-dweller) and *G. truncatulinoides* (deep-dweller) indicates the subsurface temperature of MIS 6 to be ~2 to ~3°C warmer than during the LGM. As the SOIWs are particularly important for the ventilation of the South Pacific Gyre, the results of *Chapter 5* show that the transfer of climatic and oceanic signals from the Southern Ocean to lower latitudes is strongly influenced by subsurface processes in these waters.

As it was concluded above, the aims, introduced in *Chapter 1.4* were achieved by the results of the different manuscripts, combined in this thesis. Summarizing, the results of these manuscripts clearly point to the importance of the Pacific Ocean in general, and of circulation and ventilation processes in detail on the global climate on glacial/interglacial timescales.

6.2 The Last Ocean: Constraining the carbon pool in the glacial Indian Ocean

As we showed in *Chapter 3*, the role of the Pacific return flow has been underestimated in most reconstructions of the glacial carbon cycle.

The modern Indian Ocean (IO) as well houses an old deep-water return flow (however, less pronounced as in the Pacific; Fig. 6.1; Mantyla and Reid, 1995; Talley, 2013). These old Indian Deep Waters received only negligible attention in the "*ventilation branch*" of the paleoceanographic community.

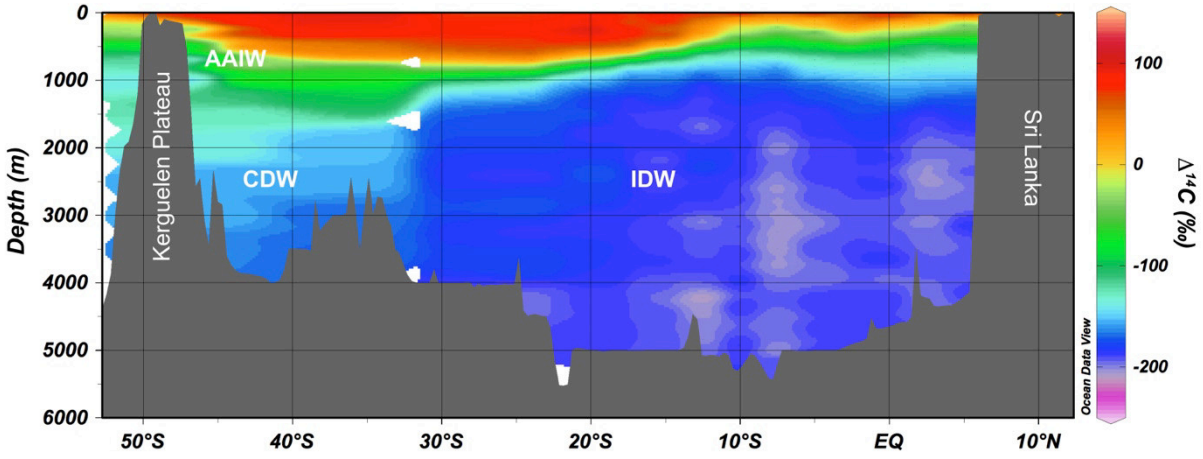

Figure 6.1: Indian Ocean $\Delta^{14}C$ distribution along ~80° E (Key et al., 2004). Antarctic Intermediate Water – AAIW; Circumpolar Deep Water – CDW; Indian Deep Water – IDW.

However, to constrain the glacial carbon cycle, the extent of old CO_2-rich deep-waters and to allow better simulations of the oceans carbon budget as well as its interaction with the atmosphere, reconstructions from the IO are of great importance. Isotopic data from the western side of the IO indeed point to the existence of old waters in the intermediate-water level off Tanzania during Termination 1 (Romahn et al., 2014). Nevertheless, (De Pol-Holz et al., 2012) showed that intermediate-water in the Indonesian Throughflow off Sumatra was constantly in equilibrium with the contemporaneous atmosphere over the last 45,000 years. Considering these ambiguous results, new analyses on a transect of sediment cores, covering the major water masses in the IO, are desirable. Located close to the upwelling regions in the IO sector of the Southern Ocean, just downstream of the ACC (Carter et al., 2009; Zhou et al., 2014), the Kerguelen Plateau might provide an interesting region for the analysis of IO ventilation. However, as You (2000) showed, the return flow of Circumpolar Deep Water in the IO is more pronounced in the South Australian Basin than towards the north of the

Kerguelen Plateau. Wrytki (1973) as well suggested that the deep-waters surrounding the Kerguelen Plateau derive primarily from Atlantic deep-water. Nevertheless, as it is shown in figure 6.1, a sediment core depth transect at the Kerguelen Plateau might provide significant insight in the recirculation of old and $\Delta^{14}C$-depleted CDW, particularly during glacial times that yielded a more extensive carbon pool. Furthermore, an ongoing project (Michel et al., 2014) is currently aiming to decipher changes in surface reservoir ages of the Kerguelen area over the time of the last deglaciation. These reconstructions would significantly improve ventilation age reconstructions using planktic and benthic foraminifera by constraining the ^{14}C-age of surface-dwelling organisms.

6.3 Improvement of data-model-comparisons

The Atlantic centered view of many modeling studies (e.g. Hain et al., 2010; Hesse et al., 2011; Kwon et al., 2012; Matsumoto and Yokoyama, 2013) might result in spurious reconstructions of oceanic patterns in the other ocean basins like the South Pacific (e.g. Butzin et al., 2005). These authors suggested an increased glacial ventilation of the deep Pacific Ocean at ~45° S, clearly contradicting the findings shown in *Chapter 3*. Therefore a better combination of ocean and climate models with proxy data from the Pacific Ocean is desirable. In combination with state of the art circulation and climate models, the data shown in this study might help to better evaluate glacial and interglacial processes in the global carbon cycle. As well, these results could be used to quantify the amount of CO_2 contained in the deep-ocean, and considering the AAIW ventilation history also to assess the quantity of CO_2 that was released to the atmosphere via deep-water upwelling in the Pacific Southern Ocean.

Regarding the complex ventilation-pattern of the glacial ocean (young AAIW; increasing age below 2000 m; highest ages between 2500 and 3600 m; and decreasing ages towards 4300 m)

it is furthermore desirable to improve the depth resolution of circulation models that tend to apply an increasing layer spacing in bottomward direction (e.g. **HAM**burg **O**cean **C**arbon **C**ycle Model – HAMOCC; Maier-Reimer et al., 2005).

6.4 Beyond MIS 2-3

The reconstruction of water mass ventilation ages shown in *Chapter 3* ends basically at the onset of MIS 3 (MIS 3 - ~27kyr to 60 kyr B.P.; Van Meerbeeck et al., 2009). As the deep-water masses are significantly better ventilated during MIS 3 than during MIS 2 (Fig. 6.2), ventilation reconstructions over the whole radiocarbon timescale (IntCal13 0 – ~50,000 calendar years B.P.; Reimer et al., 2013) can be of great importance for the understanding of long-term ventilation changes in the Southern Ocean.

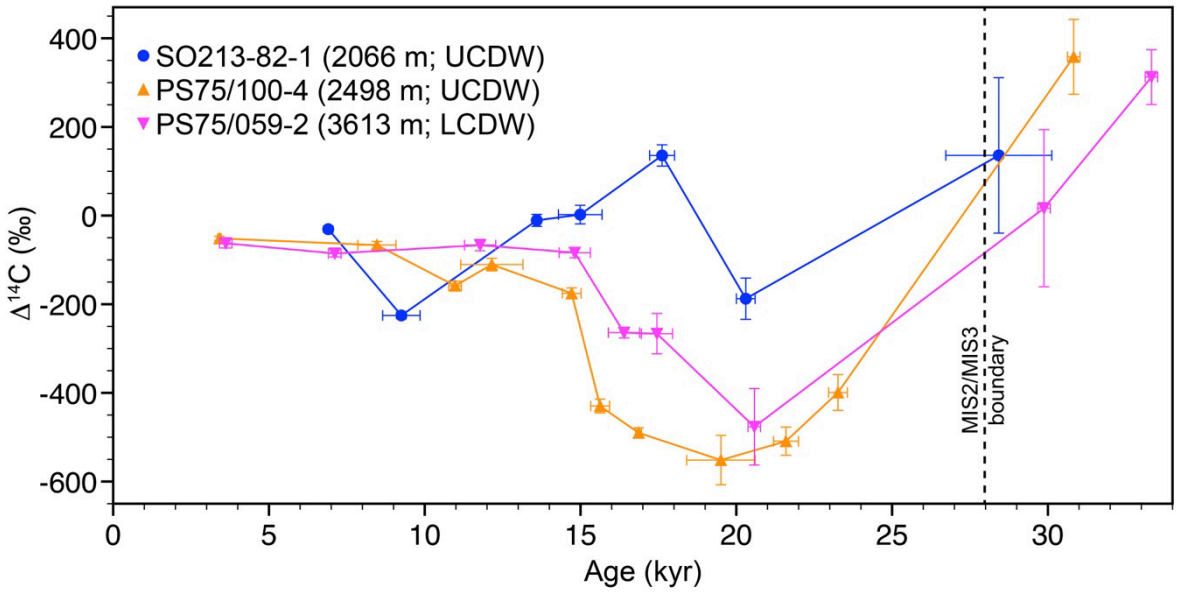

Figure 6.2: Circumpolar Deep Water $\Delta^{14}C$ history. The dashed line marks the boundary between MIS 2 and MIS 3.

Beyond the range of radiocarbon, a combination of other ventilation-proxies like $\delta^{13}C$ or carbonate ion concentrations together with (quasi-) conservative water mass tracers like ε_{Nd} can be very instructive for the reconstruction of Pleistocene carbon cycle processes.

Understanding the processes that conditioned the last interglacial (MIS 5) might further help to understand glacial to interglacial transitions. In particular the reconstruction of MIS 5e, where the global sea level is assumed to have been several meters higher than today (Shackleton et al., 2003), would help to understand and predict the events affecting our modern climate system.

6.5 Assessing AAIW variability in other regions

As it was shown in *Chapter 3*, several controversial records of AAIW ventilation were published over the last years (e.g. Marchitto et al., 2007; Stott et al., 2009; Bryan et al., 2010). Despite the intriguing pattern of extremely decreased ventilation during Heinrich Stadial 1 (HS 1) and the Younger Dryas (YD), these extreme results could not be reproduced by SO records of decreased AAIW ventilation (De Pol-Holz et al., 2010; Rose et al., 2010; results of *Chapter 3*; Fig. 6.3). However, the common denominator of all records, yielding extreme AAIW ventilation ages is that these sediment cores were recovered from upwelling regions off Baja California (Marchitto et al., 2007), Galapagos (Stott et al., 2009) and Oman (Bryan et al., 2010; Fig. 6.4). As today, these cores lie close to the boundary of intermediate-water and underlying deep-water. Therefore it can not be ruled out that the pronounced depletion was caused by contact to underlying old deep-water, induced by shoaling of intermediate-water as discussed in *Chapter 4*. This process could have enabled the upward extension of radiocarbon depleted deep-water during these time intervals, hence explaining the aberrant patterns from the SO and the lower latitude upwelling regions.

Basak et al. (2010) suggested that the ε_{Nd}-signal of the sediment record off Baja California (MV99-MC19/GC31/PC08; 705 m water depth) indicates the presence of AAIW during the pronounced $\Delta^{14}C$-depletion events coinciding with HS1 and the YD. However, according to the findings of Noble et al. (2013), the negative ε_{Nd}-values found by Basak et al. (2010) can

also be explained by contact to underlying deep-water. Therefore, a more precise analysis of the vertical AAIW extent at these (Baja California, Galapagos and Oman) and other sites could bring a new a perspective into the debate on pathways of upwelled, deglacial CO_2.

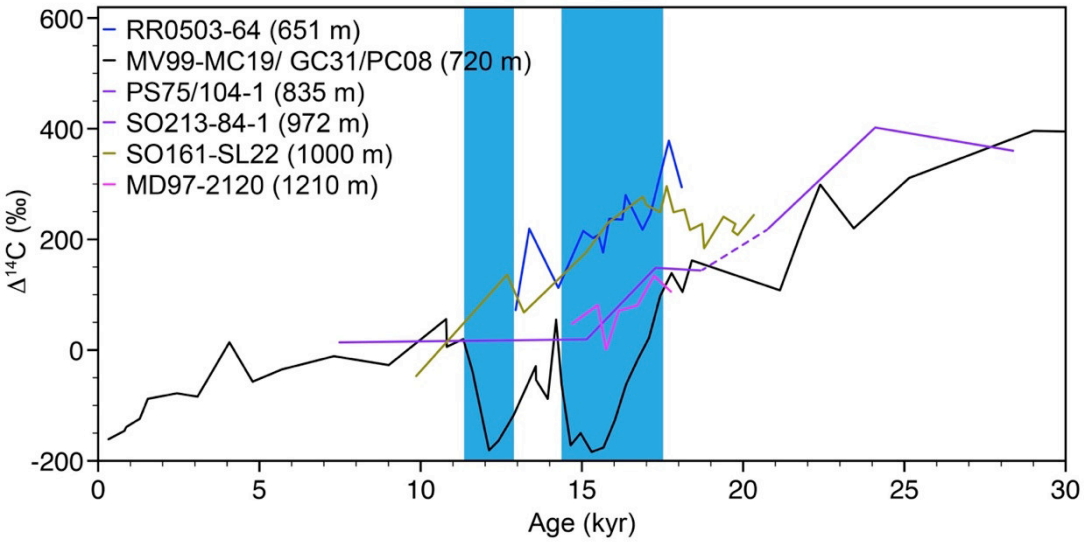

Figure 6.3: AAIW $\Delta^{14}C$ records for the last 30,000 years. RR0503-64 (Bay of Plenty, NZ) and MD97-2120 (Bounty Trough, NZ) by Rose et al. (2010); MV99-MC19/BG31/PC08 (Baja California) by Marchitto et al. (2007); SO161-SL22 (Chile) by De Pol-Holz et al. (2010). Records PS75/104-1 and SO213-84-1 (Bounty Trough, NZ) originate from this study. The blue bars indicate the Younger Dryas (left) and Heinrich Stadial 1 (right).

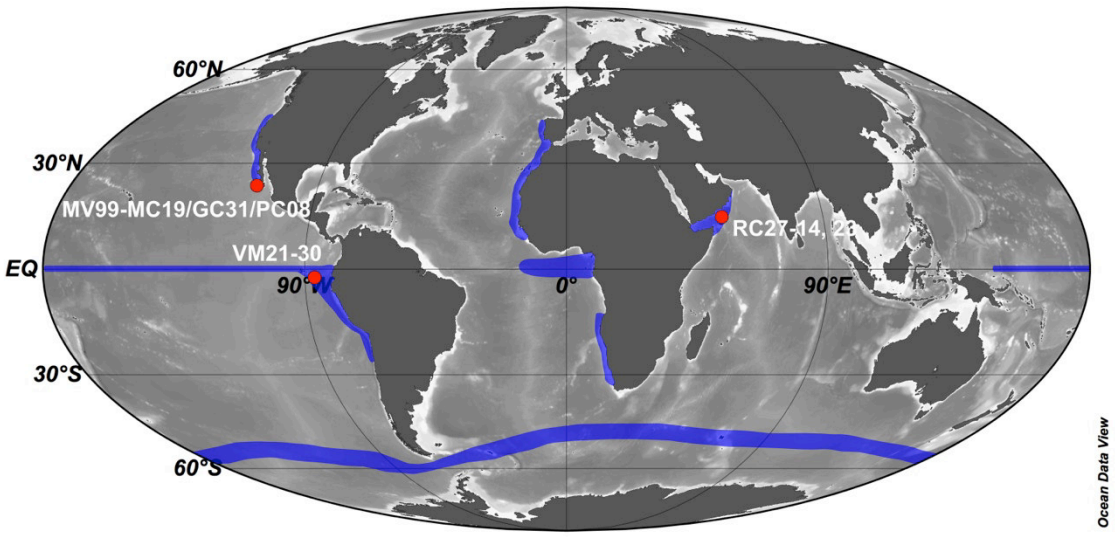

Figure 6.4: Approximate locations of global upwelling systems (blue shadings) according to Anderson and Lucas (2008). Red dots indicate core positions. MV99-MC19/GC31/PC08 (Marchitto et al., 2007); VM21-30 (Stott et al., 2009) and RC27-14, 23 (Bryan et al., 2010).

In addition, other records as well should be re-evaluated, regarding the findings of *Chapter 4*. For example, Leduc et al. (2010) discuss a shift from more positive to more negative $\delta^{13}C$-values in sediment core MD02-2529 (1619 mbsl off Costa Rica). They interpret this pattern as a competition between northern-sourced nutrient-rich (low in $\delta^{13}C$) and southern-sourced nutrient-poor (high in $\delta^{13}C$) water masses. However, this sediment core as well lies very close to the AAIW/NPIW to PDW boundary. Hence, a shoaling of intermediate-water could as well plausibly explain the $\delta^{13}C$ record of Leduc et al. (2010; Fig. 6.5). In this light, isotope records from sediment cores, peculiarly close to the intermediate-/deep-water boundary, should be re-evaluated on the process of intermediate-water-shoaling.

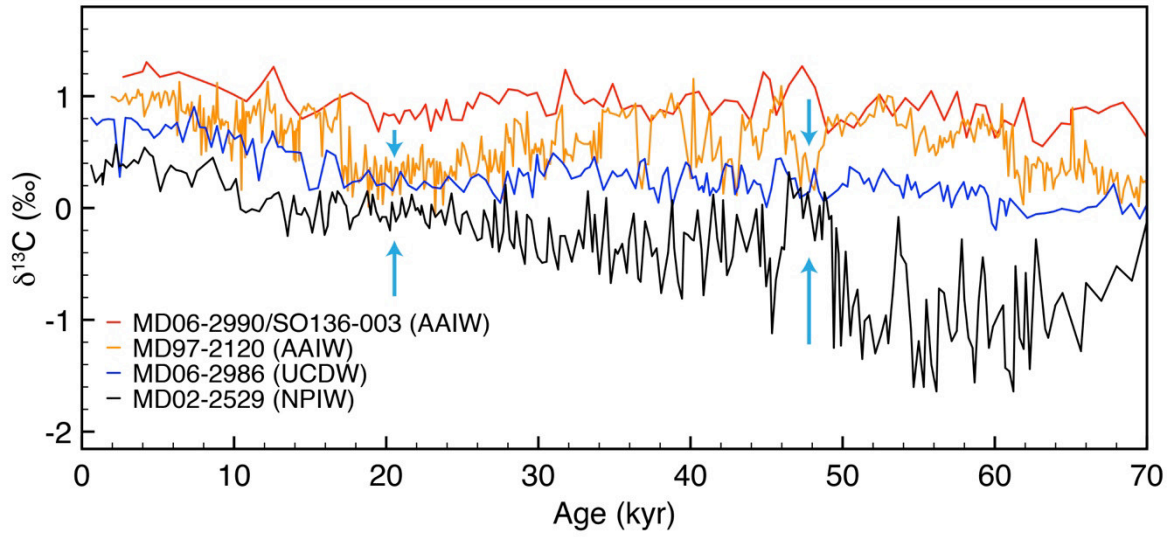

Figure 6.5: Intermediate-water variability in the southwest and equatorial Pacific. The blue arrows mark intervals of possible intermediate-water shoaling. Modern water masses are indicated in brackets. In the SW-Pacific (MD97-2120; orange line; Pahnke and Zahn, 2005) the isotopic values drop to the level of the UCDW (MD06-2986; blue line; this study), while the values in the equatorial Pacific (MD02-2529; black line; Leduc et al., 2010) rise from more negative NPIW-like values (Key et al., 2004) to Southern Ocean UCDW-like values. During these intervals, a record, more distant from the AAIW/UCDW-boundary (MD06-2990/SO136-003; red line; this study), shows that the drop in $\delta^{13}C$ did not affect the entire SW-Pacific AAIW.

Chapter 7

Epilogue

Nowadays, the discussion on the topic of climate change is more vivid than ever. Everyday, in news, social-media and blogs, one or the other aspect of anthropogenic caused climate change (AC^3) and its consequences are discussed in length.

Despite all the evidence pointing towards AC^3 and global warming (IPCC Members 2007/2013), the public opinion on whether AC^3 is true or not is still somewhat ambiguous. In addition, about 40% of the public doubt the level of scientific consensus on AC^3 (Nisbet and Myers, 2007). However, in reality, about 97% of all papers written on this subject, endorse the view of the *Intergovernmental Panel on Climate Change* (IPCC) and only an absolute minority among the scientific community is not convinced of AC^3 (Anderegg et al., 2010; Cook et al., 2013).

I write this epilogue because global climate change occurred throughout the entire history of our planet. Therefore, some people tend to use this fact to raise doubts on the anthropogenic cause for the current processes in our climate system.

Now that I showed that the deep-ocean released large amounts of stored CO_2 to the deglacial atmosphere, I can already anticipate people exploiting these findings to reason that this process might also be in operation today, causing the current rise in modern CO_2.

True, deep-water is upwelled around Antarctica (e.g. Talley, 2013; Fig. 1.2), but this deep-water is substantially younger than the waters described in *Chapter 3*, and due to the high partial pressure of atmospheric CO_2, the modern Southern Ocean acts as a sink rather than as a source of CO_2 (Gruber et al., 2009). In particular, the salient position of modern atmospheric CO_2 is displayed in figure 7.1 (red).

Furthermore, the data shown in *Chapter 3* indicate an end of the deep-water rejuvenation and therefore an end of the pronounced outgassing period, which coincided already with the onset

of the warm Holocene. Although the CO_2-fluctuations of the last 800,000 years can be explained by natural processes (including the processes described in this thesis), our data and the unprecedented trend in atmospheric CO_2 over the last 270 years (Neftel et al., 1994; Tans and Keeling, 2014) clearly show that other (e.g. anthropogenic) factors are ultimately driving the modern CO_2-pattern.

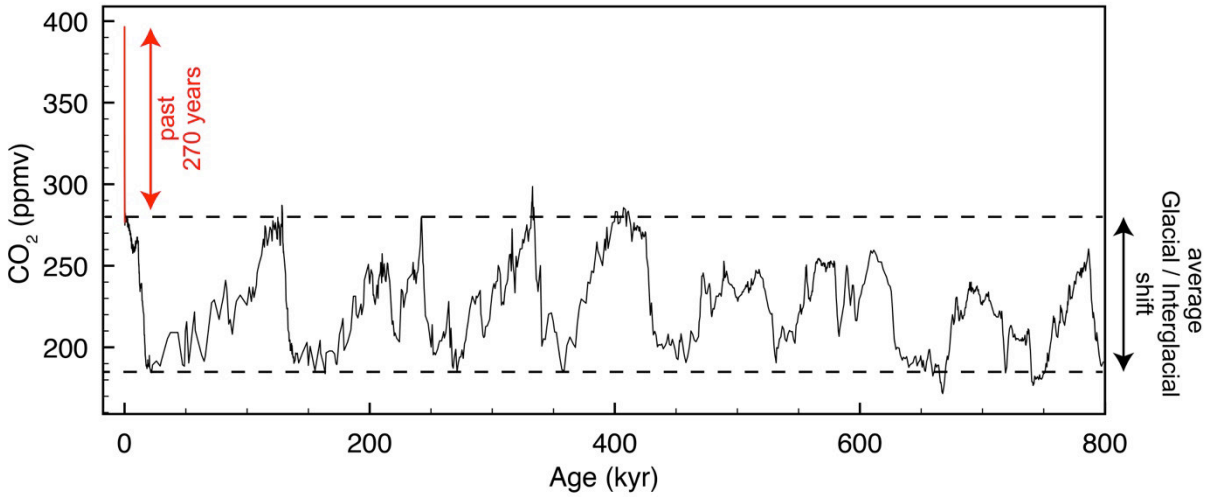

Figure 7.1: Record of atmospheric CO_2 over the last 800,000 years. 0 – 59 years (Tans and Keeling, 2014); 59 – 270 years (Neftel et al., 1994); 270 – 22,000 years (Monnin et al., 2001); 22,000 – 393,000 years (Pépin et al., 2001; Petit et al., 1999; Raynaud et al., 2005); 393,000 – 664,000 years (Siegenthaler et al., 2005); 664,000 – 800,000 years (Lüthi et al., 2008).

References

Adkins, J.F., 2013. The role of deep ocean circulation in setting glacial climates. Paleoceanography 28, 539-561.

Adkins, J.F., Boyle, E.A., 1997. Changing atmospheric $\Delta^{14}C$ and the record of deepwater paleoventilation ages. Paleoceanography 12, 337-344.

Alloway, B., Lowe, D.J., Barrell, D.J.A., Newnham, R.M., Almond, P.C., Augustinus, P.C., Bertler, N.A.N., Carter, L., Litchfield, N.J., McGlone, M.S., Jamie, S., Vandergoes, M.J., Williams, P.W., members, N.-I., 2007. Towards a climate event stratigraphy for New Zealand over the past 30,000 years (NZ-INTIMATE project). Journal of Quaternary Science 22, 9-35.

Alloway, B.V., Pillans, B., Carter, L., Naish, T.R., Westgate, J.A., 2005. Onshore–offshore correlation of Pleistocene rhyolitic eruptions from New Zealand: implications for TVZ eruptive history and paleoenvironmental construction. Quaternary Science Reviews 24, 1601-1622.

Anderegg, W.R.L., Prall, J.W., Harold, J., Schneider, S.H., 2010. Expert credibility in climate change. PNAS, 1-3.

Anderson, R.F., Ali, S., Bradtmiller, L.I., Nielsen, S.H.H., Fleischer, M.Q., Anderson, B.E., Burckle, L.H., 2009. Wind-Driven Upwelling in the Southern Ocean and the Deglacial Rise in Atmospheric CO_2. Science 323, 1443-1448.

Anderson, R.F., Carr, M.-E., 2010. Uncorking the Southern Ocean's Vintage CO_2. Science 328, 1117-1118.

Anderson, T.E., Lucas, M.I., 2008. Upwelling Ecosystems, in: Jorgensen, S.E., Fath, B. (Eds.), Encyclopedia of Ecology. Elsevier Science, New York, pp. 3651-3661.

Antonov, J.I., Seidov, D., Boyer, T.P., Locarnini, R.A., Mishonov, A.V., Garcia, H.E., Baranova, O.K., Zweng, M.M., Johnson, D.R., 2010. World Ocean Atlas 2009, Volume 2: Salinity, in: Levitus, S. (Ed.), NOAA Atlas NESDIS 69. NOAA.

Ayers, J.M., Strutton, P.G., 2013. Nutrient variability in Subantarctic Mode Waters forced by the Southern Annular Mode and ENSO. Geophysical Research Letters 40, 3419-3423.

Bard, E., 1988. Correction of Accelerator Mass Spectrometry ^{14}C Ages Measured in Planktonic Foraminifera: Paleoceanographic Implications. Paleoceanography 3, 635-645.

Barker, S., Greaves, M., Elderfield, H., 2003. A study of cleaning procedures used for foraminiferal Mg/Ca paleothermometry. Geochemistry Geophysics Geosystems 4, 1-20.

Barker, S., Knorr, G., Vautravers, M.J., Diz, P., Skinner, L.C., 2010. Extreme deepening of the Atlantic overturning circulation during deglaciation. Nature Geoscience 3, 567-571.

Basak, C., Martin, E.E., Horikawa, K., Marchitto, T.M., 2010. Southern Ocean source of ^{14}C-depleted carbon in the North Pacific Ocean during the last deglaciation. Nature Geoscience 3, 770-773.

Beck, J.W., Richards, D.A., Edwards, R.L., Silverman, B.W., Smart, P.L., Donahue, D.J., Herrera-Osterheld, S., Burr, G.S., Calsoyas, L., Jull, A.J.T., Biddulph, D., 2001. Extremly large variations of atmospheric ^{14}C concentration during the last glacial period. Science 292, 2453-2458.

Bianchi, C., Gersonde, R., 2004. Climate evolution at the last deglaciation: the role of the Southern Ocean. Earth and Planetary Science Letters 228, 407-424.

Bostock, H.C., Barrows, T.T., Carter, L., Chase, Z., Cortese, G., Dunbar, G.B., Ellwood, M., Hayward, B.W., Howard, W.R., Neil, H.L., Noble, T.L., Mackintosh, A., Moss, P.T., Moy, A.D., White, D., Williams, M.J.M., Armand, L.K., 2013b. A review of the Australian-New Zealand sector of the Southern Ocean over the last 30 ka (Aus-INTIMATE project). Quaternary Science Reviews 74, 35-57.

Bostock, H.C., Hayward, B.W., Neil, H.L., Currie, K.I., Dunbar, G.B., 2011. Deep-water carbonate concentrations in the southwest Pacific. Deep-Sea Research I 58, 72-85.

Bostock, H.C., Opdyke, B.N., Gagan, M.K., Fifield, L.K., 2004. Carbon isotope evidence for changes in Antarctic Intermediate Water circulation and ocean ventilation in the southwest Pacific during the last deglaciation. Paleoceanography 19, 1-15.

Bostock, H.C., Opdyke, B.N., Williams, M.J.M., 2010. Characterising the intermediate depth waters of the Pacific Ocean using $\delta^{13}C$ and other geochemical tracers. Deep-Sea Research I 57, 847-859.

Bostock, H.C., Sutton, P.J., Williams, M.J.M., Opdyke, B.N., 2013a. Reviewing the circulation and mixing of Antarctic Intermediate Water in the South Pacific using evidence from geochemical tracers and Argo float trajectories. Deep-Sea Research I 73, 84-98.

Boyle, E.A., Keigwin, L.D., 1982. Deep Circulation of the North Atlantic over the Last 200,000 Years: Geochemical Evidence. Science 218, 784-787.

Brix, H., Gerdes, R., 2003. North Atlantic Deep Water and Antarctic Bottom Water: Their interaction and influence on the variability of the global ocean circulation. Journal of Geophysical Research 108, 1-17.

Broecker, W., 1982. Glacial to Interglacial Changes in Ocean Chemistry. Progress in Oceanography 11, 151-197.

Broecker, W., 2009. The Mysterious ^{14}C Decline. Radiocarbon 51, 109-119.

Broecker, W., Barker, S., 2007. A 190‰ drop in atmosphere's $\Delta^{14}C$ during the "Mystery Interval" (17.5 to 14.5 kyr). Earth and Planetary Science Letters 256, 90-99.

Broecker, W., Clark, E., 2010. Search for a glacial-age ^{14}C-depleted ocean reservoir. Geophysical Research Letters 37, 1-6.

Broecker, W., Clark, E., Barker, S., 2008. Near constancy of the Pacific Ocean surface to mid-depth radiocarbon-age difference over the last 20 kyr. Earth and Planetary Science Letters 274, 322-326.

Broecker, W., Peng, T.-H., 1987. The role of $CaCO_3$ compensation in the Glacial to Interglacial Atmospheric CO_2 Change. Global Biogeochemical Cycles 1, 15-29.

Broecker, W.S., Maier-Reimer, E., 1992. The Influence of Air and Sea Exchange on The Carbon Isotope Distribution in the Sea. Global Biochemical Chycles 6, 315-320.

Bronk Ramsey, C., Staff, R.A., Bryant, C.L., Brock, F., Kitagawa, H., van der Plicht, J., Schlolaut, G., Marshall, M.H., Brauer, A., Lamb, H.F., Payne, R.L., Tarasov, P.E., Haraguchi, T., Gotanda, K., Yonenobu, H., Yokoyama, Y., Tada, R., Nakagawa, T., 2012. A Complete Terrestrial Radiocarbon Record for 11.2 to 52.8 kyr B.P. Science 388, 370-374.

Brown, S.J., Elderfield, H., 1996. Variations in Mg/Ca and Sr/Ca ratios of planktonic foraminifera caused by postdepositional dissolution: Evidence of shallow Mg-dependent dissolution. Paleoceanography 11, 543-551.

Bryan, S.P., Marchitto, T.M., Lehman, S.J., 2010. The release of ^{14}C-depleted carbon from the deep ocean during the last deglaciation: Evidence from the Arabian Sea. Earth and Planetary Science Letters 298, 244-254.

Burke, A., Robinson, L.F., 2012. The Southern Ocean's Role in Carbon Exchange During the Last Deglaciation. Science 335, 557-561.

Butzin, M., Prange, M., Lohmann, G., 2005. Radiocarbon simulations for the glacial ocean: The effects of wind stress, Southern Ocean sea ice and Heinrich events. Earth and Planetary Science Letters 235, 45-61.

Callahan, J.E., 1972. The structure and circulation of Deep Water in the Antarctic. Deep-Sea Research 19, 563-575.

Carter, L., Garlick, R.D., Sutton, P., Chiswell, S., Oien, N.A., Stanton, B.R., 1998. Ocean Circulation New Zealand. National Institute of Water and Atmospheric Research Ltd (NIWA), Wellington, New Zealand.

Carter, L., McCave, I.N., 1997. The Sedimentary Regime Beneath the Deep Western Boundary Current Inflow to the Southwest Pacific Ocean. Journal of Sedimentary Research 67, 1005-1017.

Carter, L., McCave, I.N., Williams, M.J.M., 2009. Chapter 4: Circulation and Water Masses of the Southern Ocean: A Review, in: Florindo, F., Siegert, G. (Eds.), Developments in Earth and Environmental Science Series. Antarctic Climate Evolution. Elsevier, pp. 85-114.

Carter, L., Wilkin, J., 1999. Abyssal circulation around New Zealand – a comparison between observations and a global circulation model. Marine Geology 159, 221-239.

Charles, C.D., Fairbanks, R.G., 1992. Evidence from Southern Ocean sediments for the effect of North Atlantic deep-water flux on climate. Nature 355, 416-419.

Cléroux, C., Cortijo, E., Duplessy, J.-C., Zahn, R., 2007. Deep-dwelling foraminifera as thermocline temperature recorders. Geochemistry Geophysics Geosystems 8, 1-19.

Cléroux, C., deMenocal, P., Guilderson, T.P., 2011. Deglacial radiocarbon history of tropical Atlantic thermocline waters: absence of CO_2 reservoir purging signal. Quaternary Science Reviews 30, 1875-1882.

Cléroux, C., Lynch-Stieglitz, J., Schmidt, M.W., Cortijo, E., Duplessy, J.-C., 2009. Evidence for calcification depth change of Globorotalia truncatulinoides between deglaciation and Holocene in the Western Atlantic Ocean. Marine Micropaleontology 73, 57-61.

Collins, W.D., Bitz, C.M., Blackmon, M., L., Bonan, G.B., Bretherton, C.S., Henderson, T.B., Kiehl, J., Large, W.G., McKenna, D.S., Santer, B.D., Smith, B.E., 2006. The Community Climate System Model Version 3 (CCSM3). Journal of Climate 19, 2122-2143.

Cook, J., Nuccitelli, D., Green, S.A., Richardson, M., Winkler, B., Painting, R., Way, R., Jacobs, P., Skuce, A., 2013. Quantifying the consensus on anthropogenic global warming in the scientific literature. Environmental Research Letters 8, 1-7.

Crundwell, M., Scott, G., Naish, T., Carter, L., 2008. Glacial–interglacial ocean climate variability from planktonic foraminifera during the Mid-Pleistocene transition in the

temperate Southwest Pacific, ODP Site 1123. Palaeogeography, Palaeoclimatology, Palaeoecology 260, 202-229.

Cunningham, S.A., Alderson, S.G., King, B.A., Brandon, M.A., 2003. Transport and variability of the Antarctic Circumpolar Current in Drake Passage. Journal of Geophysical Research 108, 1-17.

Curry, W.B., Oppo, D.W., 2005. Glacial water mass geometry and the distribution of $\delta^{13}C$ of $\sum CO_2$ in the western Atlantic Ocean. Paleoceanography 20, 1-12.

De Pol-Holz, R., Keigwin, L.D., Southon, J., Hebbeln, D., Mohtadi, M., 2010. No signature of abyssal carbon in intermediate waters off Chile during deglaciation. Nature Geoscience 3, 192-195.

De Pol-Holz, R., Mohtadi, M., Southon, J.R., 2012. Intermediate water radiocarbon off west Sumatra during the last 45,000 years, EGU General Assembly, Vienna.

Dekens, P.S., Lea, D.W., Pak, D.K., Spero, H.J., 2002. Core top calibration of Mg/Ca in tropical foraminifera: Refining paleotemperature estimation. Geochemistry Geophysics Geosystems 3.

Denton, G.H., Anderson, R.F., Toggweiler, J.R., Edwards, R.L., Schaefer, J.M., Putnam, A.E., 2010. The Last Glacial Termination. Science 328, 1652-1656.

Denton, G.H., Broecker, W.S., Alley, R.B., 2006. The mystery interval 17.4 to 14-5 kyr ago. PAGES News 14, 14-16.

Deuser, W.G., Ross, E.H., 1989. Seasonally abundant planktonic foraminifera of the Sargasso Sea: Succession, deep-water fluxes, isotopic compositions and paleoceanographic implications. Journal of Foraminiferal Research 19, 268-293.

Downes, S.M., Bindoff, N.L., Rintoul, S.R., 2010. Changes in the Subduction of Southern Ocean Water Masses at the End of the Twenty-First Century in Eight IPCC Models. Journal of Climate 23, 6526-6541.

Duplessy, J.-C., Shackleton, N.J., Fairbanks, R.G., Labeyrie, L., Oppo, D., Kallel, N., 1988. Deepwater source variations during the last climate cycle and their impact on global deepwater circulation. Paleoceanography 3, 343-360.

Emiliani, C., 1955. Pleistocene Temperatures. Journal of Geology 63, 538-578.

Emiliani, C., 1991. Planktic/Planktonic, Nektic/Nektonic, Benthic/Benthonic. Journal of Paleontology 65, 329.

EPICA Community Members, 2006. One-to-one coupling of glacial climate variability in Greenland and Antarctica. Nature 444, 195-198.

Epstein, S., Mayeda, T., 1953. Variation of O^{18} content of waters from natura sources. Geochimica et Cosmochimica Acta 4, 213-224.

Fairbanks, R.G., Wiebe, P.H., Be, A.W., 1980. Vertical distribution and isotopic composition of living planktonic foraminifera in the western North Atlantic. Science 207, 61-63.

Farquhar, G.D., Ehleringer, J.R., Hubick, K.T., 1989. Carbon Isotope Discrimination and Photosynthesis. Annual Review of Plant Physiology and Plant Molecular Biology 40, 503-537.

Fischer, H., Schmitt, J., Lüthi, D., Stocker, T.F., Tschumi, T., Parekh, P., Joos, F., Köhler, P., Völker, P., Gersonde, R., Barbante, C., Le Floch, M., Raynaud, D., Wolff, E., 2010. The

role of Southern Ocean processes in orbital and millennial CO_2 variations – A synthesis. Quaternary Science Reviews 29, 193-205.

Francois, R., Altabet, M.A., Yu, E.-F., Sigman, D.M., Bacon, M.B., Frank, M., Bohrmann, G., Bareille, G., Labeyrie, L.D., 1997. Contribution of Southern Ocean surface-water stratification to low atmospheric CO_2 concentrations during the last glacial period. Nature 389, 929-935.

Franke, J., Paul, A., Schulz, M., 2008. Modeling variations of marine reservoir ages during the last 45,000 years. Climate of the Past 4, 125-136.

Friedrich, M., Remmele, S., Kromer, B., Hofnmann, J., Spurk, M., Krause, K.F., Orcel, C., Kuppers, M., 2004. The 12,460-year Hohenheim oak and pine tree-ring chronology from central Europe - A unique annual record for radiocarbon calibration and paleoenvironment reconstructions,. Radiocarbon 46, 1111-1122.

Galbraith, E.D., Jaccard, S.L., Pedersen, T.F., Sigman, D.M., Haug, G.H., Cook, M., Southon, J.R., Francois, R., 2007. Carbon dioxide release from the North Pacific abyss during the last deglaciation. Nature 449, 890-894.

Garcia, H.E., Locarnini, R.A., Boyer, T.P., Antonov, J.I., Baranova, O.K., Zweng, M.M., Johnson, D.R., 2010. World Ocean Atlas 2009, Volume 3 Dissolved Oxygen, Apparent Oxygen Utilization and Oxygen Saturation, in: Levitus, S. (Ed.), NOAA Atlas NESDIS 70, p. 344 pp.

Georgi, D.T., 1979. Modal Properties of Antarctic Intermediate Water in the Southeast Pacific and the South Atlantic. Journal of Physical Oceanography 9, 456-468.

Gersonde, R., 2011. The Expedition of the Research Vessel "Polarstern" to the polar South Pacific in 2009/2010 (ANT-XXVI/2 - BIPOMAC), Berichte zur Polar und Meeresforschung. Alfred Wegener Institute, Bremerhaven.

Gersonde, R., Abelmann, A., Brathauer, U., Becquey, S., Bianchi, C., Cortese, G., Grobe, H., Kuhn, G., Niebler, H.-S., Segl, M., Sieger, R., Zielinski, U., Fütterer, D.K., 2003. Last glacial sea surface temperatures and sea-ice extent in the Southern Ocean (Atlantic-Indian sector): A multiproxy approach. Paleoceanography 18, 1061.

Gersonde, R., Crosta, X., Abelmann, A., Armand, L., 2005. Sea-surface temperature and sea ice distribution of the Southern Ocean at the EPILOG Last Glacial Maximum—a circum-Antarctic view based on siliceous microfossil records. Quaternary Science Reviews 24, 869-896.

Godwin, H., 1962. Half-life of Radiocarbon. Nature 195, 984.

Goldstein, S.J., Lea, D.W., Chakraborty, S., Kashgarian, M., Murrell, M.T., 2001. Uranium-series and radiocarbon geochronology of deep-sea corals: implications for Southern Ocean ventilation rates and the oceanic carbon cycle. Earth and Planetary Science Letters 193, 167-182.

Groeneveld, J., Chiessi, C.M., 2011. Mg/Ca of Globorotalia inflata as a recorder of permanent thermocline temperatures in the South Atlantic. Paleoceanography 26, 1-12.

Gross, O., 2014. Uvigernia peregrina, in: Hayward, B.W., Cedhagen, T., Kaminski, M., Gross, O. (Eds.), World Foraminifera Database.

Gruber, N., Gloor, M., Mikaloff-Fletcher, S.E., Doney, S.C., Dutkiewicz, S., Follows, M., Gerber, M., Jacobson, A.R., Joos, F., Lindsay, K., Menemenlis, D., Mouchet, A.,

Sarmiento, J.L., Takahashi, T., 2009. Oceanic sources and sinks of atmospheric CO_2. Journal of Geophysical Research 23, 1-21.

Hain, M.P., Sigman, D.M., Haug, G.H., 2010. Carbon dioxide effects of Antarctic stratification, North Atlantic Intermediate Water formation, and subantarctic nutrient drawdown during the last ice age: Diagnosis and synthesis in a geochemical box model. Global Biochemical Chycles 24, 1-19.

Hall, A., Visbeck, M., 2002. Synchronous Variability in the Southern Hemisphere Atmosphere, Sea Ice, and Ocean Resulting from the Annular Mode. Journal of Climate 15, 3043-3057.

Hanawa, K., Talley, L.D., 2001. Mode Waters, in: Siedler, G., Church, J., Gould, J. (Eds.), Ocean Circulation and Climate. Academic, San Diego, California, pp. 373-386.

Hartin, C.A., Fine, R.A., Sloyan, B.M., Talley, L.D., Chereskin, T.K., Happell, J., 2011. Formation rates of Subantarctic mode water and Antarctic intermediate water within the South Pacific. Deep-Sea Research I 58, 524-534.

Hasson, A., Koch-Larrouy, A., Morrow, R., Juza, M., Penduff, T., 2011. The origin and fate of mode water in the southern Pacific Ocean. Ocean Dynamics 62, 335-354.

Hayward, B.W., Gross, O., 2014. Cibicidoides wuellerstorfi, in: Hayward, B.W., Cedhagen, T., Karminski, T., Gross, O. (Eds.), World Foraminifera Database.

Hayward, B.W., Neil, H.L., Carter, R., Grenfell, H.R., Hayward, J.J., 2002. Factors influencing the distribution patterns of Recent deep-sea benthic foraminifera, east of New Zealand, Southwest Pacific Ocean. Marine Micropaleontology 46, 139-176.

Hayward, B.W., Sabaa, A.T., Grenfell, H.R., 2004. Benthic foraminifera and the late Quaternary (last 150 ka) paleoceanographic and sedimentary history of the Bounty Trough, east of New Zealand. Palaeogeography, Palaeoclimatology, Palaeoecology 211, 59-92.

Hayward, B.W., Scott, G.H., Crundwell, M.P., Kennet, J.P., Carter, L., Neil, H.L., Sabaa, A.T., Wilson, K., Rodger, J.S., Schaefer, G., Grenfell, H.R., Li, Q., 2008. The effect of submerged plateaux on Pleistocene gyral circulation and sea-surface temperatures in the Southwest Pacific. Global and Planetary Change 63, 309-316.

Heath, R.A., 1981. Oceanic fronts around southern New Zealand. Deep-Sea Research 28A, 547-560.

Heath, R.A., 1985. A review of the physical oceanography of the seas around New Zealand — 1982. New Zealand Journal of Marine and Freshwater Research 19, 79-124.

Herguera, J.C., Herbert, T., Kashgarian, M., Charles, C., 2010. Intermediate and deep water mass distribution in the Pacific during the Last Glacial Maximum inferred from oxygen and carbon stable isotopes. Quaternary Science Reviews 29, 1228-1245.

Herraiz-Borreguero, L., Rintoul, S.R., 2011. Subantarctic mode water: distribution and circulation. Ocean Dynamics 61, 103-126.

Hesse, T., Butzin, M., Bickert, T., Lohmann, G., 2011. A model-data comparison of $\delta^{13}C$ in the glacial Atlantic Ocean. Paleoceanography 26, 1-16.

Ho, S.L., Mollenhauer, G., Lamy, F., Martinez-Garcia, A., Mohtadi, M., Gersonde, R., Hebbeln, D., Nunez-Ricardo, S., Rosell-Melé, A., Tiedemann, R., 2012. Sea surface temperature variability in the Pacific sector of the Southern Ocean over the past 700 kyr. Paleoceanography 27, 1-15.

Hoffmann, D.L., Beck, J.W., Richards, D.A., Smart, P.L., Singarayer, J.S., Ketchmark, T., Hawkesworth, C.J., 2010. Towards radiocarbon calibration beyond 29 ka using speleothems from the Bahamas. Earth and Planetary Science Letters 289, 1-10.

Holte, J.W., Talley, L.D., Chereskin, T.K., Sloyan, B.M., 2012. The role of air-sea fluxes in Subantarctic Mode Water formation. Journal of Geophysical Research 117, 1-17.

Holte, J.W., Talley, L.D., Chereskin, T.K., Sloyan, B.M., 2013. Subantarctic mode water in the southeast Pacific: Effect of exchange across the Subantarctic Front. Journal of Geophysical Research 118, 2052-2066.

IPCC Members, 2007. Climate Change 2007: Synthesis Report, in: Pachauri, R.K., Reisinger, A. (Eds.). IPCC, Geneva.

IPCC Members, 2013. Climate Change 2013: The Physical Science Basis. IPCC, Geneva.

Jenkins, A., 1999. The Impact of Melting Ice on Ocean Waters. Journal of Physical Oceanography 29, 2370-2381.

Jochum, K.P., Weis, U., Stoll, B., Kuzmin, D., Yang, Q., Raczek, I., Jacob, D.E., Stracke, A., Birbaum, K., Frick, D.A., Günther, D., Enzweiler, J., 2011. Determination of Reference Values for NIST SRM 610--617 Glasses Following ISO Guidelines. Geostandards and Geoanalytical Research 35, 397-429.

Jouzel, J., Masson-Delmotte, V., Cattani, O., Dreyfus, G., Falourd, S., Hoffmann, G., Minster, B., Nouet, J., Barnola, J.-M., Chappellaz, J., Fischer, H., Gallet, J.C., Johnsen, S., Leuenberger, M., Loulergue, L., Luethi, D., Oerter, H., Parrenin, F., Raisbeck, G.M., Raynaud, D., Schilt, A., Schwander, J., Selmo, E., Souchez, R., Spahni, R., Stauffer, B., Steffensen, J.P., Stenni, B., Stocker, T.F., Tison, J.L., Werner, M., Wolff, E.W., 2007. Orbital and Millennial Antarctic Climate Variability over the Past 800,000 Years. Science 317, 793-796.

Kaiser, J., Lamy, F., Hebbeln, D., 2005. A 70-kyr sea surface temperature record off southern Chile (Ocean Drilling Program Site 1233). Paleoceanography 20, 1-15.

Keigwin, L.D., 2004. Radiocarbon and stable isotope constraints on Last Glacial Maximum and Younger Dryas ventilation in the western North Atlantic. Paleoceanography 19, 1-15.

Kennicutt II, M.C., Chown, S.L., 2014. Six priorities for Antarctic science. Nature 512, 23-25.

Kersten, F., 2013. Last Glacial to Holocene changes of deep and intermediate water carbonate ion concentrations in the Southern Ocean: Constraints from foraminiferal Boron/Calcium ratios, FB5. University of Bremen, Bremen, p. 111.

Key, R.M., Kozyr, A., Sabine, C.L., Lee, K., Wanninkhof, R., Bullister, J.L., Feely, R.A., Millero, F.J., Mordy, C., Peng, T.-H., 2004. A global ocean carbon climatology: Results from Global Data Analysis Project (GLODAP). Global Biochemical Chycles 18, 1-23.

Key, R.M., T., T., Olsen, A., Hoppema, M., Jutterström, S., Schirnick, C., Van Heuven, S., Kozyr, A., Lin, X., Velo, A., 2010. The CARINA data synthesis project: introduction and overview. Earth System Science Data 2, 105-121.

King, A.L., Howard, W.R., 2003. lanktonic foraminiferal flux seasonality in Subantarctic sediment traps: A test for paleoclimate reconstructions. Paleoceanography 18, 1019.

Kitagawa, H., van der Plicht, J., 1998. A 40,000-year varved chronology frome Lake Suigetsu, Japan: extension of the ^{14}C calibration curve. Radiocarbon 40, 505-515.

Kitagawa, H., van der Plicht, J., 2000. Atmospheric radiocarbon calibration beyond 11,900 cal BP from Lake Suigetsu laminated sediments. Radiocarbon 42, 369-380.

Klages, J.P., Kuhn, G., Hillenbrand, C.-D., Graham, A., G. C., Smith, J.A., Larter, R.D., Gohl, K., Wacker, L., 2014. Retreat of the West Antarctic Ice Sheet from the western Amundsen Sea shelf at a pre- or early LGM stage. Quaternary Science Reviews 91, 1-15.

Kohfeld, K.E., Graham, R.M., de Boer, A.M., Sime, L.C., Wolff, E.W., Le Quéré, C., Bopp, L., 2013. Southern Hemisphere westerly wind changes during the Last Glacial Maximum: paleo-data synthesis. Quaternary Science Reviews 68, 76-95.

Kroopnick, P.M., 1985. The distribution of ^{13}C of $\sum CO_2$ in the world oceans. Deep-Sea Research 32, 57-84.

Kwon, E.Y., Hain, M.P., Sigman, D.M., Galbraith, E.D., Sarmiento, J.L., Toggweiler, J.R., 2012. North Atlantic ventilation of "southern-sourced" deep water in the glacial ocean. Paleoceanography 27, 1-12.

Lambert, F., Delmonte, B., Petit, J.R., Bigler, M., Kaufmann, P.R., Hutterli, M.A., Stocker, T.F., Ruth, U., Steffensen, J.P., Maggi, V., 2008. Dust-climate couplings over the past 800,000 years from the EPICA Dome C ice core. Nature 452, 616-619.

Lamy, F., Gersonde, R., Winckler, G., Esper, O., Jaeschke, A., Kuhn, G., Ullermann, J., Martinez-Garcia, A., Lambert, F., Kilian, R., 2014. Increased Dust Deposition in the Pacific Southern Ocean During Glacial Periods. Science 343, 403-407.

Lamy, F., Kaiser, J., Ninnemann, U., Hebbeln, D., Arz, H., Stoner, J.S., 2004. Antarctic Timing of Surface Water Changes off Chile and Patagonian Ice Sheet Response. Science 304.

Le Grande, A.N., Schmidt, G.A., 2006. Global gridded data set of the oxygen isotopic composition in seawater. Geophysical Research Letters 33, 1-5.

Le Grande, A.N., Schmidt, G.A., 2011. Water isotopologues as a quantitative paleosalinity proxy. Paleoceanography 26, 1-10.

Le Quéré, C., Rödenbeck, C., Buitenhuis, E.T., Conway, T.J., Langenfelds, R., Gomez, A., Labuschagne, C., Ramonet, M., Nakazawa, T., Metzl, N., Gillett, N.P., Heimann, M., 2007. Saturation of the Southern Ocean CO_2 Sink Due to Recent Climate Change. Science 316, 1735-1738.

Leduc, G., Vidal, L., Tachikawa, K., Bard, B., 2010. Changes in Eastern Pacific ocean ventilation at intermediate depth over the last 150 kyr BP. Earth and Planetary Science Letters 298, 217-228.

Lenton, A., Matear, R.J., 2007. Role of the Southern Annular Mode (SAM) in Southern Ocean CO_2 uptake. Global Biochemical Cycles 21, 1-17.

Lisiecki, L.E., Raymo, M.E., 2005. A Pliocene-Pleistocene stack of 57 globally distributed benthic $\delta^{18}O$ records. Paleoceanography 20, 1-17.

Liu, Z., Shin, S.-I., Otto-Bliesner, B., Kutzbach, J., Brady, E.C., Lee, D.E., 2002. Tropical cooling at the last glacial maximum and extratropical ocean ventilation. Geophysical Research Letters 29, 1409.

Locarnini, R.A., Mishonov, A.V., Antonov, J.I., Boyer, T.P., Garcia, H.E., Baranova, O.K., Zweng, M.M., Johnson, D.R., 2010. World Ocean Atlas 2009, Vol. 1. Temperature. NOAA Atlas NESDIS 68.

Loncarcic, N., Peeters, F.J.C., Kroon, D., Brummer, G.-J., 2006. Oxygen isotope ecology of recent planktic foraminifera at the central Walvis Ridge (SE Atlantic). Paleoceanography 21, 1-18.

Lovenduski, N.S., Gruber, N., 2005. Impact of the Southern Annular Mode on Southern Ocean circulation and biology. Geophysical Research Letters 32, 1-4.

Lowe, D.J., Blaauw, M., Hogg, A.G., Newnham, R.M., 2012. Ages of 24 widespread tephras erupted since 30,000 years ago in New Zealand, with re-evaluation of the timing and palaeoclimatic implications of the Lateglacial cool episode recorded at Kaipo bog. Quaternary Science Reviews, 1-25.

Lund, D.C., 2013. Deep Pacific ventilation ages during the last deglaciation: Evaluating the influence of diffusive mixing and source region reservoir age. Earth and Planetary Science Letters 381, 52-62.

Lund, D.C., Mix, A.C., Southon, J., 2011. Increased ventilation age of the deep northeast Pacific Ocean during the last deglaciation. Nature Geoscience 4, 771-774.

Lüthi, D., Le Floch, M., Bereiter, B., Blunier, T., Barnola, J.-M., Siegenthaler, U., Raynaud, D., Jouzel, J., Fischer, H., Kawamura, K., Stocker, T.F., 2008. High-resolution carbon dioxide concentration record 650,000–800,000 years before present. Nature 453, 379-382.

Luz, B., 1977. Late Pleistocene paleoclimates of the South Pacific based on statistical analysis of planktonic foraminifers. Palaeogeography, Palaeoclimatology, Palaeoecology 22, 61-78.

Mackensen, A., 2012. Strong thermodynamic imprint on Recent bottom-water and epibenthic $\delta^{13}C$ in the Weddell Sea revealed: Implications for glacial Southern Ocean ventilation. Earth and Planetary Science Letters 317-318, 20-26.

Mackensen, A., Hubberton, H.-W., Bickert, T., Fischer, G., Fütterer, D.K., 1993. The $\delta^{13}C$ in Benthic Foraminiferal Tests of Fontbotia Wuellerstorfi (Schwager) Realtive to the $\delta^{13}C$ of Dissolved Inorganic Carbon in Southern Ocean Deep Water: Implications for Glacial Ocean Circulation Models. Paleoceanography 8, 587-610.

Mackensen, A., Schumacher, S., Radke, J., Schmidt, D.N., 2000. Microhabitat preferences and stable carbon isotopes of endobenthic foraminifera: clue to quantitative reconstruction of oceanic new production? Marine Micropaleontology 40, 233-258.

Maier-Reimer, E., Kriest, I., Segschneider, J., Wetzel, P., 2005. The HAMburg Ocean Carbon Cycle Modell HAMOCC 5.1 - Technical Description Release 1.1 -. Reports on Earth System Science, 1-57.

Manabe, S., Stouffer, R.J., 1993. Century-scale effects of increased atmospheric CO_2 on the ocean-atmosphere sytem. Nature 364, 215.

Mangini, A., Godoy, J.M., Godoy, M.L., Kowsmann, R., Santos, G.M., Ruckelshausen, M., Schröder-Ritzrau, A., Wacker, L., 2010. Deep sea corals off Brazil verify a poorly ventilated Southern Pacific Ocean during H2, H1 and the Younger Dryas. Earth and Planetary Science Letters 293, 269-276.

Mantyla, A.W., Reid, J.L., 1995. On the origins of deep and bottom waters of the Indian Ocean. Journal of Geophysical Research 100, 2417-2439.

Marchitto, T.M., Lehman, S.J., Ortiz, J.D., Flückinger, J., van Geen, A., 2007. Marine Radiocarbon Evidence for the Mechanism of Deglacial Atmospheric CO_2 Rise. Science 316, 1456-1459.

Markgraf, V., Dodson, J.R., Kershaw, A.P., McGlone, M.S., Nicholls, N., 1992. Evolution of late Pleistocene and Holocene climates in the circum-South Pacific land areas. Climate Dynamics 6, 193-211.

Marr, J.P., Bostock, H.C., Carter, L., Bolton, A., Smith, E., 2013. Differential effects of cleaning procedures on the trace element chemistry of planktonic foraminifera. Chemical Geology 351, 310-323.

Martinez-Garcia, A., Rosell-Melé, A., Geibert, W., Gersonde, R., Masqué, P., Gaspari, V., Barbante, C., 2009. Links between iron supply, marine productivity, sea surface temperature, and CO_2 over the last 1.1 Ma. Paleoceanography 24, 1-14.

Martínez-Méndez, G., Hebbeln, D., Mohtadi, M., Lamy, F., De Pol-Holz, R., Reyes-Macaya, D., Freudenthal, T., 2013. Changes in the advection of Antarctic Intermediate Water to the northern Chilean coast during the last 970 kyr. Paleoceanography 28, 607-618.

Mashiotta, T.A., Lea, D.W., Spero, H.J., 1999. Glacial–interglacial changes in Subantarctic sea surface temperature and δ^{18}O-water using foraminiferal Mg. Earth and Planetary Science Letters 170, 417-432.

Matsumoto, K., Lynch-Stieglitz, J., Anderson, R.F., 2001. Similar glacial and Holocene Southern Ocean hydrography. Paleoceanography 16, 445-454.

Matsumoto, K., Oba, T., Lynch-Stieglitz, J., Yamamoto, H., 2002. Interior hydrography and circulation of the glacial Pacific Ocean. Quaternary Science Reviews 21, 1693-1704.

Matsumoto, K., Yokoyama, Y., 2013. Atmospheric Δ^{14}C reduction in simulations of Atlantic overturning circulation shutdown. Global Biogeochemical Cycles 27, 1-9.

Mazzullo, J.M., A., M., Kidd, R.B., 1988. New sediment classification scheme for the Ocean Drilling Program, in: Mazzullo, J.M., Graham, A.G. (Eds.), Handbook for Shipboard Sedimentologists, pp. 45-67.

McCartney, M.S., 1977. Subantarctic Mode Water, in: Angel, M.V. (Ed.), A Voyage of Discovery: George Deacon 70th Anniversary Volume, supplement to Deep-sea research and oceanographic abstracts. Pergamon Press, Oxford, pp. 103-119.

McCave, I.N., Carter, L., 1997. Recent sedimentation beneath the Deep Western Boundary Current off northern New Zealand. Deep-Sea Research I 44, 1203-1237.

McCave, I.N., Carter, L., Hall, I.R., 2008. Glacial–interglacial changes in water mass structure and flow in the SW Pacific Ocean. Quaternary Science Reviews 27, 1886-1908.

McManus, J.F., Francois, R., Gherardi, J.-M., Keigwin, L.D., Brown-Leger, S., 2004. Collapse and rapid resumption of Atlantic meridional circulation linked to deglacial climate changes. Nature 428, 834-837.

McNeil, B., Matear, R.J., Key, R.M., Bullister, J.L., Sarmiento, J.L., 2003. Antrhopogenic CO2 uptake by the ocean based on the global chlorofluorocarbon data set. Science 299, 235-239.

Meissner, K.J., Galbraith, E.D., Völker, C., 2005. Denitrification under glacial and interglacial conditions: A physical approach. Paleoceanography 20, 1-13.

Mekik, F., Francois, R., Soon, M., 2007. A novel approach to dissolution correction of Mg/Ca-based paleothermometry in the tropical Pacific. Paleoceanography 22, 1-12.

Merkel, U., Prange, M., Schulz, M., 2010. ENSO variability and teleconnections during glacial climates. Quaternary Science Reviews 29, 86-100.

Michel, E., Siani, G., Mazaud, A., Paterne, M., Waelbroeck, C., de Vries, T., Van der Putten, N., Björck, S., Jaccard, S.L., De Pol-Holz, R., Skinner, L.C., Muscheler, R., Kissel, C., 2014. Southern Ocean records across the last deglaciation and their timing, SCAR 2014 Open Science Conference, Auckland.

Mohtadi, M., Hebbeln, D., 2004. Mechanisms and variations of the paleoproductivity off northern Chile (24°S–33°S) during the last 40,000 years. Paleoceanography 19, 1-15.

Molinelli, E., 1981. The Antarctic influence in Antarctic Intermediate Water. Journal of Marine Research 39, 267-293.

Monnin, E., Indermühle, A., Dällenbach, A., Flückiger, J., Stauffer, B., Stocker, T.F., Raynaud, D., Barnola, J.-M., 2001. Atmospheric CO2 Concentrations over the Last Glacial Termination. Science 291, 112-114.

Moreno, P.I., Lowell, T.V., Jacobson, G.L., Denton, G.H., 1999. Abrupt Vegetation and Climate Changes During the Last Glacial Maximum and Last Termination in the Chilean Lake District: A Case Study From Canal de la Puntilla (41°S). Geografiska Annaler 81, 285-311.

Moreno, P.I., Vilanova, I., Villa-Martínez, R., 2014. Southern Annular Mode-like changes in southwestern Patagonia at centennial timescales over the last three millennia. Nature Communications 5, 1-7.

Morris, M.Y., Stanton, B., Neil, H.L., 2001. Subantarctic oceanography around New Zealand: preliminary results from an ongoing survey. New Zealand Journal of Marine and Freshwater Research 35, 499.519.

Mortyn, P.G., Charles, C.D., 2003. Planktonic foraminiferal depth habitat and $\delta^{18}O$ calibrations: Plankton tow results from the Atlantic sector of the Southern Ocean. Paleoceanography 18, 1-14.

Murata, A., Kumamoto, Y., Sasaki, K.-i., Watanabe, S., Fukasawa, M., 2010. Decadal increases in anthropogenic CO2 along 20°S in the South Indian Ocean. Journal of Geophysical Research 115, 1-15.

Murata, A., Kumamoto, Y., Watanabe, S., Fukasawa, M., 2007. Decadal increases of anthropogenic CO_2 in the South Pacific subtropical ocean along 32°S. Journal of Geophysical Research 112, 1-11.

Muratli, J.M., Chase, Z., Mix, A.C., McManus, J., 2010. Increased glacial-age ventilation of the Chilean margin by Antarctic Intermediate Water. Nature Geoscience 3, 23-26.

Neftel, A., Friedli, H., Moor, E., Lötscher, H., Oeschger, H., Siegenthaler, U., Stauffer, B., 1994. Historical CO_2 record from the Siple Station ice core, A Compendioum of Data on Global Change. Carbon Dioxide Analysis Center, Oak Ridge.

Newnham, R.M., Vandergoes, M.J., Hendy, C.H., Lowe, D.J., Preusser, F., 2007. A terrestrial palynological record for the last two glacial cycles from southwestern New Zealand. Quaternary Science Reviews 26, 517-535.

Niebler, H.-S., Hubberton, H.-W., Gersonde, R., 1999. Oxygen Isotope Values of Planktic Foraminifera: A Tool for the Reconstruction of Surface Water Stratification, in: Fischer,

G., Wefer, G. (Eds.), Use of Proxies in Paleoceanography: Examples from the South Atlantic. Springer-Verlag, Berlin, pp. 165-189.

Ninnemann, U.S., Charles, C.D., 2002. Changes in the mode of Southern Ocean circulation over the last glacial cycle revealed by foraminiferal stable isotopic variability. Earth and Planetary Science Letters 201, 383-396.

Nisbet, M.C., Myers, T., 2007. Twenty Years of Public Opinion About Global Warming. Public Opinion Quaterly 71, 444-470.

Noble, T.L., Piotrowski, A.M., McCave, I.N., 2013. Neodymium isotopic composition of intermediate and deep waters in the glacial southwest Pacific. Earth and Planetary Science Letters 384, 27-36.

Northcote, L.C., Neil, H.L., 2005. Seasonal variations in foraminiferal flux in the Southern Ocean, Campbell Plateau, New Zealand. Marine Micropaleontology 56, 122-137.

Nürnberg, D., Groeneveld, J., 2006. Pleistocene variability of the Subtropical Convergence at East Tasman Plateau: Evidence from planktonic foraminiferal Mg/Ca (ODP Site 1172A). Geochemistry Geophysics Geosystems 7, 1-18.

Oke, P.R., England, M.H., 2004. Oceanic response to changes in the latitude of the Southern Hemisphere subpolar westerly winds. Journal of Climate 17, 1040-1054.

Orsi, A.H., Johnson, G.C., Bullister, J.L., 1999. Circulation, mixing, and production of Antarctic Bottom Water. Progress in Oceanography 43, 55-109.

Orsi, A.H., Whitworth III, T., Nowlin Jr, W.D., 1995. On the meridional extent and fronts of the Antarctic Circumpolar Current. Deep-Sea Research I 42, 641-673.

Otto-Bliesner, B., Brady, E.C., Clauzet, G., Tomas, R., Levis, S., Kothavala, Z., 2006. Last Glacial Maximum and Holocene Climate in CCSM3. Journal of Climate 19, 2526-2544.

Pahnke, K., Goldstein, S.L., Hemming, S.R., 2008. Abrupt changes in Antarctic Intermediate Water circulation over the past 25,000 years. Nature Geoscience 1, 870-874.

Pahnke, K., Zahn, R., 2005. Southern Hemisphere Water Mass Conversion Linked with North Atlantic Climate Variability. Science 307, 1741-1746.

Pahnke, K., Zahn, R., Elderfield, H., Schulz, M., 2003. 340,000-Year Centennial-Scale Marine Record of Southern Hemisphere Climatic Oscillation. Science 301, 948-952.

Paillard, D., Labeyrie, L., Yiou, P., 1996. Macintosh Program Performs Time-Series Analysis. Eos, Transactions, American Geophysical Union 77.

Parrenin, F., Masson-Delmotte, V., Köhler, P., Raynaud, D., Paillard, D., Schwander, J., Barbante, C., Landais, A., Wegner, A., Jouzel, J., 2013. Synchronous Change of Atmospheric CO_2 and Antarctic Temperature During the Last Deglacial Warming. Science 339, 1060-1063.

Pena, L.D., Cacho, I., Ferretti, P., Hall, M.A., 2008. El Niño–Southern Oscillation–like variability during glacial terminations and interlatitudinal teleconnections. Paleoceanography 23, 1-8.

Pena, L.D., Goldstein, S.L., Hemming, S.R., Jones, K.M., Calvo, E., Pelejero, C., Cacho, I., 2013. Rapid changes in meridional advection of Southern Ocean intermediate waters to the tropical Pacific during the last 30 kyr. Earth and Planetary Science Letters 368, 20-32.

Pépin, L., Raynaud, D., Barnola, J.-M., Loutre, M.F., 2001. Hemispheric roles of climate forcings during glacial- interglacial transitions as deduced from the Vostok record and LLN-2D model experiments. Journal of Geophysical Research 106, 31,885-831,892.

Peterson, C.D., Lisiecki, L.E., Stern, J.V., 2014. Deglacial whole-ocean $\delta^{13}C$ change estimated from 480 benthic foraminiferal records. Paleoceanography 29, 1-15.

Petit, J.R., Jouzel, J., Raynaud, D., Barkov, N.I., Barnola, J.-M., Basile, I., Bender, M., Chappellaz, J., Davis, M., Delaygue, G., Delmotte, M., Kotlyakov, V.M., Legrand, M., Lipenkov, V.Y., Lorius, C., Pépin, L., Ritz, C., Saltzman, E., Stievenard, M., 1999. Climate and atmospheric history of the past 420,000 years from the Vostok ice core, Antarctica. Nature 399, 429-436.

Piola, A.R., Georgi, D.T., 1982. Circumpolar properties of Antarctic Intermediate Water and Subantarctic Water. Deep-Sea Research 29, 687-711.

Piola, A.R., Gordon, A.L., 1989. Intermediate water in the southwestern South Atlantic. Deep-Sea Research 36, 1-16.

Piotrowski, A.M., Goldstein, S.L., Hemming, S.R., Fairbanks, R.G., 2004. Intensification and variability of ocean thermohaline circulation through the last deglaciation. Earth and Planetary Science Letters 225, 205-220.

Proust, J.-N., Lamarche, G., Migeon, S., Neil, H.L., 2006. Geoscience Cruise, MD152/MATACORE (24 January-7 February 2006) on R/V Marion-Dufresne", Tectonic and Climatic Controls on Sediment Budget, Les rapports de campagnes à la mer. Institut polaire français Paul-Émile Victor, p. 107.

Raynaud, D., Barnola, J.-M., Souchez, R., Lorrain, R., Petit, J.-R., Duval, P., Lipenkov, V.Y., 2005. Palaeoclimatology: The record for marine isotopic stage 11. Nature 436, 39-40.

Regenberg, M., Nürnberg, D., Steph, S., Groeneveld, J., Garbe-Schönberg, D., Tiedemann, R., Dullo, W.-C., 2006. Assessing the effect of dissolution on planktonic foraminiferal Mg/Ca ratios: Evidence from Caribbean core tops. Geochemistry Geophysics Geosystems 7, 1-23.

Regenberg, M., Regenberg, A., Garbe-Schönberg, D., Lea, D.W., 2014. Global dissolution effects on planktonic foraminiferal Mg/Ca ratios controlled by the calcite-saturation state of bottom waters. Paleoceanography 29, 127-142.

Regenberg, M., Steph, S., Nürnberg, D., Tiedemann, R., Garbe-Schönberg, D., 2009. Calibrating Mg/Ca ratios of multiple planktonic foraminiferal species with $\delta^{18}O$-calcification temperatures: Paleothermometry for the upper water column. Earth and Planetary Science Letters 278, 324-336.

Reimer, P.J., Baillie, M.G.L., Bard, E., Bayliss, A., Beck, J.W., Bertrand, C.J., H., Blackwell, P.G., Buck, C.E., Burr, G.S., Cutler, K.B., Damon, P.E., Edwards, L., Fairbanks, R.G., Friedrich, M., Guilderson, T.P., Hogg, A.G., Hughen, K., Kromer, B., McCormac, G., Mannin, S., Bronk Ramsey, C., Reimer, R.W., Remmele, S., Southon, J.R., Stuiver, M., Talamo, S., Taylor, F.W., van der Plicht, J., Weyhenmeyer, C.E., 2004. IntCal04 terrestrial radiocarbon age calibration, 0-26 cal kyr BP. Radiocarbon 46, 1029-1058.

Reimer, P.J., Baillie, M.G.L., Bard, E., Bayliss, A., Beck, J.W., Blackwell, P.G., Bronk Ramsey, C., Buck, C.E., Burr, G.S., Edwards, R.L., Friedrich, M., Grootes, P.M., Guilderson, T.P., Hajdas, I., Heaton, T.J., Hogg, A.G., Hughen, K.A., Kaiser, K.F.,

Kromer, B., McCormac, F.G., Manning, S.W., Reimer, R.W., Richards, D.A., Southon, J.R., Talamo, S., Turney, C.S.M., van der Pflicht, J., Weyhenmeyer, C.E., 2009. INTCAL09 AND MARINE09 RADIOCARBON AGE CALIBRATION CURVES, 0–50,000 YEARS CAL BP. Radiocarbon 51, 1111-1150.

Reimer, P.J., Bard, E., Bayliss, A., Beck, J.W., Blackwell, P.G., Bronk Ramsey, C., Buck, C.E., Cheng, H., Edwards, R.L., Friedrich, M., Grootes, P.M., Guilderson, T.P., Haflidason, H., Hajdas, I., Hatté, C., Heaton, T.J., Hoffmann, D.L., Hogg, A.G., Hughen, K.A., Kaiser, K.F., Kromer, B., Manning, S.W., Niu, M., Reimer, R.W., Richards, D.A., Scott, E.M., Southon, J.R., Staff, R.A., Turney, C.S.M., van der Plicht, J., 2013. IntCal13 and Marine13 Radiocarbon Age Calibration Curves 0-50,000 Years Cal BP. Radiocarbon 55, 1869-1887.

Ribbe, J., 2001. Intermediate Water Mass Production Controlled by Southern Hemisphere Winds. Geophysical Research Letters 28, 535-538.

Rintoul, S.R., Bullister, J.L., 1999. A late winter hydrographic section from Tasmania to Antarctica. Deep-Sea Research I 46, 1417-1454.

Rintoul, S.R., England, M.H., 2002. Ekman Transport Dominates Local Air–Sea Fluxes in Driving Variability of Subantarctic Mode Water. Journal of Physical Oceanography 32, 1308-1321.

Rintoul, S.R., Hughes, C., Olbers, D., 2001. The Antarctic Circumpolar Current System, in: Siedler, G., Church, J., Gould, J. (Eds.), Ocean, Ice and Atmosphere - Interactions at the Antarctic Continental Margin, pp. 151-171.

Robinson, L.F., Adkins, J.F., Keigwin, L.D., Southon, J., Fernandez, D.P., Wang, S.-L., Scheirer, D.S., 2005. Radiocarbon Variability in the Western North Atlantic During the Last Deglaciation. Science 310, 1469-1473.

Robinson, L.F., van de Flierdt, T., 2009. Southern Ocean evidence for reduced export of North Atlantic Deep Water during Heinrich event 1. Geology 37, 195-198.

Rohling, E.J., 2007. Progress in paleosalinity: Overview and presentation of a new approach. Paleoceanography 22, 1-9.

Rohling, E.J., Cooke, S., 1999. Stable oxygen and carbon isotopes in foraminiferal carbonate shells, in: Gupta, S. (Ed.), Modern Foraminifera. Kluwer Academic Publishers, Dordrecht, pp. 239-258.

Rojas, M., Moreno, P., Kageyama, M., Crucifix, M., Hewitt, C., Abe-Ouchi, A., Ohgaito, R., Brady, E.C., Hope, P., 2009. The Southern Westerlies during the last glacial maximum in PMIP2 simulations. Climate Dynamics 32, 525-548.

Romahn, S., Mackensen, A., Groeneveld, J., Pätzold, J., 2014. Deglacial intermediate water reorganization: new evidence from the Indian Ocean. Climate of the Past 10, 293-303.

Ronge, T.A., Tiedemann, R., Lamy, F., Kersten, F., Frische, M., Fietzke, J., De Pol-Holz, R., Pahnke, K., Alloway, B.V., Wacker, L., Southon, J., Constraining the extent and evolution of the Southwest Pacific glacial carbon pool. submitted.

Rose, K.A., Sikes, E.L., Guilderson, T.P., Shane, P., Hill, T.M., Zahn, R., Spero, H.J., 2010. Upper-ocean-to-atmosphere radiocarbon offsets imply fast deglacial carbon dioxide release. Nature 466, 1093-1097.

Russell, J.L., Dickson, A.G., 2003. Variability in oxygen and nutrients in South Pacific Antarctic Intermediate Water. Global Biochemical Chycles 17, 1033.

Ryan, M.T., Dunbar, G.B., Vandergoes, M.J., Neil, H.L., Hannah, M.J., Newnham, R.M., Bostock, H.C., Alloway, B.V., 2012. Vegetation and climate in Southern Hemisphere mid-latitudes since 210 ka: new insights from marine and terrestrial pollen records from New Zealand. Quaternary Science Reviews 48, 80-98.

Sabine, C.L., Feely, R.A., Gruber, N., Key, R.M., Lee, K., Bullister, J.L., Wanninkhof, R., Wong, C.S., Wallace, D.W.R., Tilbrook, B., Millero, F.J., Peng, T.-H., Kozyr, A., Ono, T., Rios, A.F., 2004. The Oceanic Sink for Anthropogenic CO_2. Science 305, 367-371.

Saenko, O.A., Fyfe, J.C., England, M.H., 2005. On the response of the oceanic wind-driven circulation to atmospheric CO2 increase. Climate Dynamics 25, 415-426.

Saenko, O.A., Weaver, A.J., 2001. Importance of wind-driven sea ice motion for the formation of Antarctic Intermediate Water in a global climate model. Geophysical Research Letters 28, 4147-4150.

Saenko, O.A., Weaver, A.J., Gregory, J.M., 2003. On the Link between the Two Modes of the Ocean Thermohaline Circulation and the Formation of Global-Scale Water Masses. Journal of Climate 16, 2797-2801.

Sallée, J.-B., Speer, K., Rintoul, S., Wijffels, S., 2010. Southern Ocean Thermocline Ventilation. Journal of Physical Oceanography 40, 509-529.

Sallée, J.-B., Wienders, N., Speer, K., Morrow, R., 2006. Formation of subantarctic mode water in the southeastern Indian Ocean. Ocean Dynamics 56, 525-542.

Sarmiento, J.L., Gruber, N., Brzezinski, M.A., Dunne, J.P., 2004. High-latitude controls of thermocline nutrients and low latitude biological productivity. Nature 427, 56-60.

Sarnthein, M., Grootes, P.M., Kennet, J.P., Nadeau, M.-J., 2007. ^{14}C Reservoir Ages Show Deglacial Changes in Ocean Currents and Carbon Cycle, in: Schmittner, A., Chiang, J.C.H., Hemming, S.R. (Eds.), Ocean Circulation: Mechanisms and Impacts—Past and Future Changes of Meridional Overturning. AGU, Geophysical Monograph Series, pp. 175-196.

Sarnthein, M., Schneider, B., Grootes, P.M., 2013. Peak glacial ^{14}C ventilation ages suggest major draw-down of carbon into the abyssal ocean. Climate of the Past 9, 929-965.

Schaub, M., Büntgen, U., Kaiser, K.F., Kromer, B., Talamo, S., Anderson, K.K., Rasmussen, S.O., 2008. Late glacial environmental variability from Swiss tree rings. Quaternary Science Reviews 27, 29-41.

Schlitzer, R., 2014. Ocean Data View, 4.6.1. ed, owa.awi.de.

Schmitt, J., Schneider, R., Elsig, J., Leuenberger, D., Lourantou, A., Chappelaz, J., Köhler, P., Joos, F., Stocker, T.F., Leuenberger, M., Fischer, H., 2012. Carbon Isotope Constraints on the Deglacial CO_2 Rise from Ice Cores. Science 336, 711-714.

Schmitz, W.J., 1995. On the interbasin-scale thermohaline circulation. Reviews of Geophysics 33, 151-173.

Schneider, W., Bravo, L., 2006. Argo profiling floats document Subantarctic Mode Water formation west of Drake Passage. Geophysical Research Letters 33, 1-4.

Schulz, K.G., Zeebe, R.E., 2006. Pleistocene glacial terminations triggered by synchronous changes in Southern and Northern Hemisphere insolation: The insolation canon hypothesis. Earth and Planetary Science Letters 249, 326-336.

Shackleton, N.J., 1974. Attainment of Isotopic Equilibrium Between Ocean Water and the Benthonic Foraminifera Genus Uvigerina: Isotopic Changes in the Ocean During the Last Glacial. Colloques Internationaux du C.N.R.S 219, 203-209.

Shackleton, N.J., 1977. The oxygen isotope stratigraphic record of the Late Pleistocene. Philosophical Transactions of the Royal Society 280, 169-182.

Shackleton, N.J., Opdyke, N.D., 1973. Oxygen Isotope and Palaeomagnetic Stratigraphy of Equatorial Pacific Core V28-238: Oxygen Isotope Temperatures and Ice Volumes on a 10" Year and 10" Year Scale*. Quaternary Research 3, 17.

Shackleton, N.J., Sánchez-Goni, M.F., Pailler, D., Lancelot, Y., 2003. Marine Isotope Substage 5e and the Eemian Interglacial. Global and Planetary Change 36, 151-155.

Shin, S.-I., Liu, Z., Otto-Bliesner, B., Brady, E.C., Kutzbach, J., Harrison, S.P., 2003. A simulation of the Last Glacial Maximum climate using the NCAR-CCSM. Climate Dynamics 20, 127-151.

Siani, G., Michel, E., De Pol-Holz, R., DeVries, T., Lamy, F., Carel, M., Isguder, G., Dewilde, F., Lourantou, A., 2013. Siani 2013, Carbon isotope records reveal precise timing of enhanced Southern Ocean upwelling during the last deglaciation. Nature Communications 4, 1-9.

Siegenthaler, U., Stocker, T.F., Monnin, E., Lüthi, D., Schwander, J., Stauffer, B., Raynaud, D., Barnola, J.-M., Fischer, G., Masson-Delmotte, V., Jouzel, J., 2005. Stable Carbon Cycle–Climate Relationship During the Late Pleistocene. Science 310, 1313-1317.

Sigman, D.M., Boyle, E.A., 2000. Glacial/interglacial variations in atmospheric carbon dioxide. Nature 407, 859-869.

Sigman, D.M., Hain, M.P., Haug, G.H., 2010. The polar ocean and glacial cycles in atmospheric CO_2 concentration. Nature 466, 47-55.

Sikes, E.L., Howard, W.R., Samson, C.R., Mahan, T.S., Robertson, L.G., Volkman, J.K., 2009. Southern Ocean seasonal temperature and Subtropical Front movement on the South Tasman Rise in the late Quaternary. Paleoceanography 24, 1-13.

Sikes, E.L., Samson, C.R., Gullderson, T.P., Howard, W.R., 2000. Old radiocarbon ages in the southwest Pacifc Ocean during the last glacial period and deglaciation. Nature 405, 555-559.

Sime, L.C., Kohfeld, K.E., Le Quéré, C., Wolff, E.W., de Boer, A.M., Graham, R.M., Bopp, L., 2013. Southern Hemisphere westerly wind changes during the Last Glacial Maximum: model-data comparison. Quaternary Science Reviews 64, 104-120.

Skinner, L.C., Fallon, S., Waelbroeck, C., Michel, E., Barker, S., 2010. Ventilation of the Deep Southern Ocean and Deglacial CO_2 Rise. Science 328, 1147-1151.

Skinner, L.C., Scrivner, A.E., Vance, D., Barker, S., Fallon, S., Waelbroeck, C., 2013. North Atlantic versus Southern Ocean contributions to a deglacial surge in deep ocean ventilation. Geology, 1-4.

Skinner, L.C., Shackleton, N.J., 2004. Rapid transient changes in northeast Atlantic deep water ventilation age across Termination I. Paleoceanography 19, 1-11.

Skinner, L.C., Waelbroeck, C., Scrivner, A.E., Fallon, S.J., 2014. Radiocarbon evidence for alternating northern and southern sources of ventilation of the deep Atlantic carbon pool during the last deglaciation. PNAS 111, 5480-5484.

Sloyan, B.M., Talley, L.D., Chereskin, T.K., Fine, R.A., Holte, J., 2010. Antarctic Intermediate Water and Subantarctic Mode Water Formation in the Southeast Pacific: The Role of Turbulent Mixing. Journal of Physical Oceanography 40, 1558-1574.

Southon, J.R., Noronha, A.L., Cheng, H., Edwards, R.L., Wang, Y., 2012. A high-resolution record of atmospheric ^{14}C based on Hulu Cave speleothem H82. Quaternary Science Reviews 33, 32-41.

Spero, H.J., Lea, D.W., 1996. Experimental determination of stable isotope variability in Globigerina bulloides: implications for paleoceanographic reconstructions. Marine Micropaleontology 28, 231-246.

Spero, H.J., Lea, D.W., 2002. The Cause of Carbon Isotope Minimum Events on Glacial Terminations. Science 296, 522-525.

Spero, H.J., Mielke, K.M., Kalve, E.M., Lea, D.W., Pak, D.K., 2003. Multispecies approach to reconstructing eastern equatorial Pacific thermocline hydrography during the past 360 kyr. Paleoceanography 18, 1-16.

Steph, S., Regenberg, M., Tiedemann, R., Mulitza, S., Nürnberg, D., 2009. Stable isotopes of planktonic foraminifera from tropical Atlantic/Caribbean core- tops: Implications for reconstructing upper ocean stratification. Marine Micropaleontology 71, 1-19.

Stephens, B., Keeling, R.F., 2000. The influence of Antarctic sea ice on glacial-interglacial CO_2 variations. Nature 404, 171-174.

Stott, L.D., Southon, J., Timmermann, A., Koutavas, A., 2009. Radiocarbon age anomaly at intermediate water depth in the Pacific Ocean during the last deglaciation. Paleoceanography 24, 1-10.

Stuiver, M., Polach, H.A., 1977. Discussion and reporting of ^{14}C data. Radiocarbon 19, 355-363.

Stuiver, M., Reimer, P.J., 1993. Extended 14C Data Base and Revised Calib 3.0 ^{14}C Age Calibration Program. Radiocarbon 35, 215-230.

Stuiver, M., Reimer, P.J., Bard, E., Beck, J.W., Burr, G.S., Hughen, K., Kromer, B., McGormac, G., van der Plicht, J., Spurk, M., 1998. INTCAL98 Radiocarbon Age Calibration 24000-0 cal BP. Radiocarbon 40, 1041-1083.

Stuiver, M., Reimer, P.J., Reimer, R.W., 2005. Calib, 7.0 ed, calib.qub.ac.uk.

Stuut, J.-B.W., Lamy, F., 2004. Climate variability at the southern boundaries of the Namib (southwestern Africa) and Atacama (northern Chile) coastal deserts during the last 120,000 yr. Quaternary Research 62, 301-309.

Sutton, P.J.H., 2003. The Southland Current: a subantarctic current. New Zealand Journal of Marine and Freshwater Research 37, 645-652.

Synal, H.-A., Stocker, M., Suter, M., 2007. MICADAS: A new compact radiocarbon AMS system. Nuclear Instruments and Methods in Physics Research B 259, 7-13.

Takahashi, T., Sweeny, C., Hales, B., Chipman, D.W., Newberger, T., Goddard, J.G., Ianuzzi, R.A., Sutherland, S.C., 2012. The Changing Carbon Cycle in the Southern Ocean. Oceanography 25, 26-37.

Talley, L.D., 2013. Closure of the global overturning circulation through the Indian, Pacific, and Southern Oceans: Schematics and transports. Oceanography 26, 80-97.

Tans, P., Keeling, R.F., 2014. Trends in Atmospheric Carbon Dioxide (NOAA Homepage).

Tessin, A.C., Lund, D.C., 2013. Isotopically depleted carbon in the mid-depth South Atlantic during the last deglaciation. Paleoceanography 28, 296-306.

Thiede, J., 1999. FS Sonne - Fahrtbericht SO136, cruise report SO136 - TASQWA: quaternary variability of water masses in Southern Tasman sea and the southern ocean (sw pacific sector); Wellington - Hobart, October 16 - November 12, in: TASQWA, s.s.p.o., Thiede, J. (Eds.). GEOMAR, Kiel, p. 106.

Thompson, D.W.J., Solomon, S., 2002. Interpretation of Recent Southern Hemisphere Climate Change. Science 296, 895-899.

Thornalley, D.J.R., Elderfield, H., McCave, I.N., 2010. Intermediate and deep water paleoceanography of the northern North Atlantic over the past 21,000 years. Paleoceanography 25, 1-17.

Tiedemann, R., 2012. FS Sonne Fahrtbericht / Cruise Report SO213. Alfred Wegener Institute, Bremerhaven.

Toggweiler, J.R., Dixon, K., 1991. The Peru Upwelling and the Ventilation of the South Pacific Thermocline. Journal of Geophysical Research 96, 20,467-420,497.

Toggweiler, J.R., Dixon, K., Broecker, W., 1991. The Peru upwelling and the ventilation of the South Pacific thermocline. Journal of Geophysical Research 96, 20,467-420,497.

Toggweiler, J.R., Russell, J.L., Carson, S.R., 2006. Midlatitude westerlies, atmospheric CO2, and climate change during the ice ages. Paleoceanography 21, 1-15.

Tomczak, M., Godfrey, J.S., 1994. Regional Oceanography: An Introduction.

Tsuchiya, M., Talley, L.D., 1998. A Pacific hydrographic section at 88°W: Water-property distribution. Journal of Geophysical Research 103, 12899-12918.

Van Meerbeeck, C.J., Renssen, H., Roche, D.M., 2009. How did Marine Isotope Stage 3 and Last Glacial Maximum climates differ? – Perspectives from equilibrium simulations. Climate of the Past 5, 33-51.

Vandergoes, M.J., Hogg, A.G., Lowe, D.J., Newnham, R.M., Denton, G.H., Southon, J., Barrell, D.J.A., Wilson, C.J.N., McGlone, M.S., Allan, A.S.R., Almond, P.C., Petchey, F., Dabell, K., Dieffenbacher-Krall, A.C., Blaauw, M., 2012. A revised age for the Kawakawa/Oruanui tephra, a key marker for the Last Glacial Maximum in New Zealand. Quaternary Science Reviews, 1-7.

Varma, V., Prange, M., Lamy, F., Merkel, U., Schulz, M., 2011. Solar-forced shifts of the Southern Hemisphere Westerlies during the Holocene. Climate of the Past 7, 339-347.

Veres, D., Bazin, L., Landais, A., Toyé Mahamadou Kele, H., Lemieux-Dudon, B., Parrenin, F., Martinerie, P., Blayo, E., Blunier, T., Capron, E., Chappelaz, J., Rasmussen, S.O., Severi, M., Svensson, A., Vinther, B., Wolff, E.W., 2013. The Antarctic ice core chronology (AICC2012): an optimized thousand yearsmulti-parameter and multi-site dating approach for the last 120. Climate of the Past 9, 1773-1748.

Villamor, P., Van Dissen, R., Alloway, B.V., Palmer, A.S., Lichfield, N., 2007. The Rangipo fault, Taupo rift, New Zealand: An example of temporal slip-rate and single-event displacement variability in a volcanic environment. Geological Society of America Bulletin 119, 529-547.

Waelbroeck, C., Labeyrie, L., Michel, E., Duplessy, J.-C., McManus, J.F., Lambeck, K., Balbon, E., Labracherie, M., 2002. Sea-level and deep water temperature changes

derived from benthic foraminifera isotopic records. Quaternary Science Reviews 21, 295-305.

WAIS Divide Project Members, 2013. Onset of deglacial warming in West Antarctica driven by local orbital forcing. Nature 500, 440-444.

Weaver, A.J., Saenko, O.A., Clark, P.U., Mitrovica, J.X., 2003. Meltwater Pulse 1A from Antarctica as a Trigger of the Bølling-Allerød Warm Interval. Science 299, 1709-1713.

Wentworth, C.K., 1922. A scale of grade and class terms of clastic sediments. Journal of Geology 30, 377-392.

Whithworth, T., 1988. The Antarctic Circumpolar Current. Oceanus 32, 53-58.

Wilke, I., Meggers, H., Bickert, T., 2009. Depth habitats and seasonal distributions of recent planktic foraminifers in the Canary Islands region (29 N) based on oxygen isotopes. Deep-Sea Research I 56.

Wrytki, K., 1973. Physical oceanography of the Indian Ocean, The biology of the Indian Ocean. Springer, Heidelberg, pp. 18-36.

Yeager, S.G., Shields, C.A., Large, W.G., Hack, J.J., 2006. The Low-Resolution CCSM3. Journal of Climate 19, 2545-2566.

You, Y., 2000. Implications of the deep circulation and ventilation of the Indian Ocean on the renewal mechanism of North Atlantic Deep Water. Journal of Geophysical Research 105, 23895-23926.

Yu, J., Anderson, R.F., Jin, Z., Menviel, L., Zhang, F., Ryerson, F.J., Rohling, E.J., 2014. Deep South Atlantic carbonate chemistry and increased interocean deep water exchange during last deglaciation. Quaternary Science Reviews 90, 80-89.

Yu, J., Elderfield, H., 2007. Benthic foraminiferal B/Ca ratios reflect deep water carbonate saturation state. Earth and Planetary Science Letters 258, 73.

Zahn, R., Pedersen, T.F., Bornhold, B.D., Mix, A.C., 1991. Water Mass Conversion in the Glacial Subarctic Pacific (54°N, 148°W): Physical Constraints and the Benthic-Planktonic Stable Isotope Record. Paleoceanography 6, 543-560.

Zeebe, R.E., Wolf-Gladrow, D., 2001. Stable Isotope Fractionation, in: Zeebe, R.E., Wolf-Gladrow, D. (Eds.), CO_2 in Seawater: Equilibrium, Kinetics, Isotopes. Elsevier, pp. 141-250.

Zhou, M., Zhu, Y., d'Ovidio, F., Park, Y.-H., Durand, I., Kestenare, E., Sanial, V., Van-Beek, P., Queguiner, B., Carlotti, F., Blain, S., 2014. Surface currents and upwelling in Kerguelen Plateau regions. Biogeosciences.

Ziegler, M., Diz, P., Hall, I.R., Zahn, R., 2013. Millennial-scale changes in atmospheric CO_2 levels linked to the Southern Ocean carbon isotope gradient and dust flux. Nature Geoscience, 1-5.

Zillman, J.W., 1972. Solar radiation and sea-air interaction south of Australia, in: Hayes, D.T. (Ed.), Antarctic Oceanology II. AGU, Washington, pp. 11-40.

Appendix

A1 – List of Abbreviations

Water masses, climatic intervals, and (pale-) oceanographic terms

AAIW	Antarctic Intermediate Water
AABW	Antarctic Bottom Water
ACC	Antarctic Circumpolar Current
ACR	Antarctic Cold Reversal
CDW	Circumpolar Deep Water
CFZ	Chile Fracture Zone
ChiRi	Chile Rise
DWBC	Deep Western Boundary Current
EPR	East Pacific Rise
HS1	Heinrich Stadial 1
IDW	Indian Deep Water
KOT	Kawakawa/Oruanui Tephra
LCDW	Lower Circumpolar Deep Water
LGM	Last Glacial Maximum
NADW	North Atlantic Deep Water
NPIW	North Pacific Intermediate Water
NZM	New Zealand Margin
PDW	Pacific Deep Water
PF	Polar Front
SAF	Subantarctic Front
SAM	Southern Annular Mode
SAMW	Subantarctic Mode Water
SASW	Subantarctic Surface Water
SAW	Subantarctic Water
SO	Southern Ocean
SOIW	Southern Ocean Intermediate Water
SPG	South Pacific Gyre
STF	Subtropical Front
STW	Subtropical Water
SWW	Southern Westerly Winds
THC	Thermohaline Circulation
UCDW	Upper Circumpolar Deep Water
WAIS	West Antarctic Ice Sheet
YD	Younger Dryas

Proxy and analytical definitions

AMS	Accelerator Mass Spectrometry
CCSM3	Community Climate System Model version 3
$CO_{2\ atm}$	Atmospheric CO_2

DIC	Dissolved Inorganic Carbon
$DI^{14}C$	^{14}C component of DIC
DTT	Deep thermocline temperatures
$\Delta^{14}C$	As defined by Stuiver and Polach (1977): The relative difference of the sample ^{14}C activity (age and $\delta^{13}C$ corrected) to the *absolute international standard* (base-year 1950)
$\Delta\Delta^{14}C$	$\Delta^{14}C$ offset of the sample to the atmospheric $\Delta^{14}C$ (Reimer et al., 2013)
$\delta^{18}O/\delta^{13}C_{Cib}$	*Cibicidoides wuellerstorfi* $\delta^{18}O/\delta^{13}C$
$\delta^{18}O/\delta^{13}O_{Uvi}$	*Uvigerina peregrina* $\delta^{18}O/\delta^{13}C$
$\delta^{18}O_{sw}$	Seawater $\delta^{18}O$
$\delta^{18}O_{sw\text{-}ivc}$	Ice volume corrected seawater $\delta^{18}O$
ICP-AES	Inductively Couples Plasma Atomic Emission Spectrometry
ICP-OES	Inductively Coupled Plasma Optical Emission Spectrometry
L*	Sediment lightness
Magsus	Magnetic Susceptibility
MICADAS	Micro Carbon Dating System
SST	Sea surface temperatures
TOC	Total Organic Carbon
TOC_{AR}	TOC accumulation rate
TT	Thermocline temperatures

Project names, facilities, and institutes

AWI	Alfred Wegener Institute
BMBF	Bundesministerium für Bildung und Forschung
BIPOMAC	Bipolar Climate Machinery
IPCC	Intergovernmental Panel on Climate Change
ETH	Eidgenössische Technische Hochschule
EPICA	European Project for Ice Coring in Antarctica
IODP	Integrated Ocean Drilling Program / International Ocean Discovery Program
NOSAMS	National Ocean Science AMS
ODP	Ocean Drilling Program
SOPATRA	South Pacific Paleoceanographic Transects

Cruise names (sediment core names)

MD97/06	R/V *Marion Dufresne* cruises MD106 and MD152 (year 1997 and 2006)
PS75	R/V *Polarstern* cruise ANTXXVI-26 (year 2009/2010)
SO136/213	R/V *Sonne* cruises 136 and 213 (year 1998 and 2010/2011)

Other

AC^3	Anthropogenic caused climate change
SW	Southwest

A2 – Core descriptions of SO213 sediment cores

In this section only core descriptions are shown that were made by me. For the core descriptions of the PS75 sediment cores, please refer to Gersonde (2011). David Poggeman (GEOMAR) measured the sediment lightness (L*) onboard SO213, while I measured the magsus and performed the core descriptions. Color codes are according to the *1990 Munsell Soil Color Charts*. THS – thin section (smear slide for biostratigraphy).

Figure A4.1: Core description, L* and magsus of SO213-59-1.

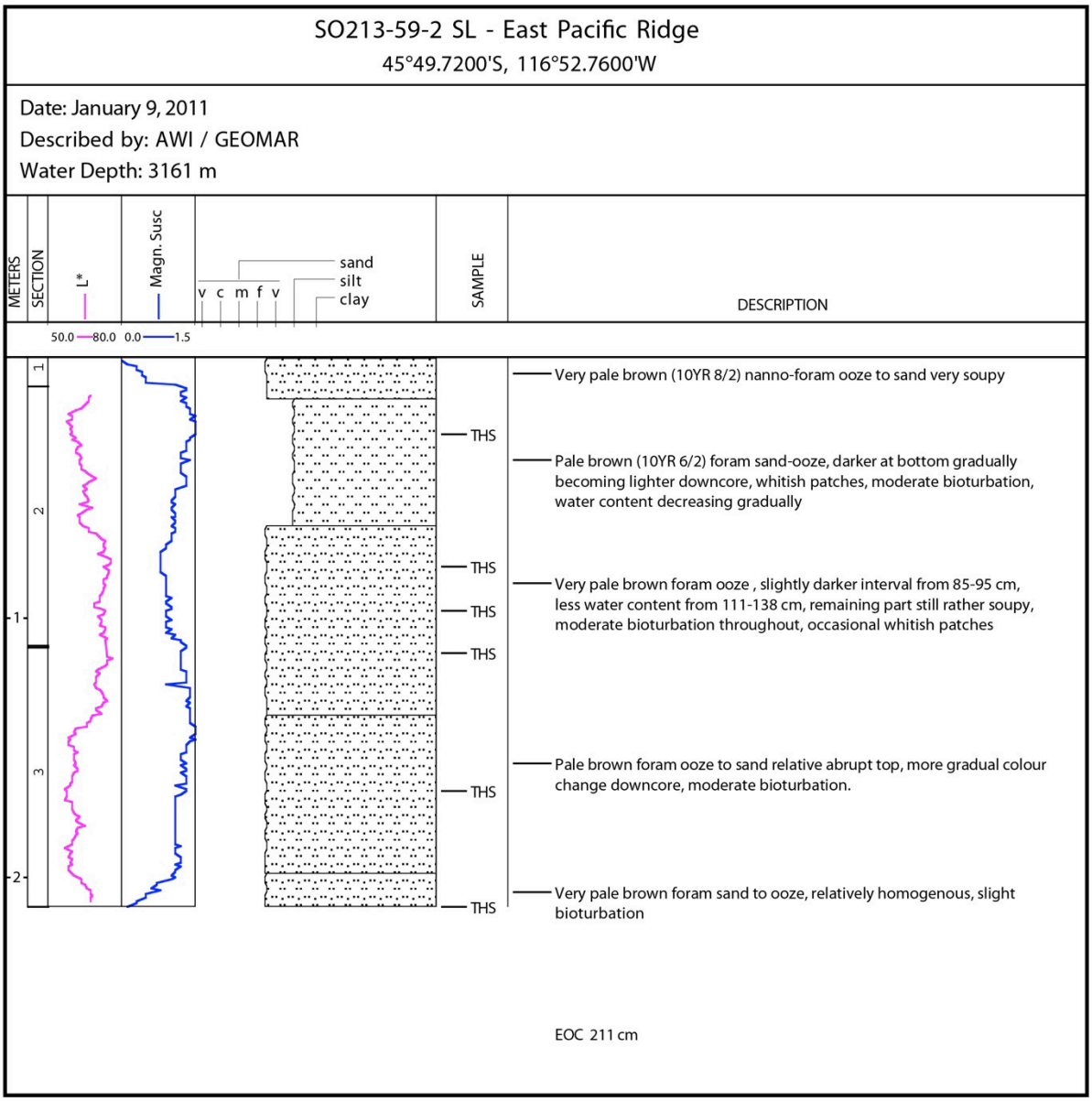

Figure A4.2: Core description, L* and magsus of SO213-76-2 (*part 1*).

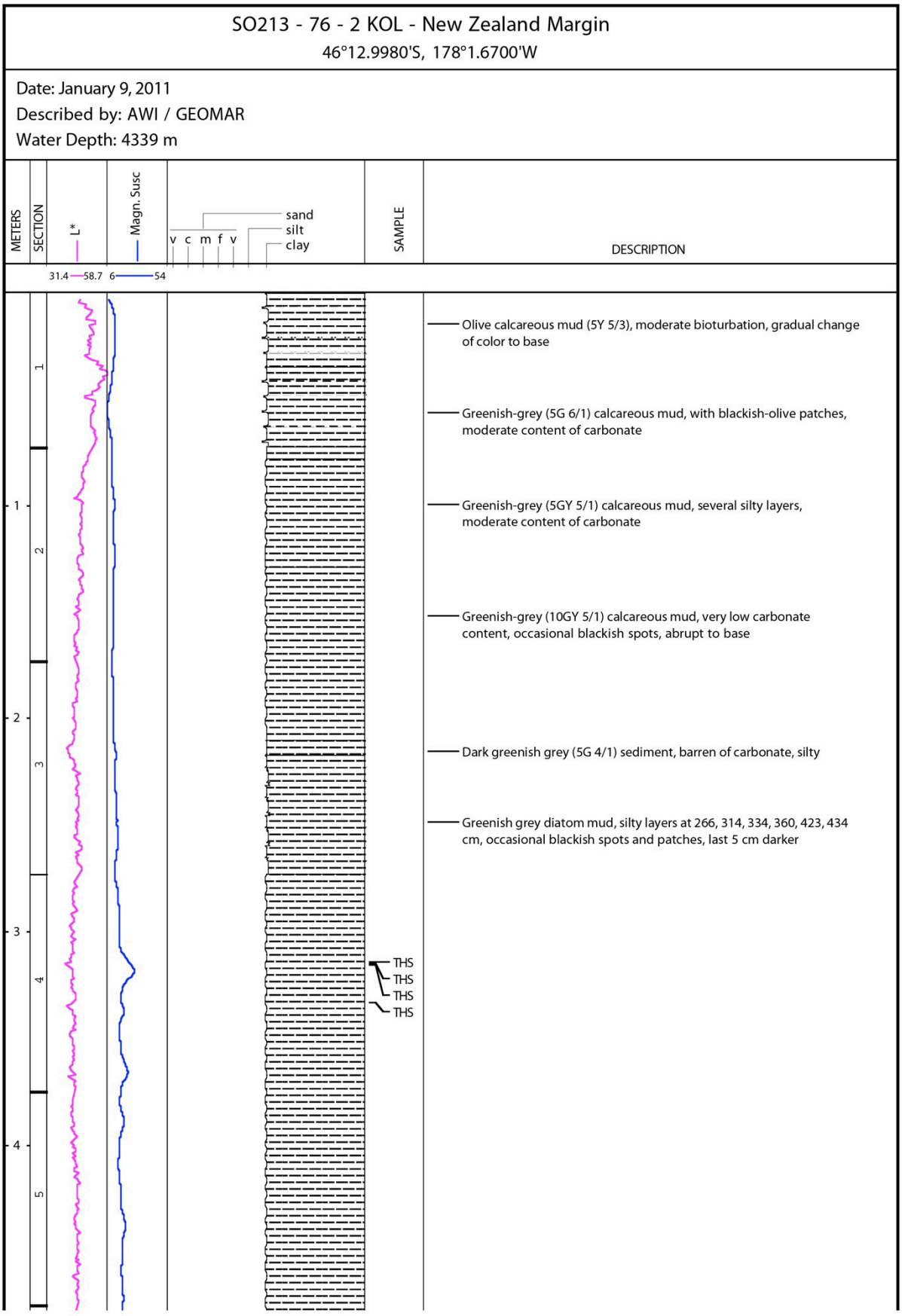

Figure A4.2: Core description, L* and magsus of SO213-76-2 (*part 2*).

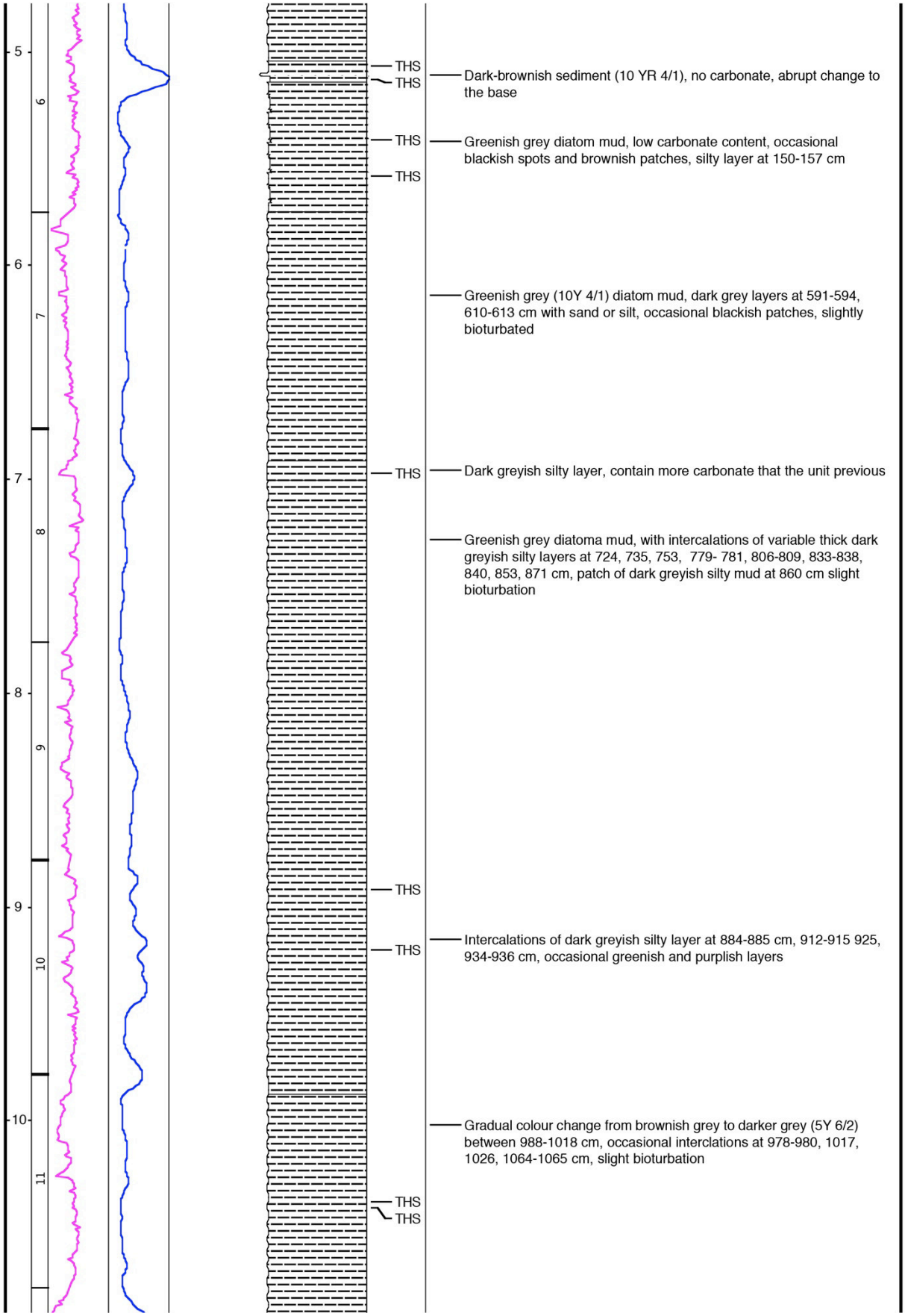

Figure A4.2: Core description, L* and magsus of SO213-76-2 (*part 3*).

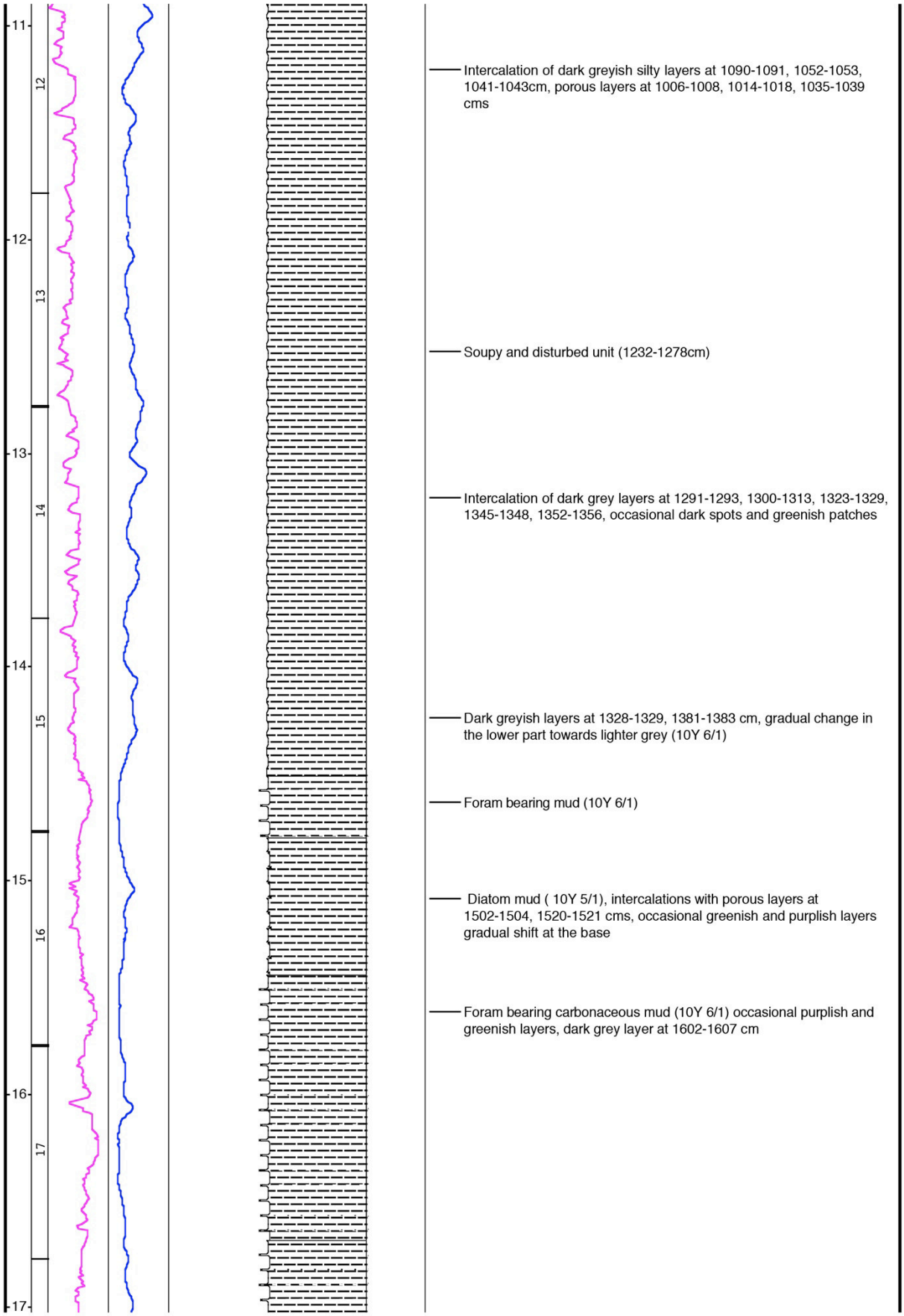

Figure A4.2: Core description, L* and magsus of SO213-76-2 (*part 4*).

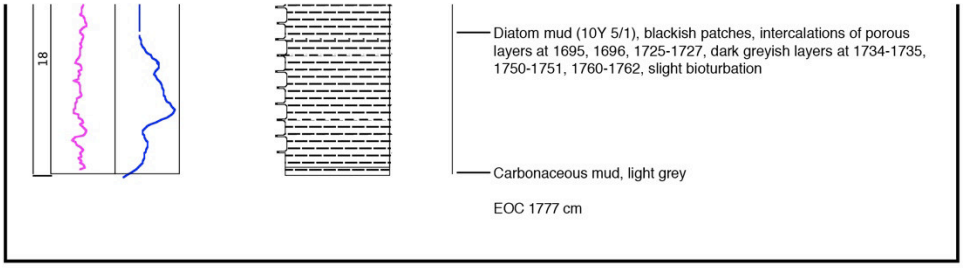

Figure A4.3: Core description, L* and magsus of SO213-79-2 (*part 1*).

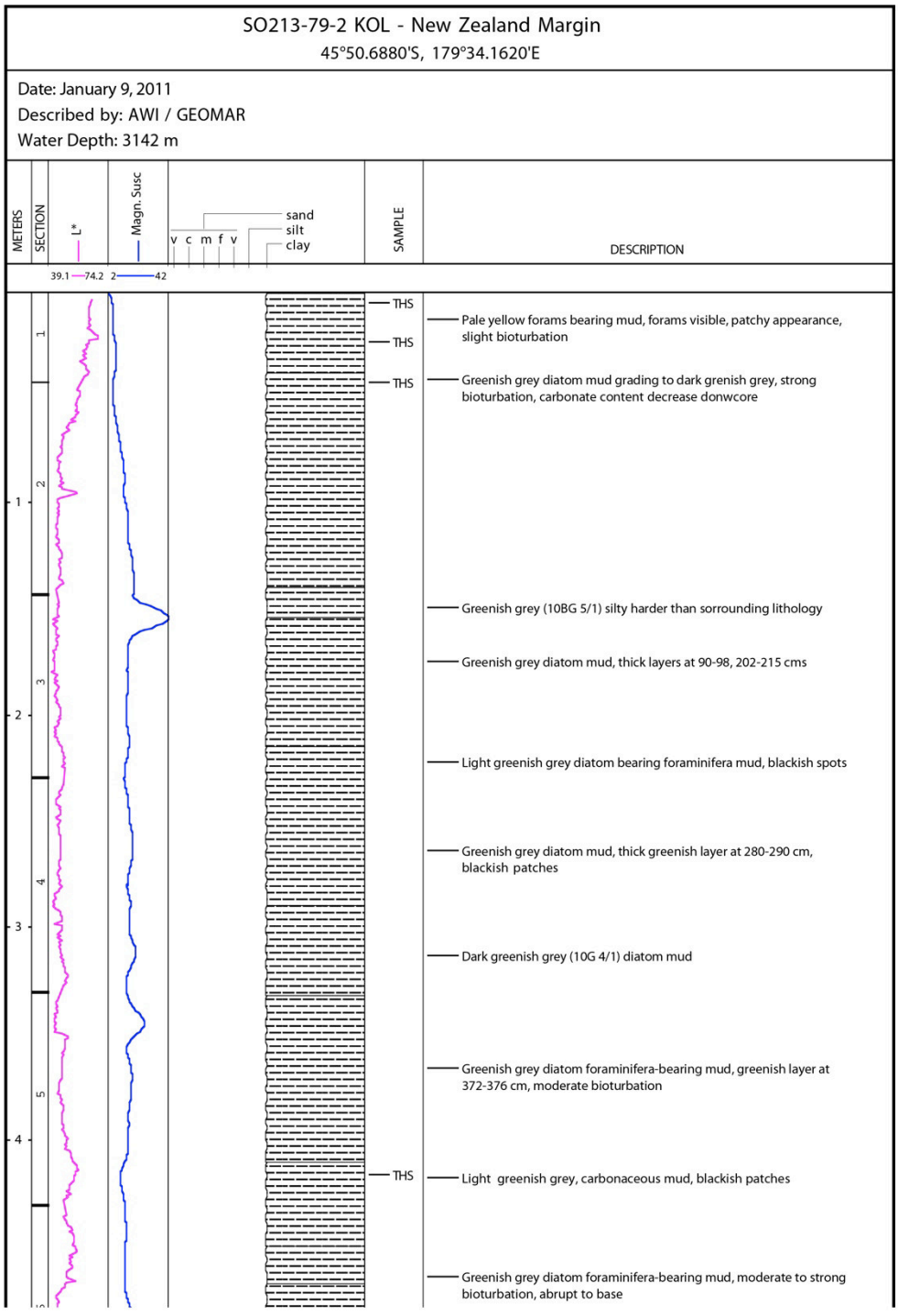

Figure A4.3: Core description, L* and magsus of SO213-79-2 (*part 2*).

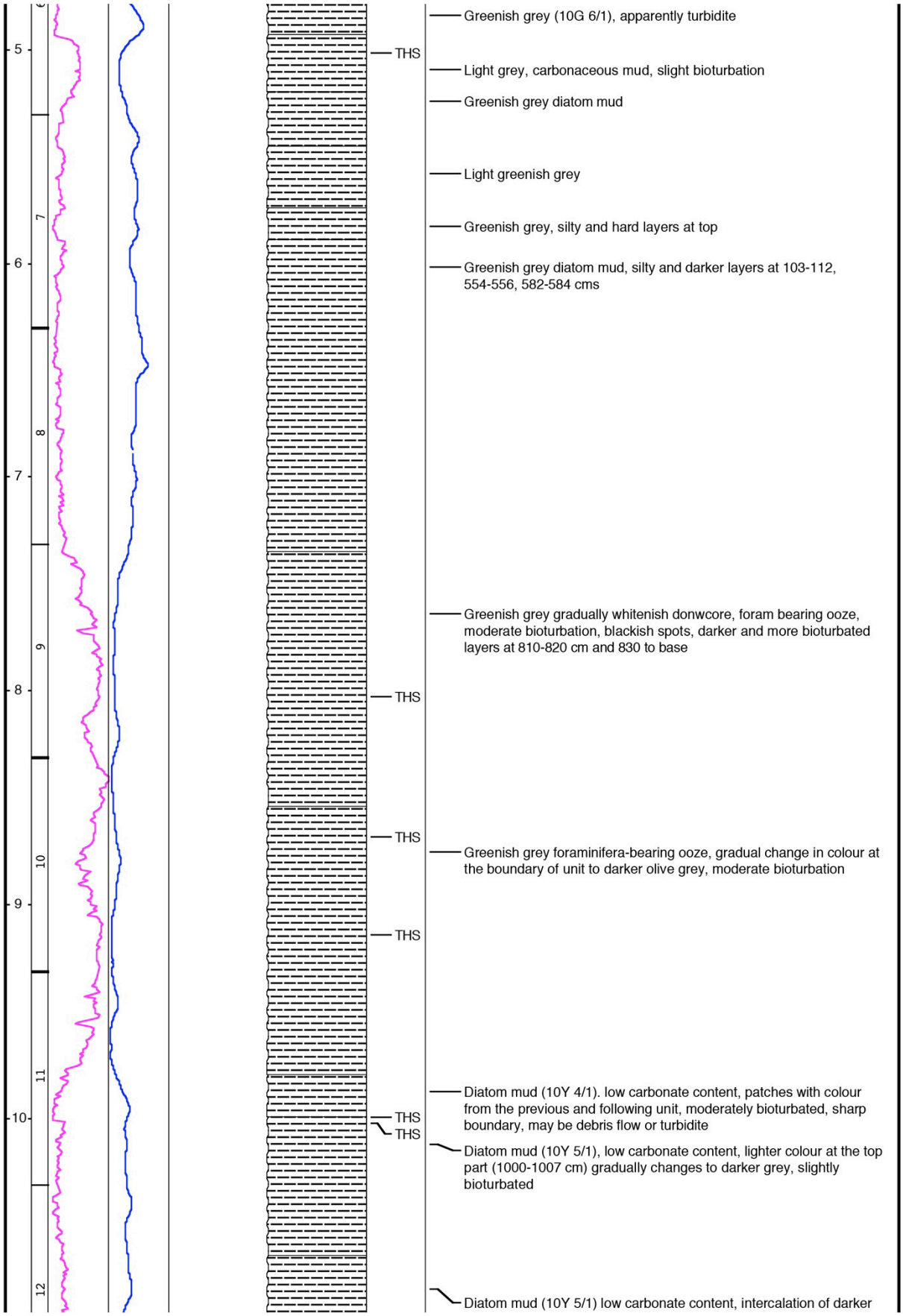

Figure A4.3: Core description, L* and magsus of SO213-79-2 (*part 3*).

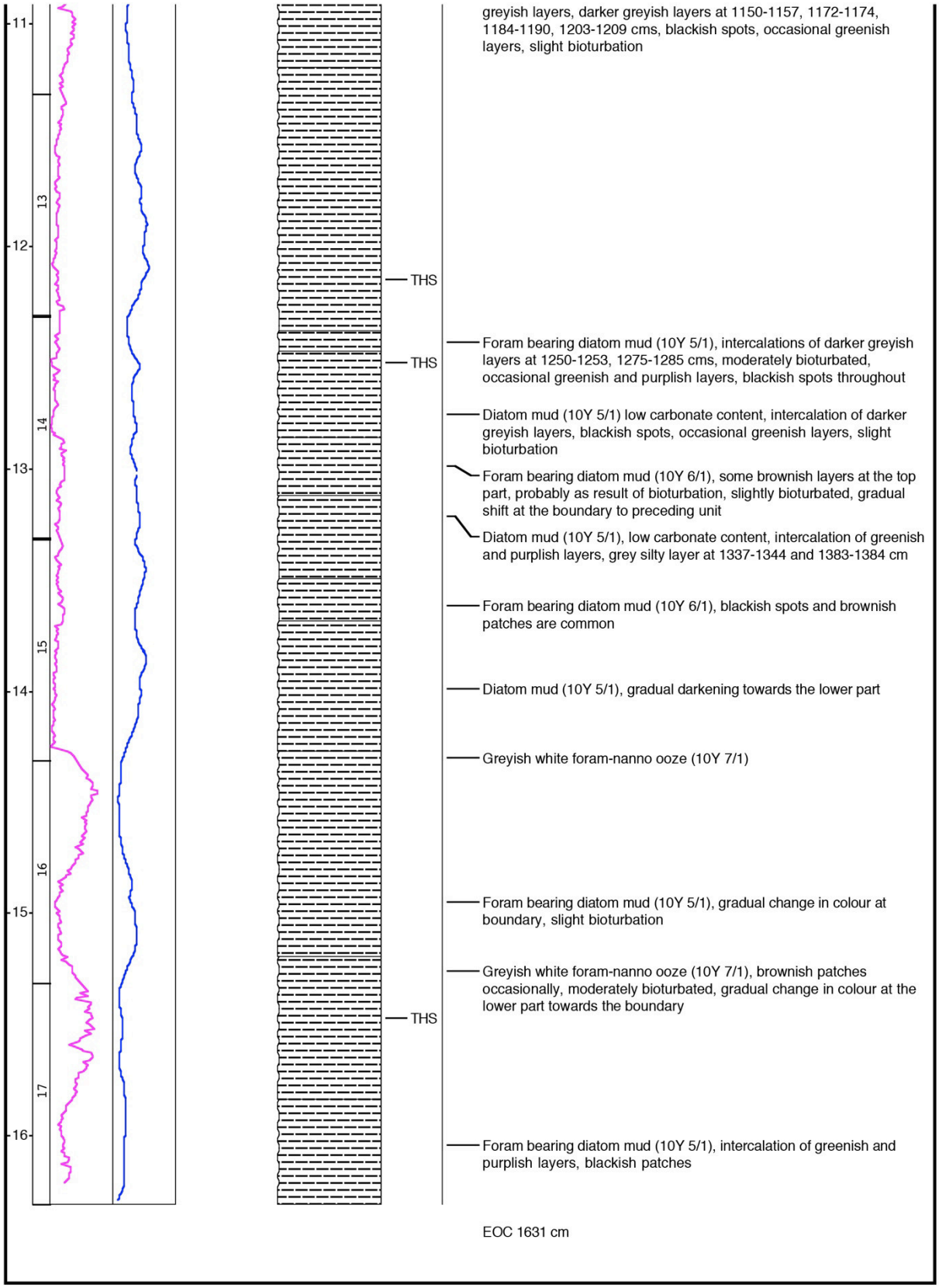

Figure A4.4: Core description, L* and magsus of SO213-84-2.

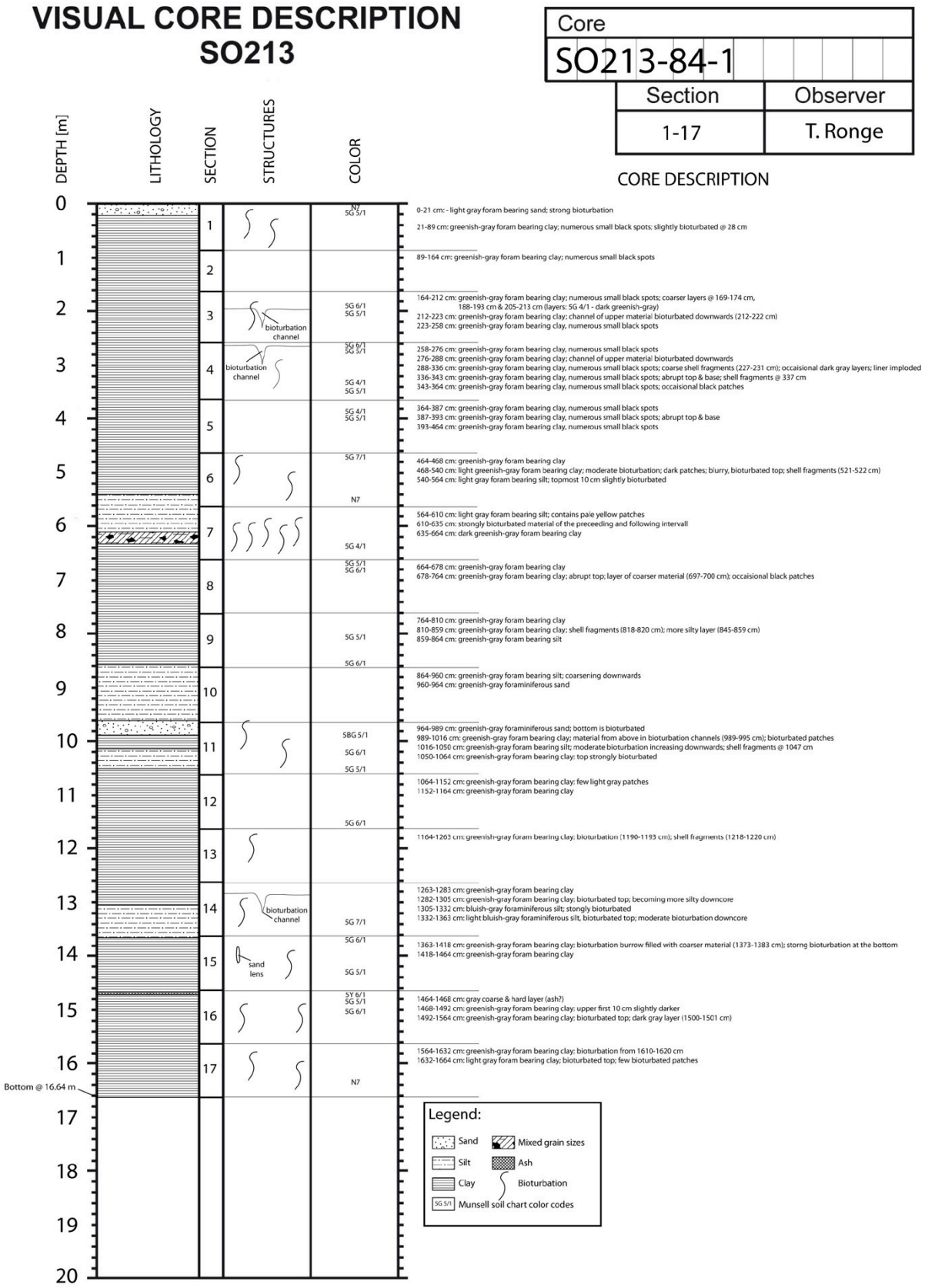

Data handling

All data presented in this thesis will be publicly available online in the PANGAEA-database at *www.pangaea.de*

For the first and second manuscript, combined DOI-packages exist that can be accessed at:

http://doi.pangaea.de/10.1594/PANGAEA.833663 (first manuscript; *Chapter 3*)

http://doi.pangaea.de/10.1594/PANGAEA.835498 (second manuscript; *Chapter 4*)